# Ferrocenyl-substituted Thiophenes –
# Electrochemical Behavior and Charge Transfer

von der Fakultät der Naturwissenschaften

der Technischen Universität Chemnitz genehmigte

# Dissertation

Zur Erlangung des akademischen Grades

doctor rerum naturalium

(Dr. rer. nat.)

vorgelegt von Diplom-Chemiker J. Matthäus Speck,

geboren am 15. Februar 1986 in Meerane

eingereicht am 16.03.2016

Gutachter:      Prof. Dr. Heinrich Lang – Technische Universität Chemnitz

Prof. Dr. Rainer Winter – Universität Konstanz

Tag der Verteidigung: 20.06.2016

## BIBLIOGRAPHISCHE BESCHREIBUNG UND REFERAT

J. Matthäus Speck

**Ferrocenyl-substituted Thiophenes – Electrochemical Behavior and Charge Transfer**

Technische Universität Chemnitz, Fakultät für Naturwissenschaften
Dissertation 2016, 232 Seiten, 101 Abbildungen, 6 Schemata, 28 Tabellen

Die vorliegende Dissertation beschäftigt sich mit dem elektrochemischen Verhalten verschiedener Ferrocenyl-substituierter Thiophene. Dabei wird sich zunächst mit dem elektrochemischen Verhalten der Serie der Ferrocenylthiophene beschäftigt, die Anzahl der Ferrocenyleinheiten variiert von n = 1 – 4. Die Abhängigkeit der elektronischen Eigenschaften von numerischen und konstitutionellen Veränderungen der redox-aktiven Gruppen wird evaluiert. Daraus resultierend wird sich einer eingehenderen Untersuchung und Modifikation des 2,5-Diferrocenylthiophen-Motivs zugewandt. Diese Modifikationen werden im Kontext möglicher Ladungstransferprozesse zwischen den Ferrocenyleinheiten in den verschiedenen Redoxzuständen und unter Beeinflussung durch den Thiophen-Brückenliganden diskutiert. Es folgen des Weiteren Ausführungen zu Substitutionen an den Ferrocenylen (Einführung elektronen-ziehender Funktionalitäten) sowie der Vergleich zwischen einer Thiophen- und der Ethylendioxythiophen-Brückeneinheit. Anschließend wird sich mit der elektronischen Variation des Brückenliganden durch die Einführung von $N$-haltigen Substituenten befasst. In den abschließenden Kapiteln wird der Einfluss zusätzlicher $\sigma$- (Fischercarben-Komplexe) oder $\pi$-gebundener ($[\mathrm{Ru}(\eta^5\text{-}C_5H_5)]^+/[\mathrm{Ru}(\eta^5\text{-}C_5Me_5)]^+$) Übergangsmetallkomplexfragmente auf Ladungstransferwechselwirkungen im 2,5-Diferrocenylthiophen in verschiedenen Redoxzuständen beleuchtet.

*Stichworte: Ferrocen, Heterozyklen, Thiophen, Ladungstransfer, Elektrochemie, Elektronische Kommunikation, Solvatochromie, Spektroelektrochemie, Nahes Infrarot*

*„Nichts tut die Natur zwecklos."*

ARISTOTELES
(384 – 322 v. Chr., GRIECHISCHER PHILOSOPH)

*„Man kommt nicht zur Wahrheit, als bis man seinen
eigenen Ideen ganz abgestorben ist, nichts Eigenes
dabei sucht und alles von vorn gelernt hat."*

FRIEDRICH CHRISTOPH OETINGER
(1702 – 1782, SCHWÄBISCHER THEOLOGE)

Die vorliegende Dissertation wurde im Zeitraum von Dezember 2010 bis Oktober 2015 unter Anleitung von Herrn Professor Dr. Heinrich Lang am Lehrstuhl für Anorganische Chemie der Technischen Universität Chemnitz angefertigt.

*Meinen Eltern und Geschwistern*

# TABLE OF CONTENTS

## LIST OF FIGURES

## LIST OF SCHEMES AND TABLES

## LIST OF ABBREVIATIONS

| | |
|---|---|
| Ac | Acetyl |
| AN | Acetonitrile |
| ArF | 3,5-Bis(trifluoromethyl)phenyl |
| a. u. | Arbitrary unit |
| BArF$_{24}$ | Tetrakis(3,5-bis(trifluoromethyl)phenyl)borate |
| Bfc | 1,1''-Biferrocenyl |
| bfc | 1,1''-Biferrocene-1,1'''-diyl |
| BFD | Bisfulvalenediiron |
| $^{n}$Bu | $n$-Butyl |
| $^{t}$Bu | $tert$-Butyl |
| CCDC | Cambridge Crystallographic Data Centre |
| CERN | Conseil Européen pour la Recherche Nucléaire |
| COSMO | Conductor-like screening model |
| Cp | Cyclopentadienyl |
| Cp* | 1,2,3,4,5-Pentamethylcyclopentadienyl |
| CR | Charge resonance |
| Ct | Centroid |
| CT | Charge transfer |
| CV | Cyclic voltammetry |
| DCC | $N,N'$-Dicyclohexylcarbodiimide |
| DCM | Dichloromethane |
| DEC | Deconvolution |
| DFT | Density functional theory |
| DMSO | Dimethyl sulfoxide |
| dppf | 1,1'-Bis(diphenylphosphino)ferrocene |
| DPV | Differential pulse voltammetry |
| EDOT | 3,4-ethylenedioxy thiophene |
| ESI | Electrospray ionization |
| ET | Electron transfer |
| Fc | Ferrocenyl |
| fc | Ferrocene-1,1'-diyl |
| FES | Free energy surface |
| FT | Fourier transform |

| | |
|---|---|
| HMBC | Heteronuclear Multiple Bond Correlation |
| HR | High resolution |
| HSQC | Heteronuclear Single Quantum Coherence |
| HTL | Hole transport layer |
| IBT | Intrabiferrocenyl charge transfer |
| IC | Interconfigurational transition |
| ICP | Intrinsic conducting polymer |
| IR | Infrared |
| IUPAC | International Union of Pure and Applied Chemistry |
| IVCR | Inter valence charge resonance |
| IVCT | Inter valence charge transfer |
| LF | Ligand field |
| LMCT | Ligand to metal charge transfer |
| Me | Methyl |
| MLCT | Metal to ligand charge transfer |
| MMCT | Metal metal charge transfer |
| Mp | Melting point |
| MS | Mass spectrometry |
| MV | Mixed valence |
| NIR | Near infrared |
| NLO | Nonlinear optics |
| NMR | Nuclear magnetic resonance |
| NPV | Normal pulse voltammetry |
| OLED | Organic light emitting diode |
| OSWV | Osteryoung square wave voltammetry |
| OTf | Trifluoromethanesulfonate (triflate) |
| OTTLE | Optically Transparent Thin Layer Electrochemistry |
| PC | Propylene carbonate |
| PEDOT | Poly(3,4-ethylenedioxy thiophene) |
| Ph | Phenyl |
| ppm | Parts per million |
| Pr | 1-Propyl |
| SCE | Saturated calomel electrode |
| SEC | Spectroelectrochemistry |

| | |
|---|---|
| SWV | <u>S</u>quare <u>w</u>ave <u>v</u>oltammetry |
| TBA | Tetra-*n*-butylammonium |
| TFAB | Tetrakis(pentafluorophenyl)borate |
| Th | 2-Thienyl |
| th | Thiophene-2,5-diyl |
| thf | Tetrahydrofuran |
| TMEDA | *N,N,N',N'*-Tetramethylethylenediamine |
| TOF | <u>T</u>ime <u>o</u>f <u>f</u>light |
| UV | <u>U</u>ltra<u>vi</u>olet |
| VE | <u>V</u>alence <u>e</u>lectron |
| Vis | <u>Vis</u>ible |
| WCA | <u>W</u>eakly <u>c</u>oordinating <u>a</u>nion |
| XPS | <u>X</u>-ray <u>p</u>hotoelectron <u>s</u>pectroscopy |
| | |
| bzw. | beziehungsweise |
| d. h. | das heißt |
| u. a. | unter anderem |
| z. B. | zum Beispiel |

| | |
|---|---|
| $\alpha$ | Hydrogen bond donor strength (Kamlet-Taft) |
| $A$ | Electrode surface [cm$^2$] |
| $\alpha, \beta$ | Charge transfer coefficients (Butler-Volmer, $\alpha + \beta = 1$) |
| $\beta$ | Hydrogen bond acceptor strength (Kamlet-Taft) |
| $c$ | Concentration [molL$^{-1}$] |
| $D$ | Diffusion coefficient [cm$^2$s$^{-1}$] |
| $e$ | Elementary charge ($\approx 1.6022 \cdot 10^{-19}$ C) |
| $E$ | Electrochemical potential [mV] |
| $E^{0'}$ | Formal potential (redox potential) [mV] |
| $\Delta E^{0'}$ | Potential separation between two redox processes [mV] |
| $E_{1/2}$ | Half wave potential [mV] |
| $\varepsilon$ | Extinction coefficient [Lmol$^{-1}$cm$^{-1}$] |
| $E_{a,c\text{-}onset}$ | Onset-potential during an anodic (*a*) or cathodic (*c*) electrode reaction [mV] |
| $\varepsilon_{max}$ | Extinction coefficient at $\lambda_{max}$ [Lmol$^{-1}$cm$^{-1}$] |
| $\Delta E_p$ | Potential separation between $E_{pa}$ and its related $E_{pc}$ [mV] |
| $E_{pa,c}$ | Potential at $i_p$ for anodic (*a*) or cathodic (*c*) electrode reactions [mV] |

| | |
|---|---|
| $E_{th}$ ($\Delta G^*$) | Thermal activation energy [cm$^{-1}$] |
| $E_{turn}$ | Reversal potential (Change of potential direction) |
| $F$ | Faraday constant ($\approx$ 96485 Cmol$^{-1}$) |
| $f$ | Oscillator strength |
| $\Delta G$ | Gibbs energy [cm$^{-1}$] |
| $\Delta G_C$ | Gibbs energy of comproportionation [cm$^{-1}$] |
| $\Delta G^{00}$ ($\Delta G^0$) | Ground state separation between educt and product state [cm$^{-1}$] |
| $\vartheta$ | Celsius temperature [°C] |
| $h$ | Planck constant ($\approx$ 6.6261·10$^{-34}$ Js) |
| $\Delta H^{\ddagger}$ | Enthalpy of activation [kJmol$^{-1}$] |
| $H_{ab}$ | Electronic coupling matrix element (electronic coupling) [cm$^{-1}$] |
| $\eta$ | Activation overpotential (Butler-Volmer) [mV] |
| $i$ | Current [µA] |
| $i_p$ | Peak current [µA] |
| $i_{pa,c}$ | Oxidation (anodic, $a$) or reduction (cathodic, $c$) peak current [µA] |
| $k_B$ | Boltzmann constant ($\approx$ 1.3807·10$^{-23}$ JK$^{-1}$) |
| $K_C$ | Comproportionation constant |
| $k_s$ | Heterogeneous electron transfer rate constant [cms$^{-1}$] |
| $\lambda$ | Marcus reorganization energy [cm$^{-1}$] |
| $\lambda_{max}$ | Wavelength of the most probable excitation of a transition [nm] |
| $\lambda_o$ | Environmental term of the Marcus reorganization energy [cm$^{-1}$] |
| $\lambda_v$ | Compound-specific term of the Marcus reorganization energy [cm$^{-1}$] |
| $\mu$ | Dipole moment [D] |
| $\mu_{eg}$ | Transition dipole moment [D] |
| $n$ | Number of charge equivalents |
| $v$ | Scan rate [mVs$^{-1}$] |
| $\Delta\tilde{v}_{1/2}$ | Bandwidth at half height [cm$^{-1}$] |
| $\Delta\tilde{v}_{1/2(theo)}$ | Expected value for $\Delta\tilde{v}_{1/2}$ from the Hush theory [cm$^{-1}$] |
| $\tilde{v}_{max}$ | Wavenumber of the most probable excitation of a transition [cm$^{-1}$] |
| $\Delta\tilde{v}_{max\text{-}IVCT}$ | Solvatochromic shift of IVCT absorption band [cm$^{-1}$] |
| $\pi^*$ | Dipolarity/polarizability (Kamlet-Taft) |
| $Q$ | Charge [C] |
| $R$ | Gas constant ($\approx$ 8.3145 JK$^{-1}$mol$^{-1}$) |

| | |
|---|---|
| $r_{ab}$ | Effective charge transfer distance (separation between the donor and acceptor charge centroids) [Å] |
| $\Delta S^{\ddagger}$ | Entropy of activation [$JK^{-1}mol^{-1}$] |
| SA | <u>S</u>olvent <u>a</u>cidity (Catalán) |
| SB | <u>S</u>olvent <u>b</u>asicity (Catalán) |
| SdP | <u>S</u>olvent <u>d</u>i<u>p</u>olarity (Catalán) |
| SP | <u>S</u>olvent <u>p</u>olarizability (Catalán) |
| $\sigma_p$ | Hammett substituent constant (*para*-effect) |
| $T$ | Temperature [K] |
| $t$ | Time [s] |

## PRÄAMBEL

Der wissenschaftliche Teil der vorliegenden Dissertation ist in englischer Sprache verfasst. Im Rahmen dieser Promotionsarbeit am Lehrstuhl für Anorganische Chemie der Technischen Universität Chemnitz wurden sechs, das Thema der Dissertation betreffende, Publikationen erstellt.

Diese Artikel sind inhaltlich unverändert und mit Genehmigung der Copyright-Inhaber als jeweils eigenständige Kapitel bzw. Unterkapitel abgebildet. Weitere noch unveröffentlichte Arbeiten sind in Manuskriptform an entsprechender Stelle eingebettet. Alle wissenschaftlichen Arbeiten und Publikationen wurden selbstständig unter Anleitung von Herrn Prof. Dr. Heinrich Lang angefertigt.

Der jeweilige individuell geleistete wissenschaftliche Beitrag, zum Beispiel im Rahmen von arbeitsgruppenübergreifenden Kooperationen, ist in den nachfolgenden Kapiteln gesondert ausgewiesen.

Die für den kausalen Zusammenhang der einzelnen Arbeiten (Kapitel) wichtigen Zusatzinformationen (Supporting Information) sind in der Appendix-Sektion entsprechend angeführt. Weiterhin ist die Bezeichnung der aufgeführten chemischen Verbindungen an die Nummerierung der entsprechenden Publikation angelehnt, in welcher die wissenschaftlichen Ergebnisse veröffentlicht wurden.

Im Anhang „Publications" wird auf alle Vorträge, Posterbeiträge und Veröffentlichungen des Promovenden verwiesen.

# A INTRODUCTION

Our daily life is fulfilled with a diversity of charge transfer phenomena, *e.g.* from electron transfer reactions in biological cells to running spark-ignition internal combustion engines in anybody's car.

Since the discovery of the electricity and its extensive introduction, *i.e.* the electric light with all the required power plants and power lines, the development of potentially conductive materials gained more and more importance. Thus, consecutive investigations on metallic materials regarding their temperature-dependent electric conductivity were carried out. Within this context the phenomenon of superconductivity was discovered by Kamerlingh Onnes in 1911 during low temperature experiments on mercury.[1] Later, the superconductivity of ceramics as high temperature superconductive materials was found – a breakthrough for the use of superconducting devices into areas such as high-field magnetic engineering or high current technologies (Figure A1).[2,3]
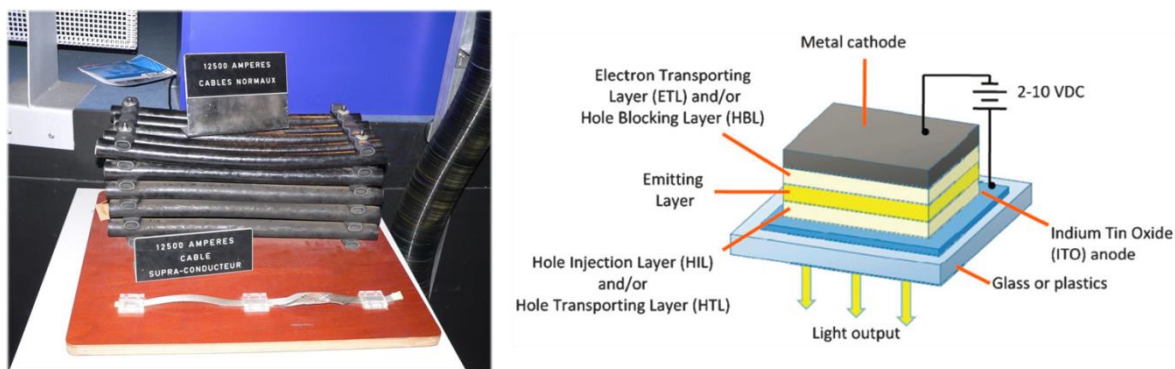


**Figure A1**. Left: Electric cables (12,500 Amperes) for accelerators at CERN. Conventional cables used for the Large Electron–Positron Collider (top) and superconductor-based cables applied for the Large Hadron Collider (bottom) (*reproduced from reference* 4). Right: Schematic construction of an organic light-emitting diode (OLED) (*reproduced from reference* 5 *with permission of the Royal Society of Chemistry*).

Looking for organic materials with metallic properties, origins could be found in the 1950s where the preparation of polyacetylene as a black powder was reported by Giulio Natta *et al.*[6,7] and the first polyacetylene films made by Shirakawa *et al.* 20 years later.[8] However, only a behavior typical for an electrical semiconductor could be observed. By the way of doping of the latter intrinsically conducting polymer (ICP), the conductivity could be increased by fourteen orders of magnitude – a milestone in the field of organic electronics.[9–11] In the following decades a widely diversified portfolio of ICPs was developed, *e.g.* poly-*para*-phenylenes, polyphenylene vinylenes, polyanilines, polyfurans, polypyrroles and polythiophenes.[12–14] Potential applications reach *inter alia* from flexible electrode materials, anticorrosive applications, the usage as antistatic coatings or their application in organic light-emitting diodes (OLEDs, Figure A1).[15–24] Especially

polythiophenes have received much attention due to their remarkable stability against aerobic conditions in the neutral and in the doped states.[13,25,26] For instance, poly(3,4-ethylenedioxythiophene) (PEDOT) became a standard material for the construction of transparent and pliable electrodes or in application as hole-transport layer (HTL) in OLEDs (Figure A1).[15,18,21,27,28] Regarding this, the application depends strongly on the ICP's electronic properties/electronic structure and the interaction between the repeating units as well as on selectively made functionalizations.[21,25,29]

Therefore, it is important to get a profound insight into charge transfer processes in that kind of macromolecular systems. Thus, a decrease of the systems to a small number of repeating units and their functionalization with well-known redox-active probes (the design of model systems) should provide to a better understanding of charge transfer phenomena in these systems.[29–37] Moreover, the permanent miniaturization process of electronic devices requires well-designed innovative materials (molecular wires), too.[38–42] Thus aromatics, modified with organometallic redox-active transition metal fragments, should be interesting molecules regarding their use in molecular electronics.[38,43–48] Due to their reversible redox behavior, ferrocene derivatives are often applied as versatile building blocks for the investigation of electronic properties and electron excitation phenomena.[37,46–51]

Within this thesis, the electronic interactions of ferrocenyl moieties over the thiophene aromatic system are investigated. Initially, an overview regarding $\pi$-conjugated systems/aromatics with redox active entities is given in the corresponding theoretical background. Afterward, the discussion devotes to the influence on electronic properties of ferrocenyl thiophenes during a numeric variation of metallocenyl increments in dependency of the substitution pattern. The following part deals with the consequences of well-directed functionalizations. A final study on thiophene-$\pi$-complexes of transition complex fragments on ferrocenyl thiophenes completes the thesis.

# B STATE OF KNOWLEDGE

## B1 BACKGROUND THEORY

In the field of transition metal chemistry, electron excitation phenomena are often related to optical *d-d* transitions (ligand field, LF) as one origin of color in transition metal compounds.[52,53] However, "pure" *d-d* absorptions usually have a low intensity as a consequence of formal transitional forbids (spin multiplicity and parity), due to a high symmetry of the transition metal's coordination environment. These forbids could be circumvented *inter alia* by symmetry distortion, vibronic and spin-orbit coupling.[37,49] Nevertheless, the strong color of transition metal complexes comes mostly from several charge transfer excitations.

Prime examples display dimanganese heptoxide ($Mn_2O_7$) and chromium trioxide ($CrO_3$), wherein optically-introduced ligand to metal charge transfer (LMCT, oxygen-to-metal) interactions are the origin of color.[53] In general an electron is formally transferred from an electron-donor to an -acceptor when a charge transfer takes place. This kind of redox processes can appear as inter- or intramolecular reactions. One special type of donor-acceptor complexes embody mixed-valence (MV) complexes (*vide infra*, Chapter B3). A first approach of a qualitative description of electron transfer (ET) reactions in solution was given by R. A. Marcus.[54,55] The reaction can occur as either a thermally or an optically induced process (Figure B1).
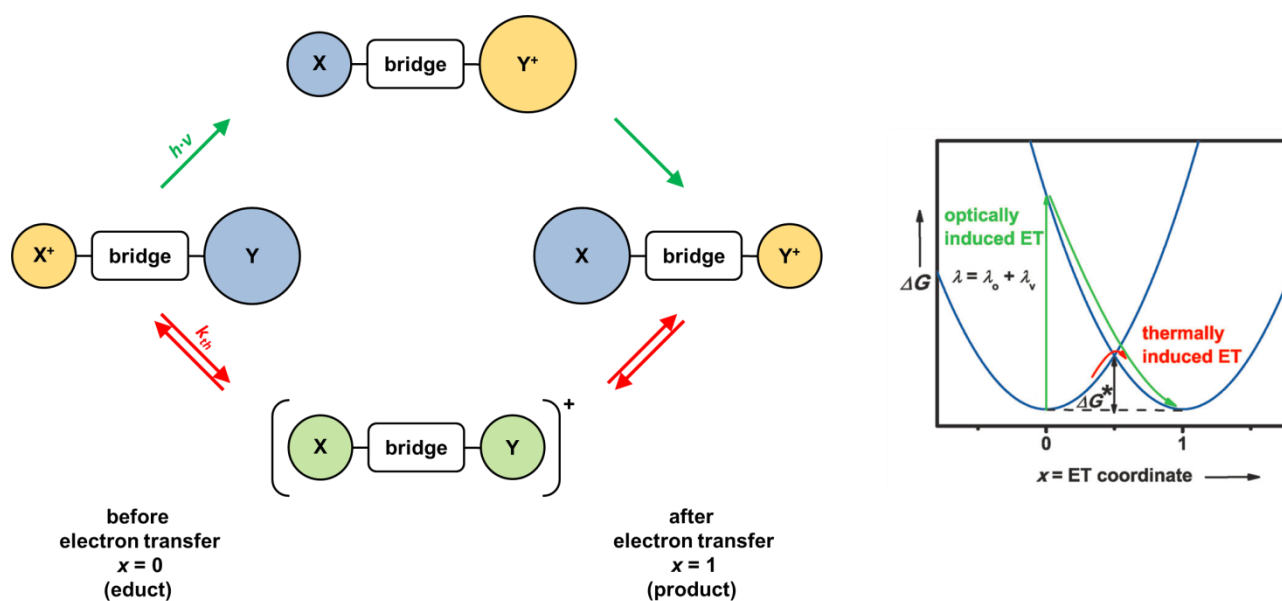


**Figure B1**. Left: Comparison of thermally (red) and optically (green) induced electron transfer reaction pathways in mixed-valence complexes. The size of redox centers **X** and **Y** denotes schematically the change of geometry between different redox states. Right: Non-coupled (diabatic) free energy surfaces of a MV with degenerate educt and product states (*adapted from reference 37 with permission of John Wiley and Sons*).

On the thermal pathway, the electron transfer from donor Y to the acceptor $X^+$ (educt state) happens by expending of an activation energy ($\Delta G^*$). Thus, a simultaneous adjustment of changing the solvation shell, the reorganization of geometries and electron transfer lead to the final MV-species at $x = 1$ (Figure B1). In contrast, during an optically induced process, the electron transfer step itself occurs before inner and outer relaxation events take place (Figure B1).[37,56] Therefore, a vertical excitation from the ground state (according to the Franck-Condon principle), at $x = 0$ along the ET coordinate through absorption of a photon leads directly to the electron transfer. The required energy $\lambda$ for this process, which consists of an environmental ($\lambda_o$) and a compound-specific ($\lambda_v$) term, is called Marcus reorganization energy (Figure B1).[54,55]

However, the Marcus (diabatic) theory is limited to systems with small electronic interactions, in relationship to the thermal energy. An adiabatic extension of the latter approach is given by the assumption of an electronic coupling larger than $k_B T$ (Marcus-Hush/Mulliken-Hush theory).[37,49,56] The corresponding electronic communication between the educt and the product states is expressed by the electronic coupling $H_{ab}$ (Figure B2, *vide infra*).[37,49,56]
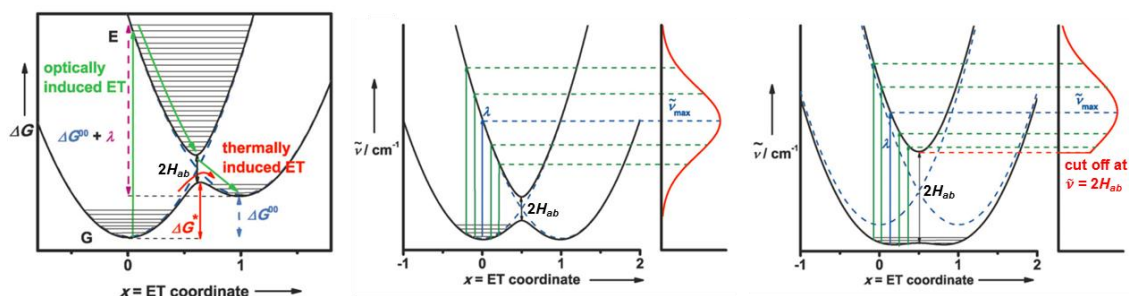


**Figure B2**. (*adapted from reference 37 with permission of John Wiley and Sons*). Left: adiabatic free energy surfaces (black lines) of a MV complex with non-degenerate MV states (degenerate states if $\Delta G^{00} = 0$, $\Delta G^*(E_{th}) = \lambda/4 - H_{ab} + H_{ab}^2/\lambda$).[37,49,57] Middle and Right: visualization of the relationship between electronic coupling $H_{ab}$ and shape of the appropriate charge transfer band (probability of individual excitations from different vibronic levels in the electronic ground state).[37] Abscissa (x) represents the electron transfer (ET) coordinate along an asymmetric stretching mode.

This parameter can be extracted from the absorption spectra of MV complexes using relationships developed by N. S. Hush.[58–60] The observation of these charge transfer absorption bands is often located in the visible and/or NIR range. Thus, for a significant electronic interaction ($0 < H_{ab} < \lambda/2$), the diabatic states (Figure B2, blue dashed lines) couple to two adiabatic free energy surfaces (FES) with two minima in the ground state. The corresponding excitation energy (most probable transition at $\tilde{\nu}_{max}$, Figure B2) is enlarged by the ground state separation $\Delta G^{00}$, if the ground state minima are thermodynamically different from each other ($\Delta G^{00} > 0$, electronically asymmetric MV

compounds).[37,49,56] An estimation of $\Delta G^{00}$ can be made by determining the redox potential difference between both individual redox sites (increments, *vide infra* Chapter F).[61] In Figure B2 the fine horizontal solid lines represent different vibronic levels in the corresponding electronic states. During an optically induced charge transfer a vertical (*vide supra*) excitation from one ground state minimum, with an Boltzmann-weighted occupation of the appropriate vibronic levels in the context of the high temperature limit (HTL)[A], takes place to vibronic levels of the excited state. A following relaxation leads to the product state (Figure B2). In the case of weakly-coupled MV systems, Gaussian-shaped charge transfer absorption bands (HTL) with its maximum at $\tilde{\nu}_{max} = \lambda + \Delta G^{00}$ are obtained (Figure B2 middle). The corresponding width at half height ($\Delta \tilde{\nu}_{1/2}$) can be estimated by using equation B1.[37,50,56,57]

$$\Delta \tilde{\nu}_{1/2}(HTL) = \sqrt{16 \ln(2)\, k_B T \tilde{\nu}_{max}} \tag{B1}$$

Moreover, by a further increasing of $H_{ab}$ the probability of transitions at $\tilde{\nu} < \tilde{\nu}_{max}$ decreases. Thus, with an increasing electronic interaction a cuff-off takes place on the low-energy side of the IVCT absorption by a continuously strong loss of intensity, until $2H_{ab} = h\tilde{\nu}_{max}$ (Figure B2 right, *vide infra*).[62,63]

Main advantages of this adiabatic theory against Marcus' diabatic approach display *inter alia* a better description of the absorption band shape as well as the possibility to determine the electronic coupling $H_{ab}$ from the experimental spectra. Thus, $H_{ab}$ can be calculated by using equation B2. The transition dipole moment ($\mu_{eg}$) can be determined by integration of the corresponding absorption band.[49,50,63,64]

$$H_{ab} = \frac{\mu_{eg}}{e r_{ab}} \tilde{\nu}_{max} \quad \text{with} \quad \mu_{eg} = 0.09584 \sqrt{\frac{\int e(\tilde{\nu})d\tilde{\nu}}{\tilde{\nu}_{max}}} \tag{B2}$$

$$H_{ab} = \frac{0.0206}{r_{ab}} \sqrt{\tilde{\nu}_{max} \varepsilon_{max} \Delta \tilde{\nu}_{1/2}} \tag{B3}$$

For true or nearly Gaussian-shaped absorption bands, *i.e.* relatively weak interacting redox centers, equation B2 can be simplified to equation B3.[49,50,63,64] However, for a consideration of further charge transfer interactions, *e.g.* between metal and bridge/ligand together with the metal-metal electronic coupling or a more straightforward access to variables like the dipole moment difference of the diabatic states it is useful to extend the model by a further symmetric stretching mode and up to three or four coupled electronic

---

[A] The required energy for population the vibronic levels is small in comparison with the thermal energy ($h\tilde{\nu} \ll k_B T$), ensuring a Boltzmann distribution of occupation.

states.[37,49,50] Furthermore, the Franck-Condon principle (Born-Oppenheimer approximation analogue) is assumed to be valid for the description of moderate and strongly-coupled MV systems, even though the investigation of electronic coupling by optical transitions potentially resonant with molecular vibration modes.[49,50,56,65–67,B]

The shape of the adiabatic FES depends on the electronic coupling of the corresponding diabatic potentials (Figure B3).
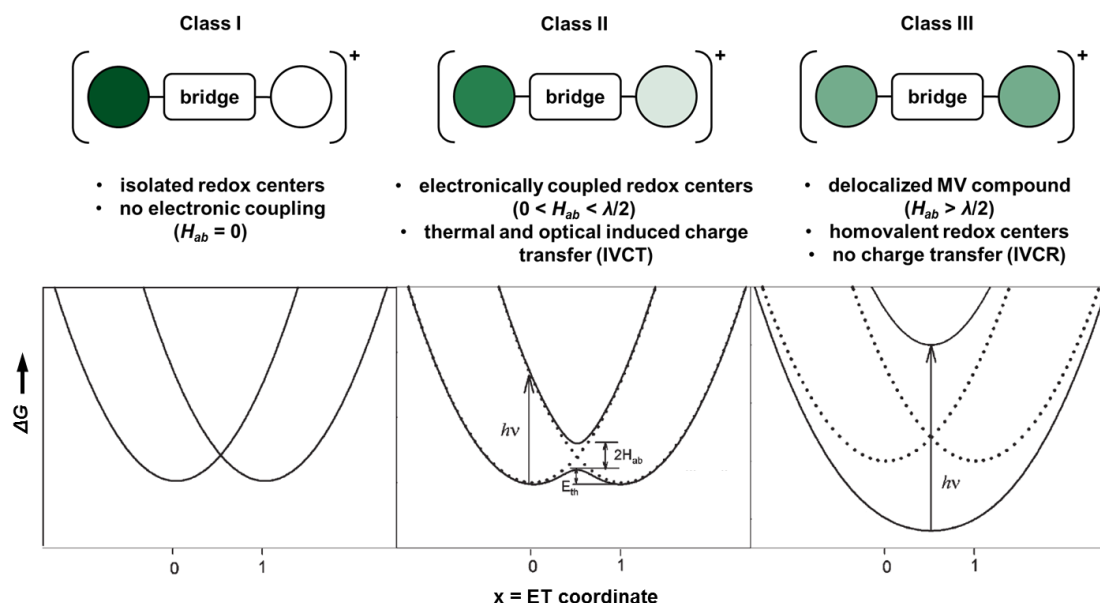


**Figure B3**. Top: schematic comparison of symmetrical mono-cationic class I to III MV complexes. Bottom: two-state model FES with different electronic couplings ($H_{ab}$). Left: $H_{ab} = 0$. Middle: $0 < H_{ab} < \lambda/2$. Right: $H_{ab} > \lambda/2$. Dotted lines represent diabatic potentials, abscissa (x) represents the electron transfer (ET) coordinate along an asymmetric stretching mode (*adapted from reference 57 with permission of the Royal Society of Chemistry*).

Hence for $0 < H_{ab} < \lambda/2$ the ground state free energy surface consists of two separated minima, while for $2H_{ab}$ larger than the Marcus reorganization energy only one minimum remains (Figure B3 right). Regarding a varying electronic interaction in donor-acceptor systems (mixed-valent species), Robin and Day have recommended a classification into three classes (Figure B3).[68] Class I systems portray mixed-valent species with no resonance interaction (charge transfer) between the donor and the acceptor moiety (no coupling between the diabatic states), theoretically $H_{ab} = 0$ (Figure B3).[37,49,68,69] Thus, the separation of the donor and acceptor charge centroids ($r_{ab}$) is equal with the geometrical distance between the redox centers. However, this assumption was often taken for weak-coupled MV compounds, due to a challenging access to $r_{ab}$.[37,49,57,63]

In the context of an experimental investigation of MV compounds, a class I classification was usually made for potentially coupled systems if the extend of electronic coupling is

---

[B] Regarding this, see also the vibronic coupling model (PKS).

beyond the limits of detection.[37] The opposite case is represented by class III mixed-valence complexes[C] in which the charge is completely delocalized ($H_{ab} > \lambda/2$, Figure B3). No charge transfer takes place in these species, the intense, non-solvatochromic[D] and asymmetric (*vide supra*) absorption bands, which can be detected in the Vis-NIR range, have their origins in *(d)π-(d)π\** transitions.[37,49] Furthermore, a designation of that kind of absorptions as inter valence charge resonances (IVCR) should be also very deftly (Figure B3).[70,71] In practice, a mixed-valent system is classified as delocalized (class III), when the corresponding species exhibit an almost homogenous ($r_{ab} \approx 0$) and less temperature-dependent charge distribution on a fast experimental time scale.[49,50,56,57,72] The majority of MV compounds offer a weak or moderate electronic interaction (class II), typical with roughly to almost Gaussian-shaped and solvatochromic inter valence charge transfer (IVCT) bands, $0 < H_{ab} < \lambda/2$ (Figure B3, middle).[37,49,50] Their valence-trapped behavior can be monitored by different spectroscopical and spectroelectrochemical techniques in dependence of the degree[E] of electronic coupling (*vide infra*).[37,47,49,72]

Moreover, the observed IVCT absorptions of the latter species show bandwidths at half height similar or larger than the Hush-prediction (*vide supra*), while a value of $\Delta\tilde{v}_{1/2}$ noticeably smaller as the theoretical expectation indicates the presence of a stronger-coupled (class II-to-III limit or class III) mixed-valent compound.[50] A further indication for a distinct electronic interaction is represented by a detectable redox splitting, *i.e.* in a symmetric homo-bimetallic species a given redox separation ($\Delta E^{0'}$) is related with $H_{ab}$.[37,47,49,51,56,57,73]



$$K_C = e^{\left(\frac{\Delta E^{0'} F}{RT}\right)} \quad \text{(B4)}$$

$$\Delta G_C = -\Delta E^{0'} F = \frac{1}{2} RT ln\left(\frac{1}{4}\right) + \underbrace{\Delta G_{estat} + \Delta G_{syn}}_{\Delta G_{nonres}} + \Delta G_{res} \quad \text{(B5)}$$
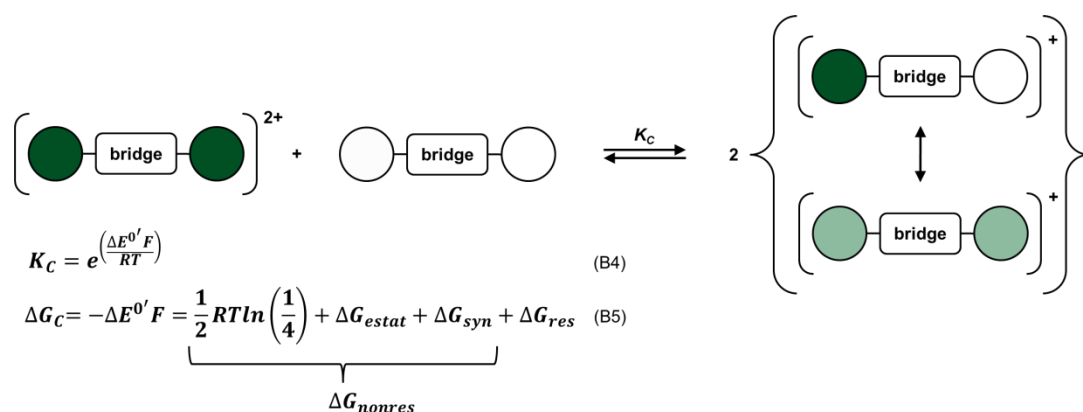
**Figure B4**. The comproportionation equilibrium and the relationship between redox separation ($\Delta E^{0'}$) and thermodynamic stability of the cationic mixed-valent complex towards neutral and doubly oxidized (dicationic) species.

---

[C] In truth, these complexes are homovalent.
[D] The dipole moment difference between the ground and excited state goes against zero.
[E] The passage from valence-trapped to delocalized goes on in a continuous "process".

The thermodynamic stability ($K_C$) of a mixed-valent species can be directly determined from the value of $\Delta E^{0'}$; it increases as the redox separation increases (Figure B4).[56,73,74] However, the Gibbs energy of comproportionation ($\Delta G_C$) consists also of terms caused by so called non-resonance interactions ($\Delta G_{nonres}$), *i.e.* an entropic stabilization, an electrostatic term $\Delta G_{estat}$ (stabilization due to charge repulsion in higher oxidized species, etc.) and a synergistic contribution ($\Delta G_{syn}$) resulting from resonance interactions between redox center and ligands (Figure B4).[56,72–74] Only from $\Delta G_{res}$ (stabilization due to resonance between the redox centers) the thermal activation barrier $E_{th}$ ($\Delta G^*$) as well as the electronic coupling $H_{ab}$ can be obtained.[56,73,74] For stronger coupled systems with a dominating resonance stabilization, the Gibbs energy of resonance can be estimated to $\Delta G_{res} \approx \Delta G_C$.[57,73]

Generally two different charge transfer mechanisms are distinguishable: A charge hopping reaction pathway in which the charge is transferred successively from one increment to another (with a temporary charged bridge), and a superexchange mechanism (tunneling process) wherein the charge transfer is only mediated by the bridge (virtual sharing of electronic bridge states).[37,49,57,75,76] In the field of organic/organometallic mixed-valence complexes the superexchange process dominates mostly during the charge transfer. Depending on the charge of the appropriate MV species as well as the involved (real/virtual) electronic states of the bridge, an electron or a hole is formally transferred.[37,63]

## B2 ELECTROCHEMICAL ASPECTS

The analysis of possible/existing Faradaic processes is very important for the investigation of charge transfer and the characterization of mixed-valence complexes. In this regard, the performing of electrochemical analyses, *e.g.* voltammetric and amperometric/coulometric experiments, should be very useful. One necessary precondition for the generation of charged mixed-valent species embody reversible redox processes, *inter alia* (thermodynamically) stable cations/anions.[56,73,74,77,78] Regarding an electrochemical reversibility, several requirements should be mentioned: A chemical (thermodynamic) reversibility must be given, *e.g.* it is not possible to regenerate the carboxylate (Figure B5, *vide infra*) from the hydrocarbon ($RCH_2CH_2R$) by applying an opposite over potential and a reverse current flow (retro-Kolbe electrolysis).[79,80]

**Kolbe electrolysis**
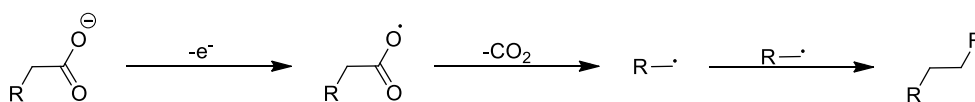


H. Kolbe
**1848**

**Figure B5**. Reaction scheme for the Kolbe electrolysis (dimerization) of alkanoic acids.[79]

Electrochemically reversible redox processes in solution include further a mass transport which is only controlled by diffusion (Nernstian behavior) as well as fast heterogenic electron transfer processes with equal rate constants (unrestrained) of the oxidation and its associated reduction electrode reaction. The influence of diffusion on the conversion of an electro-active species at a potential-controlled electrode is described by the Cottrell relationship (equation B6).[80–82]

$$i = \frac{nFAc_0\sqrt{D}}{\sqrt{\pi t}} \qquad \text{for a planar electrode} \tag{B6}$$

$$i = i_0\left\{e^{\left[\frac{\alpha nF\eta}{RT}\right]} - e^{\left[-\frac{\beta nF\eta}{RT}\right]}\right\} \quad \text{with } \beta = 1 - \alpha \text{ and } \eta = E - E^{0'} \tag{B7}$$
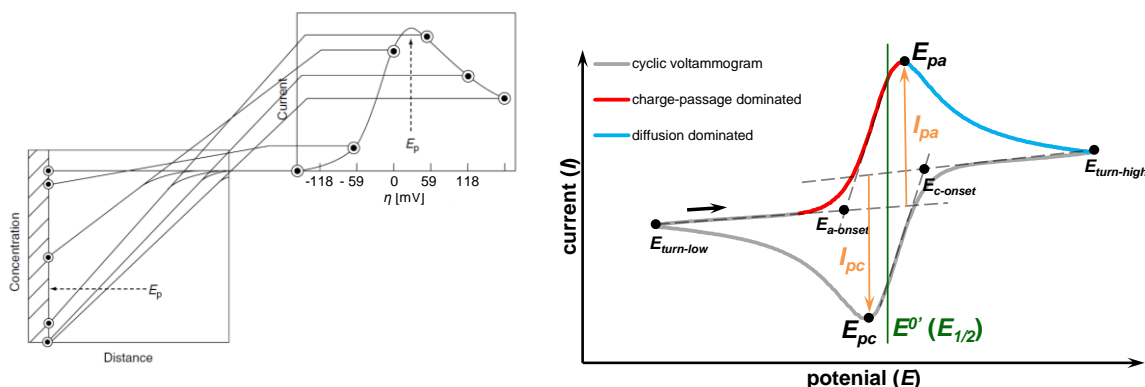


**Figure B6**. Left: Visualization of the relationship between analyte concentration at the electrode and current response (*adapted with permission from reference 83. Copyright 1983 American Chemical Society*). Right: Characteristic parameter of a cyclic voltammogram (potential sweep).

The charge passage potential dependence is expressed by the Butler-Volmer equation, in which $\eta$ denotes the activation overpotential (equation B7).[F] For an electrochemically reversible redox event the charge transfer coefficients of both electrode reactions are equal, $\alpha = \beta = 0.5$. During an anodic potential sweep and a successive increasing activation overpotential ($\eta$) the current rises due to a higher conversion of the redox-active species. By the time, the concentration of the analyte tends to zero and the current deceases (limiting current of diffusion, Figure B6).[81,83]

---

[F] The relationship between bulk-concentration and (equilibrium) electrode potential is given by the Nernst equation.[80]

Thus, throughout recording a cyclic voltammogram[G] (also during a linear sweep) a oxidation current peak ($I_{pa}$) is detected at $E_{pa}$ (analogous for reductions, Figure B6).[84–86] The arithmetic mean of both peak potentials is designated as half-wave potential $E_{1/2}$ (voltammetry with sigmoidal responses – with or without hysteresis) or more generally as formal potential $E^{0'}$ (Figure B6).[84,87,H] Furthermore, the relationship between peak current and scan rate for reversible systems is given by the Randles–Sevcik equation (equation B8).[80,81]

$$i_p = (2.69 \times 10^5)n^{3/2}AcD^{1/2}v^{1/2} \qquad \text{at 298 K} \qquad (B8)$$

The corresponding peak separation amounts $\Delta E_p \approx 57/n$ mV.[80,81] In the field of pulsed voltammetry techniques Osteryoung's square wave voltammetry (OSWV or SWV) represents one of the most applied methods.[88] In difference to differential pulse (DPV) or normal pulse voltammetry (NPV) a forward and a reverse pulse with the same magnitude (square pulse) are modulated on a staircase potential sweep, resulting in a higher sensitivity, an effective background compensation and a formal symmetrical current response.[80,88]

However, available analytical possibilities for an electrochemical investigation of sensitive redox-active materials are often limited *inter alia* due to the thermodynamic stability and dissociation capability of the conducting agent as well as the conductivity of the corresponding electrolyte especially in nonpolar solvents, such as dichloromethane or toluene.[89–91] For instance the easy decomposition of tetrafluoroborate or hexafluorophosphate, *inter alia* by fluoride transfer reactions, is well-known in the literature.[91–95] The "less reactive" and weaker coordinating tetraphenylborate exhibit a remarkable receptivity towards electrophilic $\pi$-attacks.[91,92,96] Furthermore, providing an electrochemical window for anodic electrochemistry, chemically inert conducting agents are required with high oxidation potentials (esp. the anion) *vs.* analyte, *vice versa* for electron affinity in cathodic direction.[I] Thus, the latter tetraphenylborate is not very suitable for anodic electrochemistry, having a redox potential close to the ferrocene window ($E_{1/2}$ = 0.41 V *vs.* FcH/FcH$^+$).[95,97] In fundamental studies Geiger and co-workers reported a strong dependency of the thermodynamic stability of electrochemically generated anions/cations on the chosen electrolyte.[90,98–101] The nucleophilicity of the

---

[G] After an initiation, the potential was varied between two different turning potentials (Figure B6) periodically by time. A cycle is completed if one turning potential is reached for a second time.
[H] For a reversible redox couple.
[I] Analogous for solvents.

counter-anion/electrolyte anion plays a crucial role during the investigation of cationic intermediates under low-polarity conditions (*vide infra*, see also Chapter E1).[95,102–105]

Thus, an application of large, charge-delocalized, weakly coordinating anions (WCAs, Figure B7 bottom) have several advantages in comparison with traditional[J] anions (Figure B7 top): Higher solubilities and dissociation of the electrolyte, *i.e.* a lower solution resistance (about 50 % reduced in dichloromethane).[95,101,105] Furthermore, (highly) positive-charged electrolysis products are obtained as more soluble salts, resulting in noticeably reduced adsorption problems on the electrode and decreased electrode passivation phenomena. The reduced nucleophilicity and ion-pairing (association constants are approx. 2 orders of magnitudes smaller) properties lead further to a lower degree of electronic structure distortion of the cationic species/analyte together with a kinetic stabilization of electrophilic electrode products.

A descriptive rationalization of nucleophilicity/ion-pairing properties on the size/charge distribution of such anions is given in Figure B7 (*vide supra*).[95,106]
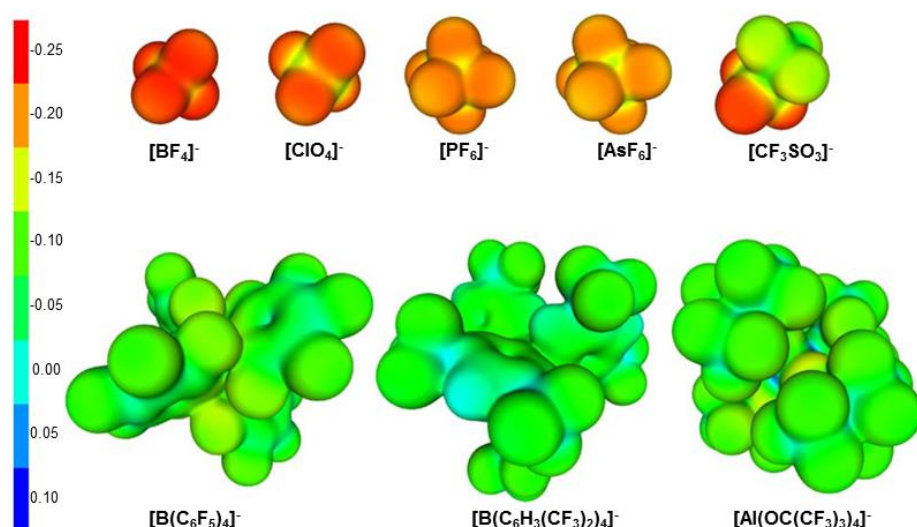


**Figure B7**. Calculated electrostatic potential distributions of representative electrochemically applied anions. Red atoms are most negatively charged, while blue represent most positively charged increments (*adapted from reference* 106 *with permission of Elsevier*).

The most widely used WCAs are represented by the perfluorinated tetraphenylborate-derivatives $[B(C_6F_5)_4]^-$ (TFAB) and $[B(C_6H_3(CF_3)_2)_4]^-$ (BArF$_{24}$), whereby the former borate is chemically more robust and BArF$_{24}$ offers lower ion-pairing and a higher solubility especially in combination with highly charged cations (multi-ferrocenium species).[89,90,95,98,100,101,105,106] Moreover, the preparation/accessibility of the latter borate is more straightforward and effective than for TFAB salts on a laboratory scale.[107]

---

[J] 1$^{st}$ generation of weak coordinating anions.

Furthermore, perfluorinated tetraalkoxyaluminates, like $[Al(OC(CF_3)_3)_4]^-$ (Figure B7), as examined by Krossing and co-workers are suitable for electrochemical investigation under "pseudo gas phase conditions", too.[91,108,109] One benefit of these aluminate-derivatives compared to latter boron-containing anions is a larger thermodynamic stability (oxidation/reduction) and the higher resistance against *inter alia* attacks of transition metal complexes (fragments).[91,95] The nucleophilicity of $[Al(OC(CF_3)_3)_4]^-$ is comparable to those of the former perfluoroborates.[106,109,110]

## B3  MIXED-VALENCE COMPLEXES – SELECTED EXAMPLES

The first use of the term mixed-valence complexes was reported by Klotz *et al.* during their work on thiolate-bridged Cu(I)/Cu(II) complexes.[111] In the context of charge transfer, this term is generally used to describe a special type of donor-acceptor complexes, in which the electronic ground and excited states (of the mixed-valent increments) have formal open-shell electron configurations.[37,49,50,56] Mixed-valence compounds like Prussian blue and Wurster's blue are well-known for centuries.[112,113] Above all, the Creutz-Taube complex (**B1**), the monocationic biferrocene (**B2**) as well as the bisfulvalene diiron (BFD, **B3**) cation represent prime examples of these species (Figure B8).[114–117] These cations, foremost **B1**, can be considered as first model compounds for the investigation of photo-introduced charge transfer between redox-active (metal) centers, as predicted by Hush (*vide supra*).[60]



| | | |
|:-:|:-:|:-:|
| **B1** | **B2** | **B3** |
| Creutz and Taube | Kaufmann and Cowan | Cowan and LeVanda |
| **1969** | **1970** | **1972** |
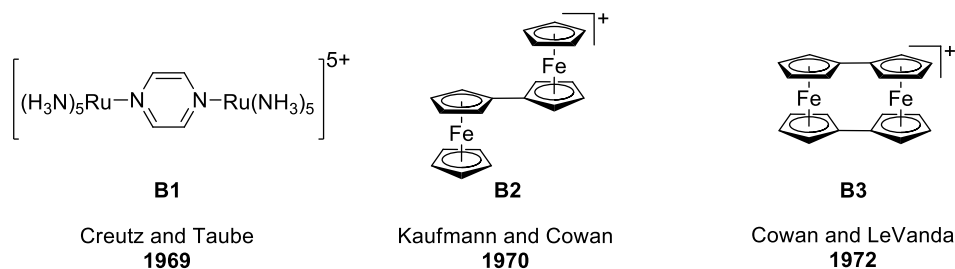
**Figure B8**. Creutz-Taube complex (**B1**), monocationic biferrocene (**B2**) and bisfulvalene diiron cation (**B3**).[114,115,117]

Thus, low-energy NIR absorptions were found regarding a direct metal-metal charge transfer/charge resonance, for **B1** at $\lambda_{max} = 1570$ nm.[114] The latter band was reported as solvent independent (strongly dependent on the bridging ligand), which could be seen as one indication for the almost charge delocalized situation (class III, *vide supra*) in **B1**.[56,59,66,114,118,119]

A similar low solvent dependency was found for the inter valence charge resonance (IVCR) absorption of the strongly-coupled bisfulvalene diiron cation (**B3**); the band could be observed at around 2000 cm$^{-1}$ in the NIR range.[70,120] Within this context, the invariance of the electronic coupling in these BFD-salts against a formal desymmetrization, by introduction of a diversity of functionalities, could be shown recently by Schmittel and co-worker.[70] During solid state investigations (Mössbauer and XPS) of **B3**, the averaged valence behavior could be verified.[116] In contrast, for **B2** only a valence-trapped situation was observed in the solid state, whereby the degree of resonance between the iron centers depends on its environmental conditions, *inter alia* on anion's nature.[121] The corresponding IVCT absorption band shows a significant solvatochromism (please see also Chapter E1, *vide infra*).[58,70,122–125] Regarding this, the biferrocene cation is classified as a strongly-coupled class II or even a borderline class II/III system, according to Robin and Day.[68,70,116,126,127]

However, metal-metal CT/CR absorption bands of transition metal complexes are often accompanied by further low-energy transitions, *e.g.* ligand-field (LF) or interconfigurational (IC) transitions, which makes the band (shape) analysis difficult.[37,47,49,57] Thus "purely" organic mixed valence compounds should be more suitable for a qualitative study of the transformation of IVCT/IVCR absorptions (band shape analysis) during an increasing electronic coupling between the redox centers. Within this context, amines functionalized with charge-stabilizing (aromatic) substituents and protected against oligomerization/polymerization should be suitable redox-active probes. For instance, tris(*para*-bromophenyl)amminium hexachloroantimonate (Magic Blue) is well-known as oxidizing reagent in organometallic electrochemistry.[78,128–130]

Lambert and co-workers have applied *N,N*-dianisylamino groups, linked by organic π-systems of varying lengths, for the investigation of charge transfer interactions (Figure B9).[63,131] For weakly-coupled mixed-valence compounds **B4$^+$** ($\Delta E^{0'}$ = 60 mV) and **B5$^+$** ($\Delta E^{0'}$ = 100 mV), the authors found, as is typical for class II systems, Gaussian-shaped and relatively weak IVCT absorptions (Figure B9).[63,131] During a decreasing of the bridging ligand, until the constitution in 1,4-diamino benzene **B9**, a successive increasing of the redox separation ($\Delta E^{0'}$) was observed together with an ongoing rise of the electronic coupling matrix element $H_{ab}$ (*vide supra* and Figure B9).[63] Moreover, a steady desymmetrization of the IVCT/IVCR absorption, *i.e.* the loss of intensity on the low-energy side of the band (cut-off, *vide supra*), by an increasing electronic coupling between the redox centers in the mixed-valent species could be recorded experimentally for the first

time, in excellent accordance with the theoretical prediction (Figure B9 and Chapter B1).[37,49,50,60,63]
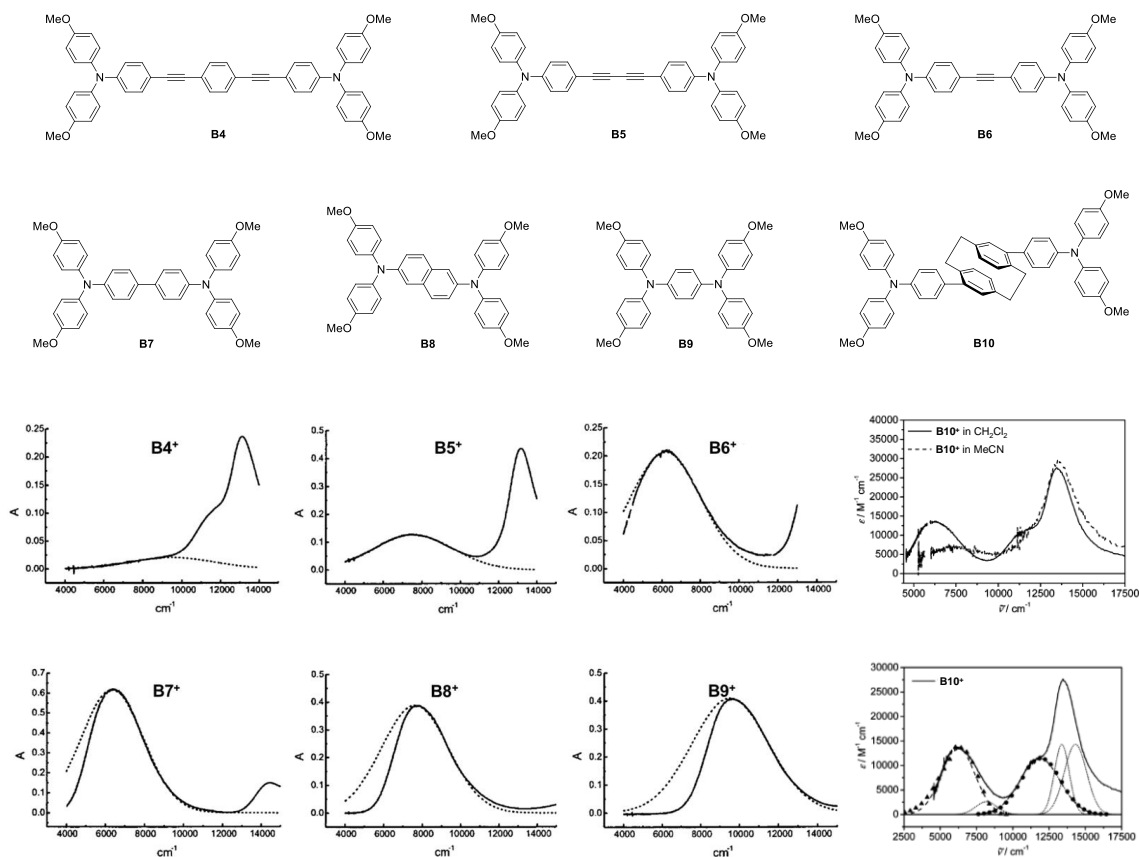


**Figure B9**. Top: triarylamine redox systems **B4** – **B10**.[63,131] Bottom (left): IVCT bands of **B4** – **B9** (solid lines) from spectroelectrochemistry in $CH_2Cl_2$ containing 0.1 M TBAPF$_6$. Dotted lines denote Gaussian band fits (*adapted with permission from reference 63. Copyright 1999 American Chemical Society*). Bottom (right): absorption spectra of **B10**$^+$ in different solvents and deconvolution of the absorption spectrum of **B10**$^+$ in $CH_2Cl_2$ by Gaussian functions (IVCT, dashed; bridge, dash-dotted; $\pi$-$\pi^*$, dotted), PES spectra simulation (IVCT, ▲; bridge, ●) (*adapted with permission from reference 132. Copyright 2006 American Chemical Society*).

The possibility of a (partial) through-space electronic interaction, *i.e.* without any direct $\pi$-conjugation, could be shown by connecting two triaryl amine increments via a [2.2]paracyclophane linker in **B10**$^+$ (Figure B9).[132] Looking for cyclophane derivatives with redox-active transition metal fragments, Stoll *et al.* reported substantial metal-metal electronic coupling in mixed-valent organocobalt superphanes (alkanediyl-bridged cyclopentadienylcobalt cyclobutadiene moieties), in strong dependence on the formal $\pi$-$\pi$ through space gap.[133] In the field of face-to-face metallocenes, for instance studies on [3.3](1,3)ferrocenophane are known.[47,134]

In electrochemical investigations on naphthalene-bridged metallocenes, Lee *et al.* reported two well-separated Fc/Fc$^+$ redox processes ($\Delta E^{0'}$ = 195 mV) for **B11** (Figure B10).[47,135] The valence-trapped situation in **B11**$^+$, in which a direct, cofacial interaction between the ferrocenyls is formally possible, was determined by UV-Vis-NIR and infrared

spectroscopy of the corresponding tetrafluoroborate.[47,135] During investigations on ferrocenylvinyl-substituted [2.2]paracyclophanes no IVCT absorptions were detected for the corresponding MV species (**B12**$^+$, Figure B10), despite significant observed redox separations.[136,137] It was reported that the electronic coupling in these species is not only affected by the $\pi$-$\pi$ interaction (through space) in the cyclophane, also a $\sigma$-bond electron density-mediated coupling (through bond) could provide a contribution.[136,138–142]



**B11**
Lee *et al.*
**1985**

**B12**
Mücke *et al.*
**2013**

**B13**

**B14**
Atzkern *et al.*
**1991**
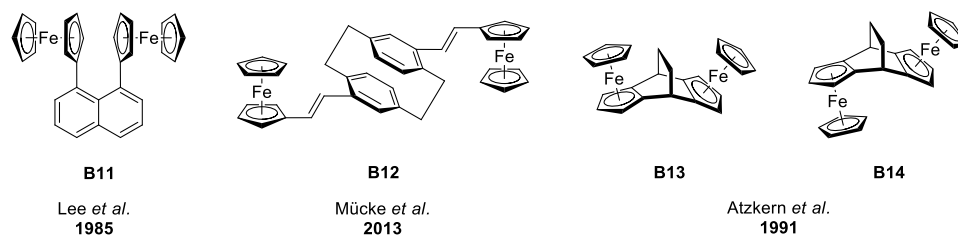
**Figure B10**. 1,8-Diferrocenyl naphthalene (**B11**), [2.2]paracyclophane **B12** and the 4,8-ethano-2,4,6,8-tetrahydro-*s*-indacene-2,6-diide complexes **B13** and **B14**.[47,137,143,144]

Dealing with ferrocenyl compounds including paraffinic bridges, Atzkern *et al.* have synthesized molecules **B13** and **B14** (Figure B10) for which under the chosen conditions notable redox separations were found ($\Delta E^{0'}$ = 200 mV and 195 mV, PrCN/0.1 M TBA[PF$_6$]), indicating significant thermodynamic stabilities of the appropriate cationic mixed-valent species.[144] During electrochemical studies on diferrocenyl methane, well-separated iron-based redox waves could be recorded ($\Delta E^{0'}$ = 170 mV, AN/0.1 M TBA[ClO$_4$]).[145,146] In further studies regarding the resonance interaction in these kind of bonding motifs, Jones *et al.* found low-energy charge transfer absorptions (IVCT) for the mono-cations. The observed low intensities of latter transitions in combination with large experimental widths at half-height ($\Delta\tilde{\nu}_{1/2}$), in relation to the Hush-prediction (*vide supra*), and a strong solvatochromism indicate a classification as weakly-coupled class II systems.[60,68,147]

Regarding ferrocenyls connected with C$_2$-building blocks, for 1,2-diferrocenyl ethane only non-separated Fc/Fc$^+$ redox processes ($\Delta E^{0'} \approx$ 40 mV) were reported under classical (*vide supra*) electrochemical conditions, as expected.[98,145,148] However, by the use of WCA-containing electrolytes in low-polarity media (DCM/TBA[B(C$_6$F$_5$)$_4$]) a remarkable thermodynamic stability ($\Delta E^{0'}$ = 180 mV) of the relevant monocationic species with respect to the appropriate dication and neutral compound could be detected.[98] The higher ability of the unsaturated C$_2$-moieties to foster electronic coupling between the redox-

active entities decreases in the series HC=CH[K] > C≡C > C=CH$_2$ and with an increasing chain length, as well.[47,149–156]

In systems with cumulenic linkers, the metal-metal electronic interaction decreases noticeable by the use of an odd-number of bridging carbon atoms as well as by the chain length.[157–162] Regarding ferrocenyl-substituted aromatics, the electronic coupling in mixed-valent diferrocenyl benzenes is preferred along the *para*-substitution.[150,163,164] A further decreasing of the metal-metal interaction in these systems can be induced by functionalization of the benzene-bridge with electron-withdrawing moieties or by using electron-poor heterocycles.[164–166] Thus, for relevant azabenzene-derivatives, *e.g.* ferrocenyl-substituted pyridines and triazines, decreased electronic interactions were found with regard to the appropriate benzenes.[166–168]

Looking for ferrocenyl-functionalized 5-membered aromatic heterocycles, *inter alia* a portfolio of different boroles,[169,170] furanes,[171,172] phospholes,[173–175] pyrroles,[176–181] siloles[182] and thiophenes[163,167,171,183–185] as well as metallacycles[186–188] were investigated. Upon using a pyrrole-core for the linking of ferrocenyls, relatively large redox separations ($\Delta E^{0'}$) were found together with intense low-energy NIR absorption bands.[171,179] In contrast, less intense IVCT-absorptions as observed for *in situ* generated mixed-valent diferrocenyl furans and thiophenes in combination with decreased $K_C$ values indicate a lower degree of electronic metal-metal interaction in the latter species.[171,185] An increasing of the bridging unit results also in a decreased electronic interaction, as outlined elsewhere (*quod vide*).[48,172,178,185,189–194] A variation of the electronic coupling should be possible through modifications on these heterocyclic systems, by the introduction of electron-donating and/or electron-withdrawing substituents. Thus, Hildebrandt *et al.* have executed selective functionalizations on the phenyl moiety of 2,5-diferrocenyl-*N*-phenylpyrrole (compounds **B15** – **B20**, Figure B11). A significant gain of redox separations in combination with rising oscillator strengths (*f*) were reported by introducing more electron-donating substituents on the *N*-phenyl group (Figure B11).[179,180] However, the impact of these modifications on the electronic coupling is less pronounced with regard to the influence of functionalizations in 1'-positions of the metallocenyl increments. Lehrich *et al.* have reported a better stabilization ($K_C$) of **B24**$^+$, due to the electron-withdrawing C≡N-groups, by approx. 3 times the magnitude of **B18**$^+$ (Figure B11).[176] Nevertheless, the authors note a decreasing metal-metal resonance interaction with increasing redox

---

[K] Difficult E/Z-differentiation due to isomerization.[47,149,150,156]

separations[L], larger $\Delta E^{0'}$ values should originate from electrostatic interactions ("non-conformist" behavior).[74,176] The interpretation of the UV-Vis-NIR spectroelectrochemical data supports this conclusion.[176]
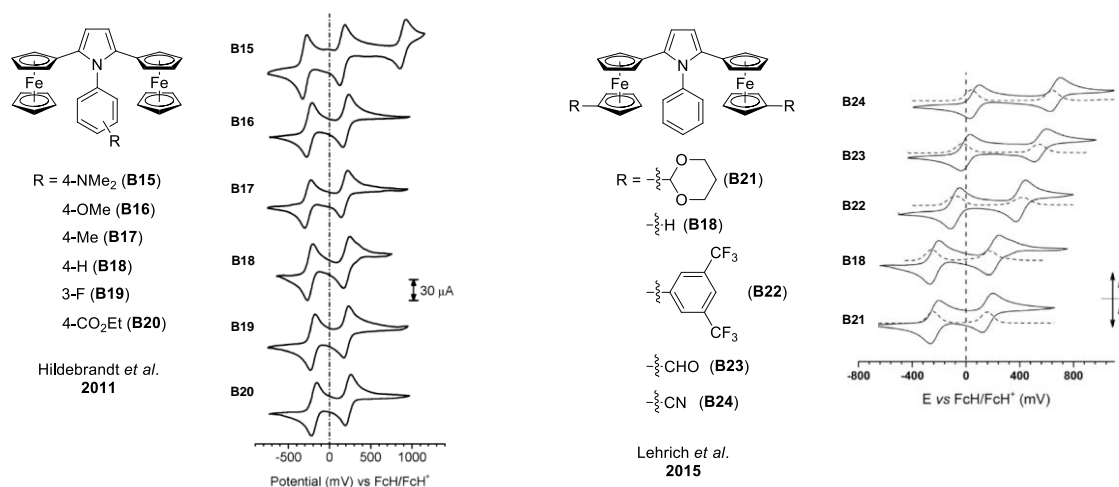


**Figure B11**. Influence of electron-donating and electron-withdrawing functionalities on the thermodynamic stability ($\Delta E^{0'}$, $K_C$) of mixed-valent 2,5-diferrocenyl-*N*-phenylpyrroles (**B15** – **B24**).[176,179,180] Scan rate: 100 mVs$^{-1}$ in dichloromethane solutions (1.0 mM) at 25 °C, supporting electrolyte [N$^n$Bu$_4$][B(C$_6$F$_5$)$_4$] (0.1 M), cyclic voltammogram (solid line) square wave voltammogram (dashed line). *Cyclic voltammograms left: adapted from reference* 180 *with permission of the Royal Society of Chemistry. Cyclic voltammograms right: adapted from reference* 176 *with permission of Elsevier.*

Looking for thiophenes modified with metallocenyl entities, symmetric diferrocenyl derivatives **B25** and **B26** are well-known in the literature (Figure B12).[167] Similar redox separations were found during their electrochemical characterization ($\Delta E^{0'}$ = 140 mV (**B25**), $\Delta E^{0'}$ = 150 mV (**B26**)), indicating comparable thermodynamic stabilities of the corresponding monocations. Moreover, the 1$^{st}$ Fc/Fc$^+$ redox process for **B26** was observed as significantly cathodically shifted with regard to ferrocene, revealing a notable electronic metal-metal coupling in **B26$^+$**.[47,167] The observed low-energy charge transfer band for the latter species reveals a valence-trapped situation, class II according to Robin and Day.[68,171] For the appropriate benzo[*c*] derivative **B29** a clearly larger redox separation ($\Delta E^{0'}$ = 280 mV) was found compared to **B26** under similar conditions (*vide supra*, Figure B12).[163,167,195,196] Thus an enlarged π-bridging system, *inter alia* throughout annulation, should result in an increasing electronic coupling at comparable geometrical distances of the redox sites. During the electrochemical analysis of 2,3-diferrocenyl benzo[*b*]thiophene (**B28**), a significantly decreased thermodynamic stability for **B28$^+$** could be detected[M].[195,196] Electrochemical studies on 2,3- and 2,4-diferrocenyl thiophene are still not reported, except for application-related investigations on their potential in semiconductor devices.[197]

---

[L] from **B21$^+$** to **B24$^+$**, except for **B18$^+$**.[176]
[M] *vs.* **B29$^+$**
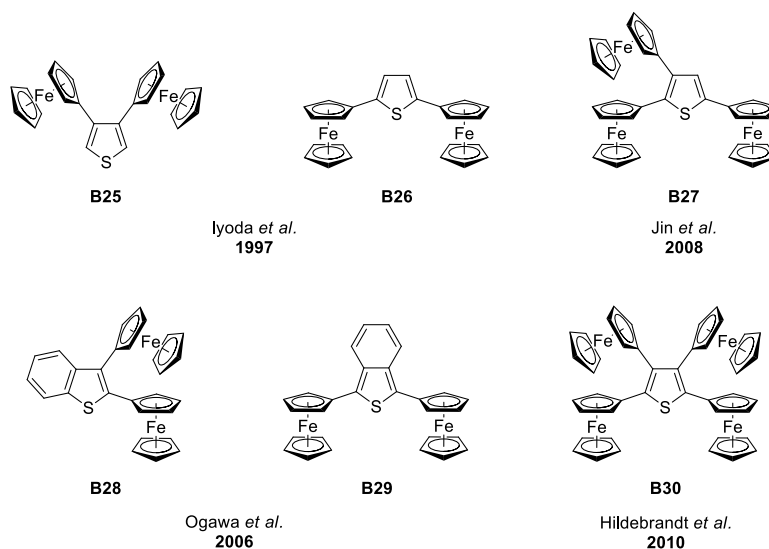
**Figure B12**. Several oligoferrocenyl-substituted thiophenes (**B25** – **B30**).[163,167,183,195,196]

As an example of a triferrocenyl thiophene, Jin *et al*. reported the synthesis of thiophene **B27** together with electrochemical investigations on a series of different ferrocenyl aromatics.[163] Furthermore, the authors attribute mixed-valent biferrocenes with thiophene-2,5-diyl spacers, instead of *para*-phenylene bridges, a stronger coupling. For **B27**, three consecutive ferrocenyl-based one-electron redox events were found, whereby the *α*-ferrocenyls will be oxidized first.[163] Moreover, four well-separated Fc/Fc$^+$ redox processes could be detected during the electrochemical examinations on tetraferrocenyl thiophene (**B30**), using a 0.1 M solution of $[N^nBu_4][B(C_6F_5)_4]$ in dichloromethane as supporting electrolyte (Figure B12).[183] However, no low-energy charge transfer absorptions, suggesting direct iron-iron interactions, could be recorded in the NIR range during the successive oxidation process of **B30**.[183]

# C ELECTRON TRANSFER STUDIES ON FERROCENYL THIOPHENES - SYNTHESIS, PROPERTIES AND ELECTROCHEMISTRY

J. M. Speck, R. Claus, A. Hildebrandt, T. Rüffer, E. Erasmus,[#] L. van As,[#] J. C. Swarts[#] and Heinrich Lang

*Section C was generated within collaboration with J. C. Swarts (#) and co-worker from the University of the Free State, Bloemfontein, ZA (comparative electrochemical studies, manuscript preparation).The author of the present doctoral thesis has carried out the synthesis and characterization of compounds C1, C11 and C12, together with all the published electrochemical and spectroelectrochemical investigations, discussion of the results and manuscript preparation. Further work was done by R. Claus and A. Hildebrandt (synthesis and characterization of compounds C2, C3, C4, C9, C10 and C13, manuscript preparation), T. Rüffer (solid-state structure determination, discussion) and Prof. Dr. Heinrich Lang (manuscript preparation and supervision).*

## INTRODUCTION

Recently, organometallic and metal-organic building blocks attached to a $\pi$-conjugated core have gained topical interest, due to their conceivable application as model compounds for transition-metal-containing polymers and, for example, in the study of electron-transfer in the respective mixed-valent species and magnetic exchange interactions.[35,119,164,195,198–203]

The use of redox-active metal-based termini offers the possibility to design new materials, like semi-conducting polymers or molecular wires.[40,47,147,204–208] In this relationship, the ferrocenyl moiety is a very promising candidate for using it as a redox-active group with a very good stability in the neutral as well as oxidized state during one-electron transfer processes.[166,171,179,180,183,186,189,209–211]

Ferrocene derivatives were studied in a wide range of organometallic chemistry: *e.g.*, as active component in new anticancer drugs,[212–215] as catalyst component in catalytic processes,[216–220] as high burning rate catalysts in solid fuels and as donors in energy transfer processes.[221,222] So far, extensive research has been carried out on ferrocenyls linked with different $\pi$-conjugated connectivities, including arenes, annulenes, five- or six-membered heterocycles, porphyrins and alkynes.[166,171,179,180,183,186,189,209–211] An example of ferrocenyl-functionalized aromatic compounds is hexaferrocenyl benzene. Electrochemical studies showed that this species can be oxidized in three separate redox events.[223]

Furthermore, the hexakis(ferrocenylethynyl)benzene shows, depending on the electrolyte counterion and the number of methyl substituents on the ferrocenyl units, cyclic voltammograms with a single six-electron response, three distinct two-electron events, or a cascade of six single-electron waves.[224]

In contrast, aromatic heterocycles including 2,5- and 3,4-diferrocenylthiophene as well as 2,6-diferrocenylpyridine, exhibit no observable metal-metal interactions, if the ferrocenyl units were oxidized simultaneously.[167] Larger peak separations between the first and second oxidations ($\Delta E^{0'}$) among symmetric ferrocenyl heteroaromatics have been reported in 1,3-di(ferrocenyl)benzo[*b*]thiophene and 1,3-di(ferrocenyl)benzo[*b*]selenophene.[196] In addition, electrochemical studies were carried out on azaferrocenes with pyridine or thiophene connectivities between the metallocenyl termini, resulting in excellent $\Delta E^{0'}$ values.[184,225]

Very recently, a series of 2,5-diferrocenyl and 2,3,4,5-tetraferrocenyl-substituted thiophenes, furans and pyrroles as well as 3,3',4,4',5,5'-hexaferrocenyl-2,2'-bithiophene were synthesized using the Negishi *C,C* cross-coupling protocol.[171,179,180,183,210] The electronic and electrochemical properties of these compounds were investigated by cyclic voltammetry (CV), square wave voltammetry (SWV) and *in situ* UV-Vis-NIR spectroscopy. It was found that the ferrocenyl termini can be separately oxidized, giving up to six reversible responses for the appropriate ferrocenyl-substituted heterocyclic molecules. NIR measurements confirmed electronic communication, as IVCT absorptions were found in the corresponding mixed-valent species.[166,171,179,180,183,186,189,209–211] Hence, the compounds were classified as class II molecules according to Robin and Day.[68] However, during the stepwise oxidation of 2,3,4,5-tetraferrocenylthiophene and 3,3',4,4',5,5'-hexaferrocenyl-2,2'-bithiophene no notable transitions which could be attributed to IVCT absorptions were observed in the NIR region, *i.e.* the electrochemically generated ferrocenium units mostly communicate electrostatically with each other.[183,210]
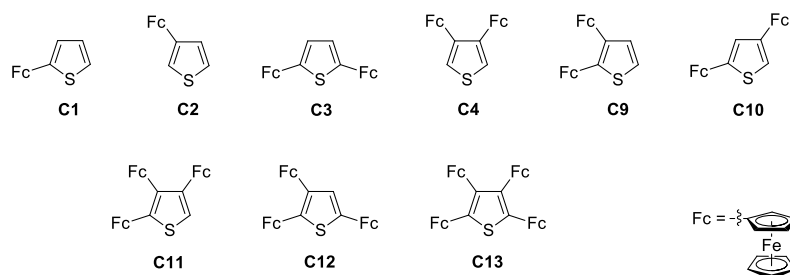


**Figure C1**. Ferrocenyl thiophenes **C1** – **C4** and **C9** – **C13**.[163,167,183,226,227]

In continuation of this work, we recently became interested in the preparation of ferrocenyl-functionalized heteroaromatics as well as their spectroelectrochemical behavior. Thus, we report herein the synthesis of the di- and tri-ferrocenyl thiophenes 2,3-Fc$_2$-$^c$C$_4$H$_2$S, 2,4-Fc$_2$-$^c$C$_4$H$_2$S and 2,3,4-Fc$_3$-$^c$C$_4$HS (Figure C1). In the investigation of electron transfer interactions between the ferrocenyl units on the thiophene, the electrochemical and spectroelectrochemical properties of these species together with a series of mono-, di-, tri- and tetra-ferrocenyl thiophenes (Figure C1) are discussed.

RESULTS AND DISCUSSION

The known ferrocenyl thiophenes **C1** – **C4**, **C12** and **C13** are accessible by different synthetic routes.[163,166,167,171,179,180,183,186,189,209–211,226,227] Nevertheless, we synthesized all of these compounds applying the palladium-promoted Negishi *C,C* cross-coupling protocol. The thiophenes 2,3-Fc$_2$-$^c$C$_4$H$_2$S (**C9**), 2,4-Fc$_2$-$^c$C$_4$H$_2$S (**C10**) and 2,3,4-Fc$_3$-$^c$C$_4$HS (**C11**) are available by a two- or three-fold Negishi *C,C* cross-coupling of the bromo thiophenes 2,3-Br$_2$-$^c$C$_4$H$_2$S (**C5**), 2,4-Br$_2$-$^c$C$_4$H$_2$S (**C6**) and 2,3,4-Br$_3$-$^c$C$_4$HS (**C7**) with FcZnCl (**C8**; Fc = Fe($\eta^5$-C$_5$H$_4$)($\eta^5$-C$_5$H$_5$)) (Scheme C1).[228]

**Scheme C1. Synthesis of ferrocenyl thiophenes C9 – C11.**



[Pd] = [Pd(CH$_2$CMe$_2$P$^t$Bu$_2$)($\mu$-Cl)]$_2$, [Pd(PPh$_3$)$_4$]
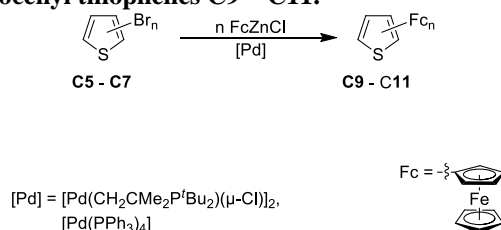
As catalyst, either [Pd(PPh$_3$)$_4$] or [Pd(CH$_2$CMe$_2$P$^t$Bu$_2$)($\mu$-Cl)]$_2$ was used (Experimental Section).[229,230] After appropriate work-up, molecules **C9** − **C11** could be isolated as orange solid materials.

They are soluble in most common organic solvents such as toluene, tetrahydrofuran, and dichloromethane and are stable in the solid state as well as in solution toward air and moisture. The ferrocenyl thiophenes **C9** – **C11** have been identified by elemental analysis, IR and NMR ($^1$H, $^{13}$C{$^1$H}) spectroscopy. Furthermore, the solid state structure of **C10** was determined by single-crystal X-ray structure analysis.

All ferrocenyl thiophenes were electrochemically analyzed by cyclic voltammetry (CV) and square wave voltammetry (SWV) as well as UV-VIS-NIR spectroelectrochemistry.

The IR spectra of **C9** – **C11** are not very expressive, and the $^1$H and $^{13}$C{$^1$H} NMR spectra of thiophenes **C9** – **C11** show the expected signal patterns in the predicted range (Experimental Section).

Single crystals of **C10** suitable for X-ray diffraction studies could be obtained by diffusion of *n*-hexane into a chloroform solution containing **C10** at ambient temperature. The molecular structure of **C10** in the solid state is shown in Figure C2 together with selected bond distances (Å), bond angles and torsion angles (°). 2,4-Diferrocenyl thiophene (**C10**) crystallizes in the orthorhombic space group *Pnma* in which **C10** is statistically disordered along a crystallographically imposed mirror plane going through C12, S1 and C13A of the thiophene ring. The two different molecules of **C10** are disordered and thus are superimposed above each other, since different atomic positions could be refined for S1 and C13.

The molecular structure of **C10** (Figure C2) does not imply the crystallographically imposed C$_S$ symmetry. Furthermore, **C10** is isomorphic to 2,5-diferrocenyl thiophene (**C3**).[231] As observed for the latter thiophene, molecule **C10** possesses a *syn*-conformation in the solid state with regard to the orientation of the two ferrocenyl units on the thiophene core. In this context, the ferrocenyl moieties are rotated by 10.4 ° out of the plane of the thiophene core. As expressed by the torsion angle C1-D1-D2-C6 = 6.8 °, the cyclopentadienyl ligands at the iron atoms exhibit an almost eclipsed conformation. A comparison of the Fe-D distances shows no significant differences (Figure C2).
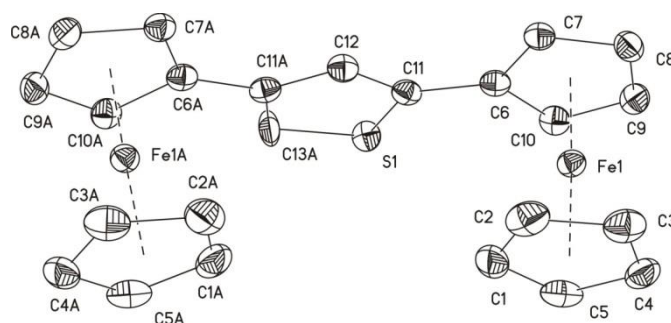


**Figure C2**. ORTEP diagram of thiophene **C10** (50 % displacement ellipsoids). Hydrogen atoms are omitted for clarity. Selected bond distances (Å), bond angles and torsion angles (°): Fe1–D1 1.648(1), Fe1-D2 1.643(1), S-C11 1.687(5), S-C13A 1.720(18), C11-C12 1.394(3), C6-C11 1.464(3), C11-S1-C13A 97.6(7), C12-C11-S1 108.8(3), C11-C12-C11A 113.9(3), C12-C11-S1-C13A 0.3(10), C10-C6-C11-S1 -9.7(4) (D1 = centroid of C$_5$H$_5$ at Fe1, D2 = centroid of C$_5$H$_4$ at Fe1). (Symmetry generated atoms are indicated by the suffix A; symmetry code: x, -y+1/2, z.)

A calculation of the mean plane from the thiophene core reveals a high degree of planarity (rms. deviation from planarity: 0.007 Å; highest deviation from planarity calculated for C11A, 0.012 Å) similar to thiophene **C13**.[183] This observation is in contrast to Mn($\eta^5$-

$C_5Fc_5)(CO)_3$, $C_5HFc_5$, and $C_6Fc_6$, where the central core deviates much more from planarity (*e.g.* 0.152(6) Å in hexaferrocenyl benzene).[223,232] Due to the intrinsic statistic disorder of **C10** a further discussion of the thiophene core bond lengths and its connection to the ferrocenyl units is hampered by the fact that carbon-carbon single and double bonds are superimposed to each other. The observed thiophene C-C bond distances with 1.394(3) Å (C11-C12, C12-C11A) and 1.450(13) Å (C11A-C13A) are significantly shorter than the corresponding values in **C3**, the C-S bond lengths with 1.687(5) Å (S1-C11) and 1.720(18) Å (S1-C13A) are observed as expected, lying between C-S single and C=S double bonds.[233] The C-C bond connecting the thiophene ring and the ferrocenyl units (C6-C11) is, at a length of 1.464(3) Å, very similar to the corresponding bond length in **C3**.[231]

The redox properties of **C1** – **C4** and **C9** – **C13** were studied by cyclic voltammetry (CV), square wave voltammetry (SWV) and UV-Vis-NIR spectroelectrochemistry. As supporting electrolyte, a 0.1 M dichloromethane solution of $[N^nBu_4][B(C_6F_5)_4]$ was used.[90,100] The electrochemical data are summarized in Table C1 and presented in Figure C3.

**Table C1. Cyclic voltammetry data (potentials *vs.* FcH/FcH$^+$) of 1.0 mmol·L$^{-1}$ solutions of C1 – C4 and C9 – C13 in dry dichloromethane containing 0.1 mol·L$^{-1}$ of $[N^nBu_4][B(C_6F_5)_4]$ as supporting electrolyte at 25 °C.**

| Compd. | $E^{0'}/\Delta E_p/\Delta E^{0'}$ [mV]$^a$ $(i_{pc}/i_{pa})^b$ Wave (no.) | | | |
| --- | --- | --- | --- | --- |
| | (1) | (2) | (3) | (4) |
| **C1** | 16/60 (0.99) | | | |
| **C2** | –9/67 (0.99) | | | |
| **C3** | –53/60 (1.00) | 195/62/248 (1.00) | | |
| **C4** | –49/71 (0.99) | 195/70/244 (1.00) | | |
| **C9** | –51/71 (0.99) | 232/73/283 (0.99) | | |
| **C10** | –21/68 (0.98) | 148/69/169 (0.98) | | |
| **C11** | –118/63 (0.99) | 148/61/266 (0.99) | 427/61/279 (1.00) | |
| **C12** | –71/66 (1.00) | 151/62/222 (0.99) | 374/70/223 (1.00) | |
| **C13**[183] | –161/62 (1.00) | 58/64/219 (1.00) | 418/64/360 (0.99) | 604/60/186 (0.99) |

$^a$ Formal potential ($E^{0'}$). Difference between the oxidation ($E_{pa}$) and reduction ($E_{pc}$) peak potential ($\Delta E_p$). Redox separation between the formal iron-based redox events ($\Delta E^{0'} = E^{0'}(2) – E^{0'}(1)$). $^b$ Ratio of current peaks at $E_{pc}$ and $E_{pa}$.

From Table C1, all electrochemical processes involving the oxidation of a ferrocenyl group could be assigned as electrochemically reversible, as the $\Delta E_p$ values were all smaller than 80 mV at slow scan rates. Theoretically, the $\Delta E_p$ for electrochemically reversible processes should be 59 mV.[85,234–237]

All ferrocenyl oxidations were observed as chemically reversible, since the $i_{pc}/i_{pa}$ ratios are approximately unity in all cases. Mono-substituted thiophenes **C1** and **C2** show only one ferrocenyl oxidation. The ferrocenyl group of 3-ferrocenylthiophene (**C2**) is oxidized at a

potential 25 mV lower than that of 2-ferrocenylthiophene (**C1**), having a redox potential of $E^{0'} = 16$ mV (Table C1 and Figure C3). This indicates a higher degree of electronic interaction between the thiophene core and the $\alpha$-ferrocenyl in comparison to the situation in 3-ferrocenylthiophene. The diferrocenyl thiophenes **C3**, **C4**, **C9** and **C10** show two well-resolved one-electron transfer processes (Figure C3). For thiophene **C10** the potential of the 1$^{st}$ wave ($E^{0'} = -21$ mV) is shifted to higher potentials in comparison to that of the other diferrocenyl thiophenes, for which the first redox event occurs nearly at the same potential (Table C1).
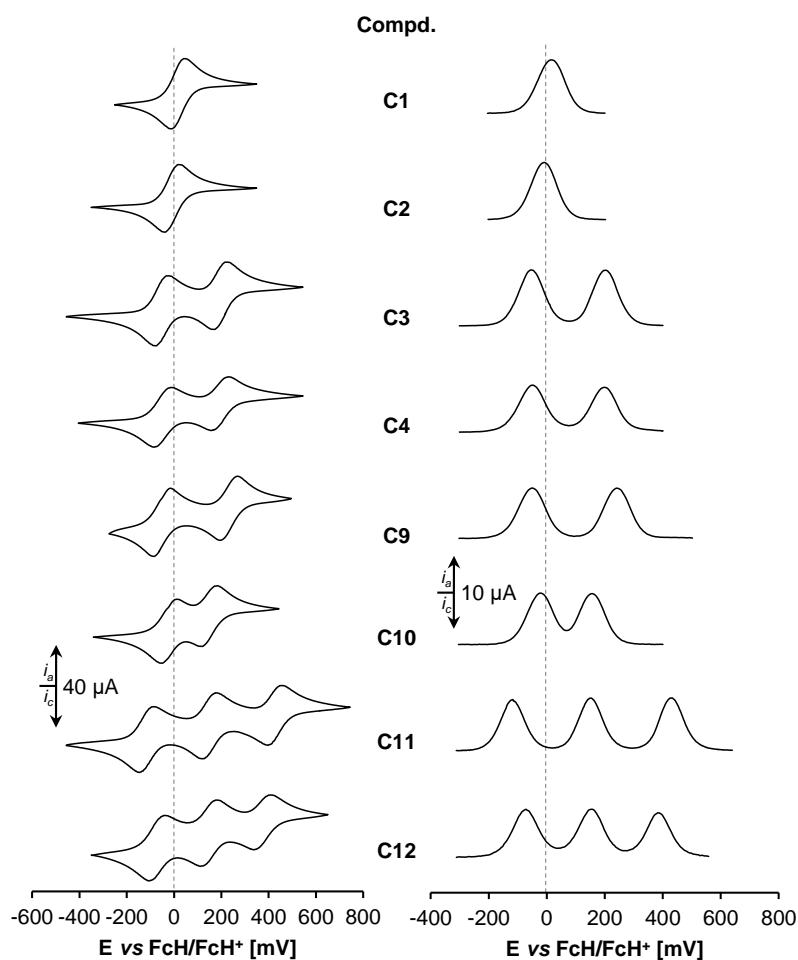


**Figure C3**. Left: cyclic voltammograms (CV) of ferrocenyl thiophenes **C1** – **C4** and **C9** – **C12**, scan rate: 100 mVs$^{-1}$ in dichloromethane solutions (1.0 mM) at 25 °C, supporting electrolyte [N$^n$Bu$_4$][B(C$_6$F$_5$)$_4$] (0.1 M). Right: square wave voltammograms (SWV) of ferrocenyl thiophenes **C1** – **C4** and **C9** – **C12**. Conditions: 5 Hz (**C1**, **C2**, **C9**, **C10**), 2.5 Hz (**C12**), and 2 Hz (**C3**, **C4**, **C11**)) in dichloromethane solutions (1.0 mM) at 25 °C, supporting electrolyte [N$^n$Bu$_4$][B(C$_6$F$_5$)$_4$] (0.1 M). For cyclic voltammetry data see Table C1; for CV and SWV of **C13** see ref 183.

The separation of the redox potentials ($\Delta E^{0'}$) decreases in the series of diferrocenylthiophenes as **C9** > **C3** ≈ **C4** > **C10**, in which the largest value was observed for 2,3-diferrocenyl thiophene (**C9**) ($\Delta E^{0'} = 283$ mV), while for the 2,4-derivative (**C10**) only a redox separation of $\Delta E^{0'} = 169$ mV was found (Table C1, Figure C3). However, the

communication between the ferrocenyl units in such molecules cannot directly be derived from the separation of the redox potentials ($\Delta E^{0'}$), since the free energy of comproportionation ($\Delta G_c$, *vide supra*) is not only a function of the resonance stabilization ($\Delta G_{res}$). $\Delta G_c$ includes also terms corresponding to the Coulomb energy, to a statistic contribution and to bonding synergisms.[50,57,73] The electrochemistry of tetraferrocenyl thiophene (**C13**) was described in detail in a previous work and the results are presented in Table C1.[183]

In order to get more insight into the oxidation process of thiophenes **C1** – **C4** and **C9** – **C13**, we carried out spectroelectrochemical studies by a stepwise increase of the potential *vs.* Ag/AgCl in an OTTLE cell (= Optically Transparent Thin Layer Electrochemistry),[238] using a 0.1 M dichloromethane solution of [N$^n$Bu$_4$][B(C$_6$F$_5$)$_4$] as supporting electrolyte. This procedure allows the in situ generation of species such as **C1$^+$**, **C2$^+$**, **C3$^{n+}$**, **C4$^{n+}$**, **C9$^{n+}$**, **C10$^{n+}$** (n = 1, 2), **C11$^{n+}$**, **C12$^{n+}$** (n = 1 – 3) and **C13$^{n+}$** (n = 1 – 4).

**Table C2. NIR data of C1 – C4 and C9 – C13 in dry dichloromethane containing 0.1 M of [N$^n$Bu$_4$][B(C$_6$F$_5$)$_4$] as supporting electrolyte at 25 °C.**

| Compd. | Transition | $\tilde{v}_{max}$ [cm$^{-1}$] ($\varepsilon_{max}$ [Lmol$^{-1}$cm$^{-1}$])$^a$ | $\Delta\tilde{v}_{1/2}$ [cm$^{-1}$]$^b$ | $\Delta\tilde{v}_{1/2(theo)}$ [cm$^{-1}$]$^c$ |
|---|---|---|---|---|
| **C1$^+$** | LMCT | 10917 (1295) | 2984 | |
| | LF | 4234 (70) | 1096 | |
| **C2$^+$** | LMCT | 11905 (943) | 2985 | |
| | LF | 4241 (46) | 1223 | |
| **C3$^+$** | LMCT | 10080 (624) | 2884 | |
| | IVCT | 4994 (2129) | 3843 | 3397 |
| | LF | 4054 (572) | 439 | |
| | MLCT/LMCT | 3524 (831) | 989 | |
| **C4$^+$** | LMCT | 12180 (824) | 3522 | |
| | IVCT | 5405 (70) | 7761 | 3534 |
| | LF | 4208 (31) | 902 | |
| **C9$^+$** | LMCT | 11534 (946) | n. a. | |
| | IVCT | 5300 (401) | 5492 | 3499 |
| | LF | 4065 (66) | 769 | |
| **C10$^+$** | LMCT | 12005 (1429) | 3263 | |
| | IVCT | 6098 (151) | 5620 | 3753 |
| | LF | 4143 (78) | 857 | |
| **C11$^+$** | LMCT | 12225 (547) | n. a. | |
| | IVCT | 6628 (184) | 5736 | 3913 |
| | LF | 4039 (31) | 1019 | |
| **C11$^{2+}$** | LMCT | 13193 (1075) | n. a. | |
| | IVCT | 7511 (244) | 6733 | 4165 |
| | LF | 4094 (54) | 978 | |
| **C12$^+$** | LMCT | 10129 (515) | 3314 | |
| | IVCT | 4914 (1583) | 4628 | 3369 |
| | LF | 4062 (326) | 475 | |
| | MLCT/LMCT | 3568 (353) | 862 | |
| **C12$^{2+}$** | LMCT | 11761 (1654) | 3170 | |
| | IVCT | 5975 (639) | 5895 | 3715 |
| | LF | 4012 (135) | 712 | |
| **C13** | | see reference 183 | | |

$^a$ Wavenumber of the bands maximum intensity ($\tilde{v}_{max}$), extinction coefficient at $\tilde{v}_{max}$ ($\varepsilon_{max}$). $^b$ Bandwidth at half height ($\Delta\tilde{v}_{1/2}$). $^c$ Bandwidth at half height expected from the Hush theory ($\Delta\tilde{v}_{1/2(theo)} = (2310\tilde{v}_{max})^{1/2}$).

If deconvolution of NIR absorptions was used, transitions with Gaussian shapes were taken to get fits good enough to allow an almost exact overlay of the sum of the spectral components with the experimental spectra. All neutral ferrocenyl thiophenes do not contain, as expected, any absorptions in the NIR range (Figures C4 and C5 and Appendix Figures AC-1 – AC-4). During the oxidation process of **C1** typical absorptions in the UV-Vis region of inner ferrocenyl ligand-to-metal charge transfer (LMCT) transitions as well as absorptions, which are attributed to LMCT interactions between the thiophene core and the ferrocenyl moieties could be observed (Table C2, Figure C4).[30,239–241] The latter absorption was found for **C1**$^+$ in the border section close to the NIR range at $\tilde{v}_{max} = 10917$ cm$^{-1}$ (Table C2). The corresponding transition for **C2**$^+$ was observed as less intensive than for **C1**$^+$ and suggests a lower degree of electronic interaction between the thiophene core and the ferrocenyl unit (*vide supra*, Figure AC-1).[30,31] Furthermore, a very weak, low-energy absorption band was found for **C1**$^+$ and **C2**$^+$ around 4200 cm$^{-1}$, which is attributed to a forbidden ligand field transition (LF, Figures C4, AC-1).[210,242–244]
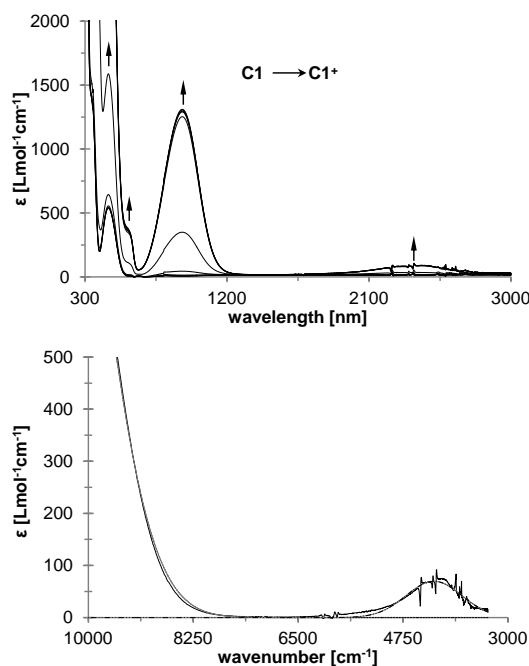


**Figure C4**. UV-Vis-NIR spectra of **C1** at rising potentials. Top: –500 to 350 mV. Bottom: deconvolution of NIR absorptions at 350 mV, using transitions with Gaussian shapes (dotted line corresponds to absorptions caused by interactions between ligand and metal, dotted dashed line represents ligand field transitions). All potentials *vs.* Ag/AgCl at 25 °C in dichloromethane, supporting electrolyte [N$^n$Bu$_4$][B(C$_6$F$_5$)$_4$] (0.1 M). Arrows indicate increasing or decreasing absorptions.

During the generation of **C3**$^+$ typical absorption bands were observed in the UV-Vis region (*vide supra*, Figure C5). A low energy absorption band was still detected at $\tilde{v}_{max} = 4994$ cm$^{-1}$, which is attributed to an intervalence charge transfer (IVCT) transition. The peak width at half-height ($\varDelta\tilde{v}_{1/2}$) of the latter band shows still a larger value than the predicted peak width at half-height ($\varDelta\tilde{v}_{1/2(theo)}$), since class II systems typically show bandwidths 30 –

40 % in excess of the Hush prediction, due to various contributory factors overlooked in Hush's treatment (Table C2).[56,60,61,68,245] The IVCT absorption is accompanied by bands at 10080 cm$^{-1}$ (LMCT), 4054 cm$^{-1}$ (LF) and a transition at $\tilde{v}_{max}$ = 3524 cm$^{-1}$ attributed to charge transfer interactions between metal and ligand (Table C2 and Figure C5).[166,171,179,180,183,186,189,209–211,242–244] Further oxidation of **C3$^+$** to **C3$^{2+}$** results in a decrease of the IVCT absorption band (Figure C5).
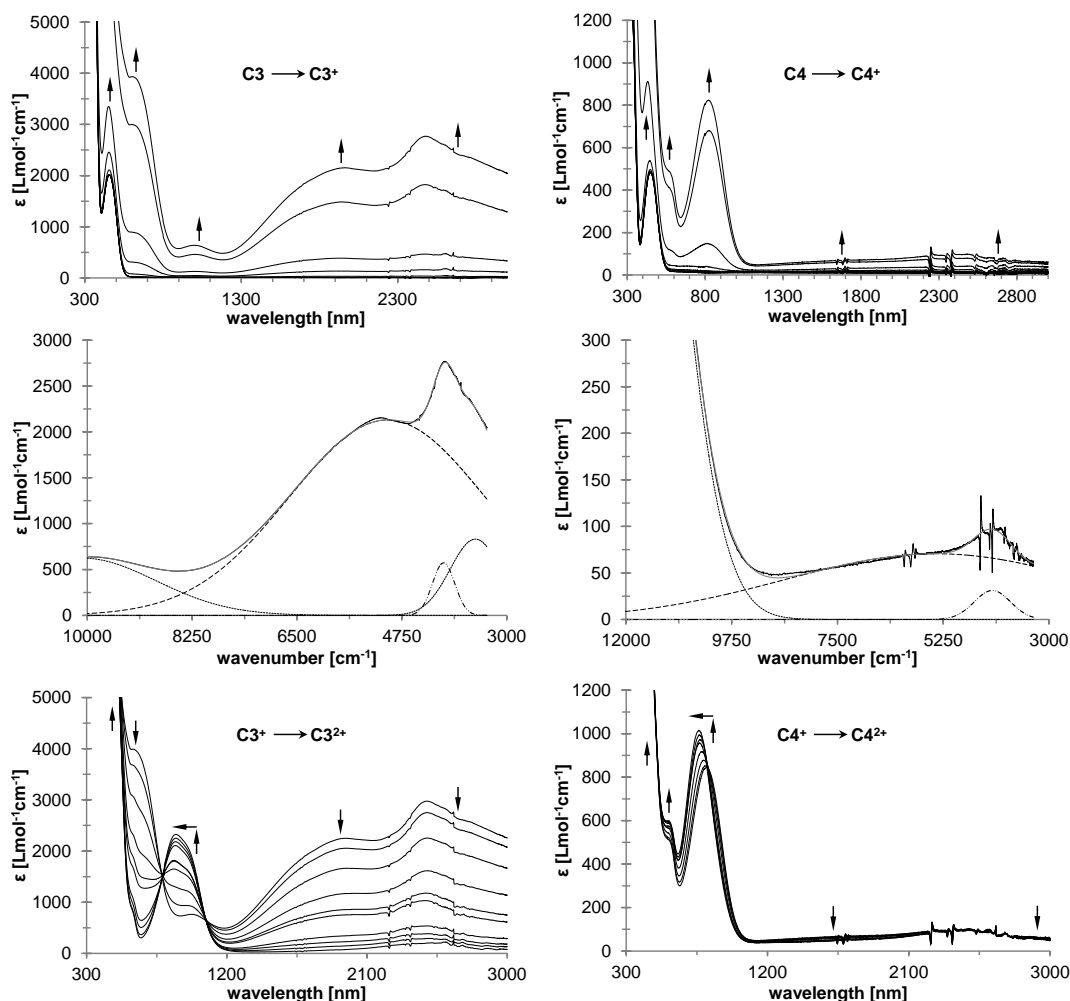


**Figure C5**. Left: UV-Vis-NIR spectra of **C3** at rising potentials. Top: –500 to 600 mV. Middle: deconvolution of NIR absorptions at 600 mV, using four distinct overlapping transitions with Gaussian shapes (dashed line indicates IVCT absorption, dotted line corresponds to absorptions caused by interactions between ligand and metal, dotted dashed line represents ligand field transitions). Bottom: 650 to 1400 mV. Right: UV-Vis-NIR spectra of **C4** at rising potentials. Top: –500 to 500 mV. Middle: deconvolution of NIR absorptions at 500 mV using three distinct overlapping transitions with Gaussian shapes (dashed line indicates IVCT absorption, dotted line corresponds to absorptions caused by interactions between ligand and metal, dotted dashed line represents ligand field transitions). Bottom: 550 to 1500 mV. All potentials *vs.* Ag/AgCl at 25 °C in dichloromethane, supporting electrolyte [N$^n$Bu$_4$][B(C$_6$F$_5$)$_4$] (0.1 M). Arrows indicate increasing or decreasing as well as shifting absorptions.

During spectroelectrochemical studies on the 3,4-diferrocenyl derivative **C4,** a very weak absorption around 5400 cm$^{-1}$ was found upon generation of **C4$^+$**, which can also be assigned to an IVCT transition (Table C2 and Figure C5). However, the corresponding $\Delta\tilde{v}_{1/2}$ value is to be treated with caution, since the investigated peak width at half-height is

more than twice as large as the predicted value and it can be an artifact, due to its very low intensity (Table C2 and Figure C5). A similar behavior was found recently for the corresponding cationic species of 1,3,5-triferrocenyl benzene.[166] Furthermore, an absorption band in the NIR region, close to the IR range, which is caused by charge transfer interactions between metal and ligand is missing, whereas the band at $\tilde{v}_{max}$ = 4208 cm$^{-1}$ can be assigned to a ligand field transition (Figure C5).[210,242–244]

For the monocation of 2,3-diferrocenyl thiophene ($\mathbf{C9^+}$) three absorptions in the NIR region were observed at 11534 cm$^{-1}$ (LMCT), 5300 cm$^{-1}$ (IVCT) and a very weak absorption at 4065 cm$^{-1}$, which can be assigned again to a forbidden ligand field transition (LF, Table C2, Figure AC-2). After the oxidation process was finished, the potential was set again at –500 mV *vs.* Ag/AgCl for checking the reversibility. The corresponding absorption spectrum differs only slightly from the original curve (Figure AC-2 bottom, grey line). During successive oxidation process of the diferrocenyl derivative $\mathbf{C10}$, characteristic absorptions were found for $\mathbf{C10^+}$ in the NIR range at $\tilde{v}_{max}$ = 12005 cm$^{-1}$, 6098 cm$^{-1}$ and 4143 cm$^{-1}$ in which the weak absorption band around 6100 cm$^{-1}$ is attributed to an IVCT transition as well (Table C2, Figure AC-3).

As a result, in the series of diferrocenyl thiophenes the interaction between the iron centers in the mono-oxidized compounds decreases in the series $\mathbf{C3^+} > \mathbf{C9^+} > \mathbf{C10^+} > \mathbf{C4^+}$. Thus, the monocation of 2,5-diferrocenyl thiophene ($\mathbf{C3^+}$) shows by far the largest interaction and for the 3,4-diferrocenyl thiophene derivative $\mathbf{C4^+}$ only a very weak intervalence charge transfer interaction was observed.

Successive oxidation of triferrocenyl thiophene $\mathbf{C11}$ leads to the formation of $\mathbf{C11^+}$, for which low energy absorption bands were found at $\tilde{v}_{max}$ = 12225 cm$^{-1}$ (LMCT), 6628 cm$^{-1}$ (IVCT) and 4039 cm$^{-1}$ (LF, Table C2, Figure AC-3). A comparison of IVCT absorptions from $\mathbf{C11^+}$ with the corresponding band of the 2-bromo-3,4,5-triferrocenyl thiophene derivative shows a slight decrease of extinction coefficient for $\mathbf{C11^+}$ (*vide infra*).[210] Further oxidation up to $\mathbf{C11^{2+}}$ results in a slight hypsochromic and hyperchromic shift of the IVCT absorption band ($\tilde{v}_{max}$ = 7511 cm$^{-1}$, $\varepsilon_{max}$ = 301 Lmol$^{-1}$cm$^{-1}$), similar to those previously observed for 2-bromo-3,4,5-triferrocenyl thiophene.[210] During the generation of $\mathbf{C12^+}$ NIR-absorptions at $\tilde{v}_{max}$ = 10129 cm$^{-1}$ (LMCT), 4914 cm$^{-1}$ (IVCT), 4062 cm$^{-1}$ (LF) and 3568 cm$^{-1}$ could be observed, the last band of which is also attributed to charge transfer transitions, caused by interactions between metal and ligand (Table C2, Figure AC-4). The relatively large extinction coefficient of the absorption around 4900 cm$^{-1}$ suggests similar transitions to those observed for $\mathbf{C3^+}$. This issue is in a good agreement with the work of

Jin *et al.* and their infrared spectroelectrochemical studies on **C3** and **C12**.[163] The oxidation of **C12$^+$** up to the respective dicationic compound results in a hypsochromic shifting of the LMCT absorption, in the border section between the visible and the NIR regions, as for the IVCT absorption band as well (Table C2, Figure AC-4). Moreover, a disappearance of the low-energy absorption band around 3600 cm$^{-1}$ was observed, similar to that found for thiophene **C3** (Table C2, Figure AC-4). The spectroelectrochemical behavior of tetraferrocenyl compound **C13** was previously described, whereas no notable absorptions attributing to intervalence charge transfer could be observed in the NIR region during the successive oxidations process of **C13**.[183]

CONCLUSION

The diferrocenylthiophenes **C9** and **C10** and the triferrocenyl derivative **C11** are available in straightforward palladium-promoted Negishi *C,C* coupling reactions of the corresponding bromo thiophenes and ferrocenyl zinc chloride.

The structure of 2,4-diferrocenyl thiophene (**C10**) in the solid state was determined by single crystal X-ray structure analysis and confirms that compound **C10** crystallizes in the orthorhombic space group *Pnma*, in which **C10** is statistically disordered and thus isomorphic to 2,5-diferrocenyl thiophene (**C3**).

The redox properties of **C1** – **C4** and **C9** – **C13** were studied by cyclic voltammetry (CV), square wave voltammetry (SWV) and UV-Vis-NIR spectroelectrochemistry. The studied ferrocenyl thiophenes display either one (**C1**, **C2**), two (**C3**, **C4**, **C9**, **C10**), three (**C11**, **C12**) or four (**C13**) well-resolved electrochemically reversible one-electron transfer processes. During the spectroelectrochemical studies of ferrocenyl thiophenes **C1** and **C2**, the LMCT absorption for **C2$^+$** around 11000 cm$^{-1}$ was observed as less intensive than for **C1$^+$**, suggesting a lower degree of electronic interaction between the thiophene core and the ferrocenyl unit. The spectroelectrochemical studies of the oligoferrocenyl molecules suggest weak metal-metal interactions in the corresponding mixed-valent species (Table C2), while in the series of diferrocenyl thiophenes the interaction between the iron centers in the monooxidized compounds decreases in the series **C3$^+$** > **C9$^+$** > **C10$^+$** > **C4$^+$**. Furthermore, a comparison between the peak width at half-height $\Delta\tilde{v}_{1/2}$ (IVCT) and the Hush prediction $\Delta\tilde{v}_{1/2(theo)}$ (of **C3$^+$**, **C4$^+$**, **C9$^+$**, **C10$^+$**, **C11$^+$**, **C11$^{2+}$**, **C12$^+$** and **C12$^{2+}$**) is clearly consistent with the identification of the low-energy absorptions of this class of compounds as class II according to Robin and Day.[68] However, during the stepwise oxidation of **C13** no notable transition, which could be attributed to IVCT absorptions, was

observed in the NIR region. These results emphasize that the electrochemically generated ferrocenium units mostly communicate electrostatically with each other.[183]

In summary, it has been found that the ferrocenium units, placed in α-position of the thiophene, interact more strongly with the five-membered heterocycle: *i.e.* larger values of the extinction coefficient can be detected for the corresponding ligand-to-metal and intervalence charge transfer absorptions of the individual cationic species.

EXPERIMENTAL SECTION

**General Procedures**. All reactions were carried out under an argon atmosphere using standard Schlenk techniques. Tetrahydrofuran, toluene and *n*-hexane were purified by distillation from sodium/benzophenone ketyl. Dichloromethane was purified by distillation from $P_4O_{10}$.

**Reagents**. Tetra-*n*-butylammonium tetrakis(pentafluorophenyl) borate was prepared by metathesis of lithium tetrakis(pentafluorophenyl)borate etherate (Boulder Scientific) with tetra-*n*-butylammonium bromide, according the published procedure.[101] All other chemicals were purchased from commercial suppliers and were used as received.

**Instruments**. Infrared spectra were obtained with a Thermo Nicolet 200 FT-IR spectrometer using KBr press techniques for sample preparation. NMR spectra were recorded using an Bruker Avance III 500 FT-NMR spectrometer ($^1$H NMR at 500.303 MHz, $^{13}$C{$^1$H} NMR at 125.813 MHz) at ambient temperature, unless otherwise noted. Chemical shifts ($\delta$) are reported in parts per million (ppm) relative to tetramethylsilane (TMS) using the solvent as internal reference (CDCl$_3$: 1H NMR $\delta = 7.26$ ppm; $^{13}$C{$^1$H}-NMR $\delta = 77.16$ ppm).[246] Coupling constants ($J$) are reported in Hertz (Hz) and integrations are reported in number of protons. The following abbreviations are used to describe peak patterns: s = singlet, d = doublet, pt = pseudotriplet. The melting points (sealed off in argon flushed capillaries) were determined using a Gallenkamp MFB 595 010 M melting point apparatus. Microanalysis was performed by using a Thermo FLASHEA 1112 Series instrument. High resolution mass spectra were recorded with a Bruker micrOTOF QII with an Apollo II ESI-source.

**Synthesis of 2,3-diferrocenyl thiophene (C9)**. A solution of ferrocene (5.0 g, 26.9 mmol) and 0.125 eq of KO$^t$Bu (0.38 g) in 60 mL tetrahydrofuran was cooled to –80 °C. Afterward, 2.0 eq (33.6 mL) of an 1.6 M *tert*-butyllithium solution in *n*-pentane was added

dropwise during a period of 15 min.[247] After 1 h isothermal stirring, one equivalent (7.53 g) of [$ZnCl_2 \cdot 2thf$] was added in a single portion and the resulting reaction mixture was warmed to 0 °C for 30 min. Furthermore, 0.4 eq (1.18 mL) of 2,3-dibromothiophene (**C5**) as well as 67,0 µmol (0.046 g) of [$Pd(CH_2CMe_2P^tBu2)(\mu\text{-}Cl)]_2$[229,230] or 0.13 mmol (0.15 g) of [$Pd(PPh_3)_4$] were added in a single portion. The resulting preparation was kept at 55 °C for 36 h. After cooling down to ambient temperature the reaction mixture was hydrolyzed with 1 M hydrochloric acid and the aqueous layer was separated and extracted three times with 20 mL of dichloromethane. The combined organic layers were dried over $MgSO_4$ and after evaporation of all volatiles, the crude product was adsorbed on alumina and purified by column chromatography (column size: 15 x 3 cm) on alumina using a *n*-hexane/toluene mixture of ratio 4:1 (v:v) as eluent. All volatiles were removed under reduced pressure and compound **C9** was obtained as an orange solid. Yield [$Pd(CH_2CMe_2P^tBu_2(\mu\text{-}Cl)]_2$: 3.60 g (8.0 mmol, 74 % based on 2,3-dibromothiophene); [$Pd(PPh_3)_4$]: 2.80 g (6.2 mmol, 57 % based on 2,3-dibromothiophene) Anal. Calcd for $C_{24}H_{20}Fe_2S$ (452.17): C,63.75; H, 4.46. Found; C, 63.40; H, 4.47. Mp: 212°C. IR data (KBr)[$cm^{-1}$]: 3090 m, 2925 w, 1590 w, 1500 s, 1420 s. $^1H$-NMR (CDCl$_3$)[$\delta$]: 7.13 (d, $J_{HH}$ = 5.3 Hz, 1H, C$_4$H$_2$S), 7.11 (d, $J_{HH}$ = 5.3 Hz, 1H, C$_4$H$_2$S), 4.37 (pt, $J_{HH}$ = 1.8 Hz, 2H, C$_5$H$_4$), 4.25 (pt, $J_{HH}$ = 1.8 Hz, 2H, C$_5$H$_4$), 4.23 (pt, $J_{HH}$ = 1.8 Hz, 2H, C$_5$H$_4$), 4.17 (s, 5H, C$_5$H$_5$), 4.15 (pt, $J_{HH}$ = 1.8 Hz, 2H, C$_5$H$_4$), 4.03 (s, 5H, C$_5$H$_5$). $^{13}C\{^1H\}$ NMR (CDCl$_3$)[$\delta$]: 136.0 (C$_i$-C$_4$H$_2$S), 135.9 (C$_i$-C$_4$H$_2$S), 130.1 (C$_4$H$_2$S), 122.3 (C$_4$H$_2$S), 82.0 (C$_i$-C$_5$H$_4$), 80.7 (C$_i$-C$_5$H$_4$), 70.6 (C$_5$H$_4$), 70.0 (C$_5$H$_5$), 69.4 (C$_5$H$_5$), 68.8 (C$_5$H$_4$), 68.1 (C$_5$H$_4$), 67.9 (C$_5$H$_4$). HR-ESI MS (calc) [m/z]: 451.9957 (451.9980) [M]$^+$.

**Synthesis of 2,4-diferrocenyl thiophene (C10)**. A solution of ferrocene (5.4 mmol, 1.0 g) and 0.125 eq (75 mg) KO$^t$Bu in 20 mL tetrahydrofuran was cooled down to –80 °C followed by an addition of 1.5 eq (5.0 mL) of an 1.6 M solution of *tert*-butyllithium in *n*-pentane within 5 min. After 30 min of isothermal stirring, 1.5 eq (2.26 g) of [$ZnCl_2 \cdot 2thf$] were added in a single portion and the reaction mixture was kept for 30 min at 0 °C. Afterward, 29 µmol (20 mg) of [$Pd(CH_2CMe_2P^tBu)_2(\mu\text{-}Cl)]_2$[229,230] and 0.5 eq (0.65 g) of 2,4-dibromothiophene (**C6**) were added in a single portion and the reaction mixture was stirred for 4 h at 30 °C. After evaporation of all volatiles, the precipitate was dissolved in 50 mL of diethyl ether and washed three times with 50 mL portions of water. The organic layer was dried over $MgSO_4$ and evaporated to dryness. The remaining solid was purified by column chromatography (column size: 20 x 3 cm) on silica using *n*-hexane as eluent. All volatiles were removed under reduced pressure and thiophene **C10** was obtained as an orange solid. Yield: 150 mg (0.33 mmol, 12.3 % based on **C6**). Anal. Calcd for $C_{24}H_{20}Fe_2S$

(452.17): C, 63.75; H, 4.46. Found; C, 63.54; H, 4.45; Mp: 214°C. IR data (KBr)[cm$^{-1}$]: 3089 m, 2923 w, 1597 w, 1498 s, 1417 s. $^1$H-NMR (CDCl$_3$)[$\delta$]: 7.09 (d, $J_{HH}$ = 1.4 Hz, 1H, C$_4$H$_2$S), 6.97 (d, $J_{HH}$ = 1.4 Hz, 1H, C$_4$H$_2$S), 4.61 (pt, $J_{HH}$ = 1.8 Hz, 2H, C$_5$H$_4$), 4.55 (pt, $J_{HH}$ = 1.8 Hz, 2H, C$_5$H$_4$), 4.30 (pt, $J_{HH}$ = 1.8 Hz, 2H, C$_5$H$_4$), 4.26 (pt, $J_{HH}$ = 1.8 Hz, 2H, C$_5$H$_4$), 4.12 (s, 5H, C$_5$H$_5$), 4.08 (s, 5H, C$_5$H$_5$). $^{13}$C{$^1$H} NMR (CDCl$_3$)[$\delta$]: 143.2 (C$_i$-C$_4$H$_2$S), 140.0 (C$_i$-C$_4$H$_2$S), 121.9 (C$_4$H$_2$S), 115.7 (C$_4$H$_2$S), 81.6 (C$_i$-C$_5$H$_4$), 80.4 (C$_i$-C$_5$H$_4$), 70.2 (C$_5$H$_5$), 69.6 (C$_5$H$_5$), 68.8 (C$_5$H$_4$), 68.5 (C$_5$H$_4$), 67.1 (C$_5$H$_4$), 66.7 (C$_5$H$_4$). HR-ESI-MS [m/z] (calc): 452.0010 (451.9980) [M]$^+$.

**Synthesis of 2,3,4-triferrocenyl thiophene (C11)**. A tetrahydrofuran solution (80 mL) of ferrocene (23.4 mmol, 4.35 g) and 0.125 eq (0.33 g) of KO$^t$Bu was cooled to –80 °C, and then 2 eq (29.15 mL) of an 1.6 M *tert*-butyllithium solution in *n*-pentane were added within 15 min.[247] After 1 h isothermal stirring one equivalent (6.54 g) of [ZnCl$_2$·2thf] was added in a single portion and resulting reaction mixture was kept at 0 °C for 30 min. Afterward, 0.27 eq (2.00 g) of 2,3,4-tribromothiophene[248] (**C7**) as well as 58.3 μmol (40 mg) of [Pd(CH$_2$CMe$_2$P$^t$Bu)$_2$($\mu$-Cl)]$_2$[229,230] were added in a single portion. The resulting reaction mixture was kept at 55 °C for 40 h. After cooling down to ambient temperature the mixture was hydrolysed with 1 M hydrochloric acid. Furthermore, the aqueous layer was separated and extracted with dichloromethane and the combined organic layers were dried over MgSO$_4$. After evaporation of all volatiles, the crude product was purified by column chromatography (column size: 20 x 3 cm) on alumina using a *n*-hexane/toluene mixture of ratio 5:1 (v:v) as eluent. Compound **C11** was obtained as an orange solid. Yield: 2.18 g (3.43 mmol, 55 % based on **C7**). Anal. Calcd for C$_{34}$H$_{28}$Fe$_3$S (636.19): C, 64.19; H, 4.44. Found: C, 64.46; H, 4.73. Mp: 232 °C (dec). IR data (KBr)[cm$^{-1}$]: 3092 m, 2928 w, 1595 w, 1495 s, 1416 s. $^1$H-NMR (CDCl$_3$)[$\delta$]: 7.46 (s, 1H, C$_4$H$_S$), 4.49 (pt, $J_{HH}$ = 1.8 Hz, 2H, C$_5$H$_4$), 4.33 (pt, $J_{HH}$ = 1.8 Hz, 2H, C$_5$H$_4$), 4.31 (pt, $J_{HH}$ = 1.8 Hz, 2H, C$_5$H$_4$), 4.30 (s, 5H, C$_5$H$_5$), 4.23 (pt, $J_{HH}$ = 1.8 Hz, 2H, C$_5$H$_4$), 4.22 (s, 5H, C$_5$H$_5$), 3.95 (pt, $J_{HH}$ = 1.8 Hz, 2H, C$_5$H$_4$), 3.89 (pt, $J_{HH}$ = 1.8 Hz, 2H, C$_5$H$_4$), 3.81 (s, 5H, C$_5$H$_5$). $^{13}$C{$^1$H}-NMR (CDCl$_3$)[$\delta$]: 139.9 (C$_i$-C$_4$H$_S$), 137.6 (C$_i$-C$_4$H$_S$), 136.4 (C$_i$-C$_4$HS), 123.4 (C$_4$HS), 86.5 (C$_i$-C$_5$H$_4$), 83.3 (C$_i$-C$_5$H$_4$), 81.5 (C$_i$-C$_5$H$_4$), 72.5 (C$_5$H$_4$), 71.9 (C$_5$H$_4$), 70.3 (C$_5$H$_4$), 70.0 (C$_5$H$_5$), 69.5 (C$_5$H$_5$), 69.0 (C$_5$H$_5$), 68.0 (C$_5$H$_4$), 67.2 (C$_5$H$_4$), 66.9 (C$_5$H$_4$). HR-ESI-MS [m/z] (calc): 635.9973 (635.9956) [M]$^+$.

**Electrochemistry.** The electrochemical measurements were carried out under an argon atmosphere on 1.0 mM dichloromethane solutions containing 0.1 M [N$^n$Bu$_4$][B(C$_6$F$_5$)$_4$] as supporting electrolyte utilizing a Voltalab 10 electrochemical laboratory from Radiometer

Analytical.[90,100] Furthermore, an OTTLE cell (= Optically Transparent Thin Layer Electrochemistry) placed in a Varian Cary 5000 UV-VIS-NIR absorption spectrometer was used for spectroelectrochemical measurements.[238] For voltammetry, a three-electrode cell with a platinum auxiliary electrode, a glassy carbon working electrode and a $Ag/Ag^+$ reference electrode were used. The working electrode was prepared by polishing with a Buehler micro cloth using Buehler diamond pastes with decreasing sizes (1 to 0.25 μm). The $Ag/Ag^+$ reference electrode was constructed from a silver wire inserted into a Luggin capillary with a Vycor tip containing 0.01 M $[AgNO_3]$ as well as 0.1 M $[N^nBu_4][B(C_6F_5)_4]$ in acetonitrile. This Luggin capillary was inserted into a second Luggin capillary with Vycor tip filled with as 0.1 M $[N^nBu_4][B(C_6F_5)_4]$ solution in dichloromethane. Successive experiments under the same experimental conditions showed that all formal reduction and oxidation potentials were reproducible within 5 mV. Experimentally potentials were referenced against a $Ag/Ag^+$ reference electrode but the results are presented referenced against the FcH/FcH$^+$ couple ($E^{0'}$ = 0.0 V) as required by IUPAC.[249] When decamethylferrocene was used as an internal standard, the experimentally measured potential was converted in to E $vs.$ FcH/FcH$^+$ by addition of –0.61 V.[250] The cyclic voltammograms were taken after typical two scans and are considered to be steady state cyclic voltammograms, in which the signal pattern differs not from the initial sweep. Finally, the experimental data were processed on Microsoft Excel worksheets.

**Crystallography**. Crystal data for **C10**, $C_{24}H_{20}Fe_2S$, Mr = 452.16 gmol$^{-1}$, orthorhombic, *Pnma*, $\lambda$ = 0.71073 Å, $a$ = 8.2562(2) Å, $b$ = 23.3232(6) Å, $c$ = 9.7291(2) Å, $V$ = 1873.51(8) Å$^3$, Z = 4, $\rho_{calcd}$ = 1.603 gcm$^{-3}$, $\mu$ = 1665 mm$^{-1}$, T = 115 K, $\Theta$ range = 3.24 – 25 °, reflections collected: 4650, independent: ($R_{int}$ = 0.0278), R1 = 0.0284, wR2 = 0.0652 [$I$> 2$\sigma$($I$)]. Single crystals of **C10** were obtained by diffusion of *n*-hexane into a chloroform solution containing **C10** at 298 K. Data were collected with an Oxford Gemini S Diffractometer, with graphite monochromatized Mo K$\alpha$ radiation ($\lambda$ = 0.71073 Å) using oil-coated shock-cooled crystals. The structure was solved by direct methods and refined by full-matrix least square procedures on $F^2$.[251,252]

**Supporting Information**. UV-Vis-NIR spectra of **C2**, **C9**, **C10**, **C11** and **C12** in dichloromethane are available in the Appendix Section (Chapter AC, *vide infra*).

ACKNOWLEDGEMENT

# D   ATROPISOMERIC   3,3',4,4',5,5'-HEXAFERROCENYL-2,2'-BITHIOPHENE: SYNTHESIS, SOLID-STATE STRUCTURE AND ELECTROCHEMISTRY

J. M. Speck, D. Schaarschmidt and Heinrich Lang

*Section D was made by the author of the present doctoral thesis (synthesis (diploma thesis), characterization, electrochemistry, interpretation of results and manuscript preparation) together with D. Schaarschmidt (solid-state structure determination, discussion) and Prof. Dr. Heinrich Lang (manuscript preparation and supervision).*

INTRODUCTION

There is an enduring interest in the chemistry of ferrocenyl-substituted homo- and hetero-aromatics because such molecules can be regarded as model species for studying metal-metal electronic interactions.[119,164,195,198–200,202,203] Furthermore, these $\pi$-conjugated organometallic compounds are qualified to design innovative electro-active materials.[40,47,147,204–208]

For the investigation of electron transfer between metal atoms, electrochemical studies, especially cyclic voltammetry (CV) and square wave voltammetry (SWV) are most common. In comparison with the high number of electrochemical studies on organometallic compounds which are published to date, spectroelectrochemical examinations have been reported only sporadically. An example of ferrocenyl-functionalized aromatic compounds is hexaferrocenyl benzene.[223] Electrochemical studies showed that this species can be oxidized in three separated redox events at –162.8, –32.2 and 222.4 mV, respectively.[223]

Hexa(ferrocenylethynyl)benzene derivatives were synthesized by Negishi *C,C* coupling from ethynylferrocenes and $C_6Br_6$, also.[224] Depending on the electrolyte counterion and the number of methyl substituents on the ferrocenyl units, their cyclic voltammograms show a single six-electron response, three distinct two-electron events, or a cascade of six single-electron waves. In contrast, aromatic heterocycles including 2,5- ($\Delta E^{0'}$ = 150 mV) and 3,4-diferrocenyl thiophene ($\Delta E^{0'}$ = 140 mV) as well as 2,6-diferrocenyl pyridine exhibit weak or nearly no observable metal-metal communication if the two ferrocenyls were oxidized simultaneously.[163,167] Higher peak separations between the first and second oxidation ($\Delta E^{0'}$) among symmetric ferrocenyl heteroaromatics have been reported in 1,3-diferrocenyl

benzo[*b*]thiophene ($\Delta E^{0'} = 280$ mV) and 1,3-diferrocenyl benzo[*b*]selenophene ($\Delta E^{0'} = 305$ mV).[196] In addition, electrochemical studies were carried out on azaferrocenes with pyridine or thiophene connectivities between the metallocenyl termini, resulting in excellent $\Delta E^{0'}$ values.[184,225]

Recently, we enriched the family of ferrocenyl-substituted 5-membered heterocycles including furan, thiophene, and 1-R-pyrrols (R = Me, Ph) by the synthesis and electrochemistry of several di-, tri- and tetra-ferrocenyl derivatives thereof.[171,179,180,183,186,189,209,253] Cyclic, square wave and linear sweep voltammetry together with *in situ* NIR spectroelectrochemistry highlight that these molecules display up to four separated electrochemical reversible one-electron transfer processes. Spectroelectrochemistry confirmed that positive charges are localized on the Fc$^+$ groups (Fc = ferrocenyl; Fe($\eta^5$-C$_5$H$_4$)($\eta^5$-C$_5$H$_5$)) in the mixed-valent intermediates if no charge transfer bands of a significant strength could be detected.

In continuation of this work, we recently became interested in the preparation of ferrocenyl-functionalized oligo-heteroaromatics. We report here on the synthesis, properties and electrochemical behavior of atropisomeric 3,3',4,4',5,5'-hexaferrocenyl-2,2'-bithiophene.

RESULTS AND DISCUSSION

For the preparation of 3,3',4,4',5,5'-hexaferrocenyl-2,2'-bithiophene (**D3**) two synthesis methodologies were applied, as shown in Scheme D1, whereby the palladium-promoted Negishi *C,C* cross-coupling of 2-Br-3,4,5-Fc$_3$-$^c$C$_4$S (**D1**) with 2-ZnCl-3,4,5-Fc$_3$-$^c$C$_4$S (**D2**) can be considered as a key step. 2,3,4-Triferrocenyl thiophene[253] (**C11**) was reacted with one equivalent of $^n$BuLi to obtain the appropriate lithio-species, which on treatment with [ZnCl$_2$·2thf] should give the respective zincate **D2** (Scheme D1). However, it appeared that incomplete lithiation always occurred, even using different reaction conditions (temperature, solvent, excess of $^n$BuLi).

As a result, a more straightforward synthesis procedure was developed including the formation of the organo-zinc compound **D2** from bromo thiophene **D1**, since this molecule enables a selective bromo-lithium exchange. Molecule **D1** was accessible by the consecutive reaction of 2,3,4-triferrocenylthiophene (**C11**), prepared from 2,3,4-tribromo thiophene and ferrocenyl zinc chloride,[253] with $^n$BuLi and 1,1,2,2-tetrabromoethane in tetrahydrofuran at low temperature (Scheme D1). Addition of $^n$BuLi to thiophene **D1** and

metathesis of the appropriate lithium intermediate with [ZnCl$_2$·2thf] gave 2-ZnCl-3,4,5-Fc$_3$-$^c$C$_4$S (**D2**).

**Scheme D1. Consecutive synthesis of 3,3',4,4',5,5'-hexaferrocenyl-2,2'-bithiophene (D3).**$^a$
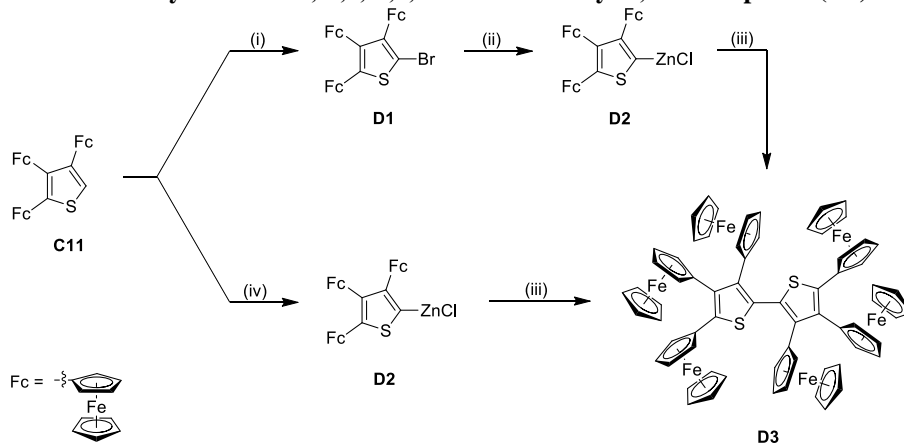


$^a$ Conditions: (i) Tetrahydrofuran; 1$^{st}$: $^n$BuLi, –25 °C, 35 min; 2$^{nd}$: 1,1,2,2-tetrabromoethane, 25 °C, 1 h. (ii) Tetrahydrofuran; 1$^{st}$: $^n$BuLi, –50 °C, 45 min; 2$^{nd}$: [ZnCl$_2$·2thf], 0 °C, 1 h. (iii) 1$^{st}$: **D1**, 2$^{nd}$: [Pd], 55 °C, 48 h ([Pd] = [Pd(CH$_2$CMe$_2$P$^t$Bu$_2$)($\mu$-Cl)]$_2$). (iv) Tetrahydrofuran; 1$^{st}$: $^n$BuLi, –25 °C, 35 min; 2$^{nd}$: [ZnCl$_2$·2thf], 0 °C, 1 h.

Under Negishi *C,C* cross-coupling conditions, compound **D2** was treated with an further equivalent of thiophene **D1** in presence of catalytic quantities of [Pd(CH$_2$CMe$_2$P$^t$Bu$_2$)($\mu$-Cl)]$_2$[229,230] (Scheme D1). After appropriate work-up, bithiophene **D3** could be isolated as an orange solid material in an over-all yield of 18 % (Experimental Section, *vide infra*). Thiophene **D1** and bithiophene **D3** are stable to air and moisture in the solid state as well as in solution.

They are less soluble in nonpolar solvents including *n*-hexane, while in toluene, dichloromethane and tetrahydrofuran they show good (**D1**) or sufficient (**D3**) solubility. Both compounds have been characterized by elemental analysis, IR and (dynamic) NMR ($^1$H, $^{13}$C{$^1$H}) spectroscopy. ESI-TOF mass spectrometry and single-crystal X-ray structure analysis (**D3**) were additionally carried out. The electrochemical and spectroelectrochemical properties of **D1** and **D3** were determined.

Less meaningful are the IR spectra of **D1** and **D3**, since only absorptions typical for ferrocenyl units and thiophene moieties were found (Experimental Section). In contrast to thiophenes **C11**[253] and **D1** (Experimental Section), the NMR spectra of bithiophene **D3** show an unexpected signal pattern. From Figure D1 (left) it can be seen that the cyclopentadienyl C$_5$H$_5$ protons give rise to three singlets at 3.7, 4.2 and 4.4 ppm. In the case of the C$_5$H$_4$ protons a total of 12 resonance signals are observed at 25 °C, which differs from the expected six pseudo-triplets as characteristic for AA'XX' spin systems (Figure D1). This observation can be ascribed with the atropisomeric behavior of **D3** and is

based on the hindered rotation along the thiophene-thiophene *C,C* axis. Successive temperature rise to 105 °C resulted in an increasing rotation frequency (Figure D1).
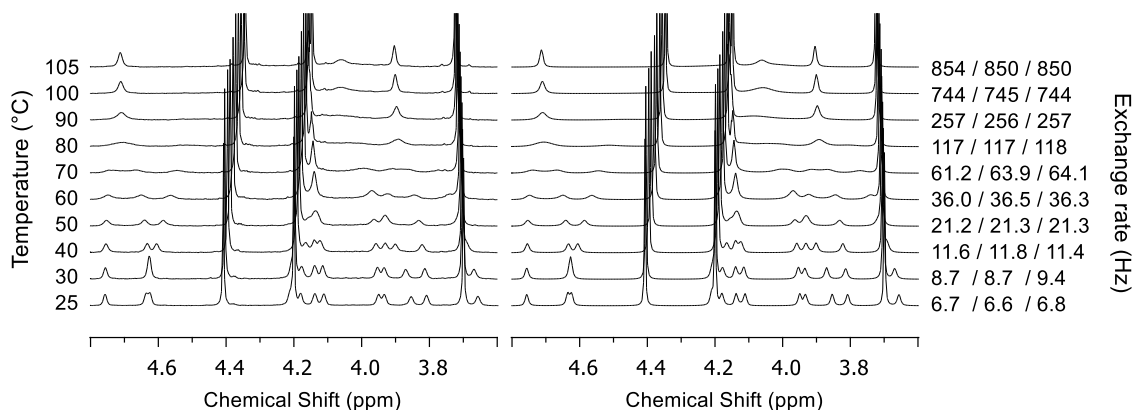


**Figure D1**. Left: ^{1}H NMR spectra of **D3** in the range of 3.6 and 4.8 ppm at various temperatures (toluene-$D_8$). Right: Simulated ^{1}H NMR spectra of **D3** with different exchange rates (separately for the ferrocenyl protons in 3,3', 4,4' and 5,5' position).

The exchange rates could be determined by line-shape-fitting of the NMR spectra at the appropriate temperatures (Figure D1, right). The activation parameters of the inner bithiophene *C,C* bond rotation could be quantified from the exchange rates using graphical methods according to Eyring.[254,255] Values for the activation enthalpy $\Delta H^{\ddagger} = 54.3(4.0)$ kJmol$^{-1}$ and activation entropy $\Delta S^{\ddagger} = -50.3(11.8)$ JK$^{-1}$mol$^{-1}$ could be determined for the rotation barrier.[254,255,N]

Single crystals of **D3** suitable for X-ray diffraction analysis could be obtained by diffusion of *n*-hexane into a toluene solution containing **D3** at ambient temperature. The molecular structure of **D3** in the solid state is shown in Figure D2. Important bond distances (Å), bond angles (°) and torsion angels (°) are summarized in the caption of Figure D2. For crystal and structure refinement data see Experimental Section (*vide infra*).

Bithiophene **D3** crystallizes in the triclinic space group $P\bar{1}$ as orange plates. The X-ray structure analysis shows that the bithiophene core unit is not coplanar, since a torsion angle of 61.4(1)° was observed between the thiophene mean planes. This differs from other bithiophene systems, such as 5,5'-bis(ferrocenylethynyl)-2,2'-bithiophene and 5-R-5'-SCN-2,2'-bithiophene (R = Br, SCN), respectivly.[256,257] The ferrocenyl substituents are rotated by 54.73(9)° (Fe1), 50.61(13)° (Fe2), 56.68(11)° (Fe3), 57.68(11)° (Fe4), 39.85(11)° (Fe5) and 53.75(10)° (Fe6) out-of-plane of the thiophene units. Both facts indicate an overstrained molecule geometry of **D3**. However, the inner C64-C68 bond with 1.456(4) Å corresponds to typical distances found for similar species and oligo aryls.[258]

---

[N] Standard error is given in parentheses.

The thiophene core bond lengths (Figure D2) show delocalization with distances between C–C/C–S single and C=C/C=S double bonds.[233]
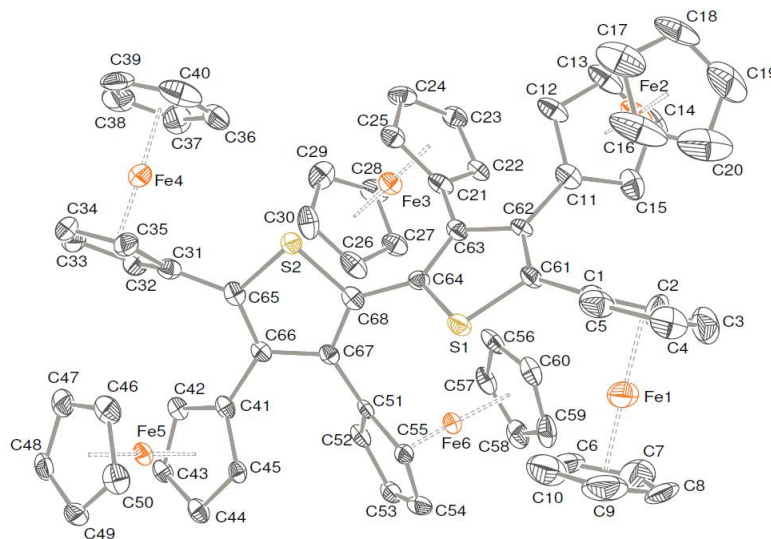


**Figure D2**. ORTEP diagram (50 % probability level) of the molecular structure of **D3**·1.5C$_7$H$_8$ with the atom-numbering scheme. All hydrogen atoms and 1.5 molecules of toluene have been omitted for clarity. Selected bond distances (Å), angles (°) and torsion angles (°): C64-C68 1.456(4), S1-C61 1.723(3), S1-C64 1.720(3), C61-C62 1.368(4), C62-C63 1.449(4), C63-C64 1.374(4), S2-C65 1.715(3), S2-C68 1.727(3), C65-C66 1.382(4), C66-C67 1.450(4), C67-C68 1.382(4), C1-C61 1.475(4), C11-C62 1.481(4), C21-C63 1.478(4), C31-C65 1.477(4), C41-C66 1.484(4), C51-C67 1.481(4); D1-Fe1 1.6573(6), D2-Fe1 1.6453(6), D1-Fe2 1.6473(5), D2-Fe2 1.6487(5), D1-Fe3 1.6488(4), D2-Fe3 1.6552(4), D1-Fe4 1.6550(6), D2-Fe4 1.6500(6), D1-Fe5 1.6559(4), D2-Fe5 1.6470(4), D1-Fe6 1.6596(4), D2-Fe6 1.6610(4); C68-C64-S1 118.5(2), C64-S1-C61 93.24(14), C64-C68-S2 118.1(2), C65-S2-C68 93.44(14), D1-Fe1-D2 178.86(4), D1-Fe2-D2 176.93(4), D1-Fe3-D2 174.56(4), D1-Fe4-D2 176.23(4), D1-Fe5-D2 178.76(3), D1-Fe6-D2 175.75(4); S1-C64-C68-S2 116.7(2), C63-C64-C68-C67 119.5(5); D denotes the centroids of the corresponding cyclopentadienyl rings (D1 = C$_5$H$_5$, D2 = C$_5$H$_4$).

The ferrocenyl cyclopentadienyl rings are rotated by 20.7(3)° (Fe1), –3.0(3)° (Fe2), –2.5(3)° (Fe3), 4.9(3)° (Fe4), –5.4(2)° (Fe5) and –12.2(2)° (Fe6) to each other, verifying almost eclipsed conformations, whereas the rotation in Fe1 is well described with a staggered arrangement. Moreover, The Fe-D distances of the ferrocenyl termini do not show significant differences (Figure D2). The Fe-C$_{ipso}$ distances (Fe1-C1 2.069(3), Fe2-C11 2.065(3), Fe3-C21 2.085(3), Fe4-C31 2.086(3), Fe5-C41 2.071(3) and Fe6-C51 2.082(3) Å) are elongated, in comparison to the other Fe-C$_{C5H4}$ bonds. A similar observation has been made for $^c$C$_4$Fc$_4$S,[183] ($\eta^5$-C$_5$Fc$_5$)Mn(CO)$_3$,[232] C$_5$HFc$_5$ and C$_6$Fc$_6$.[223]

The calculation of the mean plane of the two thiophene units reveals these five-membered heterocycles to be planar (S1, C61-C64: rms deviation from planarity 0.0128 Å; highest deviation from planarity calculated for atom C61 with –0.0169(16) Å; S2, C65-C68: rms deviation from planarity 0.0168 Å; highest deviation from planarity calculated for atom C65 with 0.0235(15) Å. A similar behavior was found for $^c$C$_4$Fc$_4$S.[183]

The redox properties of **D1** and **D3** were studied by cyclic voltammetry (CV), square wave voltammetry (SWV) (Figure D3) and UV-Vis-NIR spectroelectrochemistry (Figure D4). As supporting electrolyte dichloromethane and anisole solutions of $[N^nBu_4][B(C_6F_5)_4]$ (0.1 M) were used.[90,100] The cyclic voltammetry studies were carried out at scan rates of 100 and 200 mVs$^{-1}$, the corresponding data are summarized in Table D1. All potentials are referenced against FcH/FcH$^+$ (FcH = Fe($\eta^5$-C$_5$H$_5$)$_2$) as suggested by IUPAC.[249] The cyclic voltammogram of **D1** shows three separated ferrocenyl-related oxidation half-reactions in the anodic sweep and reduction half-reactions in the cathodic CV sweep (Figure D3, left top, and Table D1).

**Table D1. Cyclic voltammetry data (potentials *vs*. FcH/FcH$^+$) of 1.0 mmol·L$^{-1}$ (sat.) solutions of D1 and D3 in dry dichloromethane and anisole containing 0.1 mol·L$^{-1}$ of $[N^nBu_4][B(C_6F_5)_4]$ as supporting electrolyte at 25 °C and 100 °C, respectively.**

| Compd. | Solvent | $\vartheta$ [°C] | $E^{0'}/\Delta E_p/\Delta E^{0'}$ [mV]$^a$ Wave (no.) | | | | |
|---|---|---|---|---|---|---|---|
| | | | (1) | (2) | (3) | (4) | (5) |
| **D1** | CH$_2$Cl$_2$ | 25 | -103/74 | 135/70/238 | 484/68/349 | | |
| **D3** | CH$_2$Cl$_2$ | 25 | -108/123 | 279/78/387 | 489/80/210 | 623/79/134 | 775/64/152 |
| **D3** | C$_6$H$_5$OCH$_3$ | 25 | -131/102 | 260/79/391 | 471/82/211 | 569/86/98 | |
| **D3** | C$_6$H$_5$OCH$_3$ | 100 | -165/156 | 261/74/426 | 491/78/230 | 651/71/160 | 800/78/149 |

$^a$ Formal potential ($E^{0'}$). Difference between the oxidation ($E_{pa}$) and reduction ($E_{pc}$) peak potential ($\Delta E_p$). Redox separation between the formal iron-based redox events ($\Delta E^{0'} = E^{0'}(2) - E^{0'}(1)$).

The first redox event occurs at $E^{0'} = -103$ mV, the second at 135 mV and the third wave at 484 mV. Each of the three ferrocenyls shows a reversible electrochemical behavior ($68 \leq \Delta E_p \leq 74$ mV). The square wave voltammogram of **D1** is also depicted in Figure D3. With its better resolution it confirms three separated well-shaped one-electron processes, indicating a good interaction between the ferrocenyl termini. The separation between the first and second wave is $\Delta E^{0'} = 238$ mV, while $\Delta E^{0'} = 349$ mV is typical for the difference of the second and third redox process. Thus, during a subsequent oxidation process, mixed-valent intermediates **D1**$^+$ and **D1**$^{2+}$ are formed (Figure D4).

The cyclic and square wave voltammograms of **D1** differ in the potential values of the individual redox processes from **C11**, which is attributed to the various substituents (*vide supra*).[253] As it can be seen from Figure D3, the cyclic voltammogram of **D3** in dichloromethane (bottom, left), utilizing $[N^nBu_4][B(C_6F_5)_4]$ as supporting electrolyte, exhibits five ferrocenyl-related redox events at 25 °C (for data see Table D1). It is obvious that the first wave contains two redox processes close together.
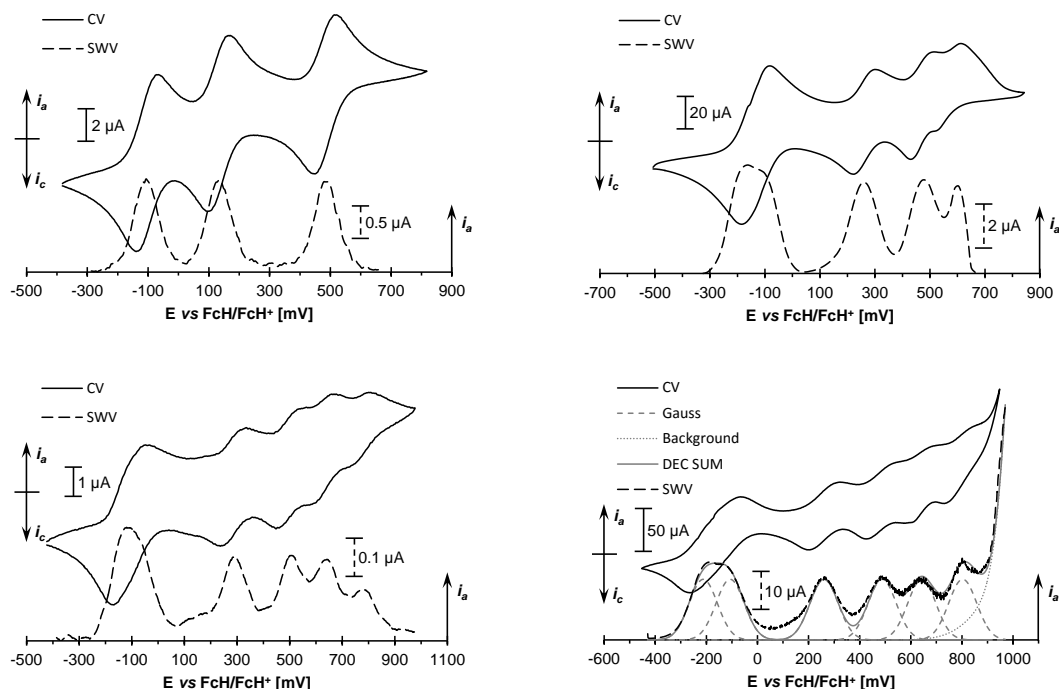
**Figure D3**. Left (top): CV (scan rate: 100 mVs$^{-1}$, left ordinate) and SWV (0.5 Hz, right ordinate) of **D1** in dichloromethane solution (1.0 mM) at 25 °C, supporting electrolyte [N$^n$Bu$_4$][B(C$_6$F$_5$)$_4$] (0.1 M). Left (bottom): CV (scan rate: 200 mV s$^{-1}$, left ordinate) and SWV (0.5 Hz, right ordinate) of **D3** in dichloromethane solution (sat.) at 25 °C, supporting electrolyte [N$^n$Bu$_4$][B(C$_6$F$_5$)$_4$] (0.1 M). Right: CV (scan rate: 100 mVs$^{-1}$, left ordinate) and SWV (1 Hz, right ordinate) of **D3** in anisole solutions (1.0 mM) at 25 °C (top) and at 100 °C (bottom), supporting electrolyte [N$^n$Bu$_4$][B(C$_6$F$_5$)$_4$] (0.1 M). For cyclic voltammetry data see Table D1, abbreviations are explained in context.

The observed current decrease of the 5$^{th}$ redox wave can be explained probably with a less solubility of **D3$^{5+}$** in dichloromethane. Anisole was chosen as further solvent because of the better solubility of **D3** in this medium. The CV measured in anisole at 25 °C (Figure D3; top right) reveals with its formally four redox events a different behavior, which is also most probably attributed to a strong adsorption of **D3$^{5+}$** onto the electrode and as a result the lack of the 6$^{th}$ redox event (*vide supra*).[224,259] To prove this issue, electrochemical experiments on **D3** were carried out at 100 °C (Figure D3; bottom, right). The corresponding cyclic voltammogram offers a similar shape as observed in dichloromethane with five waves at $E^{0'}$ = –165, 261, 491, 651, and 800 mV as well as $\Delta E_p$ values between 71 and 78 mV according to one-electron processes. However, the first redox event shows a peak separation $\Delta E_p$ of 156 mV (Table D1), indicating that this wave corresponds to two redox events close together (*vide supra*). Deconvolution of the SWV confirms this observation, whereas the superposition (DEC SUM) of all processes consists of six one-electron redox events (Gauss) and the increasing background current (background) at the anodic end of the electrochemical window (Figure D3).

In order to get more insight into the oxidation process of **D1** and **D3** we carried out spectroelectrochemical studies by the stepwise increase of the potential *vs.* Ag/AgCl in an

OTTLE (= Optically Transparent Thin Layer Electrochemistry)[238] cell by using dichloromethane (**D1**) or anisole (**D3**) solutions and $[N^nBu_4][B(C_6F_5)_4]$ as supporting electrolyte. This procedure allows the *in situ* generation of $\textbf{D1}^{n+}$ (n = 1, 2, 3) and $\textbf{D3}^{n+}$ (n = 1 – 6) (Figure D4). Compounds **D1** and **D3** do not contain, as expected, any absorptions in the NIR range (Figure D4). In contrast, the spectra of monocationic $\textbf{D1}^+$ and dicationic $\textbf{D1}^{2+}$ show characteristic absorptions for mixed-valent systems (Fe(II)/Fe(III)). Deconvolution of the NIR absorptions of $\textbf{D1}^+$ and $\textbf{D1}^{2+}$ was achieved using three distinct overlapping transitions with Gaussian shapes (Figure D4, top and middle).
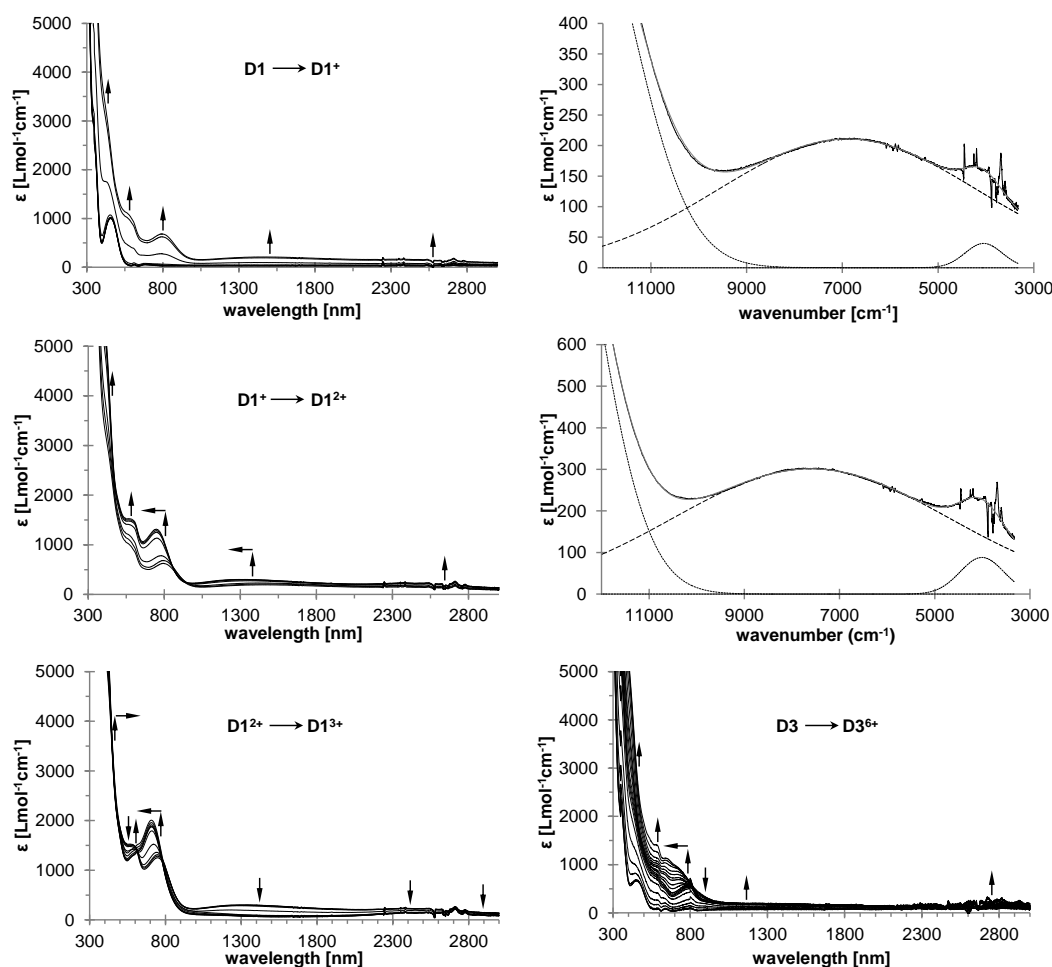


**Figure D4**. UV-Vis-NIR spectra of **D1** (left, right top and middle) and **D3** (right bottom) at rising potentials: –500 to 200 mV (left top), 175 to 400 mV (left middle), 325 to 1000 mV (left bottom) for **D1** and –500 to 1100 mV for **D3** *vs.* Ag/AgCl at 25 °C in dichloromethane (**D1**) or anisole (**D3**), supporting electrolyte $[N^nBu_4][B(C_6F_5)_4]$ (0.1 M). Expanded spectra (right top and middle) display the deconvolution of NIR absorptions at 200 mV (top) and 400 mV (middle) during the successive oxidation of **D1** (dashed line indicate IVCT absorptions, dotted line corresponds to absorptions caused by interactions between ligand and metal as well as ligand field transitions).[253] Arrows indicate increasing or decreasing as well as shifting absorptions.

The fits are good enough to allow an almost exact overlay of the sum of the spectral components with the experimental spectra. During the generation of $\textbf{D1}^+$ a weak low-energy absorption at 1450 nm ($\varepsilon_{max}$ = 210 Lmol$^{-1}$cm$^{-1}$, $\Delta\tilde{\nu}_{1/2}$ = 6367 cm$^{-1}$) was observed, which is attributed to an IVCT transition. It is already known that such class II systems

according to Robin and Day[68] show weak metal-to-metal charge transfer (MMCT) absorptions with peak widths at half height ($\Delta\tilde{v}_{1/2}$) often larger than the predicted values from the Hush model.[61,245] Upon gradual oxidation to the twice oxidized species $D1^{2+}$, a slight hypsochromic and hyperchromic shift of the IVCT band to 1316 nm ($\varepsilon_{max} = 301$ Lmol$^{-1}$cm$^{-1}$, $\Delta\tilde{v}_{1/2} = 6830$ cm$^{-1}$) was detected.

During the successive oxidation process of **D1** typical absorptions in the UV-Vis region of inner ferrocenyl ligand-to-metal charge transfer (LMCT) transitions as well as absorptions which are attributed to LMCT interactions between the thiophene core and the ferrocenyl moieties can be observed (Figure D4).[30,184,225,239–241] Furthermore, a very weak low-energy absorption band was observed close to the IR range (around 4000 cm$^{-1}$), which is too less intense as they can be explained with ligand-to-metal charge transfer interactions. For this reason we attributed this absorption band to a formal forbidden ligand field transition (Figure D4).[242–244] It is noteworthy that the NIR transitions of the mixed-valent complexes $D1^{n+}$ (n = 1, 2) are similar to those of 2,3,4-triferrocenyl thiophene (**C11**), for which IVCT absorptions between 1510 nm (**C11$^{+}$**) and 1330 nm (**C11$^{2+}$**) were found, and 2,5-diferrocenyl thiophene (**C3**) indicating electron transfer properties of the appropriate thiophene (*vide supra*).[171,253] As expected, successive generation of the triple oxidized species $D1^{3+}$ leads to a disappearance of the IVCT absorption.

*In situ* UV-Vis-NIR measurements on solutions of bithiophene **D3** show no significant absorptions between 500 – 3000 nm (Figure D4 right bottom, Figure AD-1). Stepwise oxidation of **D3** up to $D3^{6+}$ led to bands between 300 and 800 nm, similar as described above. Under our conditions no notable transitions which could be attributed to IVCT absorptions were observed in the NIR region, since the weak absorption around 1300 nm shows no decrease in intensity at high potentials (Figure D4, right bottom). However, this observation could be caused by the less solubility of multiple charged positive species (*vide supra*). If there is no IVCT absorption, the ferrocenyl/ferrocenium termini mostly interact electrostatically with each other. This means most likely that the positive charge is localized around the ferrocenium ligands in the mixed-valent partially oxidized intermediates. The same electrochemical behavior was recently found for the supercrowded tetraferrocenyl thiophene $^{c}C_4Fc_4S$.[183]

CONCLUSION

The atropisomeric 3,3',4,4',5,5'-hexaferrocenyl-2,2'-bithiophene (**D3**) is available in a straightforward palladium-promoted Negishi *C,C* coupling of 2-bromo-3,4,5-triferrocenyl thiophene (**D1**) and 2,3,4-triferrocenyl thiophene zinc chloride (**D2**).

The structure of the title compound in the solid state was determined by single crystal X-ray structure analysis, confirming the steric demand of the six ferrocenyl termini at the bithiophene core. This reflects, for example, the out-of-plane tilting of the two thiophene units, associated with the loss of coplanarity of the ferrocenyls with the bithiophene core. The atropisomerism of 3,3',4,4',5,5'-hexaferrocenyl-2,2'-bithiophene was verified by dynamic $^1$H NMR spectroscopy. The activation parameters were determined ($\Delta H^{\ddagger}$ = 54.2 kJmol$^{-1}$, $\Delta S^{\ddagger}$ = –50.4 JK$^{-1}$mol$^{-1}$).

Electrochemical as well as spectroelectrochemical studies indicate that the starting material 2-bromo-3,4,5-triferrocenyl thiophene shows weak electronic coupling between the three partially oxidized ferrocenyl termini, as evidenced by the appearance of IVCT transitions in the NIR region. However, for the hexaferrocenyl bithiophene another electrochemical behavior is characteristic. Due to less solubility of title compound in dichloromethane, as well as the less solubility of the oligo-cationic species, the respective electrochemical measurements had to be carried out in anisole. In the latter case four reversible redox events at $E^{0'}$ = –131, 260, 471, and 569 mV *vs.* FcH/FcH$^+$ are observed at ambient temperature. The formal lack of the sixth redox process is probably caused by a strong adsorption of appropriate penta-cation onto the electrode. However, when the electrochemical experiments were run at 100 °C a total number of five redox processes were observed at $E^{0'}$ = –165, 261, 491, 651, and 800 mV *vs.* FcH/FcH$^+$ with $\Delta E_p$ values between 71 and 78 mV, whereas the first event shows a peak separation $\Delta E_p$ of 156 mV, indicating that this wave corresponds to two redox events close together. Deconvolution of the square wave voltammogram supports this observation. Spectroelectrochemistry of **D3** confirms that upon stepwise oxidation the ferrocenyl termini and electrochemically generated ferrocenium units mostly communicate electrostatically with each other, since no IVCT absorptions were found in the NIR region.

These results empathize that the positive charges are mainly localized on the ferrocenium moieties in the mixed-valent species.

EXPERIMENTAL SECTION

**General Procedures**. All reactions were carried out under an argon atmosphere using standard Schlenk techniques. Tetrahydrofuran, toluene and *n*-hexane were purified by distillation from sodium/benzophenone ketyl. Dichloromethane was purified by distillation from $P_4O_{10}$ and anisole was purified by distillation from calcium hydride.

**Reagents**. Tetra-*n*-butylammonium tetrakis(pentafluorophenyl)borate was prepared by metathesis of lithium tetrakis(pentafluorophenyl)borate etherate (Boulder Scientific) with tetra-*n*-butylammonium bromide, according to a published procedure.[101] All other chemicals were purchased from commercial suppliers and were used as received.

**Instruments**. Infrared spectra were obtained with a Thermo Nicolet 200 FT-IR spectrometer using KBr press techniques for sample preparation. NMR spectra were recorded using an Bruker Avance III 500 FT-NMR spectrometer ($^1$H NMR at 500.303 MHz, $^{13}$C{$^1$H} NMR at 125.813 MHz) at ambient temperature, unless otherwise noted. Chemical shifts ($\delta$) are reported in parts per million (ppm) relative to tetramethylsilane (TMS) using the solvent as internal reference (CDCl$_3$: $^1$H NMR $\delta$ = 7.26 ppm; $^{13}$C{$^1$H} NMR $\delta$ = 77.16 ppm. Toluene-$D_8$: $^1$H NMR $\delta$ = 7.09, 7.01, 6.97, 2.08 ppm; $^{13}$C{$^1$H} NMR $\delta$ = 137.48, 128.87, 127.96, 125.13, 20.43 ppm. Thf-$D_8$: $^1$H NMR $\delta$ = 3.58, 1.72; $^{13}$C{$^1$H} NMR $\delta$ = 67.21, 25.31).[246] Coupling constants ($J$) are reported in Hertz (Hz) and the integrations in number of protons. The following abbreviations are used to describe peak patterns: m = multiplet, s = singlet, pt = pseudo triplet. The melting points (sealed off in argon flushed capillaries) were determined using a Gallenkamp MFB 595 010 M melting point apparatus. Microanalyses were performed using a Thermo FLASHEA 1112 Series instrument. High resolution mass spectra were recorded with a Bruker micrOTOF QII with an Apollo II ESI source.

**Synthesis of 2-bromo-3,4,5-triferrocenylthiophene (D1)**. Thiophene **C11**[253] (1.5 g, 2.36 mmol) was dissolved in 100 mL of tetrahydrofuran, cooled to –40 °C and 1.1 eq (1.04 mL) of an 2.5 M *n*-butyllithium solution in *n*-hexane was added dropwise. The resulting solution was warmed to –25 °C during a period of 35 min, then cooled again to –40 °C, and 1.1 eq (0.3 mL) of 1,1,2,2-tetrabromoethane were added in a single portion. The reaction mixture was warmed to ambient temperature and stirred for additional 3 h. After removal of all volatile materials, the remaining crude product was adsorbed on alumina and purified by column chromatography (column size: 25 x 3 cm) on alumina using an *n*-hexane/toluene mixture of ratio 3:1 (v:v) as eluent. Compound **D1** was obtained from the

first orange fraction (second fraction: thiophene **C11**). After evaporation of all solvents and crystallization from an *n*-hexane/toluene mixture (ratio 5:1, v:v), compound **D1** was obtained as orange needles. Yield: 654 mg (0.94 mmol, 40 % based on **C11**). Anal. calcd for $C_{34}H_{27}BrFe_3S$ (715.08): C, 57.11; H, 3.81. Found: C, 57.35; H, 3.89. Mp: 195 °C (dec). IR data (KBr) [cm$^{-1}$]: 3089 w, 1636 w, 1410 w, 1106 m, 1000 s, 814 s, 501 s, 486 s, 475 s. $^1$H NMR (CDCl$_3$) [$\delta$]: 4.74 (pt, $J_{HH}$ = 1.7 Hz, 2H, C$_5$H$_4$), 4.39 (pt, $J_{HH}$ = 1.7 Hz, 2H, C$_5$H$_4$), 4.34 (s, 5H, C$_5$H$_5$), 4.17 (s, 5H, C$_5$H$_5$), 4.12 (pt, $J_{HH}$ = 1.7 Hz, 2H, C$_5$H$_4$), 4.08 (pt, $J_{HH}$ = 1.7 Hz, 2H, C$_5$H$_4$), 4.01 (pt, $J_{HH}$ = 1.7 Hz, 2H, C$_5$H$_4$), 3.85 (pt, $J_{HH}$ = 1.7 Hz, 2H, C$_5$H$_4$), 3.66 (s, 5H, C$_5$H$_5$). $^{13}$C{$^1$H} NMR (CDCl$_3$) [$\delta$]: 138.8 (C$_i$-C$_4$BrS), 138.5 (C$_i$-C$_4$BrS), 136.8 (C$_i$-C$_4$BrS), 107.3 (C$_{Br}$-C$_4$BrS), 84.0 (C$_i$-C$_5$H$_4$), 82.2 (C$_i$-C$_5$H$_4$), 81.7 (C$_i$-C$_5$H$_4$), 73.5 (C$_5$H$_4$), 72.4 (C$_5$H$_4$), 70.8 (C$_5$H$_4$), 70.3 (C$_5$H$_5$), 69.5 (C$_5$H$_5$), 69.0 (C$_5$H$_5$), 68.3 (C$_5$H$_4$), 66.8 (C$_5$H$_4$), 66.7 (C$_5$H$_4$). HR-ESI MS (calcd) {int} [m/z]: 713.9055 (713.9065) {100} [M]$^+$, 715.9042 (715.9041) {97} [M]$^+$.

**Synthesis of 3,3',4,4',5,5'-hexaferrocenyl-2,2'-bithiophene (D3)**. Molecule **D1** (450 mg, 0.63 mmol) was dissolved in 20 mL of tetrahydrofuran. This solution was treated with 1.1 eq (0.28 mL) of a 2.5 M *n*-butyl lithium solution in *n*-hexane at –50 °C. After 45 min isotherm stirring, 1.1 eq (194.2 mg) of [ZnCl$_2$·2thf] were added in a single portion. The resulting mixture was warmed to 0 °C and stirred for 1 h at this temperature. Afterward, one equivalent of **D1** and 10 mg (14.6 μmol) of [Pd(CH$_2$CMe$_2$P$^t$Bu$_2$)($\mu$-Cl)]$_2$[229,230] were added in a single portion. The resulting reaction mixture was warmed to 55 °C and stirred for 48 h at this temperature. After evaporation of all volatiles in vacuum, the crude product was adsorbed on alumina and purified by column chromatography (column size: 15 x 3 cm) on alumina using an *n*-hexane/toluene mixture of ratio 2:1 (v:v) as eluent. Compound **D3** was obtained from the third orange fraction (eluted with toluene; first fraction: **D1**; second fraction: **C11**). After evaporation of all solvents and crystallization from an *n*-hexane/toluene mixture (ratio 4:1, v:v) orange plates could be isolated. Yield: 360 mg (0.28 mmol, 45 % based on 1 eq of **D1**). Anal. calcd for $C_{68}H_{54}Fe_6S_2$·$C_7H_8$ (1362.49): C, 66.11; H, 4.59. Found: C, 65.91; H, 4.52. Mp: 250 °C (dec). IR data (KBr) [cm$^{-1}$]: 3083 w, 2919 w, 1639 w, 1410 w, 1106 s, 999 m, 818 s, 500 s, 474 s. $^1$H NMR (thf-$D_8$) [$\delta$]: 4.98 (m, 2H, C$_5$H$_4$), 4.76 (m, 2H, C$_5$H$_4$), 4.54 (s, 10H, C$_5$H$_5$), 4.51 (m, 2H, C$_5$H$_4$), 4.47 (m, 2H, C$_5$H$_4$), 4.43 (m, 2H, C$_5$H$_4$), 4.26 (m, 2H, C$_5$H$_4$), 4.16 (s, 10H, C$_5$H$_5$), 4.14 (m, 2H, C$_5$H$_4$), 4.03 (m, 2H, C$_5$H$_4$), 3.95 (m, 2H, C$_5$H$_4$), 3.79 (m, 2H, C$_5$H$_4$), 3.65 (s, 10H, C$_5$H$_5$), 3.62 (m, 2H, C$_5$H$_4$), 3.37 (m, 2H, C$_5$H$_4$). $^{13}$C{$^1$H} NMR (thf-$D_8$) [$\delta$]: 139.6 (C$_i$-C$_4$S), 139.2 (C$_i$-C$_4$S), 138.3 (C$_i$-C$_4$S), 128.9 (C$_i$-C$_4$S), 85.5 (C$_i$-C$_5$H$_4$), 83.6 (C$_i$-C$_5$H$_4$), 83.4 (C$_i$-C$_5$H$_4$), 77.3

($C_5H_4$), 74.7 ($C_5H_4$), 73.7 ($C_5H_4$), 73.2 ($C_5H_4$), 73.0 ($C_5H_4$), 71.5 ($C_5H_4$), 70.7 ($C_5H_5$), 69.7 ($C_5H_5$), 69.2 ($C_5H_5$), 68.8 ($C_5H_4$), 68.5 ($C_5H_4$), 67.7 ($C_5H_4$), 67.4 ($C_5H_4$), 67.1 ($C_5H_4$), 66.4 ($C_5H_4$). HR-ESI-MS (calcd) [m/z]: 1269.9746 (1269.9771) $[M]^+$.

**Electrochemistry**. Electrochemical measurements were carried out under an argon atmosphere on 1.0 mM dichloromethane and anisole solutions of **D1** and **D3** containing 0.1 $molL^{-1}$ of $[N^nBu_4][B(C_6F_5)_4]$ as supporting electrolyte,[90,100] utilizing a Voltalab 10 electrochemical laboratory from Radiometer Analytical. A three-electrode cell, which utilized a platinum auxiliary electrode, a platinum working electrode and a $Ag/Ag^+$ reference electrode, was used. For high temperature electrochemistry a saturated calomel electrode (SCE) as reference electrode was applied. The working electrodes were prepared by polishing with a Buehler micro cloth using Buehler diamond pastes with decreasing sizes (1 to 0.25 μm). The $Ag/Ag^+$ reference electrode was constructed from a silver wire inserted into a Luggin capillary with a Vycor tip containing a solution of 0.01 M $[AgNO_3]$ as well as $[N^nBu_4][B(C_6F_5)_4]$ (0.1 M) in acetonitrile. This Luggin capillary was inserted into a second Luggin capillary with Vycor tip filled with a 0.1 M $[N^nBu_4][B(C_6F_5)_4]$ solution in dichloromethane. Successive experiments under the same experimental conditions showed that all formal reduction and oxidation potentials were reproducible within 5 mV. Experimentally potentials were referenced against $Ag/Ag^+$ or SCE reference electrodes, but the presented results are referenced against the $FcH/FcH^+$ couple ($E^{0'} = 0.0$ V) as required by IUPAC.[249] When decamethylferrocene was used as an internal standard, the experimentally measured potential was converted into $E$ *vs.* $FcH/FcH^+$ by addition of –0.61 V.[250] The cyclic voltammograms which are shown were taken after typical two scans and are considered to be steady-state cyclic voltammograms, in which the signal pattern differs not from the initial sweep. Finally, the experimental data were processed on Microsoft Excel worksheets.

**Crystallography**. Crystal data for **D3**·1.5$C_7H_8$, $Mr$ = 1408.53 $gmol^{-1}$, triclinic, $P\bar{1}$, $a$ = 13.1164(12) Å, $b$ = 14.1721(12) Å, $c$ = 17.7987(14) Å, $\alpha$ = 77.124(7) °, $\beta$ = 82.581(7) °, $\gamma$ = 68.966(8) °, $V$ = 3006.0(4) $Å^3$, $Z$ = 2, $\rho_{calcd}$ = 1.556 $gcm^{-3}$, $\mu$ = 1.527 $mm^{-1}$, $T$ = 110 K, $\Theta$ range = 2.98 – 26.00 °, reflections collected: 20973, independent: 11569 ($R_{int}$ = 0.0377), $R_1$ = 0.0375, $wR_2$ = 0.0773 [$I > 2\sigma(I)$]. Single crystals of **D3** were obtained by diffusion of *n*-hexane into a toluene solution containing **D3** at 25 °C. Data were collected with an Oxford Gemini S Diffractometer, with graphite monochromatized Mo K$\alpha$ radiation ($\lambda$ = 0.71073 Å) using oil-coated shock-cooled crystals. The structure was solved by direct methods and refined by full-matrix least square procedures on $F^2$.[251,252]

**Supporting Information**. UV-Vis-NIR spectra of **D3** in dichloromethane is available in the Appendix Section (Chapter AD, *vide infra*).

# E   FUNCTIONALIZATIONS ON 2,5-DIFERROCENYLTHIOPHENES AND THEIR IMPLICATIONS ONTO ELECTRONIC PROPERTIES

## E1   ANION'S ROLE CONCERNING CHARGE TRANSFER IN CATIONIC MIXED-VALENCE COMPLEXES – A COMPACT STUDY

J. M. Speck and Heinrich Lang

*Section E1 was made by the author of the present doctoral thesis, including all experimental works and the interpretation of the results, in supervision of Prof. Dr. Heinrich Lang.*

INTRODUCTION

During the last two decades, intense research activities in the field of weakly coordinating anions (WCAs) have been carried out.[89,91,95,100,101,105,106,123] Especially the possibility to analyze sensitive species electrochemically under "pseudo gas phase conditions",[91,108] *inter alia* due to the high dissociation constants of WCA salts in non-polar media, highlights their application potential (Chapter B, *quod vide*).[91,95,101,105,106] Fundamental studies on varying redox separations ($\Delta E^{0'}$) of oligometallic complexes in dependency of solvent and anion properties, reported by Geiger *et al.*, elucidate the significance of the counter ion on the thermodynamic stability ($K_C$) of oxidized or reduced species.[90,95,98–101,105,106,260] Moreover, an increased redox separation for a symmetric, bimetallic system could be an indication for a larger resonance interaction (communication) between the metal centers.[37,50,56,73] For weak and moderately coupled systems, a solvatochromic shift of the corresponding charge transfer absorption band can usually be observed, in dependence on the applied solvents as well as the degree of electronic coupling.[37,49,50,57,68,123,261] However, there is some controversy in the literature regarding the influence of anion's ion-pairing/coordinating properties on charge transfer interactions in these cationic donor-acceptor systems, *vice versa* for anionic systems.[123,262]

One well-suited reference system for the investigation of such influences should be biferrocene (BfcH). The corresponding mono-cation, known in literature for decades, is well-investigated regarding the electrochemical behavior/electronic coupling and its classification as a strongly coupled class II (borderline class II/III) system within the Robin and Day regime is commonly accepted, *inter alia* well-separated redox events in combination with relatively intense and solvatochromic inter valence charge

transfer (IVCT) absorptions (temperature-dependent charge localization-delocalization transition).[49,50,56,67,68,115–117,123,126,127,149,242,263–265]


RESULTS AND DISCUSSION

The electrochemical studies on solutions of biferrocene were carried out under an argon atmosphere using dichloromethane (DCM), acetonitrile (AN) or propylene carbonate (PC) as solvent, which contains either $[N^nBu_4][B(C_6F_5)_4]$ (0.1 M) or $[N^nBu_4][PF_6]$ (0.1 M) as supporting electrolyte (Experimental Section).

Under our conditions, biferrocene shows two well-resolved, reversible (Nernstian) ferrocenyl-based redox events with small $\Delta E_p$ values and $i_{pc}/i_{pa}$ ratios close to unity (Table E1 and Figure E1).[80,85,234,235]
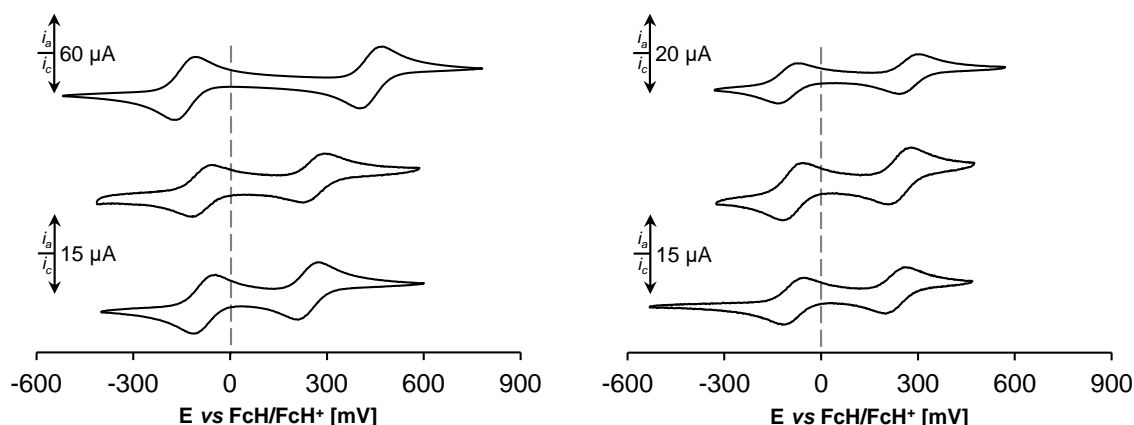


**Figure E1**. Cyclic voltammograms of biferrocene (BfcH) in dichloromethane (top), acetonitrile (middle) and propylene carbonate (bottom). Scan rate: 100 mVs$^{-1}$ in 1.0 mM (left top), 0.5 mM (right top) and 0.25 mM solutions at 25 °C, 0.1 M supporting electrolyte $[N^nBu_4][B(C_6F_5)_4]$ (left) or $[N^nBu_4][PF_6]$ (right).

Especially in low polarity media, WCA-containing electrolytes, *e.g.* $[B(C_6F_5)_4]^-$ and $[B(3,5-(CF_3)_2-C_6H_3)_4]^-$, are able to "outplay" their potential for enlarging the thermodynamic stability of mixed-valent species (*vide supra*).[90,101,266] Thus, by using DCM/$[N^nBu_4][B(C_6F_5)_4]$ a redox separation for BfcH of $\Delta E^{0'}$ = 573 mV was found, comparable to previously reported data (Table E1, Figure E1).[98] The corresponding value for $K_C$ decreases by changing the anion to hexafluorophosphate, as expected.[90,98,100,267] Further increasing of the solvent's polarity/ solvation ability leads to either slight or negligible variations in the thermodynamic stability of BfcH$^+$ (Table E1, Figure E1).[98,267,268] The related Gibbs energy consists *inter alia* of terms caused by Coulomb as well as resonance interactions (Chapter B, *vide supra*). One indication, that an increasing $\Delta E^{0'}$ (by a formal reducing the anion's ion-pairing properties) isn't mainly caused from

electrostatic interactions, is represented by a cathodic shift of the 1st bimetallocene redox process compared with the appropriate monometallic derivative (Table E1, Figure E1).[51]

**Table E1. Cyclic voltammetry data (potentials *vs.* FcH/FcH⁺) of biferrocene solutions at 25 °C.**

| solvent/supporting electrolyte (0.1 M)[a] | $E^{0'}/\Delta E_p$ [mV][e] wave (no.) (1) | (2) | $\Delta E^{0'}$ [mV][f] | $K_C$ [10⁵][g] |
|---|---|---|---|---|
| DCM/[N$^n$Bu$_4$][B(C$_6$F$_5$)$_4$][b] | –137/62 | 436/64 | 573 | 48492.5 |
| AN/[N$^n$Bu$_4$][B(C$_6$F$_5$)$_4$][c] | –89/64 | 257/64 | 346 | 7.1 |
| PC/[N$^n$Bu$_4$][B(C$_6$F$_5$)$_4$][c] | –81/64 | 241/68 | 322 | 2.8 |
| DCM/[N$^n$Bu$_4$][PF$_6$][d] | –103/62 | 272/60 | 375 | 21.8 |
| AN/[N$^n$Bu$_4$][PF$_6$][c] | –87/60 | 243/68 | 330 | 3.8 |
| PC/[N$^n$Bu$_4$][PF$_6$][c] | –84/62 | 231/68 | 315 | 2.1 |

[a] DCM = dichloromethane, AN = acetonitrile, PC = propylene carbonate. [b] 1.0 mM analyte. [c] 0.25 mM analyte. [d] 0.5 mM analyte. [e] Formal potential ($E^{0'}$). Difference between the oxidation ($E_{pa}$) and reduction ($E_{pc}$) peak potential ($\Delta E_p$). [f] Redox separation between the formal iron-based redox events ($\Delta E^{0'} = E^{0'}(2) - E^{0'}(1)$). [g] Comproportionation constant $\left(K_C = e^{\frac{\Delta E^{0'} F}{RT}}\right)$.

Furthermore during solid-state analyses, a strong dependence of iron-iron electronic coupling in mixed-valent biferrocenium salts on their environment and the anion was reported.[121] During spectroscopic studies on liquid solutions of BfcH⁺ derivatives, a solvatochromism of NIR absorptions was reported not only induced by the solvent itself.[58,122–125,269] However, in recent studies regarding the influence of the anion on inter valence charge transfer, using dinuclear ruthenium and osmium complexes in acetonitrile solutions, just a less significant effect of the anion association on the electronic coupling was noted.[262] Thus, for a deeper insight regarding this topic, *in situ* spectroelectrochemical studies were carried out by an stepwise increase of the potential (varying step heights: 5 – 100 mV) *vs.* Ag/AgCl in an OTTLE[238] (= Optically Transparent Thin Layer Electrochemistry) cell using a 0.1 M dichloromethane ($\mu$ = 1.6 D) solution of [N$^n$Bu$_4$][B(C$_6$F$_5$)$_4$] and [N$^n$Bu$_4$][PF$_6$] as supporting electrolytes.[270]

**Table E2. NIR data of BfcH⁺ at 25 °C.**

| Compd. | Transition | $\tilde{v}_{max}$ [cm⁻¹][a] ($\varepsilon_{max}$ [Lmol⁻¹cm⁻¹])[a,b] | $\Delta\tilde{v}_{1/2}$ [cm⁻¹][a,c] | $\Delta\tilde{v}_{1/2(theo)}$ [cm⁻¹][d] | $\tilde{v}_{max\text{-}IVCT\text{-}AN}$ [cm⁻¹][e] ($\Delta\tilde{v}_{1/2\text{-}AN}$ [cm⁻¹])[f] {$\Delta\tilde{v}_{max\text{-}IVCT}$ [cm⁻¹]}[g] | $\tilde{v}_{max\text{-}IVCT\text{-}PC}$ [cm⁻¹][h] ($\Delta\tilde{v}_{1/2\text{-}PC}$ [cm⁻¹])[i] {$\Delta\tilde{v}_{max\text{-}IVCT}$ [cm⁻¹]}[g] |
|---|---|---|---|---|---|---|
| **[BfcH] [B(C$_6$F$_5$)$_4$]** | IVCT | 4440 (1360) | 3510 | 3200 | 5490 | 5540 |
|  | IC/LF | 3880 (310) | 590 |  | (4160) | (4140) |
|  | IC/LF | 3330 (910) | 900 |  | {1050} | {1100} |
| **[BfcH] [PF$_6$]** | IVCT | 5030 (1010) | 3690 | 3410 | 5560 | 5570 |
|  | IC/LF | 3920 (100) | 320 |  | (4120) | (4240) |
|  | IC/LF | 3550 (490) | 1000 |  | {530} | {540} |

[a] Measured in dichloromethane. [b] Wavenumber of the bands maximum intensity ($\tilde{v}_{max}$), extinction coefficient at $\tilde{v}_{max}$ ($\varepsilon_{max}$). [c] Bandwidth at half height ($\Delta\tilde{v}_{1/2}$). [d] Bandwidth at half height expected from the Hush theory ($\Delta\tilde{v}_{1/2(theo)} = (2310\tilde{v}_{max})^{1/2}$). [e] Measured in acetonitrile (AN). [f] $\Delta\tilde{v}_{1/2}$ of the IVCT transition measured in AN. [g] Solvatochromic shift ($\Delta\tilde{v}_{max\text{-}IVCT} = \tilde{v}_{max\text{-}IVCT\text{-}AN/PC} - \tilde{v}_{max}$). [h] Measured in propylene carbonate (PC). [i] $\Delta\tilde{v}_{1/2}$ of the IVCT transition measured in PC.

The solvatochromism was evaluated by using acetonitrile ($\mu$ = 3.9 D) and propylene carbonate ($\mu$ = 4.9 D) as more polar solvents.[270] For deconvolution of NIR absorptions, three Gaussian-shaped transitions were used to get fits good enough for an almost exact overlay with the sum of the experimental spectral components. The corresponding spectra are presented in Figures E2, E3 and NIR data are presented in Table E2.
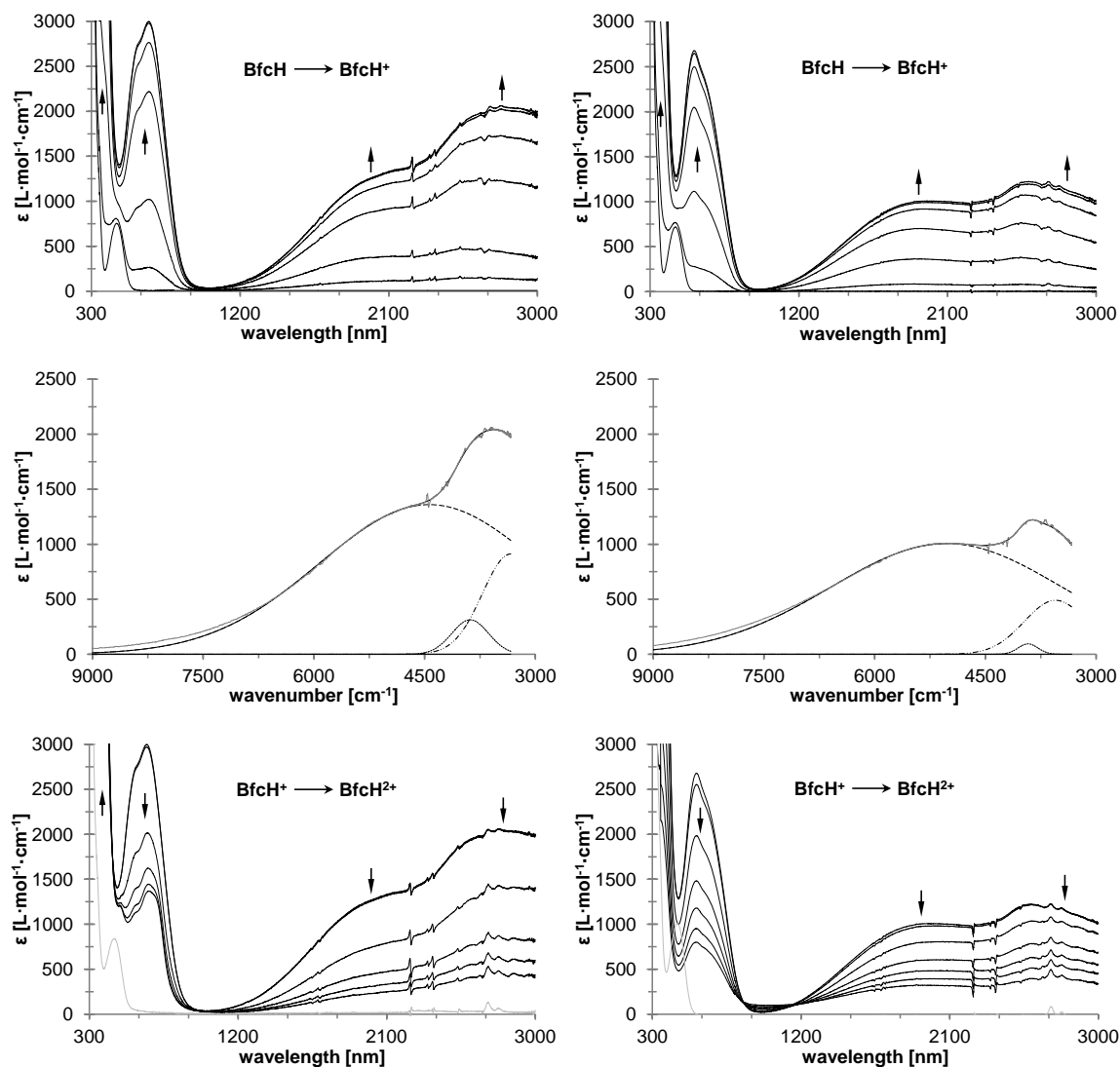


**Figure E2**. UV-Vis-NIR spectra of biferrocene (BfcH) at rising potentials, Measured in dichloromethane containing 0.1 M [N$^n$Bu$_4$][B(C$_6$F$_5$)$_4$] (left) or 0.1 M [N$^n$Bu$_4$][PF$_6$] as supporting electrolyte at 25 °C. Potentials *vs.* Ag/AgCl.[238] Left: –500 to 550 mV (top); deconvolution of NIR absorptions at 550 mV (middle) using three distinct overlapping transitions with Gaussian shapes (dashed line indicates IVCT absorption, dotted line corresponds to absorptions caused by interactions between ligand and metal, dotted dashed line indicates IC/LF transitions); 550 to 1300 mV (bottom), grey line represents re-reduction to the neutral species. Right: –100 to 400 mV (top); deconvolution of NIR absorptions at 400 mV (middle) using three distinct overlapping transitions with Gaussian shapes (dashed line indicates IVCT absorption, dotted line and dotted dashed line indicate IC/LF transitions); 400 to 900 mV (bottom), grey line represents re-reduction to the neutral species. Arrows indicate increasing or decreasing as well as shifting absorptions.

During the *in situ* generation of [BfcH][B(C$_6$F$_5$)$_4$] in dichloromethane intense low-energy NIR absorptions could be found in which the more hypsochromic shifted band (around 4400 cm$^{-1}$ under these conditions) is well-known as IVCT absorption (Figure

E2).[70,115,126,127] A very characteristic behavior of such transitions is represented by the occurrence of a negative solvatochromism when the solvent is changed.[63,70,242] Thus by varying the solvent to more polar media (AN and PC), the latter absorption band for [BfcH][B(C$_6$F$_5$)$_4$] is shifted hypsochromically (also hypochromic) by more than 1000 cm$^{-1}$ to higher energies (Table E2 and Figure E3). When the anion was changed to hexafluorophosphate, very similar results were obtained for the corresponding acetonitrile and propylene carbonate solutions (Table E2 and Figure E3).
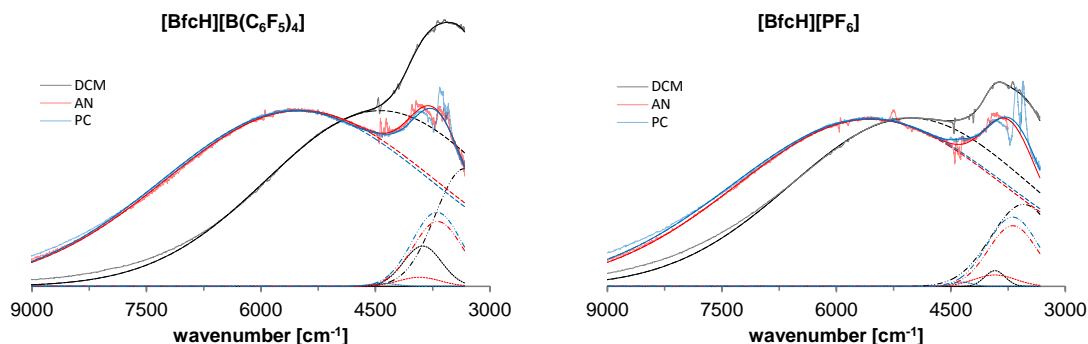


**Figure E3**. Deconvolution of NIR absorptions (normalized intensities, using three Gaussian-shaped transitions) of *in situ* generated [BfcH][B(C$_6$F$_5$)$_4$] or [BfcH][PF$_6$]. Measured in dichloromethane (DCM), acetonitrile (AN) and propylene carbonate (PC) containing 0.1 M [N$^n$Bu$_4$][B(C$_6$F$_5$)$_4$] (left) or 0.1 M [N$^n$Bu$_4$][PF$_6$] (right) as supporting electrolyte at 25 °C (dashed line indicates IVCT absorption, dotted line and dotted dashed line indicate IC/LF transitions).[238]

However, a significant difference could be recorded by comparing the NIR absorptions of [BfcH][PF$_6$] with [BfcH][B(C$_6$F$_5$)$_4$] in dichloromethane solutions (Figures E2, E3 and Table E2). Due to hexafluorophosphate's stronger coordinating properties, the inter valence charge transfer absorption band could be found as less intense and more shifted to higher energies ($\tilde{v}_{max}$ = 5030 cm$^{-1}$) with regard to the appropriate WCA electrolyte. The corresponding solvatochromic shift amounts to only $\Delta\tilde{v}_{max\text{-}IVCT}$ = 530 cm$^{-1}$ (Table E2), a verification of previously published values.[70,122]


CONCLUSION
Within this study biferrocene, taken as benchmark system, was investigated with the aim to estimate the influence of anion's coordination/pairing properties on the electronic coupling in cationic mixed valent species. The dependency on the solvent polarity was determined by using dichloromethane, acetonitrile and propylene carbonate.

During the electrochemical studies a strong influence of supporting electrolyte's anion on the thermodynamic stability of BfcH$^+$ was found, primary in low-polarity media and

similar as reported for other systems previously.[90,95,100,105] The obtained electrochemical data for biferrocene are in good agreement with literature-known values.[98,267]

Within the UV-Vis-NIR spectroelectrochemical investigations, the recorded data during the generation of [BfcH][PF$_6$] verify the already published absorption behavior.[70,122,123] However, significant differences in the NIR absorption behavior could be detected for [BfcH][B(C$_6$F$_5$)$_4$] in comparison with the hexafluorophosphate derivative, when the solvent polarity is decreased (dichloromethane). Thus, if polar solvents such as acetonitrile and propylene carbonate are applied for the investigation of mixed-valent compounds, the solvation of the latter species will de dominated by the solvent itself (ions separated by solvent molecules) and the nature of the counter ion (anion) is less important. In analogy to the strong dependence of redox separation ($E^{0'}$) on the ion-pairing in less polar solvents, the anion properties have also a huge impact on the electronic coupling of redox-active species in the corresponding inter valent states. Therefore, in dichloromethane the electronic structure of mixed valent BfcH$^+$ undergoes a higher degree of distortion in presence of stronger coordinating anions, such as hexafluorophosphate or [SbF$_6$]$^-$.[70] While, for weakly coordinating anions, *e.g.* [B(C$_6$F$_5$)$_4$]$^-$, the charge distribution in these mixed valent species reaches higher symmetry until the anion becomes infinitely large (gas phase).

Hence, the role of the anion (counter ion) should be considered as not unimportant in the context of quantum chemical verifications of such charge transfer phenomena.

EXPERIMENTAL SECTION

**Solvents and Reagents.** Biferrocene was synthesized from *in situ* generated ferrocenyl zinc chloride and bromoferrocene in a Pd-promoted Negishi *C,C* cross-coupling reaction (yield: 60 %), similar as reported previously.[210,253,271] Otherwise, biferrocene could be obtained as one side product from Negishi ferrocenylation reactions. Dichloromethane was purified by distillation from CaH$_2$ and stored over molecular sieve (4 Å). Acetonitrile (analytical grade) was ordered from Acros Organics and stored over molecular sieve (4 Å). [N$^n$Bu$_4$][B(C$_6$F$_5$)$_4$] was prepared by metathesis of Li[B(C$_6$F$_5$)$_4$]·$n$Et$_2$O (Boulder Scientific) with [N$^n$Bu$_4$]Br according to a published procedure.[101] Its purification was enhanced by a filtration step of the crude product through a pad of silica using dichloromethane as solvent. All other chemicals were purchased from commercial suppliers and were used as received.

**Electrochemistry.** For electrochemical measurements, a Voltalab 10 electrochemical laboratory from Radiometer Analytical was used. All experiments were carried out under an atmosphere of argon on dichloromethane, acetonitrile and propylene carbonate solutions of the analyte, containing 0.1 mol·$L^{-1}$ of $[N^nBu_4][B(C_6F_5)_4]$ or $[N^nBu_4][PF_6]$ as supporting electrolyte, otherwise noted.[90,100] For spectroelectrochemical measurements, an OTTLE cell (= Optically Transparent Thin Layer Electrochemistry) placed in a Varian Cary 5000 UV-VIS-NIR absorption spectrometer was used.[238] A verification of the obtained extinction coefficients was made within additional UV-Vis spectroscopic measurements. For voltammetry, a three electrode cell with a platinum auxiliary electrode, a glassy carbon working electrode (3.0 mm in diameter) and a $Ag/Ag^+$ reference electrode were used. The working electrode was prepared by polishing with Buehler MicroFloc using Buehler diamond suspensions with decreasing sizes (1 to 0.25 μm). The $Ag/Ag^+$ reference electrode was constructed from a silver wire inserted into a Luggin capillary with a Vycor tip containing a solution of 0.01 mol·$L^{-1}$ $[AgNO_3]$ and 0.1 mol·$L^{-1}$ of the supporting electrolyte in acetonitrile. This Luggin capillary was inserted into a second Luggin capillary with a Vycor tip filled with a 0.1 mol·$L^{-1}$ supporting electrolyte solution in the corresponding solvent. Alternatively, a silver wire as quasi-reference electrode was applied. Successive experiments under the same experimental conditions showed that all formal reduction and oxidation potentials were reproducible within ±5 mV. Experimentally potentials were referenced against a $Ag/Ag^+$ reference electrode but the results are presented referenced against the FcH/FcH$^+$ couple ($E^{0'}$ = 0.0 V) as required by IUPAC.[249] Within this context, decamethylferrocene was used as an internal standard and the experimentally measured potentials were converted into *E vs* FcH/FcH$^+$ by addition of -0.61 V.[250,272] The cyclic voltammograms were taken after typical two scans and are considered to be steady state cyclic voltammograms, in which the signal pattern differs not from the initial sweep. Finally, the experimental data were processed on Microsoft Excel worksheets.

## E2 SUBSTITUENT INFLUENCE ON CHARGE TRANSFER INTERACTIONS IN α,α'-DIFERROCENYLTHIOPHENES

J. M. Speck, M. Korb, T. Rüffer, A. Hildebrandt and Heinrich Lang

*Section E2 was made by the author of the present doctoral thesis (synthesis, characterization, electrochemistry, interpretation of results and manuscript preparation) together with M. Korb (solid-state structure determination, discussion), T. Rüffer (solid-state structure determination) and A. Hildebrandt (manuscript corrections), in supervision of Prof. Dr. Heinrich Lang.*

INTRODUCTION

During the rapid miniaturization process of electronic devices requires the development of well-designed new materials. Since the discovery of polyacetylene in 1977,[11] over 50,000 articles have been published regarding intrinsic conducting polymers (ICP), *inter alia* dealing with aniline, pyrrole and especially thiophene derivatives.[12–14]

Within this context, organometallic building blocks connected with such $\pi$-conjugated hydrocarbons are of potential interest concerning their application in molecular electronics.[43–45] Moreover, they can be considered as model systems for molecular wires.[38,46–48,178] In this regard, redox-active transition metal fragments, for example, the ferrocenyl moiety with its excellent stability in both, the neutral and the oxidized state, are versatile building blocks for the investigation of electronic properties,[166,171,173,179,180,183,210,224,253,273,274] and hence ferrocenyl-substituted aromatics have been applied for studying charge transfer interactions.[171–173,178–180,184,253] Fascinating examples of this family of compounds are the perferrocenylated derivatives of benzene, cyclopentadienyl-manganese(I) tricarbonyl, furan, pyrroles and thiophenes.[179,183,210,223,232] However, the electronic coupling in the corresponding mixed-valent states depends strongly on the electronic structure of the respective species: *i.e.* the nature of the arene/heterocycle and the redox-active unit itself.[31,166,171,173,180,184,253]

Recently, it was shown that a variation of the substitution pattern in ferrocenyl thiophenes reaches a maximum of electronic interaction, if the ferrocenyls are bonded at the thiophene $\alpha$-carbon atoms.[253]

In continuation of this work, we herein report on the charge transfer interactions within a series of *α,α'*-diferrocenyl thiophenes. The ferrocenyl termini are substituted by electron

withdrawing groups (Figure E4), while the thiophene itself was modified in *β*-positions with an ethylenedioxy bridge. The electronic properties of these compounds were investigated by electrochemical studies, *inter alia* by the use of UV-Vis-NIR and infrared spectroelectrochemical techniques.[171,253]
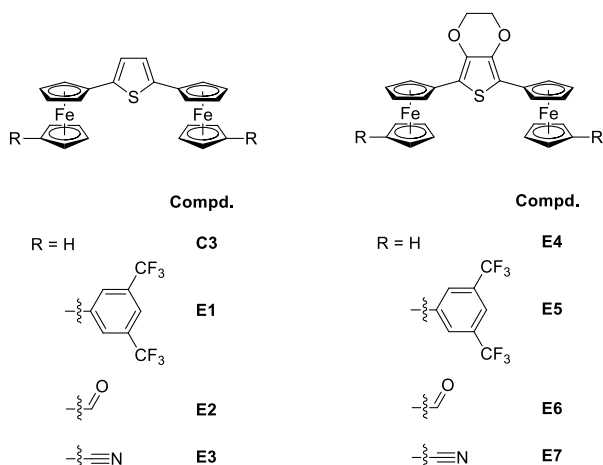


**Figure E4**. Ferrocenyl thiophenes **C3**[171,253], **E1** – **E3** and 3,4-ethylene-dioxy thiophenes **E4** – **E7**.

RESULTS AND DISCUSSION

**Synthesis and Characterization.** Within the synthesis procedures of thiophenes **E1** – **E7** (Figure E4), the linking between the thiophene core and the ferrocenyls was performed by a *C,C* cross-coupling reaction using typical Negishi conditions.[223,228,253] Thus, compound **E4** was accessible in analogy to the preparation of 2,5-diferrocenyl thiophene (**C3**) by a Pd-catalyzed[229,230,275] conversion of 2,5-dibromo-3,4-ethylenedioxy thiophene[27,167,276] with *in situ* generated ferrocenyl zinc chloride, wherein FcZnCl (Fc = Fe($\eta^5$-C$_5$H$_4$)($\eta^5$-C$_5$H$_5$)) was prepared from lithioferrocene[247] in a metathesis reaction with equimolar amounts of [ZnCl$_2$·2thf] (Experimental Section).[253]

**Scheme E1. Synthesis of E1, E2 and E4 – E6.**
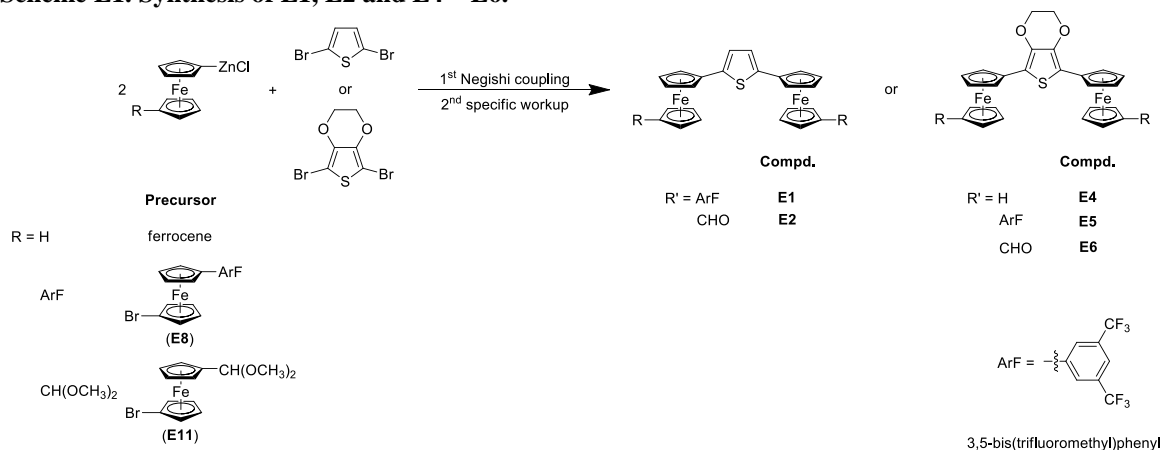


After appropriate workup, compound **E4** was isolated as an orange solid. For the synthesis of the ArF-substituted (ArF = 3,5-bis(trifluoromethyl)phenyl)[100] derivatives **E1** and **E5**

(Figure E4, Scheme E1), $Fe(\eta^5\text{-}C_5H_4Br)(\eta^5\text{-}C_5H_4ArF)$ (**E8**) was synthesized in a palladium-promoted *C,C* cross-coupling reaction of *in situ* generated $Fe(\eta^5\text{-}C_5H_4Br)(\eta^5\text{-}C_5H_4ZnCl)$ and 1-bromo-3,5-bis-(trifluoro-methyl)benzene (Scheme E1, Experimental Section, Appendix AE2). To obtain **E8** (Scheme E1) in good yields, an excess of 1-bromo-3,5-bis(trifluoromethyl)benzene and reaction temperatures below 35 °C are necessary, whereas higher temperatures resulted in an increased formation of 1-bromo-1'''-(3,5-bis(trifluoromethyl)-phenyl)-1',1''-biferrocene (**E10**) (Appendix AE2). Bromoferrocene **E8** could be converted into $Fe(\eta^5\text{-}C_5H_4ArF)(\eta^5\text{-}C_5H_4ZnCl)$ in consecutive reaction steps, applying a lithium-bromine exchange reaction followed by addition of equimolar amounts of $[ZnCl_2\cdot2thf]$. The resulting organozinc species was further reacted with either 2,5-dibromothiophene or the corresponding ethylenedioxy derivative to obtain **E1** and **E5,** respectively (Scheme E1, Experimental Section). For the preparation of diformyl compounds **E2** and **E6** (Scheme E1), 1-bromo-1'-formylferrocene[277] was converted to dimethyl acetal **E11** in a proton-catalyzed reaction with trimethoxy methane (Appendix Chapter AE2).

*Caution!* **E11** is very sensitive towards acids and hydrolyzes rapidly in solvents such as chloroform and dichloromethane. Furthermore, $Fe(\eta^5\text{-}C_5H_4CH(OMe)_2)(\eta^5\text{-}C_5H_4ZnCl)$ was accessible by a synthetic route similar to that for $Fe(\eta^5\text{-}C_5H_4ArF)(\eta^5\text{-}C_5H_4ZnCl)$ (*vide supra*). A subsequent Negishi *C,C* coupling of the latter organo-zinc species with the corresponding dibromo thiophene gave the 1'-formylferrocenyl-functionalized thiophenes **E2** and **E6** as deep red solid materials (Scheme E1, Experimental Section). The dicyano derivatives **E3** and **E7** were synthesized from **E2** and **E6** using an one-pot cyanation procedure, according to the method described by Vowinkel and Bartel (Experimental Section).[278] After appropriate workup, thiophenes **E3** and **E7** could be obtained as orange solids in good yields (Experimental Section).

Thiophenes **E1** – **E7** are soluble in most of the common organic solvents, including tetrahydrofuran, toluene and dichloromethane. They are stable towards air and moisture in the solid state as well as in solution.

Diferrocenyl thiophenes **E1** – **E7** were identified by elemental analysis, high resolution ESI-TOF mass spectrometry as well as IR and NMR ($^1$H, $^{13}$C{$^1$H}) spectroscopy. Furthermore, the solid state structures of **E1** – **E4**, [**E4**][B(C_6F_5)_4], **E5**, and **E7** were determined by single X-ray structure analysis. All compounds were electrochemically

investigated by cyclic (CV) and square wave voltammetry (SWV) and *in situ* UV-Vis-NIR and infrared spectroelectrochemistry.[238]

For **E1** – **E7** the anticipated absorptions in the infrared range could be observed (Experimental Section). Furthermore, the $^1$H and $^{13}$C{$^1$H} NMR spectra of **E1** – **E7** show the expected signal patterns in the predicted ranges (Experimental Section).

**Solid state structures**. The molecular structures of **E1** – **E4**, [**E4**][B(C$_6$F$_5$)$_4$], **E5** and **E7** in the solid state have been determined by single crystal X–ray diffraction analysis. Suitable crystals were obtained by diffusion of *n*-hexane into a saturated dichloromethane (**E1** – **E5**, **E7**) or diethyl ether ([**5**][B(C$_6$F$_5$)$_4$]) solutions containing the respective compound at –30 °C. The molecular structure of **E1** – **E4**, [**E4**][B(C$_6$F$_5$)$_4$], **E5** and **E7** together with selected bond distances and angles are depicted in Figures E5 – E8 and are summarized in the Appendix Section (Table AE2-1).
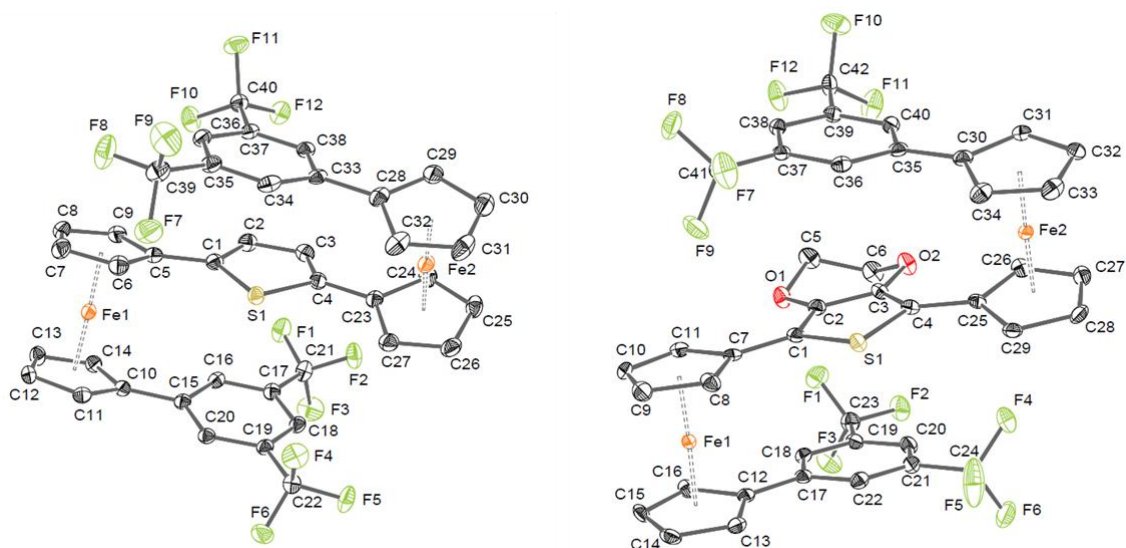


**Figure E5**. ORTEP diagrams (50% probability level) of the molecular structures of **E1** (left) and **E5** (right) with the atom numbering schemes. Hydrogen atoms are omitted for clarity. Selected bond lengths (Å) and angles (°) for **E1**: C1–C2 1.360(3), C1–S1 1.738(2), C2–C3 1.412(3), C3–C4 1.365(3), C4–S1 1.731(2), C4–S1–C1 92.08(11). **E5**: C1-C2 1.364(3), C1-S1 1.743(2), C2-C3 1.427(3), C3-C4 1.358(3), C4–S1 1.737(2), C4–S1–C1 93.13(11).

Crystal and structure refinement data are presented in the Experimental Section. In addition, the structural features of 1-bromo-1'''-(3,5-bis(trifluoromethyl)-phenyl)-1',1''-biferrocene (**E10**) are discussed in the Appendix Section (Chapter AE2). Thiophenes **E1** – **E4**, [**E4**][B(C$_6$F$_5$)$_4$], **E5**, and **E7** crystallize in the centrosymmetric triclinic space group $P\bar{1}$ ([**E4**][B(C$_6$F$_5$)$_4$]), the monoclinic space groups $P2_1/c$ (**E1**, **E5**), $P2_1/n$ (**E2**, **E3**), $P2/n$ (**E4**) and the non-centrosymmetric space group *Pbca* (**E7**) with one molecule of each compound within the asymmetric unit. Compound **E7** crystallizes with one molecule of dichloromethane as packing solvent (*vide infra*).
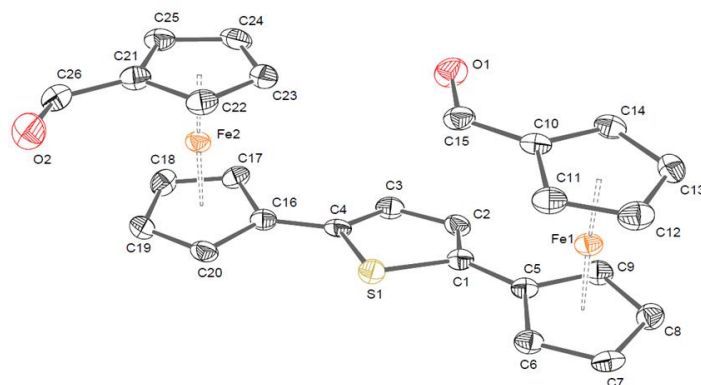
**Figure E6**. ORTEP diagram (50% probability level) of the molecular structure of **E2** with the atom numbering scheme. Hydrogen atoms are omitted for clarity. Selected bond lengths (Å) and angles (°) for **E2**: C10–C15 1.452(5), C15–O1 1.215(4), C21–C26 1.445(5), C26–O2 1.226(4), O1–C15–C10 124.6(3), O2–C26–C21 125.0(4), C4–S1–C1 92.35(16).
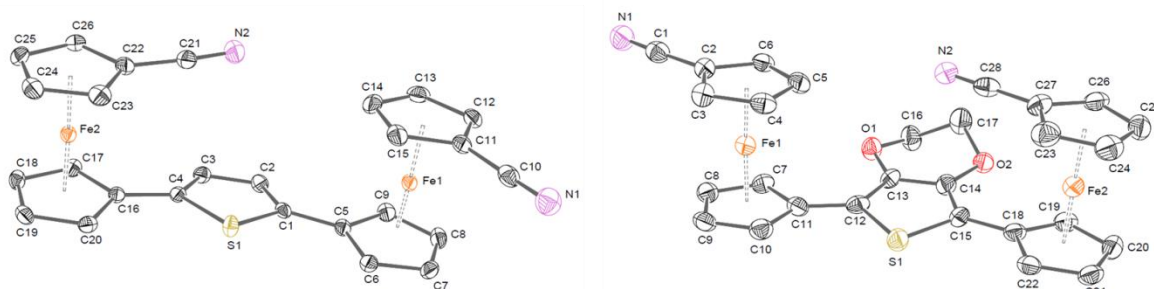


**Figure E7**. ORTEP diagrams (50% probability level) of the molecular structures of **E3** (left) and **E7** (right) with the atom numbering schemes. Hydrogen atoms and one molecule dichloromethane (right) are omitted for clarity. Selected bond lengths (Å) and angles (°) for **E3**: C10-N1 1.141(2), C10-C11 1.434(3), C21-N2 1.144(2), C21-C22 1.426(3), N1-C10-C11 178.6(2), N2-C21-C22 176.4(2), C1-S1-C4 92.26(8). **E7**: C1-N1 1.128(8), C1-C2 1.430(8), C27–C28 1.427(8), C28–N2 1.139(8), N1–C1–C2 178.0(7), N2–C28–C27 179.9(7), C12–S1–C15 92.6(3).
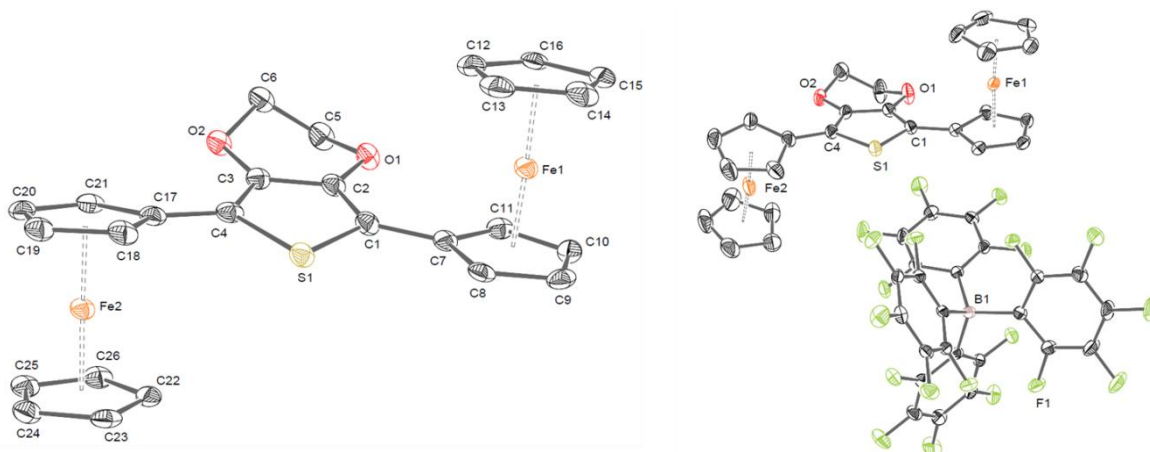


**Figure E8**. ORTEP diagrams (50 % probability level) of the molecular structures of **E4** (left) and [**E4**][B(C$_6$F$_5$)$_4$] (right) with an equal atom numbering schemes. Hydrogen atoms and one molecule diethyl ether (right) are omitted for clarity. Selected bond lengths (Å) and angles (°) **E4**: C1–S1 1.729(3), C1–C2 1.383(4), C2–C3 1.403(4), C3–C4 1.380(4), C4–S1 1.734(3), C1–S1–C4 93.30(17). For [**E4**][B(C$_6$F$_5$)$_4$]: C1–S1 1.738(3), C1–C2 1.362(5), C2–C3 1.434(5), C3–C4 1.358(5), C4–S1 1.739(3), C1–S1–C4 92.85(13).

The orientation of the ferrocenyl units depend on the substituents R at the non-thiophene bonded ferrocenyl C$_5$H$_4$ rings. With R = H (**E4**), ArF (**E1**, **E5**) an antiparallel orientation of the ferrocenyl substituents was observed, but parallel with R = CHO (**E2**), C≡N (**E3**, **E7**). For **E1** and **E5**, the ArF substituents exhibit an "S"-shaped conformation (Figure E5,

Appendix AE2). For molecule **E1** short distances between the heterocyclic core and the phenyl rings within the van der Waals radii were found (C1–C16 3.348(3) Å, C4–C48 3.346(3) Å, S1–C33 3.486(2) Å). For compounds **E2**, **E3** and **E7**, one substituent R at the ferrocenyls is rotated parallel to the heterocyclic core and thus, exhibits an almost synperiplanar orientation (**E2**, 5.9(2) °; **E3**, 4.21(12) °; **E7**, –8.1(4) °), whereas, the outward rotated group is anticlinal positioned (**E2**, – 144.5(2) °; **E3**, 141.24(12) °; **E7**, – 145.7(4) °). Within all compounds the linked $\pi$-systems (thiophene core, cyclopentadienyl and phenyl rings) exhibit a rather coplanar orientation (Table AE2-1).

An influence of the electron-rich ethylenedioxy moiety and the electron-withdrawing substituents at the ferrocenyls on the structural features of the thiophene unit could not be observed. Nevertheless, varying Fe–D distances (for example **E2**: Fe1–D1 = 1.6550(5), Fe1–D2 = 1.6600(5), Fe2–D3 = 1.6560(5), Fe2–D4 = 1.6439(5)) occur for electronically equal ferrocenyl moieties (Table AE2-1, **E2**) caused by packing effects.

The structure of [**E4**][B($C_6F_5$)$_4$] in the solid state shows no differences in its conformation compared with **E4**. However, the decreased electron density results in a higher delocalization in the thiophene core. Thus, the C1–C2 bond (**E4**, 1.362(5); [**E4**][B($C_6F_5$)$_4$], 1.383(4) Å) and the C3–C4 distance (**E4**, 1.358(5); [**E4**][B($C_6F_5$)$_4$], 1.380(4) Å) are enlarged,[O] whereas the C2–C3 bond is significantly shortened (**E4**, 1.434(5); [**E4**][B($C_6F_5$)$_4$], 1.403(4) Å). Furthermore, within [**E4**][B($C_6F_5$)$_4$] the Fe-cyclopentadienyl centroid (Fe–D) bond lengths are increased, suggesting a ferrocenium-like character, which is more pronounced for Fe2 (Fe1–D1, 1.6571(4); Fe2–D3 1.6636(4) Å and Fe1–D2 1.6668(4); Fe2–D4 1.6840(4) Å).[279,280] However, short Fe–D distances, in comparison to ferrocenium salts known in the literature,[279–281] together with a significantly reduced C2–C3 bond indicate charge delocalization in [**E4**][B($C_6F_5$)$_4$] (Figure E8, Appendix Table AE2-1).

**Electrochemistry**. Electrochemical studies of thiophenes **E1** – **E7** were carried out under an argon atmosphere in dichloromethane solutions containing [N$^n$Bu$_4$][B($C_6F_5$)$_4$] (0.1 M) as supporting electrolyte. *In situ* spectroelectrochemical investigations were performed using an OTTLE[238] (= Optically Transparent Thin Layer Electrochemistry) cell (Experimental Section). The electrochemical data are presented in Table E3 and the corresponding voltammograms are shown in Figure E10.

---

[O] With respect on a $2\sigma$ criterion.

For diferrocenyl thiophenes **E1** – **E7**, two well-resolved, reversible one-electron redox events with small $\Delta E_p$ values (Table E3) and $i_{pc}/i_{pa}$ ratios approaching unity were observed in all cases.[85,171,234,235,253] The introduction of electron withdrawing functionalities at the ferrocenyl units resulted in a shift of both redox events towards higher potential ($E^{0'}(1)$ = 82 (**E1**), 235 (**E2**), 306 mV (**E3**)) and increased redox separations ($\Delta E^{0'}$ = 325 (**E1**) 293 (**E2**) 321 mV (**E3**)) with respect to **C3**.[253]

**Table E3. Cyclic voltammetry data (potentials *vs.* FcH/FcH$^+$) of 1.0 mM solutions of C3, E1 – E7 in dry dichloromethane containing [N$^n$Bu$_4$][B(C$_6$F$_5$)$_4$] (0.1 M) as supporting electrolyte at 25 °C.**

| Compd. | $E^{0'}/\Delta E_p$ [mV][a] Wave (no.) | | $\Delta E^{0'}$ [mV][b] | $K_C$ [10$^4$][c] |
|---|---|---|---|---|
| | (1) | (2) | | |
| **C3**[253] | –53/60 | 195/62 | 248 | 1.6 |
| **E1** | 82/64 | 407/65 | 325 | 31.2 |
| **E2** | 235/63 | 528/65 | 293 | 9.0 |
| **E3** | 306/65 | 627/70 | 321 | 26.7 |
| **E4** | –160/64 | 153/66 | 313 | 19.5 |
| **E5** | –32/68 | 357/68 | 389 | 376.2 |
| **E6** | 90/65 | 488/69 | 398 | 534.1 |
| **E7** | 146/63 | 582/66 | 436 | 2343.8 |

[a] Formal potential ($E^{0'}$). Difference between the oxidation and reduction peak potential ($\Delta E_p$). [b] Redox separation ($\Delta E^{0'}$, $\Delta E^{0'} = E^{0'}(2) - E^{0'}(1)$). [c] Comproportionation constant ($K_C$, $K_C = e^{\frac{\Delta E^{0'}F}{RT}}$).

These results correspond well with similar observations from Winter and Kowalski on the example of 2,5-bis(1'-(2,5-dimethylaza-ferrocenyl))thiophene under comparable experimental conditions.[163,167,184,225]
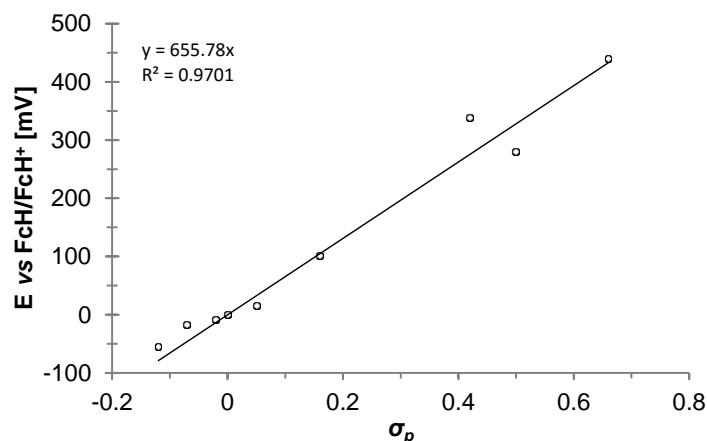


**Figure E9**. Correlation of redox potenials ($E^{0'}$) of different ferrocene derivatives with their corresponding Hammett substituent constants ($\sigma_p$).[282] For correlation data, see Table AE2-3 (Appendix Section).

Despite having the more positive redox potential for the first oxidation, thiophene **E2** exhibits a smaller redox separation, when compared to **E1** (Table E3, Figure E10). Within this context, the Hammett substituent constant for the ArF functionality could be estimated using FcArF (**E9**). Hence, in a series with other ferrocene derivatives bearing substituents

with different known electronic properties a correlation of the substituent's Hammett constant ($\sigma_p$) and the ferrocenyls redox potential gave a linear regression (Figure E9). This relationship was used to calculate $\sigma_p = 0.28$ ($\pm 0.05$) for the ArF substituent (Figure E9 and Table AE2-3, Appendix Section).[282] On the other hand, it is well established that the more electron-rich 3,4-ethylenedioxy thiophene (EDOT) has an oxidation potential ca. 0.3 V more negative than thiophene itself.[283,284] Thus, the introduction of the $OCH_2CH_2O$ group leads to a shift of the first redox process of **E4 – E7** toward more cathodic potentials, with respect to their non-substituted analogues **C3**, **E1 – E3**.[285]
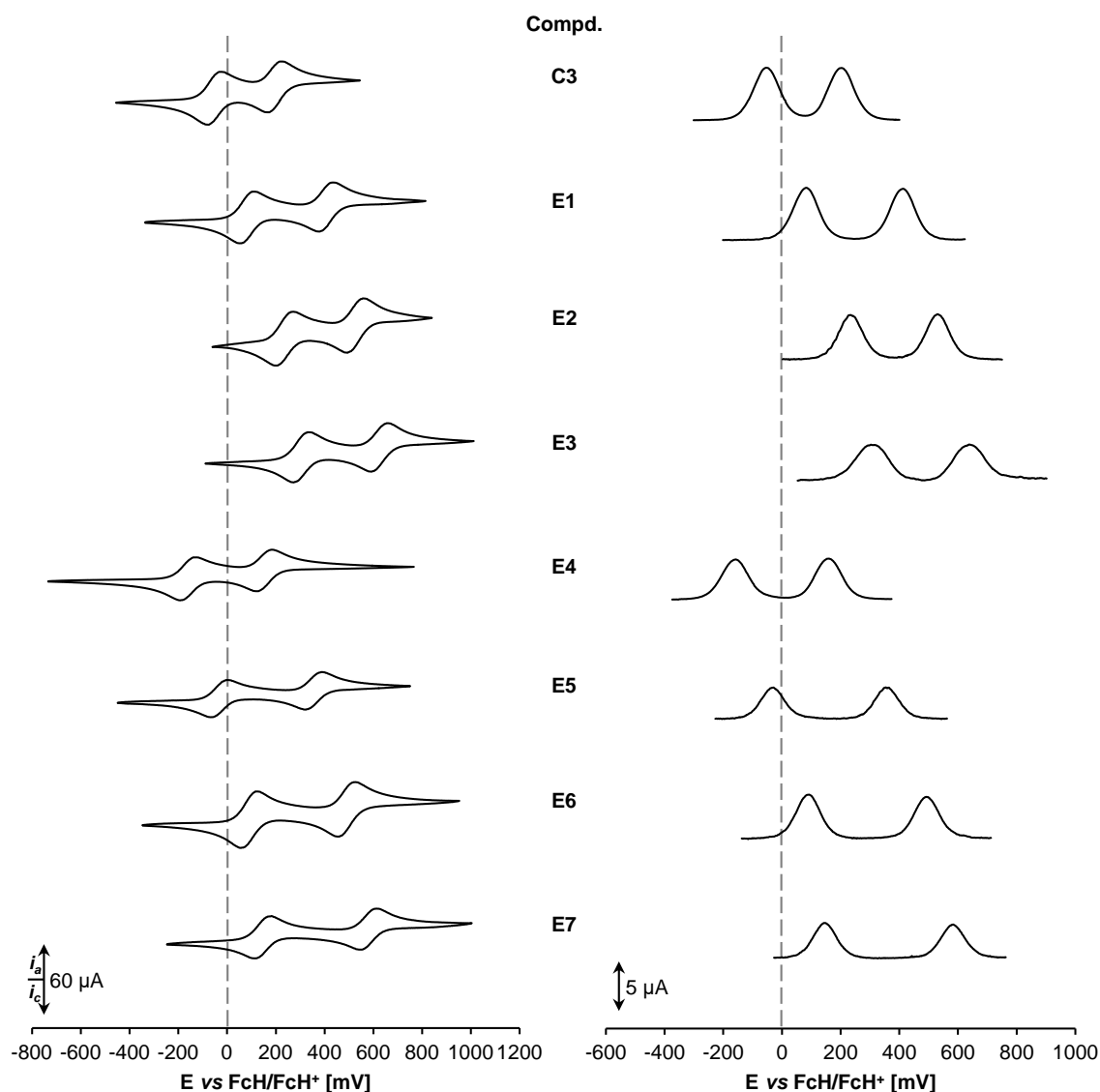


**Figure E10**. Left: Cyclic voltammograms (CV) of **C3**, **E1 – E7**, scan rate: 100 mVs$^{-1}$ in dichloromethane solutions (1.0 mM) at 25 °C, supporting electrolyte [N$^n$Bu$_4$][B(C$_6$F$_5$)$_4$] (0.1 M). Right: Square wave voltammograms (SWV) of **C3**, **E1 – E7** (**E3**, 10 Hz; **E1**, 5 Hz; **C3**, **E4**, 2 Hz; **E2**, **E5**, **E6**, **E7**, 1 Hz.) in dichloromethane solutions (1.0 mM) at 25 °C, supporting electrolyte [N$^n$Bu$_4$][B(C$_6$F$_5$)$_4$] (0.1 M).[253]

Moreover, enlarged redox separations were found (Table E3, Figure E9).[253] Similar findings were made for other metallocenyl-substituted heterocyclic systems: for example,

the electrochemical investigation of a series of 2,5-diferrocenyl-1-phenyl-1*H*-pyrroles showed that the electron-rich heterocycles facilitate a higher thermodynamic stability ($K_C$) of the mixed-valent state.[31,180,285]

In order to gain a deeper insight into the oxidation process of **E1** – **E7**, spectroelectrochemical studies were carried out by an stepwise increase of the potential (varying step heights: 5 – 100 mV) *vs.* Ag/AgCl in an OTTLE[238] cell using a 0.1 M dichloromethane ($\mu = 1.6$ D) solution of $[N^nBu_4][B(C_6F_5)_4]$ as supporting electrolyte (for data see Table E4).[270]

**Table E4. NIR data of C3, E1 – E7 in dry dichloromethane containing $[N^nBu_4][B(C_6F_5)_4]$ (0.1 M) as supporting electrolyte at 25 °C.**

| Compd. | Transition | $\tilde{v}_{max}$ [cm$^{-1}$] ($\varepsilon_{max}$ [Lmol$^{-1}$cm$^{-1}$])$^a$ | $\Delta\tilde{v}_{1/2}$ [cm$^{-1}$]$^b$ | $\Delta\tilde{v}_{1/2(theo)}$ [cm$^{-1}$]$^c$ | $\tilde{v}_{max(IVCT-PC)}$ [cm$^{-1}$]$^{d,e}$ ($\Delta\tilde{v}_{1/2}$ [cm$^{-1}$])$^d$ {$\Delta\tilde{v}_{max-IVCT}$ [cm$^{-1}$]}$^f$ |
|---|---|---|---|---|---|
| **C3$^{+253}$** | LMCT<br>IVCT | 10080 (624)<br>4994 (2129)<br>4054 (572)<br>3524 (831) | 2880<br>3840<br>440<br>990 | 3400 | 7020<br>(3950)<br>{2030} |
| **E1$^+$** | LMCT<br>IVCT | 9770 (690)<br>4130 (3290)<br>3970 (730)<br>3440 (1960) | 3190<br>3660<br>470<br>840 | 3090 | 5880<br>(3470)<br>{1750} |
| **E2$^+$** | LMCT<br>IVCT | 9320 (710)<br>4680 (3160)<br>4010 (980)<br>3460 (1540) | 2810<br>3540<br>600<br>910 | 3290 | 6500<br>(3380)<br>{1820} |
| **E3$^+$** | LMCT<br>IVCT | 9010 (770)<br>4710 (3340)<br>4100 (1210)<br>3490 (2390) | 2700<br>3270<br>630<br>1050 | 3300 | 6320<br>(3560)<br>{1610} |
| **E4$^+$** | LMCT<br>IVCT | 9160 (670)<br>4840 (3330)<br>4180 (1470)<br>3540 (2160) | 2620<br>3300<br>690<br>1010 | 3440 | 6160<br>(3090)<br>{1320} |
| **E5$^+$** | LMCT<br>IVCT | 8880 (670)<br>4200 (4600)<br>4060 (2200)<br>3420 (3560) | 2650<br>3310<br>690<br>850 | 3120 | 5140<br>(3490)<br>{940} |
| **E6$^+$** | LMCT<br>IVCT | 8780 (790)<br>4280 (4600)<br>3930 (2410) | 2180<br>3520<br>1090 | 3140 | 5290<br>(3600)<br>{1110} |
| **E7$^+$** | LMCT<br>IVCT | 8740 (800)<br>4260 (4610)<br>4230 (2090) | 2190<br>3770<br>980 | 3140 | 5150<br>(3590)<br>{890} |

$^a$ Wavenumber of the bands maximum intensity ($\tilde{v}_{max}$), extinction coefficient at $\tilde{v}_{max}$ ($\varepsilon_{max}$). $^b$ Bandwidth at half height ($\Delta\tilde{v}_{1/2}$). $^c$ Bandwidth at half height expected from the Hush theory ($\Delta\tilde{v}_{1/2(theo)} = (2310\tilde{v}_{max})^{1/2}$).
$^d$ Measured in propylene carbonate (PC). $^e$ $\tilde{v}_{max}$ of the IVCT transition ($\tilde{v}_{max(IVCT-PC)}$). $^f$ Solvatochromic shift ($\Delta\tilde{v}_{max-IVCT} = \tilde{v}_{max(IVCT-PC)} - \tilde{v}_{max}$).
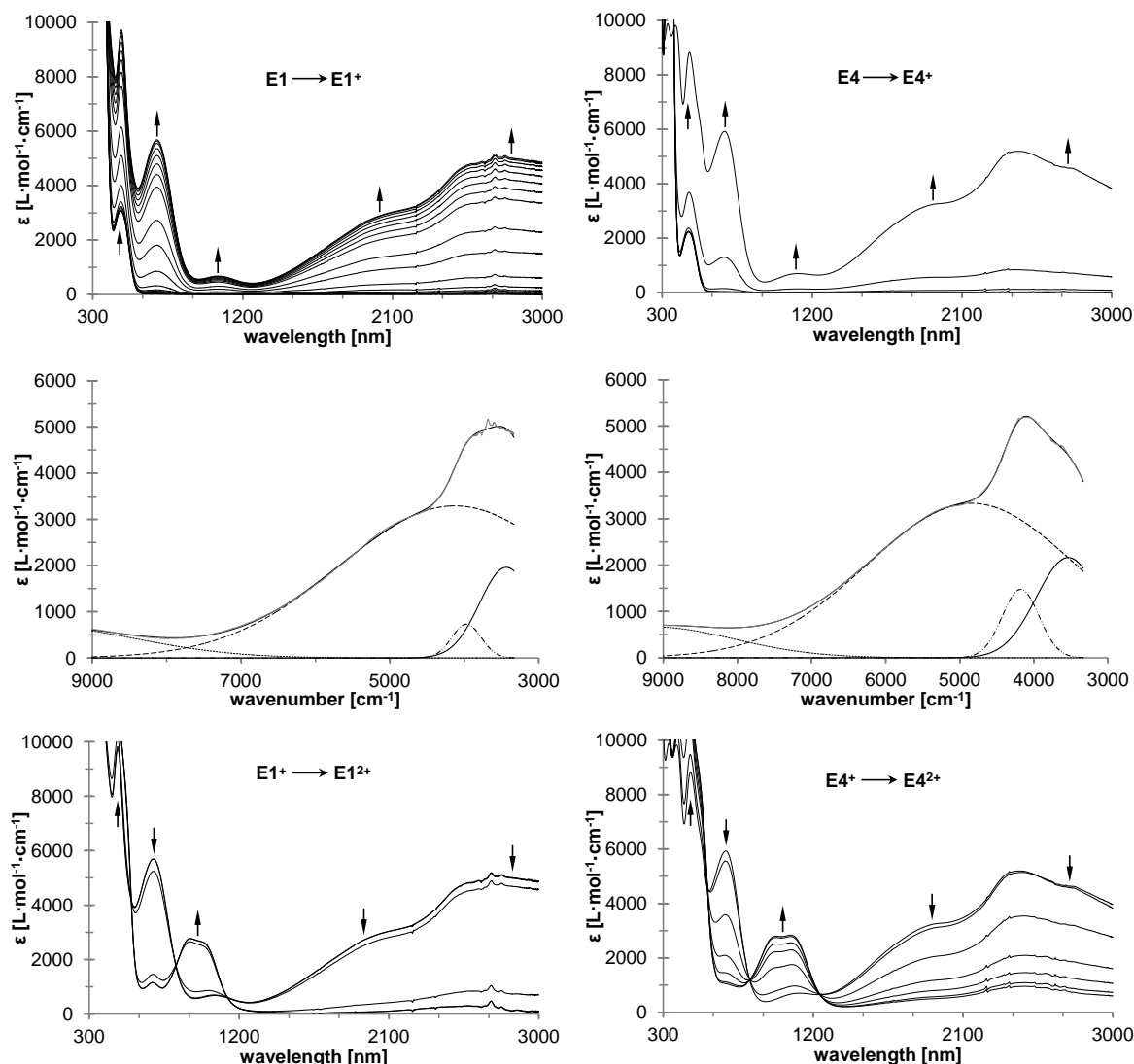
**Figure E11**. Left: UV-Vis-NIR spectra of **E1** at rising potentials. Top: –100 to 580 mV. Middle: deconvolution of NIR absorptions at 580 mV using four distinct overlapping transitions with Gaussian shapes (dashed line indicates IVCT absorption, dotted line corresponds to absorptions caused by interactions between ligand and metal). Bottom: 580 to 800 mV. Right: UV-Vis-NIR spectra of **E4** at rising potentials. Top: –200 to 300 mV. Middle: deconvolution of NIR absorptions at 300 mV using four distinct overlapping transitions with Gaussian shapes (dashed line indicates IVCT absorption, dotted line corresponds to absorptions caused by interactions between ligand and metal). Bottom: 300 to 900 mV. All potentials *vs.* Ag/AgCl at 25 °C in dichloromethane, supporting electrolyte $[N^{n}Bu_4][B(C_6F_5)_4]$ (0.1 M). Arrows indicate increasing or decreasing as well as shifting absorptions.

This procedure allows the *in situ* generation of mixed-valent species. If deconvolution of NIR absorptions was used, three to four Gaussian-shaped transitions were applied to get fits good enough to allow an almost exact overlay of the sum of the spectral components with the experimental spectra.

All neutral thiophene complexes do not display, as expected, any absorptions in the NIR range. The corresponding spectra are presented in Figures E11 and E12 and in the Appendix Section (Figures AE2-3 to AE2-8). During the oxidation of **E1** – **E7** typical absorptions in the UV-Vis (inner ferrocenyl related $\pi$-$\pi$* and MLCT/d-d transitions) and NIR region appear as mixed-valent **E1**$^+$ – **E7**$^+$ are formed (Table E4, *vide*

*supra*).[31,179,239,240,253] Within the NIR region a high-energy NIR absorption around 10000 cm$^{-1}$ can be assigned to a ligand to metal charge transfer transition (LMCT), as reported previously.[31,166,171,173,178,179,210,253,286,287] Intervalence charge transfer (IVCT) transitions were observed in the spectral range between 4000 and 5000 cm$^{-1}$ together with further low-energy NIR absorptions (Table E4).[253] These transitions are often explained with charge transfer-assisted ligand field (LF) or LMCT interactions; moreover the bandwidth at half height ($\Delta\tilde{v}_{1/2}$) for these relative intense absorptions is more narrow than the Hush theory would predict ($\Delta\tilde{v}_{1/2(theo)}$) for an IVCT transition.[49,50,57,242,244,253,265,288]
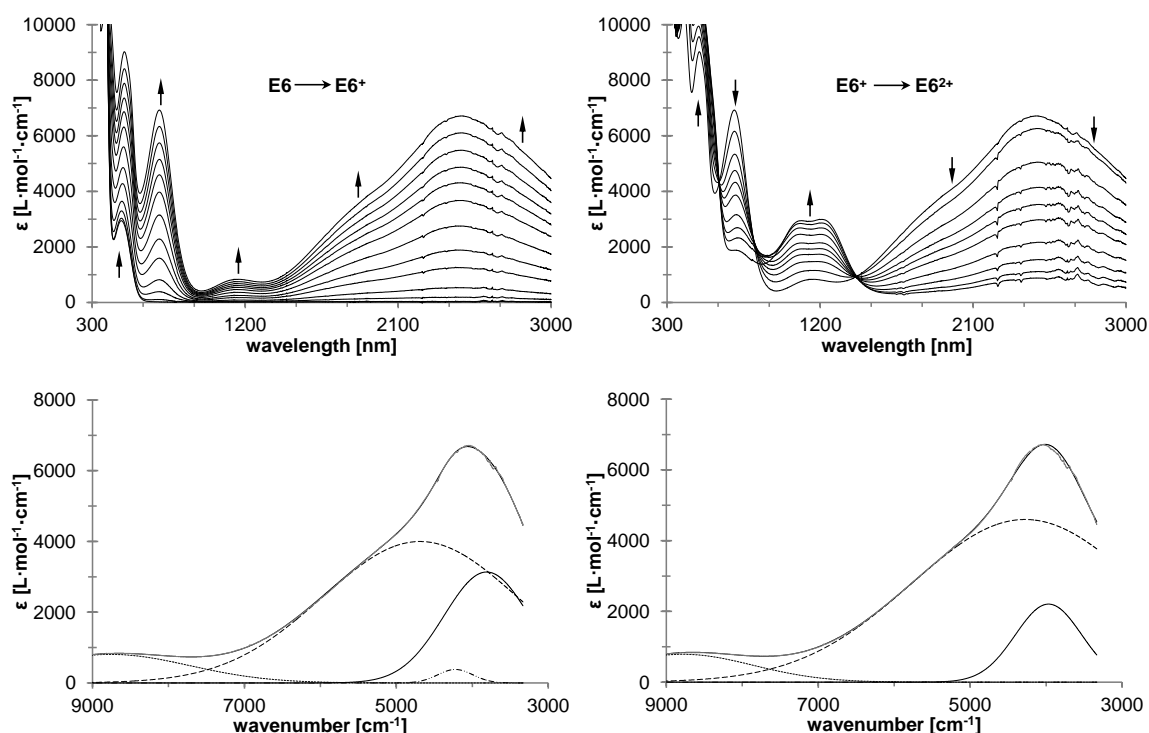


**Figure E12**. UV-Vis-NIR spectra of **E6** at rising potentials. Left top: 100 to 650 mV. Left bottom: deconvolution of NIR absorptions at 650 mV using four distinct overlapping transitions with Gaussian shapes (dashed line indicates IVCT absorption, dotted line corresponds to absorptions caused by interactions between ligand and metal). Right top: 650 to 1300 mV. Right bottom: deconvolution of NIR absorptions at 650 mV using three distinct overlapping transitions with Gaussian shapes. All potentials *vs.* Ag/AgCl at 25 °C in dichloromethane, supporting electrolyte [N$^n$Bu$_4$][B(C$_6$F$_5$)$_4$] (0.1 M). Arrows indicate increasing or decreasing as well as shifting absorptions.

Additionally, those bands are often called interconfigurational (IC) transitions ($d\pi$-$d\pi$).[49,172,289] However, Warratz *et al.* have proposed an IVCT character for such absorptions in mixed-valent non-bridged biferrocene species, similar as known for bis(fulvalene)diiron systems.[70,126,127] The physical parameters ($\tilde{v}_{max}$, $\varepsilon_{max}$, $\Delta\tilde{v}_{1/2}$; Table E4) of the IVCT absorptions could be determined by spectral simulation using Gaussian-shaped transitions. While in general four Gaussian transitions have been used to simulate the experimental spectra,[210,253,287] for compounds **E6$^+$** and **E7$^+$** it is sufficient to use only three bands to generate a fit good enough to allow an almost exact overlay with the experimental spectra

(Figures E11 and AE2-8).[P] This fact might reflect either that one of the low energy bands is decreased in intensity beyond the resolution, is shifted out of the measurement range or perfectly overlaps with other transitions. Moreover, Gaussian-shaped transitions are strictly valid only for weakly coupled (Hush) systems.[37,50,57,63] Hence, with increasing electronic coupling, a cutoff takes place on the low-energy side of the transition and the absorption becomes asymmetric. Thus, the analysis of such transitions should be handled with caution.

A comparison of the intensities of the IVCT absorpions of $C3^+$, $E1^+ - E7^+$ showed that $\varepsilon_{max}$ increases in a similar manner as the redox separation (Electrochemical Section), revealing that electron-withdrawing substituents at the ferrocenyl/ferrocenium entities and electron-donating functionalities at the thiophene core are beneficial. The corresponding NIR absorptions become more intense as the electron-withdrawing effect of the substituents as well as their ability of charge stabilization increases. Furthermore, a bridging unit with a lower oxidation potential (closer to the ferrocenyl units) has a similar influence. Moreover, electron acceptor moieties at the ferrocenyl units and an ethylenedioxy functionality on the thiophene bridge cause a bathochromic shift of the corresponding IVCT absorptions, which is most pronounced for $E1^+$ and $E5^+$ ($\tilde{v}_{max}$ = 4994 cm$^{-1}$ ($C3^+$), 4130 cm$^{-1}$ ($E1^+$), 4200 cm$^{-1}$ ($E5^+$)) (Figures E11 and AE2-6).

Within class II systems IVCT absorptions typically show a strong solvatochromism.[50,57,68] In order to investigate this behavior, propylene carbonate (PC) ($\mu$ = 4.9 D) was further chosen as additional solvent for the spectroelectrochemical measurements. In the case of $C3^+$, the IVCT transition could be detected around 7000 cm$^{-1}$ ($\tilde{v}_{max(IVCT-PC)}$) by using PC, revealing a solvatochromic shift ($\Delta\tilde{v}_{max-IVCT}$) of more than 2000 cm$^{-1}$ (Table E4, Figure AE2-3 (Appendix Section)). Within the series of $\alpha,\alpha'$-diferrocenyl thiophenes the solvatochromic shift ($\Delta\tilde{v}_{max-IVCT}$) decreases with increasing intensity of the IVCT absorptions (Table E4, Figures E11, E12 and AE2-3 to AE2-8). However, $\Delta\tilde{v}_{max-IVCT}$ for mixed-valent aldehydes $E2^+$ and $E6^+$ is not as large as those for $E1^+$ and $E5^+$, respectively, which might be due to larger resonance stabilization capabilities of the aromatic ArF units (Table E4). Nevertheless, the magnitude of $\Delta\tilde{v}_{max-IVCT}$ compared to values for very strong coupled systems[70] ($\Delta\tilde{v}_{max-IVCT} \approx$ 100 cm$^{-1}$) verify a class II classification according to Robin and Day.[68]

---

[P] By the use of four Gaussian transitions, the corresponding solvatochromic shift becomes significantly smaller together with a lower intensity and a reduced width at half-height for the IVCT transition.

Infrared spectroelectrochemical studies of thiophenes **E2**, **E3**, **E6** and **E7** were carried out, monitoring the $v(CO)$ or $v(CN)$ stretching frequencies (Figure E13). Upon generation of **E2$^+$** and **E6$^+$** the original absorptions at 1682 and 1665 cm$^{-1}$ (**E2**) or 1682 and 1664 cm$^{-1}$ (**E6**) disappeared and a broad absorption band at 1684 cm$^{-1}$ (**E2$^+$**) or 1678 cm$^{-1}$ and 1689 cm$^{-1}$ (**E6$^+$**) emerged (Figure E13).
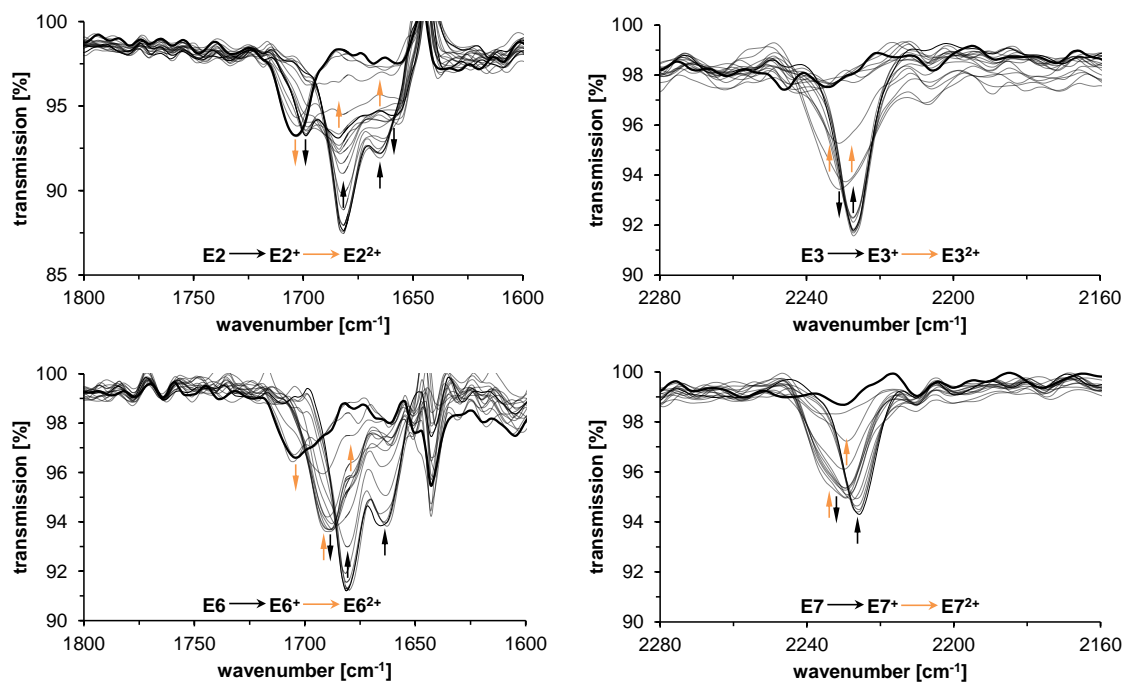


**Figure E13**. Infrared spectra of **E2**, **E3**, **E6** and **E7** at rising potentials (left top: −100 to 1000 mV; right top: −100 to 1000 mV; left bottom: −100 to 850 mV; right bottom: −100 to 1000 mV). All potentials *vs*. Ag/AgCl at 25 °C in dichloromethane on 2 mM analyte solutions, supporting electrolyte [N$^n$Bu$_4$][B(C$_6$F$_5$)$_4$] (0.1 M). Arrows indicate increasing or decreasing as well as shifting absorptions.

A further increase in the potential leads to a new band for **E2$^{2+}$** at 1703 cm$^{-1}$ and for **E6$^{2+}$** at 1695 cm$^{-1}$. A similar spectroelectrochemical behavior was found for the cyano-derivatives **E3** and **E7** by monitoring their $v(CN)$ (Figure E13). The stretching frequencies for the neutral compounds at 2226 cm$^{-1}$ shifts to 2231 cm$^{-1}$ (**E3$^+$**) and 2229 cm$^{-1}$ (**E7$^+$**) during the generation of the mixed-valent species (Figure E13). The corresponding width at half height is nearly twice as large as observed for **E3** and **E7** and suggests a valence trapped situation in the respective monocations within the infrared time scale.[49]

CONCLUSION

Within this study, the synthesis of a series of $\alpha,\alpha'$-diferrocenyl thiophenes 2,5-fc$_2$-$^cC_4H_2S$ and 2,5-fc$_2$-3,4-(OCH$_2$CH$_2$O)-$^cC_4S$ (fc = Fe($\eta^5$-C$_5$H$_4$)($\eta^5$-C$_5$H$_4$R); R = H (**C3**, **E4**), 3,5-(CF$_3$)$_2$-$^cC_6H_3$ (**E1**, **E5**), CHO (**E2**, **E6**), C≡N (**E3**, **E7**)) is reported with the aim of investigating the electronic influence of functional groups at the ferrocenyl entities and on

the heterocyclic bridging unit on low-energy charge transfer transitions. The syntheses were performed using a Pd-promoted Negishi *C,C* cross-coupling protocol. Hence, appropriate ferrocenyl zinc chloride derivatives were reacted with the corresponding 2,5-dibromo thiophene.

The obtained molecules were characterized spectroscopically. The structural properties of **E1** – **E4**, [**E4**][B(C$_6$F$_5$)$_4$], **E5** and **E7** in the solid state were investigated by single-crystal X-ray diffraction studies. The influence of the electron-rich ethylenedioxy moiety or the additional electron-withdrawing substituents at the cyclopentadienyl rings on the bond lengths in the heterocyclic core is very limited. Furthermore, a comparison of **E4** and **E4$^+$** in the solid state reveals an effect of the decreased electron density on the solid state structure. Analysis of the bond lengths within [**E4**][B(C$_6$F$_5$)$_4$] suggest delocalization in the mixed valence state.

The electrochemical studies of thiophenes **E1** – **E7** were carried out under an argon atmosphere in dichloromethane solutions containing [N$^n$Bu$_4$][B(C$_6$F$_5$)$_4$] (0.1 M) as supporting electrolyte. They exhibit an increasing redox separation/thermodynamic stability of the mixed-valent species in the series **C3** < **E2** < **E4** < **E3** ≈ **E1** < **E5** < **E6** < **E7**. Further UV-Vis-NIR and infrared spectroelectrochemical studies verified these observations. The NIR absorptions of the corresponding mixed-valent species become more intense as the electron-withdrawing effect of the substituents and their ability of charge stabilization increases. Confirming the results of previous works,[171,179,180] a more electron-rich five-membered heterocycle also facilitates the electron transfer. The electronic coupling between the iron-based redox centers over the thiophene core increases in this direction. Finally, the spectroelectrochemical investigations reveal a valence trapped situation in corresponding mixed-valent species and hence offer a class II classification according to Robin and Day.

In summary, electron-withdrawing groups at the ferrocenyls in combination with the electron-donating ethylenedioxy unit at the thiophene building block enforces the electronic coupling between the iron-based redox centers in the corresponding mixed-valent state.

EXPERIMENTAL SECTION

**General Procedures**. All reactions were carried out under an argon atmosphere using standard Schlenk techniques. Tetrahydrofuran was purified by distillation from sodium/benzophenone ketyl. Toluene were *n*-hexane were purified with a MBRAUN SPS-800 purification system. Dichloromethane was purified by distillation from $CaH_2$.

**Reagents.** Tetra-*n*-butylammonium tetrakis(pentafluorophenyl)borate was prepared by metathesis of lithium tetrakis(pentafluorophenyl)borate etherate (Boulder Scientific) with tetra-*n*-butylammonium bromide, according to a published procedure.[101] All other chemicals were purchased from commercial suppliers and were used as received.

**Instruments**. Infrared spectra were obtained with a Thermo Nicolet 200 FT-IR spectrometer using KBr press techniques for sample preparation. NMR spectra were recorded using an Bruker Avance III 500 FT-NMR spectrometer ($^1$H NMR at 500.303 MHz, $^{13}$C{$^1$H} NMR at 125.813 MHz) at ambient temperature, unless otherwise noted. Chemical shifts ($\delta$) are reported in parts per million (ppm) relative to tetramethylsilane using the solvent as internal reference ($CDCl_3$: $^1$H NMR $\delta$ = 7.26 ppm; $^{13}$C{$^1$H} NMR $\delta$ = 77.16 ppm).[246] Coupling constants (*J*) are reported in Hertz (Hz) and integrations are reported in number of protons. The following abbreviations are used to describe peak patterns: s = singlet, pt = pseudotriplet, q = quartet, m = multiplet. The melting points (sealed off in argon flushed capillaries) were determined using a Gallenkamp MFB 595 010 M melting point apparatus. Microanalysis was performed by using a Thermo FLASHEA 1112 Series instrument. High resolution mass spectra were recorded with a Bruker micrOTOF QII with an Apollo II ESI-source.

**Synthesis of 2,5-di-(1'-(3,5-bis(trifluoromethyl)phenyl)ferrocenyl)thiophene (E1)**. A solution of **E8** (Appendix Section) (0.5 g, 1.05 mmol) in 20 mL tetrahydrofuran was cooled to –90 °C and 1.1 eq (0.46 mL) of *n*-butyllithium (*n*-hexane) were added within 5 min. The resulting dark red solution was stirred at –90 °C for 45 min. Afterward, 1.1 eq (323 mg) of [$ZnCl_2$·2thf] were added in a single portion and the resulting reaction mixture was warmed to 0 °C for 30 min. Then, 0.45 eq (50 μL) of 2,5-dibromo thiophene and 11.7 μmol (8 mg) of [Pd($CH_2CMe_2P^tBu_2$)($\mu$-Cl)]$_2$[229,230] were added and the resulting reaction was kept at 55 °C for 19 h. After it was cooled to ambient temperature, the crude product was adsorbed on alumina and purified by column chromatography (column size: 20 x 3 cm, alumina) using an *n*-hexane/toluene mixture of ratio 4:1 (v:v) as eluent. After recrystallization from a dichloromethane/*n*-hexane mixture (ratio 1:4) **E1** was obtained as

red crystals. Yield: 0.22 g (0.25 mmol, 53 % based on 2,5-dibromo thiophene). Anal. Calcd for $C_{40}H_{24}F_{12}Fe_2S$ (876.4): C, 54.82; H, 2.76. Found; C, 55.26; H, 3.07. Mp: 175 °C. IR data (KBr)[cm$^{-1}$]: 3101 w, 3087 w, 1616 w, 1501 w, 1452 w, 1360 m, 1283 s, 1121 s, 889 m, 815 m, 698 m, 683 m. $^1$H NMR (CDCl$_3$)[$\delta$]: 7.58 (m, 4H, C$_6$H$_3$), 7.48 (m, 2H, C$_6$H$_3$), 6.40 (s, 2H, C$_4$H$_2$S), 4.57 (pt, $J_{HH}$ = 1.9 Hz, 4H, C$_5$H$_4$), 4.39 (pt, $J_{HH}$ = 1.9 Hz, 4H, C$_5$H$_4$), 4.34 (pt, $J_{HH}$ = 1.9 Hz, 4H, C$_5$H$_4$), 4.25 (pt, $J_{HH}$ = 1.9 Hz, 4H, C$_5$H$_4$). $^{13}$C{$^1$H} NMR (CDCl$_3$)[$\delta$]: 140.8 (C$_i$-C$_6$H$_3$), 138.4 (C$_i$-C$_4$H$_2$S), 131.5 (q, $J_{CF}$ = 33 Hz, C$_i$-C$_6$H$_3$), 125.5 (m, C$_6$H$_3$), 123.5 (q, $J_{CF}$ = 273 Hz, CF$_3$), 122.8 (C$_4$H$_2$S), 119.2 (m, C$_6$H$_3$), 83.2 (C$_i$-C$_5$H$_4$), 82.1 (C$_i$-C$_5$H$_4$), 71.4 (C$_5$H$_4$), 69.9 (C$_5$H$_4$), 68.3 (C$_5$H$_4$), 67.7 (C$_5$H$_4$). HR-ESI MS (calc) [m/z]: 876.0118 (876.0102) [M]$^+$. Crystal data for **E1**, $C_{40}H_{24}F_{12}Fe_2S$, $M_r$ = 876.35 g·mol$^{-1}$, monoclinic, $P2_1/c$, $\lambda$ = 0.71073 Å, $a$ = 11.3424(3) Å, $b$ = 14.3516(4) Å, $c$ = 20.4730(4) Å, $\beta$ = 96.798(2) °, $V$ = 3309.20(14) Å$^3$, $Z$ = 4, $\rho_{calcd}$ = 1.759 g·cm$^{-3}$, $\mu$ = 1.040 mm-1, $T$ = 103.3(2) K, $\Theta$ range = 2.85 – 25.50 °, reflections collected: 16182, independent: 6141 ($R_{int}$ = 0.0347), R1 = 0.0333, wR2 = 0.0706 [$I > 2\sigma(I)$].

**Synthesis of 2,5-di-(1'-formylferrocenyl)thiophene (E2)**. A solution of E11 (Appendix Section) (2.15 g, 6.34 mmol) in 40 mL tetrahydrofuran was cooled to –90 °C and 1.1 eq (2.8 mL) of 2.5 M *n*-butyllithium (*n*-hexane) were added within 5 min. After 45 min of stirring, 1.1 eq (1.96 g) of [ZnCl$_2$·2thf] were added in a single portion and the resulting reaction mixture was warmed to 0 °C within 30 min. Afterward, 0.45 eq (0.32 mL) of 2,5-dibromo thiophene and 26.2 μmol (18 mg) of [Pd(CH$_2$CMe$_2$P$^t$Bu$_2$)($\mu$-Cl)]$_2$[229,230] were added and resulting reaction mixture was warmed to 55 °C for 48 h. After cooling to ambient temperature, the reaction was hydrolyzed with 1 M degassed hydrochloric acid (25 mL) and was extracted with dichloromethane (100 mL). The combined organic phases were dried over MgSO$_4$ and the solvent was removed in vacuum. The remaining crude product was adsorbed on alumina and purified by column chromatography (column size: 20 x 3 cm, alumina) using an *n*-hexane/ethyl acetate mixture of ratio 1:1 (v:v) as eluent. After recrystallization from a dichloromethane/*n*-hexane mixture (ratio 1:4) compound **E2** was obtained as dark red crystals. Yield: 0.74 g (1.46 mmol, 51 % based on 2,5-dibromo thiophene). Anal. Calcd for $C_{26}H_{20}Fe_2O_2S$ (508.2): C, 61.45; H, 3.97. Found; C, 61.66; H, 3.85. Mp: 133 °C. IR data (KBr)[cm$^{-1}$]: 3104 w, 3091 w, 3075 w, 2884 w, 2760 w, 1679 s, 1663 s, 1452 m, 1370 m, 1244 m, 1032 m, 820 m, 795 m, 745 w. $^1$H NMR (CDCl$_3$)[$\delta$]: 9.86 (s, 2H, CHO), 6.88 (s, 2H, C$_4$H$_2$S), 4.74 (pt, $J_{HH}$ = 1.9 Hz, 4H, C$_5$H$_4$), 4.67 (pt, $J_{HH}$ = 1.9 Hz, 4H, C$_5$H$_4$), 4.55 (pt, $J_{HH}$ = 1.9 Hz, 4H, C$_5$H$_4$), 4.40 (pt, $J_{HH}$ = 1.9 Hz, 4H, C$_5$H$_4$). $_{13}$C{$_1$H} NMR (CDCl$_3$)[$\delta$]: 193.6 (CHO), 139.3 (C$_i$-C$_4$H$_2$S), 123.8 (C$_4$H$_2$S), 82.4 (C$_i$-

$C_5H_4$), 80.3 ($C_i$-$C_5H_4$), 75.3 ($C_5H_4$), 71.4 ($C_5H_4$), 70.2 ($C_5H_4$), 67.8 ($C_5H_4$). HR-ESI MS (calc) [m/z]: 507.9909 (507.9878) [M]$^+$. Crystal data for **E2**, $C_{26}H_{20}Fe_2O_2S$, $M_r = 508.18$ g·mol$^{-1}$, monoclinic, $P2_1/n$, $\lambda = 0.71073$ Å, $a = 11.8158(8)$ Å, $b = 9.6818(6)$ Å, $c = 18.0526(10)$ Å, $\beta = 102.988(6)$ °, $V = 2012.3(2)$ Å$^3$, $Z = 4$, $\rho_{calcd} = 1.677$ g·cm$^{-3}$, $\mu = 1.568$ mm$^{-1}$, $T = 103.50(14)$ K, $\Theta$ range = 3.13 – 25.50 °, reflections collected: 7745, independent: 3727 ($R_{int} = 0.0603$), R1 = 0.0559, wR2 = 0.1440 [$I > 2\sigma(I)$].

**Synthesis of 2,5-di-(1'-cyanoferrocenyl)thiophene (E3).** To a solution of hydroxylamine hydrochloride (40 mg, 0.56 mmol) in 1 mL degassed $H_2O$ were added 0.22 mmol of **E2** dissolved in 3 mL pyridine. The resulting reaction mixture was stirred for 60 min at ambient temperature. Afterward, vitriol (40 mg, 0.16 mmol) and a mixture of triethylamine (0.2 mL) and dichloromethane (1 mL) were added in a single portion. *N,N'*-Dicyclohexylcarbodiimide (DCC) (0.13 g, 0.63 mmol) dissolved in 4 mL of dichloromethane was added and the reaction mixture was stirred for 16 h. After evaporation of all volatiles, the crude product was purified by column chromatography (column size: 20 x 3 cm, alumina) using dichloromethane as eluent. After recrystallization from a dichloromethane/*n*-hexane mixture (ratio 1:4) **E3** was obtained as orange crystals. Yield: 75 mg (0.15 mmol, 69 % based on **E2**). Anal. Calcd for $C_{26}H_{18}Fe_2N_2S$ (502.2): C, 62.18; H, 3.61; N, 5.58. Found; C, 62.12; H, 3.38; N, 5.68. Mp: 127 °C. IR data (KBr) [cm$^{-1}$]: 3101 m, 2231 m, 2219 s, 1451 w, 1425 w, 1229 m, 1031 m, 848 m, 817 s, 792 s, 648 m. $^1$H NMR (CDCl$_3$)[$\delta$]: 6.96 (s, 2H, $C_4H_2S$), 4.71 (pt, $J_{HH} = 1.9$ Hz, 4H, $C_5H_4$), 4.57 (pt, $J_{HH} = 1.9$ Hz, 4H, $C_5H_4$), 4.46 (pt, $J_{HH} = 1.9$ Hz, 4H, $C_5H_4$), 4.35 (pt, $J_{HH} = 1.9$ Hz, 4H, $C_5H_4$). $^{13}$C{$^1$H} NMR (CDCl$_3$)[$\delta$]: 139.0 ($C_i$-$C_4H_2S$), 124.1 ($C_4H_2S$), 119.6 (CN), 82.8 ($C_i$-$C_5H_4$), 73.7 ($C_5H_4$), 72.9 ($C_5H_4$), 71.2 ($C_5H_4$), 68.7 ($C_5H_4$), 53.6 ($C_i$-$C_5H_4$). HR-ESI MS (calc) {int} [m/z]: 501.9862 (501.9890) {31} [M]$^+$, 502.9932 (502.9963) {70} [M+H]$^+$, 524.9760 (524.9782) {100} [M+Na]$^+$. Crystal data for **E3**, $C_{26}H_{18}Fe_2N_2S$, $M_r = 502.18$ g·mol$^{-1}$, monoclinic, $P2_1/n$, $\lambda = 0.71073$ Å, $a = 11.9241(2)$ Å, $b = 9.7440(2)$ Å, $c = 17.7181(4)$ Å, $\beta = 103.282(2)$ °, $V = 2003.57(7)$ Å3, $Z = 4$, $\rho_{calcd} = 1.665$ g·cm$^{-3}$, $\mu = 1.569$ mm$^{-1}$, $T = 109.90(14)$ K, $\Theta$ range = 3.13 – 26.00 °, reflections collected: 16860, independent: 3904 ($R_{int} = 0.0247$), R1 = 0.0248, wR2 = 0.0613 [$I > 2\sigma(I)$].

**Synthesis of 2,5-diferrocenyl-3,4-ethylenedioxythiophene (E4).** Ferrocene (3.0 g, 16.1 mmol) and 0.125 eq of KO$^t$Bu (226 mg) were dissolved in 50 mL of tetrahydrofuran, and the resulting solution was cooled to –90 °C. Afterward, 2 eq (20.2 mL) of 1.6 M *tert*-butyllithium (*n*-pentane) were added within 5 min. After 60 min of stirring, one eq (4.52 g) of [ZnCl$_2$·2thf] was added within 2 min and the resulting reaction mixture was warmed to

0 °C for 30 min. Finally, 0.45 eq (2.18 g) of 2,5-dibromo-3,4-ethylenedioxythiophene[27,276] and 40.8 µmol (28 mg) of $[Pd(CH_2CMe_2P^tBu_2)(\mu\text{-}Cl)]_2$[229,230] were added to the reaction mixture and stirring was continued at 55 °C for 16 h. After the reaction mixture was cooled to ambient temperature, it was hydrolyzed with 1 M hydrochloric acid (50 mL) and the organic layer was separated. The aqueous phase was extracted with diethyl ether (150 mL) and the combined organic phases were dried over $MgSO_4$. After evaporation of all volatiles, the crude product was adsorbed on alumina and purified by column chromatography (column size: 20 x 3 cm, alumina) using an *n*-hexane/toluene mixture of ratio 2:1 (v:v) as eluent. Compound **E4** was obtained as an orange solid. Yield: 1.39 g (2.72 mmol, 38 % based on 2,5-dibromo-3,4-ethylenedioxythiophene). Anal. Calcd for $C_{26}H_{22}Fe_2O_2S$ (510.2): C, 61.21; H, 4.35. Found; C, 61.20; H, 4.34. Mp: 190 °C (dec). IR data (KBr)[cm$^{-1}$]: 3080 w, 2975 w, 2870 W, 1542 m, 1438 s, 1363 s, 823 m. $^1$H NMR (CDCl$_3$)[$\delta$]: 4.66 (pt, $J_{HH}$ = 1.8 Hz, 4H, $C_5H_4$), 4.30 (s, 4H, $C_2H_4O_2$), 4.25 (pt, $J_{HH}$ = 1.8 Hz, 4H, $C_5H_4$), 4.13 (s, 10H, $C_5H_5$). $^{13}$C{$^1$H} NMR (CDCl$_3$)[$\delta$]: 137.4 ($C_i$-$C_4$S), 112.8 ($C_i$-$C_4$S), 78.9 ($C_i$-$C_5H_4$), 69.9 ($C_5H_5$), 68.2 ($C_5H_4$), 66.8 ($C_5H_4$), 64.9 ($C_2H_4O_2$). HR-ESI MS (calc) [m/z]: 510.0120 (510.0034) [M]$^+$. Crystal data for **E4**, $C_{26}H_{22}Fe_2O_2S$, $M_r$ = 510.20 g·mol$^{-1}$, monoclinic, $P2/n$, $\lambda$ = 0.71073 Å, $a$ = 14.4839(10) Å, $b$ = 7.4506(4) Å, $c$ = 19.1676(13) Å, $\beta$ = 104.881(7) °, $V$ = 1999.1(2) Å$^3$, $Z$ = 4, $\rho_{calcd}$ = 1.695 g·cm$^{-3}$, $\mu$ = 1.579 mm$^{-1}$, $T$ = 105(6) K, $\Theta$ range = 2.95 – 25.06 °, reflections collected: 8977, independent: 3523 ($R_{int}$ = 0.0548), R1 = 0.0459, wR2 = 0.1089 [$I > 2\sigma(I)$].

**Sythesis of [E4][B(C$_6$F$_5$)$_4$].** For solid state structure analysis, [**E4**][B(C$_6$F$_5$)$_4$] was prepared by treating a dichloromethane (10 mL) solution containing **E4** (98.0 µmol, 50.0 mg) with an equimolar amount of [Ag[B(C$_6$F$_5$)$_4$]·Et$_2$O]$^{290}$ at ambient temperature. The resulting crude product was washed twice with *n*-hexane (20 mL), and [**E4**][B(C$_6$F$_5$)$_4$] was crystallized by diffusion of *n*-hexane into a saturated diethyl ether solution of [**E4**][B(C$_6$F$_5$)$_4$] at –30 °C. Crystal data for [**E4**][B(C$_6$F$_5$)$_4$], $C_{54}H_{32}BF_{20}Fe_2O_3S$, $M_r$ = 1263.37 g·mol$^{-1}$, triclinic, $P\bar{1}$, $\lambda$ = 0.71073 Å, $a$ = 10.5390(5) Å, $b$ = 12.7194(6) Å, $c$ = 19.9395(7) Å, $\alpha$ = 93.121(3) °, $\beta$ = 104.227(3) °, $\gamma$ = 108.078(4) °, $V$ = 2438.10(18) Å$^3$, $Z$ = 2, $\rho_{calcd}$ = 1.721 g·cm$^{-3}$, $\mu$ = 0.762 mm$^{-1}$, $T$ = 109.90(14) K, $\Theta$ range = 3.03 – 26.00 °, reflections collected: 22177, independent: 9488 ($R_{int}$ = 0.0233), R1 = 0.0455, wR2 = 0.0962 [$I > 2\sigma(I)$].

**Synthesis of 2,5-di-(1'-(3,5-bis(trifluoromethyl)phenyl)-ferrocenyl)-3,4-ethylenedioxy-thiophene (E5).** Compound **E8** (Appendix Section) (1.0 g, 2.1 mmol) was dissolved in 50 mL tetrahydrofuran. At –90 °C this solution was treated with 1.05 eq (0.9 mL) of 2.5 M *n*-

butyllithium (*n*-hexane) within 5 min. The obtained dark red solution was stirred at –90 °C for 45 min. Afterward, 1.05 eq (0.62 g) of [ZnCl$_2$·2thf] were added in a single portion and the resulting reaction mixture was warmed to 0 °C, and after 30 min, 0.45 eq (283 mg) of 2,5-dibromo-3,4-ethylenedioxythiophene[27,276] and 20.4 µmol (14 mg) of [Pd(CH$_2$CMe$_2$P$^t$Bu$_2$)($\mu$-Cl)]$_2$[229,230] were added. The resulting mixture was warmed to 55 °C for 48 h. Afterward, the reaction mixture was hydrolyzed at ambient temperature with 1 M hydrochloric acid (30 mL), the organic layer was separated and the aqueous phase was extracted with diethyl ether (100 mL). The combined organic phases were dried over MgSO$_4$ and evaporated to dryness. The crude product was adsorbed on alumina and purified by column chromatography (column size: 20 x 3 cm, alumina) using an *n*-hexane/toluene mixture of ratio 2:1 (v:v) as eluent. After recrystallization from a dichloromethane/*n*-hexane mixture (ratio 1:4) compound **E5** was obtained as red-orange crystals. Yield: 0.61 g (0.65 mmol, 69 % based on 2,5-dibromo-3,4-ethylenedioxy-thiophene). Anal. Calcd for C$_{42}$H$_{26}$F$_{12}$Fe$_2$O$_2$S (934.4): C, 53.99; H, 2.80. Found; C, 54.02; H, 2.94. Mp: 185 °C. IR data (KBr)[cm$^{-1}$]: 3088 w, 2984 w, 2942 w, 2874 w, 1613 w, 1538 w, 1502 w, 1441 w, 1359 m, 1331 s, 1162 m, 1123 s, 1091 m, 1024 m, 886 m, 819 m, 698 m, 682 m. $^1$H NMR (CDCl$_3$)[$\delta$]: 7.71 (m, 4H, C$_6$H$_3$), 7.53 (m, 2H, C$_6$H$_3$), 4.59 (pt, $J_{HH}$ = 1.9 Hz, 4H, C$_5$H$_4$), 4.47 (pt, $J_{HH}$ = 1.9 Hz, 4H, C$_5$H$_4$), 4.38 (pt, $J_{HH}$ = 1.9 Hz, 4H, C$_5$H$_4$), 4.20 (pt, $J_{HH}$ = 1.9 Hz, 4H, C$_5$H$_4$), 4.13 (s, 4H, C$_2$H$_4$O$_2$). $^{13}$C{$^1$H} NMR (CDCl$_3$)[$\delta$]: 141.8 (C$_i$-C$_6$H$_3$), 137.8 (C$_i$-C$_4$S), 131.5 (q, $J_{CF}$ = 33 Hz, C$_i$-C$_6$H$_3$), 125.6 (m, C$_6$H$_3$), 123.6 (q, $J_{CF}$ = 273 Hz, CF$_3$), 111.1 (C$_i$-C$_4$S), 119.2 (m, C$_6$H$_3$), 83.0 (C$_i$-C$_5$H$_4$), 80.7 (C$_i$-C$_5$H$_4$), 71.4 (C$_5$H$_4$), 69.6 (C$_5$H$_4$), 68.2 (C$_5$H$_4$), 68.0 (C$_5$H$_4$), 64.5 (C$_2$H$_4$O$_2$). HR-ESI MS (calc) [m/z]: 934.0162 (934.0157) [M]$^+$. Crystal data for **E5**, C$_{42}$H$_{26}$F$_{12}$Fe$_2$O$_2$S, $M_r$ = 934.39 g·mol$^{-1}$, monoclinic, P2/*c*, $\lambda$ = 1.54184 Å, $a$ = 11.6039(3) Å, $b$ = 19.6397(6) Å, $c$ = 16.2593(5) Å, $\beta$ = 107.351(3) °, $V$ = 3536.83(18) Å$^3$, $Z$ = 4, $\rho_{calcd}$ = 1.755 g·cm$^{-3}$, $\mu$ = 8.069 mm$^{-1}$, $T$ = 109.95(10) K, $\Theta$ range = 3.63 – 65.99 °, reflections collected: 14795, independent: 6104 ($R_{int}$ = 0.0359), R1 = 0.0430, wR2 = 0.1131 [$I$> 2$\sigma$($I$)].

**Synthesis of 2,5-di-(1'-formylferrocenyl)-3,4-ethylenedioxy-thiophene (E6).** A solution of **E11** (Appendix Section) (2.52 g, 7.43 mmol) in 50 mL tetrahydrofuran was cooled to –90 °C and 1.05 eq (3.1 mL) of 2.5 M *n*-butyllithium (*n*-hexane) were added within 5 min. After 45 min of stirring, 1.05 eq (2.19 g) of [ZnCl$_2$·2thf] were added in a single portion and the resulting reaction mixture was warmed to 0 °C within 30 min. Afterward, 0.45 eq (1.00 g) of 2,5-dibromo-3,4-ethylenedioxythiophene[27,276] and 58.3 µmol (40 mg) of [Pd(CH$_2$CMe$_2$P$^t$Bu$_2$)($\mu$-Cl)]$_2$[229,230] were added in a single portion to the reaction mixture.

The resulting mixture was warmed to 55 °C for 22 h. After cooling to ambient temperature, the reaction was hydrolyzed with 1 M degassed hydrochloric acid (80 mL) and was extracted with dichloromethane (150 mL). The combined organic phases were dried over $MgSO_4$ and the solvent was removed in vacuum. The remaining crude product was adsorbed on alumina and purified by column chromatography (column size: 20 x 3 cm, alumina) using a $CH_2Cl_2$/toluene mixture of ratio 2:1 (v:v) as eluent. After recrystallization from a dichloromethane/$n$-hexane mixture (ratio 1:4) compound **E6** was obtained as red crystals. Yield: 1.20 g (2.12 mmol, 63 % based on 2,5-dibromo-3,4-ethylenedioxythiophene). Anal. Calcd for $C_{28}H_{22}Fe_2O_4S$ (566.2): C, 59.39; H, 3.92. Found; C, 59.03; H, 3.94. Mp: 142 °C. IR data (KBr)[cm$^{-1}$]: 3075 w, 2977 w, 2927 w, 2860 w, 2823 w, 2757 w, 1681 s, 1457 m, 1084 s, 828 m. $^1$H NMR (CDCl$_3$)[$\delta$]: 9.82 (s, 2H, CHO), 4.80 (pt, $J_{HH}$ = 1.9 Hz, 4H, C$_5$H$_4$), 4.75 (pt, $J_{HH}$ = 1.9 Hz, 4H, C$_5$H$_4$), 4.55 (m, 4H, C$_5$H$_4$), 4.36 (s, 4H, C$_2$H$_4$O$_2$), 4.34 (pt, $J_{HH}$ = 1.9 Hz, 4H, C$_5$H$_4$). $^{13}$C{$^1$H} NMR (CDCl$_3$)[$\delta$]: 193.5 (CHO), 138.5 (C$_i$-C$_4$S), 110.9 (C$_i$-C$_4$S), 81.3 (C$_i$-C$_5$H$_4$), 80.5 (C$_i$-C$_5$H$_4$), 74.7 (C$_5$H$_4$), 71.1 (C$_5$H$_4$), 69.7 (C$_5$H$_4$), 67.6 (C$_5$H$_4$), 64.9 (C$_2$H$_4$O$_2$). HR-ESI MS (calc) [m/z]: 565.9905 (565.9933) [M]$^+$.

**Synthesis of 2,5-di-(1'-cyanoferrocenyl)-3,4-ethylenedioxy-thiophene (E7)**. Hydroxyl-amine hydrochloride (123 mg, 1.77 mmol) was dissolved in 2 mL degassed H$_2$O and 0.71 mmol (400 mg) of **E6** dissolved in 4 mL pyridine was added in a single portion. After 40 min of stirring, vitriol (71 mg, 0.28 mmol) and a mixture of triethylamine (0.5 mL) and dichloromethane (2 mL) were added, followed by an addition of $N,N'$-dicyclohexylcarbodiimide (0.42 g, 2.04 mmol) in 8 mL of dichloromethane. After 16 h of stirring, all volatiles were evaporated and the remaining crude product was purified by column chromatography (column size: 20 x 3 cm, alumina) using dichloromethane as eluent. After recrystallization from a dichloromethane/$n$-hexane mixture (ratio 1:4) compound **E7** was obtained as orange crystals. Yield: 0.29 g (0.52 mmol, 73 % based on 7). Anal. Calcd for $C_{28}H_{20}Fe_2N_2O_2S$ (560.2): C, 60.03; H, 3.60; N, 5.00. Found; C, 60.06; H, 3.61; N, 5.00. Mp: 158 °C. IR data (KBr)[cm$^{-1}$]: 3106 w, 2990 w, 2939 w, 2870 w, 2225 m, 2219 s, 1541 m, 1458 s, 1442 s, 1366 m, 1230 m , 1217 m, 1086 s, 1032, m, 826 m, 816 w. $^1$H NMR (CDCl$_3$)[$\delta$]: 4.82 (pt, $J_{HH}$ = 1.9 Hz, 4H, C$_5$H$_4$), 4.58 (pt, $J_{HH}$ = 1.9 Hz, 4H, C$_5$H$_4$), 4.40 (m, 4H, C$_5$H$_4$), 4.38 (s, 4H, C$_2$H$_4$O$_2$), 4.35 (pt, $J_{HH}$ = 1.9 Hz, 4H, C$_5$H$_4$). $^{13}$C{$^1$H} NMR (CDCl$_3$)[$\delta$]: 138.8 (C$_i$-C$_4$S), 119.5 (CN), 110.4 (C$_i$-C$_4$S), 81.8 (C$_i$-C$_5$H$_4$), 73.4 (C$_5$H$_4$), 72.3 (C$_5$H$_4$), 70.5 (C$_5$H$_4$), 68.4 (C$_5$H$_4$), 64.9 (C$_2$H$_4$O$_2$), 58.3 (C$_i$-C$_5$H$_4$). HR-ESI MS (calc) {int} [m/z]: 559.9901 (559.9940) {100} [M]$^+$, 582.9799 (582.9837) {85}

[M+Na]$^+$. Crystal data for **E7**, $C_{29}H_{22}Cl_2Fe_2N_2O_2S$, $M_r$ = 645.15 g·mol$^{-1}$, orthorhombic, *Pbca*, $\lambda$ = 1.54184 Å, $a$ = 23.5771(12) Å, $b$ = 7.5787(5) Å, $c$ = 28.8018(14) Å, $V$ = 5146.4(5) Å$^3$, $Z$ = 8, $\rho_{calcd}$ = 1.665 g·cm$^{-3}$, $\mu$ = 11.973 mm$^{-1}$, $T$ = 104.95(10) K, $\Theta$ range = 3.07 – 65.00 °, reflections collected: 11997, independent: 4341 ($R_{int}$ = 0.0628), R1 = 0.0623, wR2 = 0.1530 [$I$> $2\sigma(I)$].

**Electrochemistry**. The electrochemical measurements were carried out under an argon atmosphere on 1.0 mmol·L-1 dichloromethane solutions containing 0.1 mol·L-1 of [N$^n$Bu$_4$][B(C$_6$F$_5$)$_4$] as supporting electrolyte utilizing a Voltalab 10 electrochemical laboratory from Radiometer Analytical.[90,100] For spectroelectrochemical measuements, an OTTLE cell (= Optically Transparent Thin Layer Electrochemistry) placed in a Varian Cary 5000 UV-VIS-NIR absorption spectrometer or an Thermo Nicolet IR 100 FT-IR spectrometer was used.[238] For voltammetry, a three electrode cell with a platinum auxiliary electrode, a glassy carbon working electrode and a Ag/Ag$^+$ reference electrode were used. The working electrode was prepared by polishing with a Buehler micro cloth using Buehler diamond pastes with decreasing sizes (1 to 0.25 μm). The Ag/Ag$^+$ reference electrode was constructed from a silver wire inserted into a Luggin capillary with a Vycor tip containing a solution of 0.01 mol·L$^{-1}$ [AgNO$_3$] and 0.1 mol·L$^{-1}$ [N$^n$Bu$_4$][B(C$_6$F$_5$)$_4$] in acetonitrile. This Luggin capillary was inserted into a second Luggin capillary with Vycor tip filled with a 0.1 mol·L$^{-1}$ [N$^n$Bu$_4$][B(C$_6$F$_5$)$_4$] solution in dichloromethane. Successive experiments under the same experimental conditions showed that all formal reduction and oxidation potentials were reproducible within 5 mV. Experimentally potentials were referenced against a Ag/Ag$^+$ reference electrode but the results are presented referenced against the FcH/FcH$^+$ couple ($E^{0'}$ = 0.0 V) as required by IUPAC.[249] When decamethylferrocene was used as an internal standard, the experimentally measured potential was converted in to E *vs.* FcH/FcH$^+$ by addition of –0.61 V.[250] The cyclic voltammograms were taken after typical two scans and are considered to be steady state cyclic voltammograms, in which the signal pattern differs not from the initial sweep. Finally, the experimental data were processed on Microsoft Excel worksheets.

**Crystallography**. Data were collected with an Oxford Gemini S diffractometer at 100 K using Mo K$\alpha$ ($\lambda$ = 0.71073 Å) radiation. The structures were solved by direct methods using SHELXS-97 and refined by full matrix least-square procedures on $F^2$ using SHELXL-97.[251,252] All non-hydrogen atoms were refined anisotropically and a riding model was employed in the refinement of the hydrogen atom positions.

Crystallographic data (see the corresponding Part in the analytical section above) for the structures in this paper have been deposited with the Cambridge Crystallographic Data Centre, CCDC, 12 Union Road, Cambridge CB21EZ, UK. Copies of the data can be obtained free of charge on quoting the depository numbers CCDC-981406 (**E1**), 981407 (**E2**), 981408 (**E3**), 981409 (**E4**), 981410 ([**E4**][B(C$_6$F$_5$)$_4$]), 981411 (**E5**), 981412 (**E7**) and 981413 (**E10**) (Fax: +44-1223-336-033; e-mail: deposit@ccdc.cam.ac.uk, http://www.ccdc.cam.ac.uk).

**Supporting Information**. The syntheses of 1-bromo-1'-(3,5-bis(trifluoromethyl)phenyl)-ferrocene (**E8**), 3,5-bis(trifluoromethyl)phenylferrocene (**E9**), 1-bromo-1'''-(3,5-bis-(trifluoromethyl)phenyl)-1',1''-biferrocene (**E10**) and 1-bromo-1'-dimethoxymethyl-ferrocene (**E11**), further solid structure details of **E1** – **E4**, [**E4**][B(C$_6$F$_5$)$_4$], **E5** and **E7**; Solid structure analysis of **E10**, cyclic voltammetry data of **E9**, formylferrocene and cyanoferrocene; linear regression data regarding the estimation of the Hammett constant $\sigma_p$ (**E9**) and the UV-Vis-NIR spectra regarding **C3**, **E1** – **E7** in dichloromethane/propylene carbonate are available in the Appendix Section (Chapter AE2).

## E3 FERROCENES BRIDGED BY ETHYLENEDIAMINO THIOPHENE – VARYING CHARGE TRANSFER PROPERTIES IN A SERIES OF 3,4-DI-*N*-SUBSTITUTED 2,5-DIFERROCENYL THIOPHENES

J. M. Speck, M. Korb, A. Schade,[#] S. Spange[#] and Heinrich Lang

*Section E3 was made by the author of the present doctoral thesis (synthesis, characterization, electrochemistry, interpretation of results and manuscript preparation) together with M. Korb (solid-state structure determination, discussion) in supervision of Prof. Dr. Heinrich Lang, and in collaboration with S. Spange (#) and A. Schade (UV-Vis solvatochromic studies of E12 and E14).*

INTRODUCTION

The continuous miniaturization process of electronic devices implements a steadily increasing demand of tailor-made innovative materials. For instance, heterocyclic and especially thiophene-based intrinsic conducting polymers (ICP) are necessary components to develop antistatic coatings or new flexible electroactive materials, *inter alia* applied in organic light-emitting diodes (OLEDs).[12–21] Moreover, thiophene derivatives, *e.g.* thienopyridines and thienopyrazines, were investigated for their application as organic light-emitting materials.[291–298] Hence, such aromatics modified with organometallic, redox-active transition metal fragments should be interesting molecules regarding their use in molecular electronics.[38,43–48] Due to their reversible redox behavior, ferrocenes are often applied as manifold building blocks for the investigation of electronic properties and electron excitation phenomena.[166,171–173,178–180,183,184,210,223,224,232,253,271,273,274] Prime examples are the perferrocenylated derivatives of benzene[223] or cyclopentadienyl-manganese(I) tricarbonyl[232] as well as a diversity of ferrocenyl-substituted heterocycles including boroles,[169,170] furanes,[171,172] group 4 metallacycles,[186–188] phospholes,[173] pyrroles,[176–181] siloles[182] and thiophenes.[163,167,183,184,210] Within this context, the electronic coupling in the corresponding mixed-valent states varies strongly with the electronic structure of the respective species.[31,166,171,173,180,184,253] It could be recently shown on α,α'-diferrocenyl thiophenes that electron-withdrawing groups on the ferrocenyls in combination with an electron-donating ethylenedioxy unit on the thiophene bridge (EDOT) enforces the electronic coupling between the iron-based redox centers in the mixed-valent state.[253,271]

In continuation of this work, we report herein the synthesis of diferrocenyl diamino thiophenes in a series of 3,4-di-*N*-substituted 2,5-diferrocenyl thiophenes (Figure E14) with the aim to improve the electronic interaction between the organometallic termini over their bridging unit.
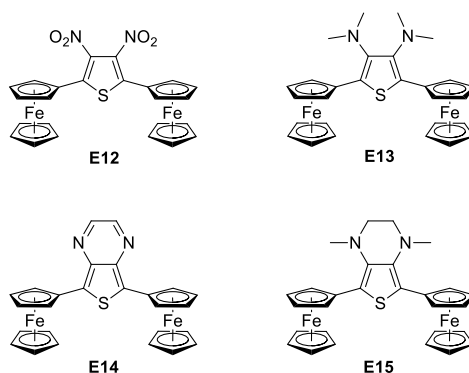


**Figure E14**. Diferrocenyl thiophenes **E12** – **E15**.

The electronic properties of these compounds were investigated by voltammetric experiments in combination with UV-Vis-NIR spectroelectrochemical measurements.[238,253,271]

RESULTS AND DISCUSSION

**Synthesis and Characterization.** The preparation of thiophene **E12** as starting material for molecules **E13** – **E15** (Figure E14) could be performed in a Pd-promoted Suzuki-Miyaura *C,C* cross-coupling reaction of 2 eq. ferroceneboronic acid with one eq of 2,5-dibromo-3,4-dinitro-thiophene[292,299] in abs. toluene, using $K_3PO_4$ as base. Within this context, it is essential to avoid water contamination of the reaction mixture; otherwise, side reactions take place on 2,5-dibromo-3,4-dinitrothiophene. After 40 h stirring at 90 °C and a chromatographic work-up, thiophene **E12** was obtained in 85 % yield as purple needles. Further reduction of **E12** with [$SnCl_2 \cdot 2H_2O$] in an ethanol/conc. hydrochloric acid mixture of ratio 2.5:1 (v:v, reflux) afforded the corresponding diamino compound **E13a** in nearly quantitative yield (Scheme E2). The latter species is very sensitive against oxygen, especially in solution. Thus, it was reacted immediately with either an excess of dimethyl sulfate (6 eq) in a tetrahydrofuran/water mixture (ratio 2.5:1, v:v) in presence of $NaHCO_3$ to synthesize thiophene **E13** (yield: 76 %), or it was treated with glyoxal (30 eq) in ethanol/water and $K_2CO_3$ to obtain thienopyrazine **E14** in an aromatizing condensation reaction as deep turquoise crystals (yield: 91 %) (Scheme E2, Experimental Section). Ethylenediamino thiophene **E15** could be synthesized in analogy to **E13** from pyrazine **E14** by reduction with an excess of $NaBH_4$ in ethanol/tetrahydrofuran of ratio 1:1 (v:v,

reflux), followed by an alkylation reaction with dimethyl sulfate, *vide supra* (Scheme E2, Experimental Section).

**Scheme E2. Synthesis of E12 – E15 (for details see Experimental Section).**
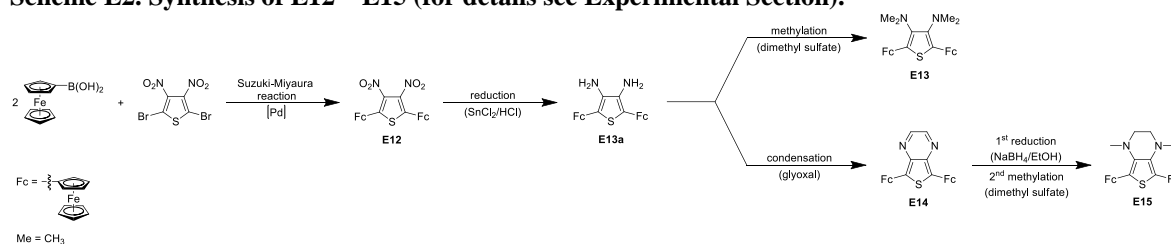


After appropriate work-up, thiophene **E15** could be obtained in acceptable yields as an orange solid material, yield: 56 % (Experimental Section).

*N*-substituted thiophenes **E12** – **E15** are soluble in most common organic solvents including acetone, tetrahydrofuran, toluene and dichloromethane. They are stable in the solid state as well as in solution, compounds **E12** and **E14** are also stable towards aerobic conditions.

Diferrocenylthiophenes **E12** – **E15** were identified by elemental analysis, high resolution ESI-TOF mass spectrometry as well as IR and NMR ($^1$H, $^{13}$C{$^1$H}) spectroscopy. The solid state structures of **E12** – **E15** were determined by single X-ray structure analysis. UV-Vis solvatochromic studies were carried out on **E12** and **E14**. All compounds were electrochemically investigated by cyclic (CV) and square wave voltammetry (SWV) as well as *in situ* spectroelectrochemistry.[238]

For compounds **E12** – **E15**, the anticipated absorptions in the infrared range could be observed, the $^1$H and $^{13}$C{$^1$H} NMR spectra show the expected signal patterns in the predicted ranges (Experimental Section).

**Solid state structures**. The molecular structures of **E12** – **E15** in the solid state have been determined by single crystal X–ray diffraction analysis. Suitable crystals were obtained by diffusion of *n*-hexane into dichloromethane (**E12**, **E14**) and ethyl acetate (**E15**) solutions or by diffusion of ethanol into a dichloromethane (**E13**) solution containing the respective compound at –35 °C (Experimental Section). The molecular structures of **E12** – **E15** together with selected bond distances (Å) and angles (°) are depicted in Figures E15 and E16 and in the Appendix Section. Crystal and structure refinement data are presented in the Experimental Section (*vide infra*).

Compounds **E12** – **E15** crystallize in the monoclinic space groups *P*2$_1$/*n* (**E12**) and *P*2$_1$/*c* (**E14**) or in orthorhombic *Fdd*2 (**E13**, **E15**) with one (**E12**, **E14**) or a half molecule (**E13**,

**E15**) in the asymmetric unit, due to a $C_2$ symmetry axis through the S atoms and the C2–C3 bond of the hetero-cyclic core. The plane intersections of the $^cC_4S$ plane with the cyclopentadienyls of the ferrocenyl moiety range from nearly coplanar (**E12**; 11.95(8) °) to a predominantly cornerwise rotation (**E12**; 39.80 (7) °) (Table AE3-1). Interestingly, the Fe(C$_5$H$_5$) moieties of the ferrocenyls in 2,5 position are directed away from the substituents in 3,4 position with an *anti* (**E13**, **E14** and **E15**) and a *syn* (**E12**) arrangement towards each other with eclipsed torsion angles for all compounds (**E14**, 1.68(4) to **E12**, 15.03(17) °).
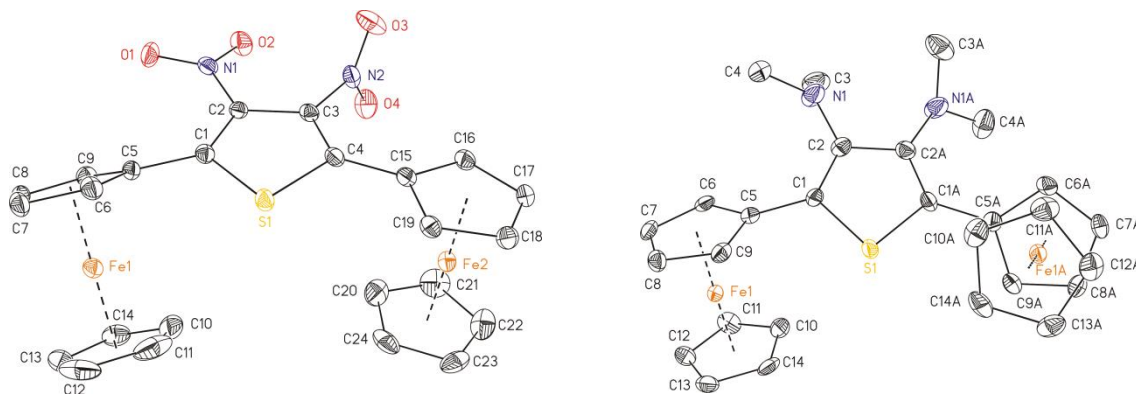


**Figure E15**. ORTEP diagrams (50% probability level) of the molecular structures of **E12** (left) and **E13** (right) with the atom numbering schemes. Hydrogen atoms are omitted for clarity. Selected bond lengths (Å) and angles (°) for **E12**: C1–C2 1.372(3), C1–S1 1.725(2), C2–C3 1.430(3), C3–C4 1.360(3), C4–S1 1.741(2), C2–N1 1.442(3), C3–N2 1.461(3), C4–S1–C1 94.19(10), O1–N1–O2 123.89(18), O3–N2–O4 124.55(19), C1–C2–N1–O1 13.7(3), C4–C3–N2–O3 90.6(3). **E13**: C1–C2 1.375(6), C1–S1 1.730(4), C2–C2A 1.449(7), C2–N1 1.406(6), C1A–S1–C1 93.3(3), C4–N1–C3 113.3(4), C1–C2–N1–C4 33.6(6), C1–C2–N1–C3 116.0(5) (Symmetry code A: –x+1, –y, z).
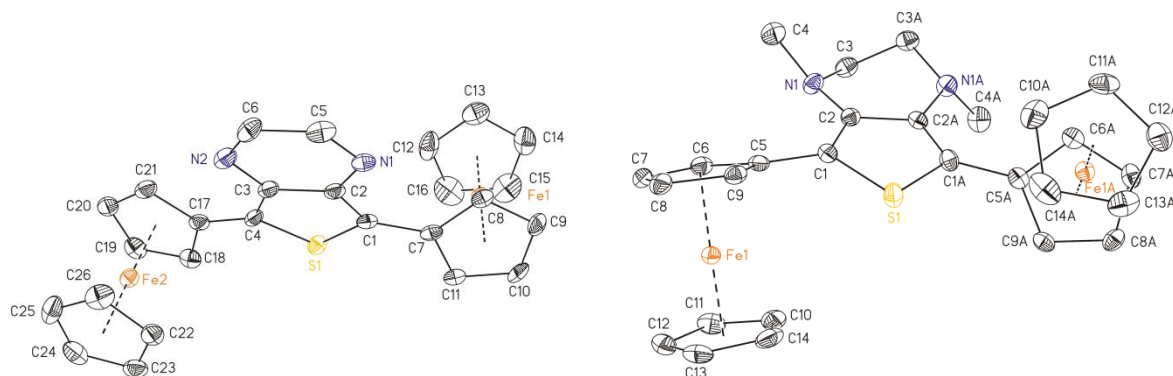


**Figure E16**. ORTEP diagrams (50% probability level) of the molecular structures of **E14** (left) and **E15** (right) with the atom numbering schemes. Hydrogen atoms are omitted for clarity. Selected bond lengths (Å) and angles (°) for **E14**: C1–C2 1.395(6), C1–S1 1.726(4), C2–C3 1.442(6), C3–C4 1.387(6), C4–S1 1.724(4), C2–N1 1.372(5), C3–N2 1.378(5), N1–C5 1.317(5), N2–C6 1.298(6), C5–C6 1.541(7), C2–N1–C5 113.9(4), C3–N2–C6 115.0(4) C1–C2–N1–C5 179.1(4), C4–C3–N2–C6 179.5(4). **E15**: C1–C2 1.373(5), C1–S1 1.731(4), C2–C2A 1.443(6), C2–N1 1.413(4), C1–S1–C1A 93.3(2), C3–N1–C4 113.9(3), C1–C2–N1–C4 59.9(4) (Symmetry code A: –x+3/2, –y+5/2, z).

The nitro groups in compound **E12** are arranged differently on the heterocyclic core, one almost coplanar (15.66(9) °) and the other one shows a perpendicular orientation (88.90(19) °, Figure E15). This results in an intermolecular electrostatic interaction between two differently rotated nitro groups at the N1 and the O3 atom of two adjacent molecules forming a dimeric structure in the crystal packing with N···O distances of

2.895(3) Å (Figure AE3-1, Table AE3-1). Molecules **E13** and **E15** exhibit similar values for the two substituents in 3,4 position, with opposite cornerwise directions (min. 33.6(6) ° (**E13**) to max. 64.0(5) ° (**E13**)), due to their $C_2$ symmetry.

In pyrazine containing **E14** the annelated aromatics are in perfect coplanarity (C5–N1–C2–C1 179.1(4), C6-N2-C3-C4 179.5(4) °) (Figure E16). The value of the X–N–X (X = O, C) angle only depends on the type of the attached atoms and decreases from 123.89(18) and 124.55(19) ° for oxygen (**E12**) to 113.3(4) and 115.0(4) ° for $sp^3$ and $sp^2$ nitrogen atoms in **E13** – **E15**. Interestingly, the bond distances and angles within the heterocycle are not affected by the electronically different substituents, whereas the C(thiophene)–N bond distance decreases from **E12** (1.442(3) Å) > **E15** (1.413(4) Å) ~ **E13** (1.406(6) Å) > **E14** (1.378(5) Å). Furthermore, the C–N distances between the two nitro groups in **E12** differ in dependence of their orientation towards the heterocyclic core. Thus, the rather coplanar oriented substituent allows a partially double bond as a resonance stabilization, which shortens the bond length (1.442(3) Å), whereas 1.461(3) Å are observed for the C–N bond to the perpendicular substituent. The pyrazine substituent in **E14**, with the shortest C–N distance, due to a delocalization with both aromatic systems, however, allows a clear distinction between formal C–N single (1.378(5) and 1.372(5) Å) and C=N double bonds (1.298(6) and 1.317(5) Å).

**UV-Vis solvatochromic studies**. The solvatochromic properties of **E12** and **E14** were investigated in 40 solvents, due to their relatively intense MLCT (*vide infra*) absorptions between 500 nm and 600 nm, and were evaluated by multiple correlation analysis using both the Kamlet-Taft (eq E1)[300–305] and Catalán relationships (eq E2).[306–312] In equation E1, the parameters are as followed: α is the hydrogen bond donor strength (HBD), β is the hydrogen bond acceptor strength (HBA) and π* corresponds to the dipolarity/polarizability of the solvent.[Q] In the multiple regression of equation E2, SA corresponds to the solvent acidity, SB to the solvent basicity, SP to the solvent polarizability, and SdP to the solvent dipolarity.[R] The solvent (*vide supra*) parameters were taken from the literature and the dataset of all measured UV-Vis absorption maxima as well as correlation analysis data are placed in the Appendix Section (Tables AE3-2 and AE3-3).[306,313]

$$\tilde{v}_{max} = \tilde{v}_{max,0} + a \cdot \alpha + b \cdot \beta + s \cdot \pi^* \qquad (E1)$$

$$\tilde{v}_{max} = \tilde{v}_{max,0} + a \cdot SA + b \cdot SB + d \cdot SP + e \cdot SdP \qquad (E2)$$

---

[Q] $\tilde{v}_{max,0}$ represents the UV-Vis absorption maximum within cyclohexane, as a defined reference.
[R] In the Catalán eq., $\tilde{v}_{max,0}$ is related to the gase phase instead of cyclohexane.

The $\lambda_{max}$ value of the UV-Vis absorption of **E12** varies from 504 nm (*n*-hexane) to 546 nm (DMSO), resulting in a positive solvatochromic shift of $\Delta\tilde{v} = 1526$ cm$^{-1}$ (Figure E17). The corresponding metal to ligand charge transfer (MLCT) absorption (*vide infra*) of compound **E14** shows a slight negative solvatochromic shift of approx. 570 cm$^{-1}$, *i.e.* from 617 nm in carbon tetrachloride to 596 nm in acetonitrile (Figure E17).
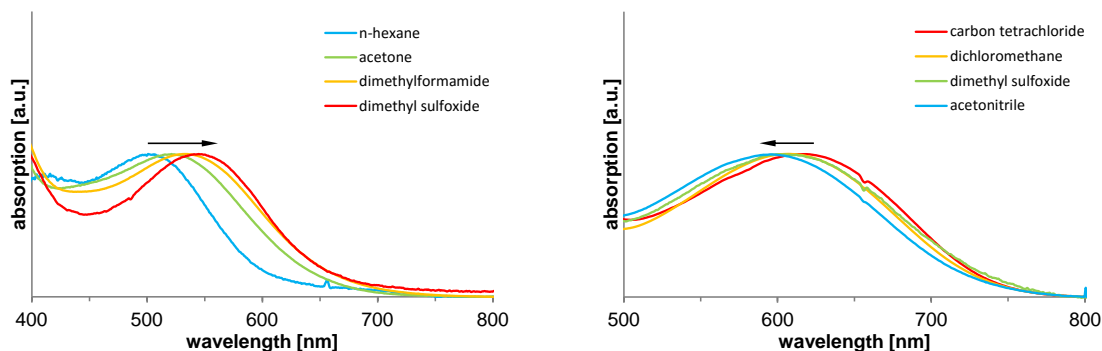


**Figure E17**. Visible absorption spectra of **E12** (left) and **E14** (right) in different solvents, for data see Table AE3-2. Arrows indicate the solvatochromic shifting.

The multiple linear correlation approaches in analogy to Kamlet-Taft and Catalán show similar results for **E12**. Thus, this dye is mainly unaffected by specific interactions, ($a = b = 0$, equations E3 and E4).

$$\tilde{v}_{max} = 19.954 - 1.290 \cdot \pi^* \tag{E3}$$

$$\tilde{v}_{max} = 21.171 - 2.071 \cdot SP - 0.797 \cdot SdP \tag{E4}$$

The unspecific interactions show typical negative coefficients for a more polar first excited state, which is better stabilized by polar solvents ($s < 0$; $d$ and $e < 0$). However, pyrazine **E14** shows a different behavior (eq E5).

$$\tilde{v}_{max} = 17.453 - 0.389 \cdot SA - 1.540 \cdot SP + 0.301 \cdot SdP \tag{E5}$$

A slight dependence on the acidity could be observed, probably due to hydrogen bond interactions incorporating the pyrazine nitrogen atoms, which results in a bathochromic shift. As a consequence of the reduced dipole moment of **E14**, the dependence on solvent dipolarity and polarizability is less pronounced when compared with **E12**. Thus, **E14** behaves like an unpolar polyene, which is mainly influenced by the solvent polarizability ($d < 0$ but $e \sim 0$). The Kamlet-Taft approach reaches his limitations for these compounds, because in the $\pi^*$-parameter the polarizability and dipolarity is combined in a 2:1 ratio.[306] Therefore, this equation is only suitable for dyes with a comparable polarizable to dipolarity ratio. Moreover, due to the small solvatochromic shift, especially for **E14**, the correlation quality is rather low (Figure AE3-2).

**Electrochemistry**. The electrochemical studies on thiophenes **E12** – **E15** were carried out under an argon atmosphere in dichloromethane solutions containing $[N^nBu_4][B(C_6F_5)_4]$ (0.1 M) as supporting electrolyte (Experimental Section). Table E5 presents the electrochemical data. The corresponding cyclic voltammograms (CV) are shown in Figure E18. Under our conditions, compounds **E12** – **E15** show two well-resolved, reversible ferrocenyl-based redox events with small $\Delta E_p$ values and $i_{pc}/i_{pa}$ ratios close to unity (Table E5 and Figure E18).[85,171,234,235,253,271]

**Table E5. Cyclic voltammetry data (potentials *vs.* FcH/FcH$^+$) of 1.0 mM solutions of E12 – E15, 2,5-DiFcTh (C3) and 2,5-DiFc-EDOT (E4), measured in dry dichloromethane containing $[N^nBu_4][B(C_6F_5)_4]$ (0.1 M) as supporting electrolyte at 25 °C.[253,271]**

| Compd. | $E^{0'}/\Delta E_p$ [mV][b] Wave (no.) | | | $\Delta E^{0'}$ [mV][c] | $K_C$ $[10^4]$[d] |
|---|---|---|---|---|---|
| | (1) | (2) | (3) | | |
| **E12** | −1539/71 | 274/66 | 429/71 | 155 | 0.04 |
| **E13** | −168/60 | 168/60 | 1018[e]/ - | 336 | 47.1 |
| **E14** | −1974/64 | −92/62 | 228/62 | 320 | 25.7 |
| **E15** | −249/62 | 169/64 | 858/72 | 418 | 1163.2 |
| **C3**[a] | −53/60 | 195/62 | - | 248 | 1.6 |
| **E4**[a] | −160/64 | 153/66 | - | 313 | 19.5 |

[a] Data from ref. 253,271 . [b] Formal potential ($E^{0'}$). Difference between the oxidation ($E_{pa}$) and reduction ($E_{pc}$) peak potential ($\Delta E_p$).[85,235] [c] Redox separation between the formal iron-based redox events ($\Delta E^{0'} = E^{0'}(n) - E^{0'}(n-1)$). [d] Comproportionation constant $\left(K_C = e^{\frac{\Delta E^{0'}F}{RT}}\right)$. [e] $E_{pa}$.

For thiophene **E12**, Fc/Fc$^+$ redox processes at $E^{0'}$ = 274 mV and 429 mV were found. The more anodic shifted formal potentials (Fc/Fc$^+$) and the reduced redox separation of **E12**, compared with 2,5-diferrocenyl thiophene (2,5-DiFcTh (**C3**))[163,167,253,271] are a consequence of the electron withdrawing properties of its nitro functionalities.[253] Thus, electron acceptor units on the bridging unit decrease the thermodynamic stability ($K_C$)[50,73] of the mixed valent species in such biferrocene systems.[165,180] The opposite case could be shown recently for the 3,4-ethylenedioxy thiophene derivative (2,5-DiFcEDOT (**E4**)), since EDOT has an oxidation potential ca. 0.3 V more cathodic than thiophene itself.[271,283,284] Moreover, an additional dinitro thiophene-based reversible one-electron reduction could be detected for **E12** during the electrochemical analysis. A similar observation was made for pyrazine **E14**, a well-known reversible bridge-based reduction event was recorded at 1.97 V, 430 mV more cathodic as detected for **E14**.[291,292,314] However, the first Fc/Fc$^+$ redox process was found at significantly lower potentials as observed for **E12** and **C3**, in combination with an increased redox separation (Table E5 and Figure E18).[253] Thus, the thieno[3,4-*b*-]pyrazine spacer with its enlarged $\pi$-system

leads to a lower-lying bridge electron density and hence to a larger thermodynamic stability ($K_C$) of **E14**$^+$. A similar "resonance effect" was previously reported for (3,5-bis(trifluoromethyl)-phenyl)ferrocenyl substituted thiophene derivatives (**E1** and **E5**) and is well known for ferrocenyl functionalized *N*-aryl pyrroles in comparison with their *N*-alkyl analogues.[179,180,271]
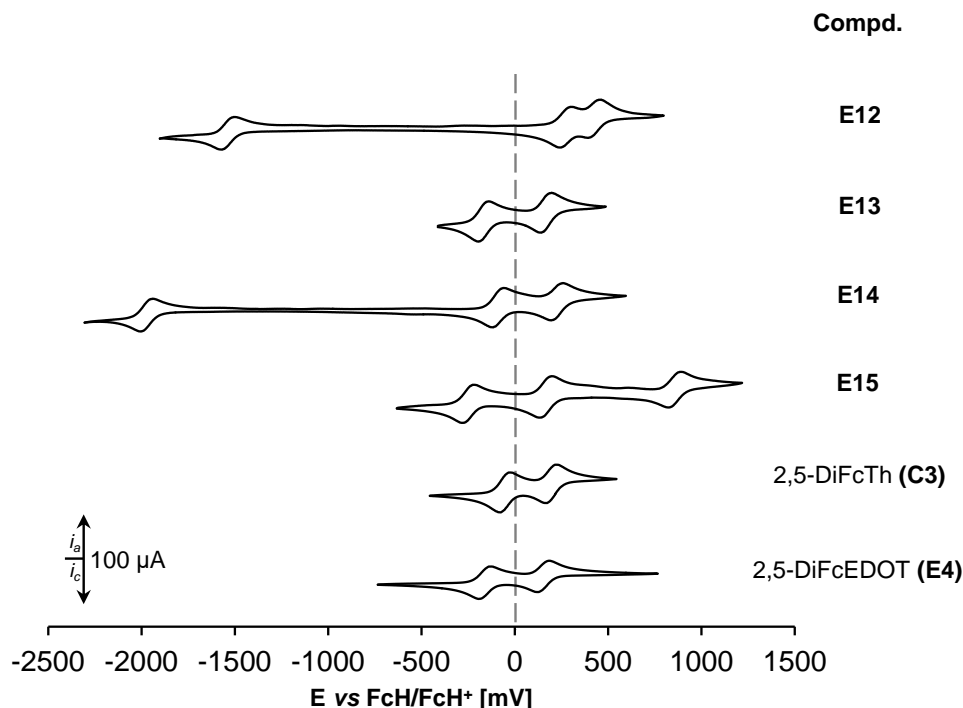


**Figure E18**. Cyclic voltammograms of **E12** – **E15**, 2,5-DiFcTh (**C3**) and 2,5-DiFcEDOT (**E4**), scan rate: 100 mVs$^{-1}$ in dichloromethane solutions (1.0 mM) at 25 °C, supporting electrolyte [N$^n$Bu$_4$][B(C$_6$F$_5$)$_4$] (0.1 M).[253,271,S]

Within this context, an amino thiophene bridge with its dramatically lower oxidation potential (*vs.* thiophene) should have a significant effect on $K_C$ of the corresponding mixed-valent diferrocenyl heterocycle.[180,271,315] However, for diamino thiophene **E13**, only a Fc/Fc$^+$ redox separation of $\Delta E^{0'} = 336$ mV was found, very similar electrochemical results compared with **E4** (Table E5, Figure E18).[271] These observations suggest an electrosteric repulsion of the *N,N*-dimethylamino groups on the thiophene ring and thus a non-ideal interaction of their non-bonding electron density with the thiophene $\pi$-system. The irreversible amino oxidation process at $E_{pa} = 1.02$ V, which is typical for non-resonance stabilized amminium species, supports this conclusion (Table E5, Figure AE3-3).[315] In this regard, a maximization of the corresponding amino-$\pi$ interaction should be possible by "forcing" the nitrogen electron lone pairs into coplanarity with the thiophene. Thus, a chemical "handle" was required to fix the nitrogen atoms, similar as known for

---

[S] SWV results confirmed perfectly the CV data.

3,4-dialkoxy thiophenes (*i.e.*, EDOT).[16,28,316] Hence, for ethylenediamino thiophene **E15** a significant cathodic shift of the first Fc/Fc$^+$ redox process could be detected together with a clearly larger redox separation (larger thermodynamic stability of **E15**$^+$) as observed for thiophene **E13** (Table E5 and Figure E18). Moreover, an additional reversible one-electron amino/amminium redox event was recorded at ca. 860 mV *vs.* FcH/FcH$^+$, similar to that known for other aryl amines, indicating a high degree of amino-$\pi$ interaction in the bridging unit of **E14/E14**$^+$.[63,128–130,317,318]

As an outcome from the electrochemical investigations, electrosteric effects have a significant influence on the electronically interacting substituents with their connected $\pi$-system, not only in the solid state (*vide supra*), but also in solution. Thus, the thermodynamic stabilities of the mixed-valent species ($K_C$) increase in the series **E12** < **E13** ≈ **E14** < **E15** (Table E5, Figure E18).

For a deeper evaluation of the electronic coupling, *in situ* spectroelectrochemical studies were carried out by an stepwise increase of the potential (varying step heights: 5 – 100 mV) *vs.* Ag/AgCl in an OTTLE[238] (= Optically Transparent Thin Layer Electrochemistry) cell using a 0.1 M dichloromethane ($\mu$ = 1.6 D) solution of [N$^n$Bu$_4$][B(C$_6$F$_5$)$_4$] as supporting electrolyte.[270] The solvatochromic behavior of NIR absorptions was determined by using propylene carbonate (PC, $\mu$ = 4.9 D) as polar solvent (*vide infra*).[50,57,68,70,270,271] If deconvolution of NIR absorptions was used, three or four Gaussian-shaped transitions were applied to get fits good enough for an almost exact overlay with the sum of the experimental spectral components. The corresponding spectra are presented in Figure E19 and in the Appendix Section (Figures AE3-4 to AE3-7).

All neutral thiophene complexes do not display any absorptions in the NIR range. During the oxidation of **E12 – E15** typical absorptions in the UV-Vis (inner ferrocenyl related $\pi$-$\pi^*$ and MLCT/d-d transitions) and NIR region were observed for mixed-valent **E12**$^+$ – **E15**$^+$ (Table E6, *vide infra*).[31,239,240,253] Thus, during the formation of **E12**$^+$ the relatively intense MLCT transition around 530 nm shifts bathochromically in combination with an occurrence of a broad near infrared absorption, which consists of two NIR absorptions close together (Figure E19). A very weak intervalence charge transfer (IVCT) absorption is accompanied by a formal forbidden ligand field transition (LF) of the ferrocenium increments, as characteristic for 17-valence electron (VE) species (Table E6, Figure E19).[210,244,319] Such a NIR absorption behavior is typical for very weakly coupled class II systems,[68,166,177,210,253] since an observed IVCT absorption with a bandwidth at half height

($\Delta\tilde{v}_{1/2}$) significantly larger than the theoretical prediction ($\Delta\tilde{v}_{1/2(theo)}$) in combination with a solvatochromic shift ($\Delta\tilde{v}_{max\text{-}IVCT}$) 900 cm$^{-1}$ larger as found for 2,5-diferrocenyl thiophene (**C3**) itself supports this classification and agrees with the electrochemical results (*vide supra*, Table E6 and Figure E19).[271] Upon generation of **E12$^{2+}$**, the IVCT absorption band disappears, while the MLCT around 600 nm undergoes a formal bathochromic and hypochromic shift. Otherwise, UV-Vis-NIR spectroelectrochemical investigations during the reduction of thiophene **E12** reveal a hypsochromic shift of the latter transition together with the appearance of two additional absorptions around 11000 cm$^{-1}$ and 18000 cm$^{-1}$, probably caused by ligand to metal charge transfer (LMCT, dinitro thiophene to ferrocenyl) interactions in **E12$^-$** (Figure AE3-4).

**Table E6. NIR data of E12 – E15 measured in dry dichloromethane containing [N$^n$Bu$_4$][B(C$_6$F$_5$)$_4$] (0.1 M) as supporting electrolyte at 25 °C.**

| Compd. | Transition | $\tilde{v}_{max}$ [cm$^{-1}$] ($\varepsilon_{max}$ [Lmol$^{-1}$cm$^{-1}$])$^a$ | $\Delta\tilde{v}_{1/2}$ [cm$^{-1}$]$^b$ | $\Delta\tilde{v}_{1/2(theo)}$ [cm$^{-1}$]$^c$ | $\tilde{v}_{max\text{-}IVCT\text{-}PC}$ [cm$^{-1}$]$^{d,e}$ ($\Delta\tilde{v}_{1/2\text{-}PC}$ [cm$^{-1}$])$^d$ \{$\Delta\tilde{v}_{max\text{-}IVCT}$ [cm$^{-1}$]\}$^f$ | $H_{ab}$ [cm$^{-1}$]$^{g,h}$ | *Ref.* |
|---|---|---|---|---|---|---|---|
| **E12$^+$** | IVCT<br>LF | 6080  (320)<br>3810    (60) | 4970<br>970 | 3750 | 9010<br>(4490)<br>\{2930\} | 270 | this work |
| **E13$^+$** | LMCT<br>IVCT<br>IC<br>IC | 8390  (700)<br>5000 (2520)<br>4210 (1130)<br>3490  (540) | 2700<br>3630<br>880<br>740 | 3400 | 6040<br>(3160)<br>\{1040\} | 590 | this work |
| **E14$^+$** | LMCT<br>IVCT<br>IC<br>IC | 9070  (670)<br>4440 (3480)<br>4030 (1400)<br>3490 (2690) | 2580<br>3130<br>560<br>950 | 3200 | 5520<br>(3340)<br>\{1080\} | 600 | this work |
| **E15$^+$** | LMCT<br>IVCT<br>IC | 8190  (830)<br>4800 (3390)<br>4310 (1370) | 3200<br>3530<br>1200 | 3330 | 5510<br>(3560)<br>\{710\} | 660 | this work |
| **C3$^+$** | LMCT<br>IVCT<br>IC<br>IC | 10080 (620)<br>4990 (2130)<br>4054  (570)<br>3524  (830) | 2880<br>3840<br>440<br>990 | 3400 | 7020<br>(3950)<br>\{2030\} | 560 | 253,271 |
| **E4$^+$** | LMCT<br>IVCT<br>IC<br>IC | 9160  (670)<br>4840 (3330)<br>4180 (1470)<br>3540 (2160) | 2620<br>3300<br>690<br>1010 | 3440 | 6160<br>(3090)<br>\{1320\} | 630 | 271 |

$^a$ Wavenumber of the bands maximum intensity ($\tilde{v}_{max}$), extinction coefficient at $\tilde{v}_{max}$ ($\varepsilon_{max}$). $^b$ Bandwidth at half height ($\Delta\tilde{v}_{1/2}$). $^c$ Bandwidth at half height expected from the Hush theory ($\Delta\tilde{v}_{1/2(theo)} = (2310\tilde{v}_{max})^{1/2}$). $^d$ Measured in propylene carbonate (PC). $^e$ $\Delta\tilde{v}_{1/2}$ of the IVCT transition measured in PC. $^f$ Solvatochromic shift ($\Delta\tilde{v}_{max\text{-}IVCT} = \tilde{v}_{max\text{-}IVCT\text{-}PC} - \tilde{v}_{max}$). $^g$ Electronic coupling, using eq E6. $^h$ Using $r_{ab}$ as separation of the donor and acceptor charge centroids.$^T$

However, no absorptions could be detected for **E12$^-$** in the NIR range. Similar findings were made for **E14$^-$**, in combination with a vanishing of the intense MLCT absorption around 600 nm (Figure AE3-6). Throughout the anodic conversion of pyrazine **E14**, a couple of absorption bands could be detected for **E14$^+$** in the NIR region: A high-energy

---

$^T$ For weakly coupled systems, $r_{ab}$ was assumed as the geometrical distance between the centroids of the thiophene-bonded cyclopentadienyl rings ($r_{ab} \approx 7.5$ Å)

NIR absorption around 9000 cm$^{-1}$, which can be attributed to a ligand to metal charge transfer (LMCT), as reported previously.[31,210,253,286,287,320] Furthermore, an intervalence charge transfer transition at ca. 4400 cm$^{-1}$ is accompanied by low-energy near-infrared absorptions which are ascribed as interconfigurational (IC) transitions.[49,172,271,289] Thus, the observed IVCT absorption of **E14$^+$** is significantly bathochromically shifted in comparison with the corresponding absorptions of monocationic **C3** and the ethylenedioxy thiophene derivative **E4** (Table E6, Figure AE3-5, *vide infra*).[253,271]
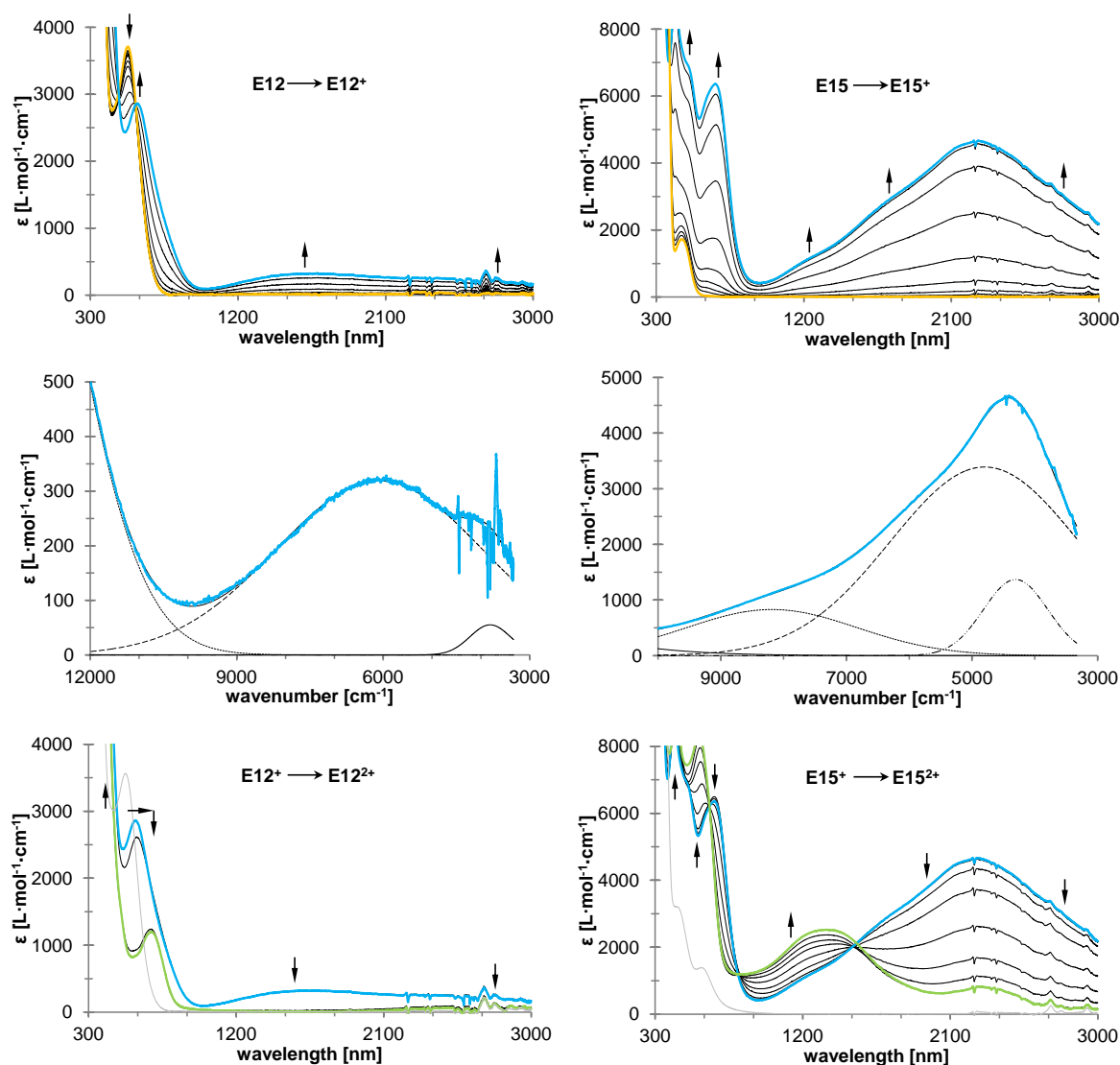


**Figure E19**. Left: UV-Vis-NIR spectra of **E12** at rising potentials. Top: –100 to 780 mV. Middle: deconvolution of NIR absorptions at 780 mV using three distinct overlapping transitions with Gaussian shapes (dashed line indicates IVCT absorption, dotted line corresponds to absorptions caused by interactions between ligand and metal, solid line indicates LF transitions). Bottom: 780 to 850 mV (grey line represents re-reduction to the neutral species). Right: UV-Vis-NIR spectra of **E15** at rising potentials. Top: –400 to 325 mV. Middle: deconvolution of NIR absorptions at 325 mV using three distinct overlapping transitions with Gaussian shapes (dashed line indicates IVCT absorption, dotted line corresponds to absorptions caused by interactions between ligand and metal, dotted dashed line indicates IC transitions). Bottom: 325 to 650 mV (grey line represents re-reduction to the neutral species). All potentials *vs.* Ag/AgCl, measured in dry dichloromethane containing [N$^n$Bu$_4$][B(C$_6$F$_5$)$_4$] (0.1 M) as supporting electrolyte at 25 °C Arrows indicate increasing or decreasing as well as shifting absorptions.

Moreover, the enlarged bridge-$\pi$-system in **E14** (**E14$^+$**) results also in a more intense and narrower IVCT as observed for 2,5-DiFcTh (**C3$^+$**), similar as detected for the mixed valent 2,5-DiFcEDOT (**E4$^+$**).[271] The associated solvatochromic shift amounts to only half of the corresponding value for 2,5-diferrocenyl thiophene (also less pronounced as determined for the EDOT derivative) and reveals a higher degree of electronic interaction in **E14$^+$** than in the mixed valent **C3$^+$** (*vide supra*, Table E6 and Figure AE3-6).[253,271] A comparable solvatochromic shift was found for **E13$^+$** ($\Delta\tilde{v}_{max\text{-}IVCT} = 1040$ cm$^{-1}$, Table E6, Figures AE3-5 and AE3-7). However, the extinction coefficient of the corresponding absorption is slightly smaller as that detected for **E14$^+$** as well as for the monocationic 2,5-DiFcEDOT (**E4$^+$**) (*vide supra*). An additional ethylene bridge between the nitrogen atoms leads to an increasing of the IVCT band intensity for **E15$^+$**, together with a significant decrease of the relevant solvatochromic shift (Table E6 and Figure E19). Devoting a quantification of the electronic interaction between the iron centers, a determination of the electronic coupling matrix element $H_{ab}$ was applied, using equation B3.[37,49,50,57,73]

$$H_{ab} = \frac{0.0206}{r_{ab}} \sqrt{v_{max}\varepsilon_{max}\Delta\tilde{v}_{1/2}}$$ (B3)

Within this context, eq B3 is only valid for very weakly coupled (Hush) systems with Gaussian-shaped IVCT absorptions (*vide supra*, Chapter B), *i.e.*, as observed for **E12$^+$**.[49,50,73,U] Thus, in the case of mixed valence complexes with stronger interacting redox centers, $H_{ab}$ will be underestimated (*vide supra*). Hence, the investigation of the electronic coupling $H_{ab}$ is more accurate by using the transition dipole moment, which can be determined from the experimental spectra through integration of the IVCT absorption band.[37,63,321] However, the observation of a couple of NIR absorptions close together, as typical for metal-containing mixed valent species, makes such a spectra analysis difficult (*vide supra*).[49,61,253,271,287,289,320] Furthermore, due to the complex capture of the effective charge transfer distance $r_{ab}$, the geometrical distance of the interacting redox centers is often taken as simplification, which is acceptable for weakly coupled systems.[37,47,49,57,63,321] Considering all these assumptions, the presented $H_{ab}$ values (Table E6) roughly verify the tendency of the increasing electronic interaction in the series of thiophenes **E12** to **E15** and in comparison with 2,5-diferrocenyl thiophene (**C3**) as well as 2,5-DiFcEDOT (**E4**). As an alternative, the investigation of the solvatochromic behavior of IVCT absorptions in a series of mixed valent compounds is also a useful tool to evaluate the magnitude of the

---

[U] With an increasing electronic coupling, a cut-off takes place on the low-energy side of the transition and the absorption becomes asymmetric.

electronic coupling, since the corresponding transitions lose solvent dependency with an increasing electronic coupling.[37,70,271,321,V] Thus, with reference to strongly coupled (class III) systems ($\Delta\tilde{v}_{max\text{-}IVCT} \leq 100$ cm$^{-1}$), the electronic interaction in the considered mixed valent thiophenes increases in the series **E12** < **C3** < **E4** < **E13** ≈ **E14** < **E15** to moderately coupled systems.[68,70,271]


CONCLUSION

Within this study, a series of 3,4-di-*N*-substituted 2,5-diferrocenyl thiophenes is reported with the aim to improve the electronic interaction between the organometallic termini over their bridging unit. The synthesis of thiophenes **E12** – **E15** were implemented on the basis of dinitro thiophene **E12**, which is accessible in excellent yield within a Pd-promoted Suzuki-Miyaura *C*,*C* cross-coupling reaction. Reduction of the nitro functionalities followed by a subsequent treating with either dimethyl sulfate or glyoxal gives compound **E13** or **E14** in very good yields. Ethylenediamino thiophene **E15** could be synthesized through the conversion of **E14** in a final two-step reduction/methylation reaction. The spectroscopic characterization of the obtained molecules was complemented with the determination of structural properties of **E12** – **E15** in the solid state by single-crystal X-ray diffraction analysis. They reveal no significant influence of the electronically different *N*-substituents on the thiophene bond distances and angles.

UV-Vis solvatochromic studies on thiophenes **E12** and **E14** reveal a moderate positive solvatochromic shift of the MLCT absorption of **E12**. However, for pyrazine **E14** a slight negative solvatochromism of the appropriate absorption band was found.

The electrochemical studies of thiophenes **E12** – **E15** were carried out under an atmosphere of argon on dichloromethane solutions containing [N$^{n}$Bu$_4$][B(C$_6$F$_5$)$_4$] (0.1 M) as supporting electrolyte. They reveal an increasing thermodynamic stability of the mixed-valent species ($K_C$) in the order **E12** < **E13** ≈ **E14** < **E15**. Subsequent *in situ* UV-Vis-NIR spectroelectrochemical studies verify these observations. Thus, the NIR absorptions of the corresponding mixed-valent species become more intense and less solvatochromic as the electron-donating effect and the extent of the electronic $\pi$-system of the bridging unit increases. Hence, electronic coupling between the iron-based redox centers over the thiophene-based core increases in this direction (**E12** < **E13** ≈ **E14** < **E15**) – from very

---

[V] This will be a topic in future works.

weakly coupled systems (**E12**) to stronger coupled (**E15**) class II systems according to Robin and Day.[68]

EXPERIMENTAL SECTION

**General Procedures.** All reactions were carried out under an atmosphere of argon using standard Schlenk techniques. Tetrahydrofuran was purified by distillation from sodium/benzophenone ketyl. Toluene and *n*-hexane were purified with a MBRAUN SPS-800 purification system. Dichloromethane was purified by distillation from $CaH_2$.

**Reagents.** Tetra-*n*-butylammonium tetrakis(pentafluorophenyl)borate was prepared by metathesis of lithium tetrakis(pentafluorophenyl)borate etherate (Boulder Scientific) with tetra-*n*-butylammonium bromide, according to a published procedure.[101] 2,5-Dibromo-3,4-dinitrothiophene was prepared according published procedures, but its purification was carried out by sublimation at 120 °C (ca. 0.5 mbar) to obtain an analytical pure compound.[292,299] Ferroceneboronic acid was either ordered from Sigma-Aldrich or it was synthesized from lithioferrocene[247] and triethyl borate based on a procedure of Nesmejanow *et al.*[322] in a high purity (yield: 70 % based on ferrocene). Both batches gave comparable results in Suzuki-Miyaura reactions. All other chemicals were purchased from commercial suppliers and were used as received.

**Instruments.** Infrared spectra were obtained with a Thermo Nicolet 200 FT-IR spectrometer using KBr press techniques for sample preparation. NMR spectra were recorded using an Bruker Avance III 500 FT-NMR spectrometer ($^1$H NMR at 500.303 MHz, $^{13}$C{$^1$H} NMR at 125.813 MHz) at ambient temperature, unless otherwise noted. Chemical shifts ($\delta$) are reported in parts per million (ppm) relative to tetramethylsilane using the solvent as internal reference ($CDCl_3$: $^1$H NMR $\delta = 7.26$ ppm; $^{13}$C{$^1$H}-NMR $\delta = 77.16$ ppm)[246]. Coupling constants ($J$) are reported in Hertz (Hz) and integrations are reported in number of protons. The following abbreviations are used to describe peak patterns: s = singlet, bs = broad singlet, pt = pseudotriplet. Resonance assignments were made using HSQC and HMBC NMR experiments. The melting points were determined using a Gallenkamp MFB 595 010 M melting point apparatus. Microanalyses were performed with a Thermo FLASHEA 1112 Series instrument. High resolution mass spectra were recorded with a Bruker micrOTOF QII with an Apollo II ESI-source. UV-Vis solvatochromic studies were carried out with a Carl Zeiss Jena MCS 400 UV-Vis spectrometer, the resulting data were processed with WIN-Aspect 1.3.1 and Origin 2015.

**Synthesis of 2,5-diferrocenyl-3,4-dinitrothiophene (E12)**. Ferroceneboronic acid (0.44 mmol, 0.1 g), 0.4 eq of 2,5-dibromo-3,4-dinitrothiophene[292,299] (58 mg) and 5 eq of $K_3PO_4$ (462 mg) were suspended in 3 mL of toluene. Afterward, Pd(dppf)Cl$_2$ (11 μmol, 8 mg) was added in a single portion and the resulting reaction mixture was stirred at 90 °C for 40 h. After cooling the reaction mixture to ambient temperature, the crude product was adsorbed on silica and purified by column chromatography (column size: 15 x 3 cm, silica) using dichloromethane as eluent. After recrystallization from a dichloromethane/*n*-hexane mixture (ratio 1:10), **E12** was obtained as deep purple crystals. Yield: 80 mg (0.15 mmol, 85 % based on 2,5-dibromo-3,4-dinitrothiophene). Anal. Calcd. for $C_{24}H_{18}Fe_2N_2O_4S$ (542.2 gmol$^{-1}$): C, 53.17; H, 3.35; N, 5.17. Found; C, 52.85; H, 3.22; N, 5.15. Mp: 207 °C. IR data (KBr) [cm$^{-1}$]: 3096 w, 3087 w, 1555 s, 1511 s, 1400 m, 1322 s, 1283 s, 1107 w, 1038 w, 818 m, 739 w. $^1$H NMR (CDCl$_3$)[$\delta$]: 4.75 (pt, $J_{HH}$ = 1.9 Hz, 4H, C$_5$H$_4$), 4.50 (pt, $J_{HH}$ = 1.9 Hz, 4H, C$_5$H$_4$), 4.24 (s, 10H, C$_5$H$_5$). $^{13}$C{$^1$H} NMR (CDCl$_3$)[$\delta$]: 140.7 (C$_i$-C$_4$S), 136.2 (C$_i$-C$_4$S), 72.8 (C$_i$-C$_5$H$_4$), 71.0 (C$_5$H$_4$), 70.7 (C$_5$H$_5$), 70.4 (C$_5$H$_4$), 67.7 (C$_5$H$_4$). HR-ESI MS (calc) [m/z]: 541.9653 (541.9681) [M]$^+$.

**Crystal data for E12**: $C_{24}H_{18}Fe_2N_2O_4S$, M$_r$ = 542.17 g·mol$^{-1}$, monoclinic, $P2_1/n$, $\lambda$ = 0.71073 Å, $a$ = 15.6921(12) Å, $b$ = 8.2846(6) Å, $c$ = 16.2955(10) Å, $\beta$ = 101.533(7) °, $V$ = 2075.7(3) Å$^3$, Z = 4, $\rho_{calcd}$ = 1.735 g·cm$^{-3}$, $\mu$ = 1.536 mm$^{-1}$, $T$ = 110.00(10) K, $\Theta$ range = 3.18 – 26.00 °, reflections collected: 10225, independent: 4063 ($R_{int}$ = 0.0318), $R_1$ = 0.0306, w$R_2$ = 0.0694 [$I > 2\sigma(I)$].

**Synthesis of 2,5-diferrocenyl-3,4-bis(*N,N*-dimethylamino)thiophene (E13)**. A solution of **E12** (0.1 g, 0.18 mmol) in 10 mL of ethanol was treated with a solution of 10 eq of [SnCl$_2$·2H$_2$O] (0.41 g) in 4 mL conc. degassed hydrochloric acid. The resulting reaction mixture was warmed to 90 °C for 15 h. Afterward, the orange mixture was cooled to 0 °C and quenched with a 4 M degassed sodium hydroxide solution (30 mL). The basic aqueous phase was extracted with diethyl ether (100 mL) and dried over MgSO$_4$. After evaporating of all volatiles in vacuum, the remaining solid (diamine **E13a**) was re-dissolved in 5 mL of tetrahydrofuran and the resulting solution was added to a suspension of sodium bicarbonate (11.9 mmol, 1 g) in 2 mL of degassed H$_2$O. The obtained reaction mixture was cooled to 0 °C and treated with 6 eq of dimethyl sulfate (0.1 mL). After 10 min of isothermal stirring, the preparation was warmed to ambient temperature and stirred for additional 24 h. Thereafter, 10 mL of conc. and degassed ammonia were added in a single portion. After 1 h of stirring at ambient temperature, the organic phase was separated and the aqueous phase was extracted with diethyl ether (100 mL). The combined organic phases were dried

over $MgSO_4$ and all volatiles were removed in vacuum. The remaining crude product was filtered over a pad of silica with ethyl acetate as eluent and crystallized finally from an ethanol/dichloromethane (ratio 3:1, v:v) mixture. Compound **E13** was obtained as orange crystals. Yield: 75 mg (0.14 mmol, 76 % based on **E12**). **E13**: Anal. Calcd. for $C_{28}H_{30}Fe_2N_2S$ (538.3 gmol$^{-1}$): C, 62.47; H, 5.62; N, 5.20. Found; C, 61.99; H, 5.74; N, 5.17. Mp: 160 °C. IR data (KBr) [cm$^{-1}$]: 3084 w, 3075 w, 2861 m, 2834 m, 2781 m, 1525 m, 1442 m, 1424 m, 1385 s, 1196 m, 1107 s, 1010 s, 998 s, 820 s, 809 s, 738 w. $^1$H NMR (acetone-$D_6$)[$\delta$]: 4.62 (pt, $J_{HH}$ = 1.9 Hz, 4H, $C_5H_4$), 4.30 (pt, $J_{HH}$ = 1.9 Hz, 4H, $C_5H_4$), 4.19 (s, 10H, $C_5H_5$), 2.72 (s, 12H, $N(CH_3)_2$). $^{13}C\{^1H\}$ NMR (acetone-$D_6$)[$\delta$]: 146.9 ($C_i$-$C_4S$), 129.6 ($C_i$-$C_4S$), 81.7 ($C_i$-$C_5H_4$), 70.4 ($C_5H_5$), 69.7 ($C_5H_4$), 68.8 ($C_5H_4$), 43.6 ($N(CH_3)_2$). HR-ESI MS (calc) [m/z]: 539.0921 (539.0902) [M+H]$^+$.

**Crystal data for E13**: $C_{28}H_{30}Fe_2N_2S$, $M_r$ = 538.31 g·mol$^{-1}$, orthorhombic, *Fdd*2, $\lambda$ = 0.71073 Å, $a$ = 20.1203(8) Å, $b$ = 17.7202(7) Å, $c$ = 12.6570(5) Å, $V$ = 4512.7(3) Å$^3$, Z = 8, $\rho_{calcd}$ = 1.585 g·cm$^{-3}$, $\mu$ = 1.399 mm$^{-1}$, $T$ = 110(2) K, $\Theta$ range = 3.064 – 24.990 °, reflections collected: 5427, independent: 1612 ($R_{int}$ = 0.0282), $R_1$ = 0.0253, w$R_2$ = 0.0584 [$I > 2\sigma(I)$], absolute structure parameter[323]: 0.020(13).

**E13a**: Anal. Calcd. for $C_{24}H_{22}Fe_2N_2S$ (482.2 gmol$^{-1}$): C, 59.78; H, 4.60; N, 5.81. Found; C, 59.66; H, 4.77; N, 5.72. Mp: 100 °C (dec). IR data (KBr) [cm$^{-1}$]: 3395 w, 3369 w, 3082 w, 1618 w, 1541 w, 1453 s, 1385 w, 1105 m, 1001 m, 875 m, 820 s, 820 m. $^1$H NMR (CDCl$_3$)[$\delta$]: 4.49 (pt, $J_{HH}$ = 1.9 Hz, 4H, $C_5H_4$), 4.28 (pt, $J_{HH}$ = 1.9 Hz, 4H, $C_5H_4$), 4.22 (s, 10H, $C_5H_5$), 3.60 (bs, 4H, $NH_2$). $^{13}C\{^1H\}$ NMR (CDCl$_3$)[$\delta$]: 133.3 ($C_i$-$C_4S$), 112.6 ($C_i$-$C_4S$), 80.7 ($C_i$-$C_5H_4$), 69.5 ($C_5H_5$), 68.3 ($C_5H_4$), 67.2 ($C_5H_4$). HR-ESI MS (calc) [m/z]: 482.0181 (482.0198) [M]$^+$.

**Synthesis of 5,7-diferrocenylthieno[3,4-*b*]pyrazine (E14)**. To a suspension of **E13a** (*vide supra*, 0.21 mmol, 0.1 g) and potassium carbonate (10.5 eq, 0.3 g) in 20 mL of ethanol were added 30 eq (0.6 mL) of glyoxal (40% in $H_2O$) in a single portion. The color of the resulting reaction mixture turned immediately to green. After 14 h of stirring at ambient temperature, the crude product was adsorbed on alumina and purified by column chromatography (column size: 10 x 3 cm, alumina) using dichloromethane as eluent. After recrystallization from a dichloromethane/*n*-hexane mixture (ratio 1:8, v:v) **3** was obtained as deep turquoise crystals. Yield: 95 mg (0.19 mmol, 91 % based on **E13a**). Anal. Calcd. for $C_{26}H_{20}Fe_2N_2S$ (504.2 gmol$^{-1}$): C, 61.93; H, 4.00; N, 5.56. Found; C, 61.67; H, 4.01; N, 5.42. Mp: 245 °C (dec). IR data (KBr) [cm$^{-1}$]: 3097 w, 3084 w, 1907 w, 1527 m, 1520 m, 1277 m, 1106 s, 1012 s, 999 m, 870 s, 809 s. $^1$H NMR (CDCl$_3$)[$\delta$]: 8.37 (s, 2H, $C_2H_2N_2$),

5.14 (pt, $J_{HH}$ = 1.9 Hz, 4H, $C_5H_4$), 4.44 (pt, $J_{HH}$ = 1.9 Hz, 4H, $C_5H_4$), 4.10 (s, 10H, $C_5H_5$). $^{13}C\{^1H\}$ NMR (CDCl$_3$)[$\delta$]: 143.5 ($C_2H_2N_2$), 139.9 ($C_i$-$C_4S$), 131.1 ($C_i$-$C_4S$), 78.3 ($C_i$-$C_5H_4$), 70.3 ($C_5H_5$), 69.4 ($C_5H_4$), 68.1 ($C_5H_4$). HR-ESI MS (calc) [m/z]: 504.0061 (504.0041) [M]$^+$.

**Crystal data for E14**: $C_{26}H_{20}Fe_2N_2S$, $M_r$ = 504.21 g·mol$^{-1}$, monoclinic, $P2_1/c$, $\lambda$ = 0.71073 Å, $a$ = 11.3226(6) Å, $b$ = 13.7160(7) Å, $c$ = 12.9074(6) Å, $\beta$ = 93.785(5) °, $V$ = 1999.95(17) Å$^3$, Z = 4, $\rho_{calcd}$ = 1.675 g·cm$^{-3}$, $\mu$ = 1.573 mm$^{-1}$, $T$ = 109.9(2) K, $\Theta$ range = 2.97 – 26.00 °, reflections collected: 15163, independent: 3908 ($R_{int}$ = 0.0642), $R_1$ = 0.0588, w$R_2$ = 0.1407 [$I > 2\sigma(I)$].

**Synthesis of 5,7-diferrocenyl-1,4-dimethyl-1,2,3,4-tetrahydrothieno[3,4-*b*]pyrazine (E15)**. A solution of **E14** (0.2 mmol, 0.1 g) in 10 mL of tetrahydrofuran and 10 mL of ethanol (90 %) was treated with 10 mmol (375 mg) NaBH$_4$. The resulting reaction mixture was heated up to reflux for 72 h. After cooling to ambient temperature all volatiles were removed in vacuum and the remaining solid was filtered over a pad of celite, using dichloromethane as solvent. Afterward, the solvent was changed to tetrahydrofuran (5 mL) and the resulting solution was added to a suspension of sodium bicarbonate (14.3 mmol, 1.2 g) in 2 mL of degassed H$_2$O. The obtained reaction mixture was cooled to 0 °C and treated with 6 eq of dimethyl sulfate (0.1 mL). After 10 min of isothermal stirring, the preparation was warmed to ambient temperature and stirred for additional 24 h. Furthermore, 10 mL of conc. and degassed ammonia were added. After 1 h of stirring at ambient temperature, the organic phase was separated and the aqueous phase was extracted with 80 mL of diethyl ether. The combined organic phases were dried over MgSO$_4$ and all volatiles were removed in vacuum. The remaining crude product was filtered over a pad of silica with ethyl acetate as eluent and was then crystallized from an ethyl acetate/*n*-hexane (ratio 1:15, v:v) mixture. Compound **E15** was obtained as orange crystals. Yield: 60 mg (0.11 mmol, 56 % based on **E14**). Anal. Calcd. for $C_{28}H_{28}Fe_2N_2S$ (536.3 gmol$^{-1}$): C, 62.71; H, 5.26; N, 5.22 Found; C, 63.20; H, 5.52; N, 5.05. Mp: 210 °C. IR data (KBr) [cm$^{-1}$]: 3097 w, 3084 w, 2951 m, 2857 m, 2799 w, 1522 m, 1467 m, 1385 s, 1348 m, 1107 s, 1001 s, 820 s 810 s. $^1H$ NMR (CDCl$_3$)[$\delta$]: 4.60 (pt, $J_{HH}$ = 1.9 Hz, 4H, $C_5H_4$), 4.25 (pt, $J_{HH}$ = 1.9 Hz, 4H, $C_5H_4$), 4.24 (s, 10H, $C_5H_5$), 2.99 (s, 4H, $C_2H_4(NR)_2$), 2.57 (s, 6H, NCH$_3$). $^{13}C\{^1H\}$ NMR (CDCl$_3$)[$\delta$]: 138.2 ($C_i$-$C_4S$), 116.6 ($C_i$-$C_4S$), 82.1 ($C_i$-$C_5H_4$), 69.9 ($C_5H_5$), 69.5 ($C_5H_4$), 67.7 ($C_5H_4$), 48.0 ($C_2H_4(NR)_2$), 42.6 (NCH$_3$). HR-ESI MS (calc) [m/z]: 536.0653 (536.0667) [M]$^+$.

**Crystal data for E15**: $C_{28}H_{28}Fe_2N_2S$, $M_r$ = 536.29 g·mol$^{-1}$, orthorhombic, *Fdd*2, $\lambda$ = 0.71073 Å, $a$ = 19.8701(5) Å, $b$ = 17.2782(5) Å, $c$ = 12.7919(4) Å, $V$ = 4391.7(2) Å$^3$, Z = 8, $\rho_{calcd}$ = 1.622 g·cm$^{-3}$, $\mu$ = 1.437 mm$^{-1}$, $T$ = 110.00(14) K, $\Theta$ range = 3.659 – 24.992 °, reflections collected: 5450, independent: 1775, ($R_{int}$ = 0.0257), $R_1$ = 0.0224, w$R_2$ = 0.0494 [$I > 2\sigma(I)$], absolute structure parameter[323]: –0.024(12).

**Electrochemistry.** The electrochemical measurements were carried out under an atmosphere of argon on 1.0 mmol·L$^{-1}$ dichloromethane solutions containing 0.1 mol·L$^{-1}$ of [N$^n$Bu$_4$][B(C$_6$F$_5$)$_4$] as supporting electrolyte utilizing a Voltalab 10 electrochemical laboratory from Radiometer analytical.[90,100] For spectroelectrochemical measuements, an OTTLE cell (= Optically Transparent Thin Layer Electrochemistry) placed in a Varian Cary 5000 UV-VIS-NIR absorption spectrometer was used.[238] For voltammetry, a three electrode cell with a platinum auxiliary electrode, a glassy carbon working electrode and a Ag/Ag$^+$ reference electrode were used. The working electrode was prepared by polishing with Buehler MicroFloc using Buehler diamond suspensions with decreasing sizes (1 to 0.25 μm). The Ag/Ag$^+$ reference electrode was constructed from a silver wire inserted into a Luggin capillary with a Vycor tip containing a solution of 0.01 mol·L$^{-1}$ [AgNO$_3$] and 0.1 mol·L$^{-1}$ [N$^n$Bu$_4$][B(C$_6$F$_5$)$_4$] in acetonitrile. This Luggin capillary was inserted into a second Luggin capillary with Vycor tip filled with a 0.1 mol·L$^{-1}$ [N$^n$Bu$_4$][B(C$_6$F$_5$)$_4$] solution in dichloromethane. Successive experiments under the same experimental conditions showed that all formal reduction and oxidation potentials were reproducible within 5 mV. Experimentally potentials were referenced against a Ag/Ag$^+$ reference electrode but the results are presented referenced against the FcH/FcH$^+$ couple ($E^{0\prime}$ = 0.0 V) as required by IUPAC.[249] Within this context, decamethylferrocene was used as an internal standard and the experimentally measured potentials were converted in to $E$ *vs*. FcH/FcH$^+$ by addition of –0.61 V.[250,272] The cyclic voltammograms were taken after typical two scans and are considered to be steady state cyclic voltammograms, in which the signal pattern differs not from the initial sweep. Finally, the experimental data were processed on Microsoft Excel worksheets.

**Crystallography.** Data were collected with an Oxford Gemini S diffractometer at 100 K using Mo Kα ($\lambda$ = 0.71073 Å) radiation. The structures were solved by direct methods using SHELXS-97 and refined by full matrix least-square procedures on F$^2$ using SHELXL-97.[251,252] All non-hydrogen atoms were refined anisotropically and a riding model was employed in the refinement of the hydrogen atom positions. Graphics of the

molecular structures have been created by using ORTEP.[324] Crystallographic data (Experimental Section) for the structures of **E12** – **E15** have been deposited with the Cambridge Crystallographic Data Centre, CCDC, 12 Union Road, Cambridge CB21EZ, UK. Copies of the data can be obtained free of charge on quoting the depository numbers CCDC-1060168 (**E12**), 1060169 (**E13**), 1060170 (**E14**), 1060171 (**E15**), (Fax: +44-1223-336-033; e-mail: deposit@ccdc.cam.ac.uk, http://www.ccdc.cam.ac.uk).

**Supporting Information**

UV-Vis absorption data of **E12** and **E14** in different solvents, the corresponding multiple correlation analysis according to Kamlet-Taft equation and Catalán as well as further UV-Vis-NIR spectra regarding **E12** – **E15** in dichloromethane/propylene carbonate and the crystallographic data of **E12** – **E15** are available in the Appendix Section (Chapter AE3).

# F  ELECTROCHEMICAL EXAMINATIONS OF FERROCENES MODIFIED BY TUNGSTEN ALKYLIDENE COMPLEXES AND THEIR ELECTRONIC INTERACTION WITH THIOPHENE

## F1  METAL-METAL INTERACTION IN FISCHER CARBENE COMPLEXES – A STUDY ON FERROCENYL AND BIFERROCENYL TUNGSTEN ALKYLIDENE COMPLEXES

B. van der Westhuizen,[#] J. M. Speck, M. Korb, J. Friedrich,[§] D. I. Bezuidenhout[#] and

Heinrich Lang

*Section F1 was made in collaboration with D. I. Bezuidenhout (#) and co-worker from the University of Pretoria, Hatfield, ZA (synthesis and characterization, manuscript preparation) and J. Friedrich (§) from the TU Chemnitz (quantum chemical calculations). The author of the present doctoral thesis has carried out educt synthesis (1,1'''-dibromobiferrocene) and all electrochemical and spectroelectrochemical investigations, discussion of the results and manuscript preparation, together with M. Korb (solid-state structure determination, discussion), in supervision of Prof. Dr. Heinrich Lang.*

## INTRODUCTION

Since the first synthesis of transition metal alkyidene complexes of type $(CO)_5M=C(OMe)R$ (M = Cr, W) by Fischer and Maasböl in the early 1960s, this family of compounds received popularity, as they are fascinating molecules and powerful tools in organic and organometallic chemistry.[72,325–329] The Dötz benzannulation reaction and the Aumann reaction procedure, a simple approach to metallaolefins, are examples of their varied application in chemistry.[330,331] By incorporating a ferrocenyl substituent with known applications in molecular sensors,[332] energy transfer processes[222] and anticancer drugs,[213,333–336] the application of Fischer carbene complexes could be extended beyond their traditional use as ligands employed for organic transformations[337–347] and as auxiliary ligands in catalysis,[348–351] to design new push-pull systems with interesting non-linear optical (NLO) properties.[352–356] It is well known that the ferrocenyl moiety as a redox-active group displays high stability in the neutral as well as the oxidized state during one-electron transfer processes.[183,196,210,357–359] Such ferrocenyl systems are ideal for studying electronic interactions by applying electrochemical and spectroelectrochemical techniques; these are efficient instruments to investigate charge transfer transitions between the separated metal entities.[180,253] This phenomenon is almost unexplored in Fischer carbene

complexes.[360–370] Moreover, studies in general concerning ferrocenyl- and biferrocenyl-functionalized Fischer carbene complexes are limited in the literature.[371–377]

We report herein the synthesis and characterization of a series of ferrocenyl (**F1**, **F2**) and biferrocenyl (**F3**, **F4**) tungsten(0) Fischer carbene complexes. Concerning the investigation of charge transfer transitions between the metallocenyl increments and the Fischer carbene units, the electrochemical and spectroelectrochemical properties of these species are discussed. These investigations are supported by computational studies.

RESULTS AND DISCUSSION

**Synthesis and Characterization.** The tungsten Fischer carbene complexes **F1** – **F4** were prepared using the classical Fischer carbene synthetic methodology in which $W(CO)_6$ was reacted with LiR (R = Fc, fc, bfc; Fc = ferrocenyl, fc = ferrocen-1,1'-diyl, bfc = 1',1'''-biferrocen-1,1'''diyl) to form the corresponding metal acylate, followed by a subsequent alkylation via addition of methyl trifluoromethanesulfonate (MeOTf) (Scheme 1, Experimental Section). Complex **F1** has been previously prepared,[378] but single X-ray diffraction data have not been reported.

**Scheme F1. Synthesis of F1 – F4.**[a]
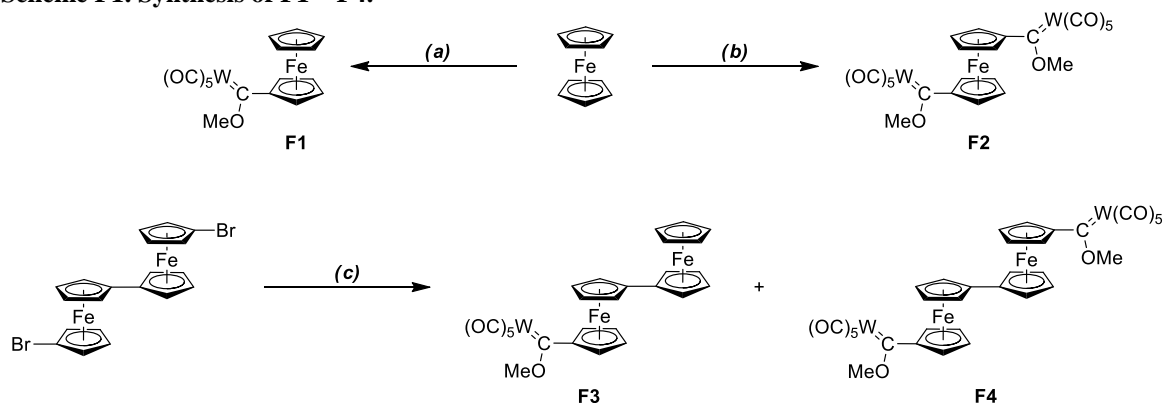


[a]Reaction conditions: (a) (i) tetrahydrofuran (thf), –80 °C, 1.06 eq $^t$BuLi, 1 eq $W(CO)_6$; (ii) dichloromethane ($CH_2Cl_2$), –50 °C, 3 eq MeOTf. (b) (i) $n$-hexane, 2 eq $^n$BuLi/TMEDA (1:1); (ii) thf, –60 °C, 2 eq $W(CO)_6$; (iii) $CH_2Cl_2$, –30 °C, 6 eq MeOTf. (c) (i) thf, –40 °C, 2.0 eq $^n$BuLi; (ii) 2 eq $W(CO)_6$; (iii) $CH_2Cl_2$, –30 °C, 6 eq MeOTf.

The lithiated ferrocenyl/biferrocenyl species were generated *in situ* from ferrocene or dibromobiferrocene by lithiation or lithium-bromine exchange reaction according to literature procedures (Scheme F1).[379,380] After purification by column chromatography, complexes **F1** – **F4** could be isolated as deep red to dark maroon solids and are very stable in the solid state as well as in solution toward moisture and air.

Complexes **F1** – **F4** were characterized by elemental analysis, IR and NMR ($^1$H, $^{13}$C{$^1$H}) spectroscopy, X-ray diffraction and mass spectrometry. Electronic effects of the carbene substituents can be followed in solution by IR and especially NMR spectroscopy.
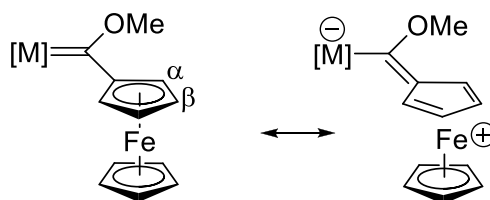


**Figure F1**. Stabilization of Fischer carbene complexes with a ferrocenyl group.

The electron withdrawing effect of the pentacarbonyl metal carbene moiety leads to a significant downfield shift of the resonances for the $H_\alpha$ protons (Figure F1) in **F1** – **F4** (4.80 – 5.00 ppm), compared to the value for ferrocene (4.15 ppm).[381] This is attributed to the $\pi$-delocalization of the positive formal charge onto the ferrocenyl substituent which aids in stabilizing the electrophilic carbene carbon atom, in addition to its inductive donating effect (Figure F1). A comparison of the $H_\alpha$ $^1$H NMR signals between complexes **F1** – **F4** as well as the $v$(CO) stretching frequencies ($A_1''$) reveal no significant differences, due to similarity of the carbene complexes (Table F1).

**Table F1. Selected NMR data and the infrared $v$(CO) stretching frequencies ($A_1''$) of Fischer carbenes F1 – F4 (Figure AF1-4).**

| Compd. | $H_\alpha$ δ $^1$H [ppm] | $C_{carbene}$ δ $^{13}$C{$^1$H} [ppm] | $A_1''$ $v$(CO) [cm$^{-1}$] |
|---|---|---|---|
| **F1** | 4.99 | 307.73 | 2063 |
| **F2** | 5.01 | 310.72 | 2063 |
| **F3** | 4.83 | 307.36 | 2062 |
| **F4** | 4.83 | 308.72 | 2062 |

**Electrochemistry and Molecular Orbital Analysis**. The electrochemical studies of Fischer carbene complexes **F1** – **F4** were carried out under an argon atmosphere in dichloromethane solutions containing [N$^n$Bu$_4$][B(C$_6$F$_5$)$_4$] (0.1 M) as supporting electrolyte and were supported by DFT calculations (computational details are given in the Experimental Section). Spectroelectrochemical investigations of **F1** – **F4** were carried out using an OTTLE[238] (= Optically Transparent Thin Layer Electrochemistry) cell (Experimental Section).

During the electrochemical studies of **F1**, three significant redox events could be observed. One reversible event was detected for **F1** at $E^{0'}$ = 300 mV, similar as detected previously,[360–370] which can be assigned to the ferrocenyl/ferrocenium (Fc/Fc$^+$) redox process (Table F2, Figures F2 and AF1-1). The significant anodic shift of this redox event,

relative to ferrocene, demonstrates the electron withdrawing effect of the Fischer carbene moiety.

**Table F2. Cyclic voltammetry data (potentials *vs.* FcH/FcH$^+$) of 1.0 mM solutions of F1 – F4 in dry dichloromethane containing [N$^n$Bu$_4$][B(C$_6$F$_5$)$_4$] (0.1 M) as supporting electrolyte at 25 °C.**

| Compd. | $E_{pa}/E_{pc}/\Delta E_p/E^{0'}/\Delta E^{0'}$ [mV] ($i_{pc}/i_{pa}$) Wave (no.) | | | | |
|---|---|---|---|---|---|
| | (1) | (2) | (3) | (4) | (5) |
| **F1** | –2053/–2133/80/ –2093 (0.46)$^a$ | 266/334/68/300 (0.95) | 1125/ – | | |
| **F2** | – /–2124 | – /–1823/301$^b$ | 554/484/70/519 (0.99) | 989/ – | 1086/ – |
| **F3** | –2072/–2166/94/ –2119 (0.54)$^a$ | 20/–48/68/–14 (0.98) | 671/604/67/637/ 651 (0.98) | 1161/ – | |
| **F4** | – /–2213 | – /–2100/113$^b$ | 261/191/70/226 (0.99) | 750/679/71/715/ 489 (0.98) | 1127/ – |

$^a$ $i_{pa}/i_{pc}$. $^b$ $\Delta E_{pc}$.
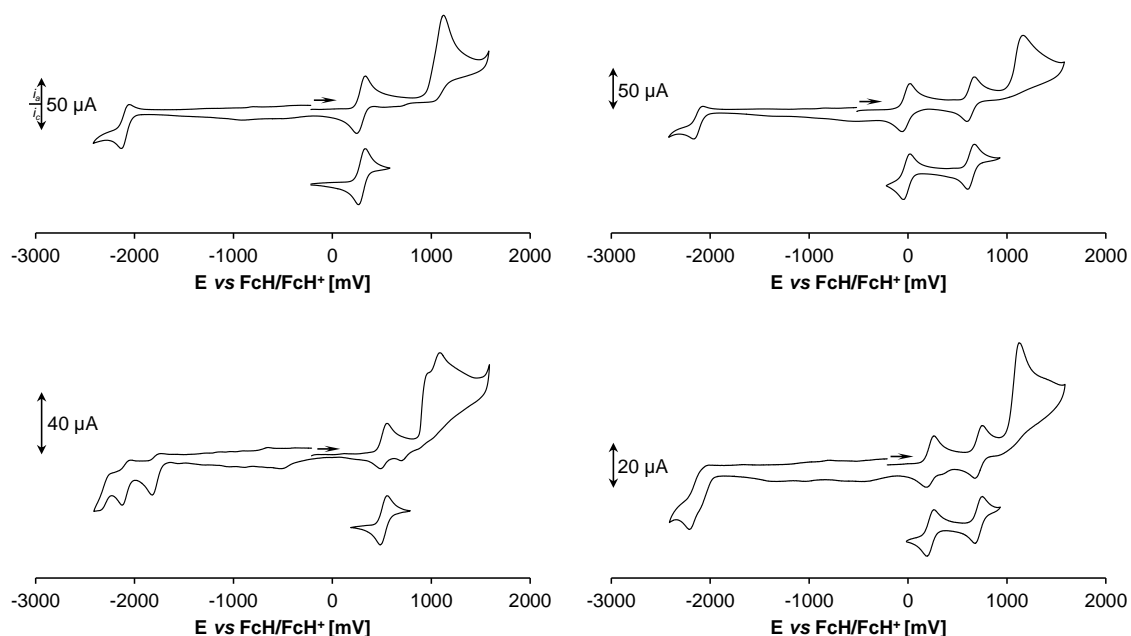


**Figure F2**. Cyclic voltammograms of Fischer carbenes **F1** (left top), **F2** (left bottom), **F3** (right top) and **F4** (right bottom). Scan rate: 100 mVs$^{-1}$ in dichloromethane solutions (1.0 mM) at 25 °C, supporting electrolyte [N$^n$Bu$_4$][B(C$_6$F$_5$)$_4$] (0.1 M). In case of the full range cyclic voltammograms the initial cycle is shown, arrows indicate the potential direction. For cyclic voltammetry data see Table F2.

Computational studies were carried out to verify the nature of the observed redox processes. The solvent effects on the ionization energies were taken into account with the conductor like screening model (COSMO) using $\varepsilon = \infty$ (Table F3, Figure F3). As a result from the DFT calculations, the oxidation potential for the first oxidation in **F1** was calculated to 0.3 V (Table F3). Considering the moderate level of theory, the theoretical value is in good agreement compared with the experimental value ($E_{ox\text{-}onset} = 0.22$ V) as well as with other considerations regarding a correlation between the electrochemical measurement and ionization energies.[382]

Furthermore, the spin density distribution of **F1$^+$** offers a localization (Mulliken spin density of 1.25) around the iron center and thus verifies the assignment to a Fc/Fc$^+$ redox event (*vide supra*, Figure F3).

**Table F3. Calculated ionization energies and oxidation/reduction potentials of F1 (computational details are given in the Experimental Section).**

| Compd. | B3LYP Ionization Energy [kJ/mol] | Incremental Ionization Energy [kJ/mol] | $E$ *vs.* FcH/FcH$^+$ [V]$^a$ |
|---|---|---|---|
| **F1$^-$** | –273.7 | | |
| **F1** | 0.0 | 273.7 | –1.5 |
| **F1$^+$** | 447.0 | 447.0 | 0.3 |
| **F1$^{2+}$** | 988.6 | 541.6 | 1.3 |
| **F1$^{3+}$** | 1632.8 | 644.2 | 2.4 |

$^a$ The ionization energy of ferrocene was calculated to 4.3 eV (414.9 kJ/mol).
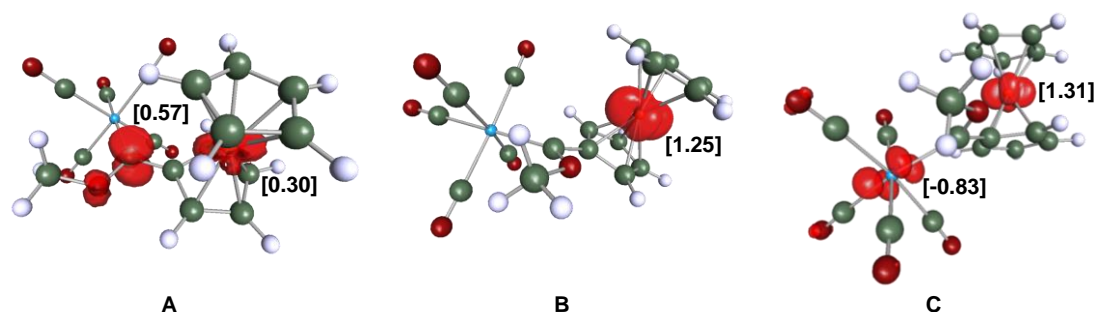


**Figure F3**. Computed spin density plots of **F1$^-$** (**A**), **F1$^+$** (**B**) and **F1$^{2+}$** (**C**). For computational details see Experimental Section. Numbers in brackets indicate the computed Mulliken spin densities.

Further increasing the potential leads to an irreversible oxidation process at $E_{pa}$ = 1.13 V, which is associated with an oxidation of the tungsten carbonyl moiety (Figures F2 and AF1-1). The peak current for this oxidation was observed as 2.5 times higher as for the ferrocenyl unit, similar as observed previously.[383] If an one step electrochemical process is assumed, the observed current reveals a two electron oxidation process, according to the Randles-Sevcik equation. However, the large differences between the calculated oxidation potentials (Table F3) suggest well-separated oxidation events during the generation of the oligocationic species. To determine the flown charge equivalents, chronocoulometric measurements were carried out. Assuming a reversible one-electron redox event for the Fc/Fc$^+$ couple (1 eq), the charge equivalents can be determined from the slope of the Anson plot, charge ($Q$) *vs* square root of time ($t^{1/2}$), with the Anson equation.[384,385] For the tungsten oxidation a value of 2.9 eq was obtained and suggests an electrode mediated successive three electron oxidation process, formal from W(0) to W(III). Nevertheless, such results should be handled with caution, due to irreversibility of the oxidation process.

Furthermore, a partially reversible reduction (Figures F2 and AF1-1) could be found in the cathodic end of the electrochemical window at $E_{pc}$ = –2.09 V (theoretical value: $E$ = –1.5

V, Table F3). This redox process is associated with a carbene center reduction/reoxidation process (Table F2, Figure F2).[386] The cyclic voltammetric as well as the chronocoulometric (1.1 eq) studies suggest a one electron redox process. From the spin density distribution in Figure F3 (**A**) localization around the carbene carbon can be seen.

A further tungsten carbene substituent on the ferrocenyl unit (complex **F2**) leads to an anodic shifting of the Fc/Fc$^+$ redox process to $E^{0'}$ = 519 mV. Within this context, the first carbene reduction should be easier than in **F1** and was observed 170 mV less cathodic compared to the carbene reduction in the ferrocenyl monocarbene complex (Table F2, Figure F2). A second carbene reduction could be found at $E_{pc}$ = –2.12 V, 300 mV more cathodic as the generation of **F1**$^-$ (Table F2, Figures F2 and AF1-2). The observation of two separated carbene reduction events leads to the conclusion that the first reduction process has an influence on the second one, depending on the bridging unit (in comparison with **F4**, *vide infra*). A similar observation was made during the oxidation events of the tungsten centers, where two separate peaks at $E_{pa}$ = 0.99 V and 1.09 V were found (Table F2). However, the oxidation potentials of both processes were found to be more cathodic as observed for **F1**.

In the case of the biferrocenyl Fischer carbene complex **F3**, one redox event was detected at $E_{pc}$ = –2.12 V and is also assigned to the carbene reduction electrode reaction (*vide supra*). For the biferrocenyl unit itself, two well separated ($\Delta E^{0'}$ = 651 mV) reversible one electron redox events at $E^{0'}$ = –14 mV and 637 mV were found (Table F2, Figure F2). A comparison of the first Bfc redox process with the corresponding event in biferrocene itself reveals an anodic shift of approx. 110 mV for the **F3**/**F3**$^+$ redox couple, only one-third of that observed for the corresponding process in **F1**.[386] Thus, the influence of the tungsten carbene moiety on the first biferrocenyl redox process in **F3** is significantly lower than that on the ferrocenyl redox event in **F1**. In addition, an oxidation peak at $E_{pa}$ = 1.16 V was noticed and is assigned to the irreversible tungsten carbonyl oxidation (*vide supra*, Table F2, Figure F2). The electrochemical investigation of the biferrocenyl carbene complex **F4** revealed two carbene reduction processes with a smaller separation ($\Delta E_{pc}$ = 113 mV) as observed for **F2**, due to the larger biferrocenyl bridge between the Fischer carbene units (*vide supra*). For the biferrocenyl increment, two reversible redox events were observed, which are separated by $\Delta E^{0'}$ = 489 mV. Hence $\Delta E^{0'}$ is smaller as detected for biferrocene ($\Delta E^{0'}$ = 530 mV) under similar experimental conditions.[98] A comparison of formal potentials for the first biferrocenyl redox processes of compounds **F3** and **F4** shows again the anodic potential shift, due to the installation of a second Fischer carbene substituent.

Finally, the irreversible oxidation of the tungsten carbonyl fragments was found at $\Delta E_{pa} =$ 1.13 V, even slightly more cathodic than for **F3**.

In order to get more insight into the oxidation processes of **F1** – **F4** spectroelectrochemical studies were carried out by a stepwise increase of the potential *vs.* Ag/AgCl in an OTTLE cell (= Optically Transparent Thin Layer Electrochemistry)[238], using a 0.1 M dichloromethane solution of $[N^{n}Bu_4][B(C_6F_5)_4]$ as supporting electrolyte. This procedure allows the *in situ* generation of mixed-valent species such as $\mathbf{F1}^{+}$, $\mathbf{F2}^{+}$, $\mathbf{F3}^{n+}$ and $\mathbf{F4}^{n+}$ (n = 1, 2). If deconvolution of NIR absorptions was used, transitions with Gaussian shapes were taken to get fits good enough to allow an almost exact overlay of the sum of the spectral components with the experimental spectra. All neutral Fischer carbene complexes do not display, as expected, any absorptions in the NIR range. The corresponding UV-Vis spectra are presented in the Supporting Information (Figures AF1-3, AF1-5 to AF1-7). For calculation of the theoretical bandwidth at half height ($\Delta\tilde{v}_{1/2(theo)}$) in asymmetric systems, the energy gap between the diabatic states ($\Delta G_0$, *vide supra* Chapter B) could be estimated, using the difference in oxidation potentials of the two redox sites. Regarding this, the oxidation potential of $(CO)_5W=C(OMe)Me^{[383]}$ as well as the formal potential of the $\mathbf{F1/F1}^{+}$ redox process were used (Table F4). Furthermore, an experimental $\Delta\tilde{v}_{1/2}$ value equal or larger than the theoretical width for symmetrical systems verifies clearly a class II assignment according to Robin and Day, since theoretical $\Delta\tilde{v}_{1/2}$ values for asymmetrical systems are generally smaller as the corresponding widths for symmetrical cases.[68]

**Table F4. NIR and infrared data of F1 – F4 in dry dichloromethane containing $[N^{n}Bu_4][B(C_6F_5)_4]$ (0.1 M) as supporting electrolyte at 25 °C.**

| Compd. | Transition | $\tilde{v}_{max}$ [cm$^{-1}$] ($\varepsilon_{max}$ [Lmol$^{-1}$cm$^{-1}$]) | $\Delta\tilde{v}_{1/2}$ [cm$^{-1}$] | $\Delta\tilde{v}_{1/2(theo)}$ [cm$^{-1}$] $\{\Delta\tilde{v}_{1/2(theo)} = (2310\lambda)^{1/2}\}^{a}$ | $v_{CO}$ [cm$^{-1}$] |
|---|---|---|---|---|---|
| $\mathbf{F1}^{+}$ | MMCT | 9270 (340) | 4660 | $2790^{c}$ ($4630^{b}$) | 1956, 2076 |
| | LF | 3930 (50) | 1280 | | $(1931, 2063)^{f}$ |
| $\mathbf{F2}^{+}$ | MMCT | 8000 (470) | 5070 | $2200^{c}$ ($4300^{b}$) | 1959, 2071, $2080^{e}$ |
| | LF | 3670 (70) | 1010 | | $(1937, 2063)^{f}$ |
| $\mathbf{F3}^{+}$ | MMCT | 8930 (65) | 2510 | $2650^{c}$ | 1935, 2065 |
| | IVCT | 5580 (930) | 3640 | $2700^{d}$ ($3590^{b}$) | $(1930, 2061)^{f}$ |
| | IBT | 3790 (340) | 820 | $1780^{d}$ | |
| $\mathbf{F3}^{2+}$ | MMCT | 8190 (280) | 4860 | $2300^{c}$ ($4140^{b}$) | 1958, 2077 |
| | LF | 3510 (120) | 1590 | | |
| $\mathbf{F4}^{+}$ | MMCT | 8870 (500) | 3170 | $2620^{c}$ | 1941, 2065, $2071^{e}$ |
| | IVCT | 4320 (1290) | 3720 | $3160^{b}$ | $(1930, 2063)^{f}$ |
| | IBT | 3320 (720) | 900 | $2770^{b}$ | |
| $\mathbf{F4}^{2+}$ | MMCT | 7870 (570) | 9030 | $2133^{c}$ ($4260^{b}$) | 1945, 2071 |
| | LF | 3600 (200) | 700 | | |

$^{a}$ $\lambda = \tilde{v}_{max} - \Delta G_0$. $^{b}$ $\lambda = \tilde{v}_{max}$. $^{c}$ $\Delta G_0 = 5900$ cm$^{-1}$. $^{d}$ $\Delta G_0 = 2420$ cm$^{-1}$. $^{e}$ Shoulder. $^{f}$ Neutral compound.

During the oxidation of **F1** typical absorptions in the UV-Vis region of inner ferrocenyl transitions ($\pi$-$\pi^*$ and MLCT/d-d) were observed (Appendix Section AF1).[239,387,388] Upon successively increasing the potential, two main absorptions at 9270 cm$^{-1}$ and 3930 cm$^{-1}$

could be detected in the NIR range during the generation of $\mathbf{F1^+}$ (in comparison with FcH$^+$, Table F4 and Figure F4).[126] The latter very weak absorption is attributed to an iron-based forbidden ligand field (LF) transition as described previously.[210,242–244,253]
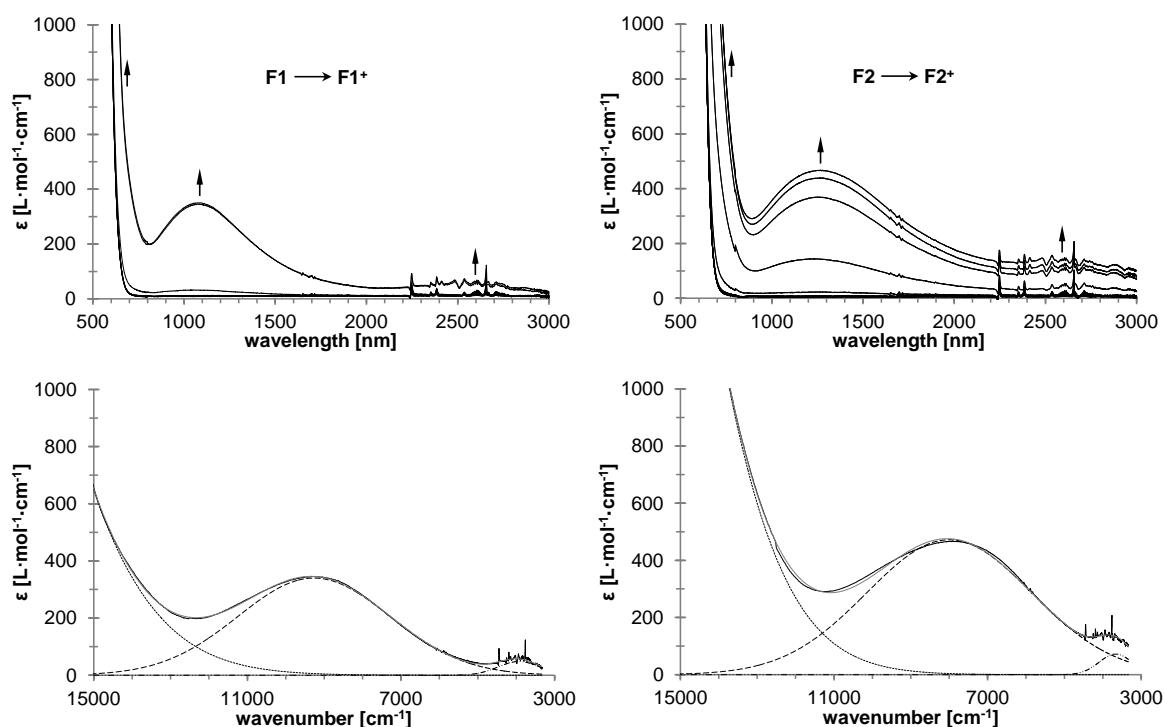


**Figure F4**. Left (top): UV-Vis-NIR spectra of **F1** at rising potentials (0 to 700 mV). Bottom: deconvolution of NIR absorptions at 700 mV using three distinct overlapping transitions with Gaussian shapes (dashed line indicates MMCT absorptions, dotted line corresponds to absorptions caused by interactions between ligand and metal, dotted-dashed line represents ligand field transitions). Right (top): UV-Vis-NIR spectra of **F2** at rising potentials (–100 to 1000 mV). Top: 500 – 3000 nm. Bottom: deconvolution of NIR absorptions at 1000 mV, using three distinct overlapping transitions with Gaussian shapes (dashed line indicates MMCT absorptions, dotted line corresponds to absorptions caused by interactions between ligand and metal, dotted dashed line represents ligand field transitions). All potentials *vs.* Ag/AgCl at 25 °C in dichloromethane, supporting electrolyte [N$^n$Bu$_4$][B(C$_6$F$_5$)$_4$] (0.1 M). Arrows indicate increasing or decreasing as well as shifting absorptions.

The weak high energy NIR absorption band at around 9300 cm$^{-1}$ can be assigned to a metal-metal charge transfer transition (MMCT) between the tungsten carbonyl fragment and the ferrocenium unit. To verify an interaction between the tungsten and the ferrocenyl building blocks, infrared spectroelectrochemical measurements monitoring the shift of $v$(CO) stretching frequencies during the oxidation process were carried out (Figures F5 and AF1-4). For carbene **F1**, absorptions could be found at 1930 cm$^{-1}$ and 2063 cm$^{-1}$, respectively (Experimental Section). Upon generation of the monocationic species **F1$^+$** a decrease of these bands takes place together with an increase of absorptions at 1956 cm$^{-1}$ and 2076 cm$^{-1}$, respectively (Table F4 and Figure F5, top left). The limited shift of the W(CO)$_5$ carbonyl stretching frequencies on oxidation is the result of conjugative and inductive effects that operate in stabilizing the positive charge on the iron nucleus by the metal carbene. Hence, the reduced back-bonding abilities of the Fc$^+$ substituent to the

carbonyl carbon atoms (compared to neutral Fc) leads to an increasing of the CO bond strengths and results in larger stretching frequencies (Figure F5). The observed carbonyl stretching frequencies are in good agreement with the calculated infrared spectra for **F1** and the corresponding monocation (Figure AF1-4, Appendix Section). Moreover, the difference ($\Delta v = 13$ cm$^{-1}$) between the two observed frequencies, 2063 cm$^{-1}$ (**F1**) and 2076 cm$^{-1}$ (**F1$^+$**), for the total symmetrical carbonyl stretching mode (A1'', *vide supra*, Figure AF1-4) differs only slightly from the corresponding value for the predicted vibrations of **F1** and **F1$^+$** ($\Delta v = 19$ cm$^{-1}$, Figure AF1-4, Table F4). Furthermore, the small magnitude of the carbonyl band shifts, compared to shifts of more than 100 cm$^{-1}$ for a metal carbonyl-based oxidation, indicates an iron based oxidation process and a valence trapped situation in **F1$^+$**. Calculation of the spin density distribution for **F1$^+$** confirms this conclusion (Figure F3). Thus, the interaction between the ferrocenyl unit and the tungsten carbene increment can be described with a weakly coupled class II system according to Robin and Day.[68]
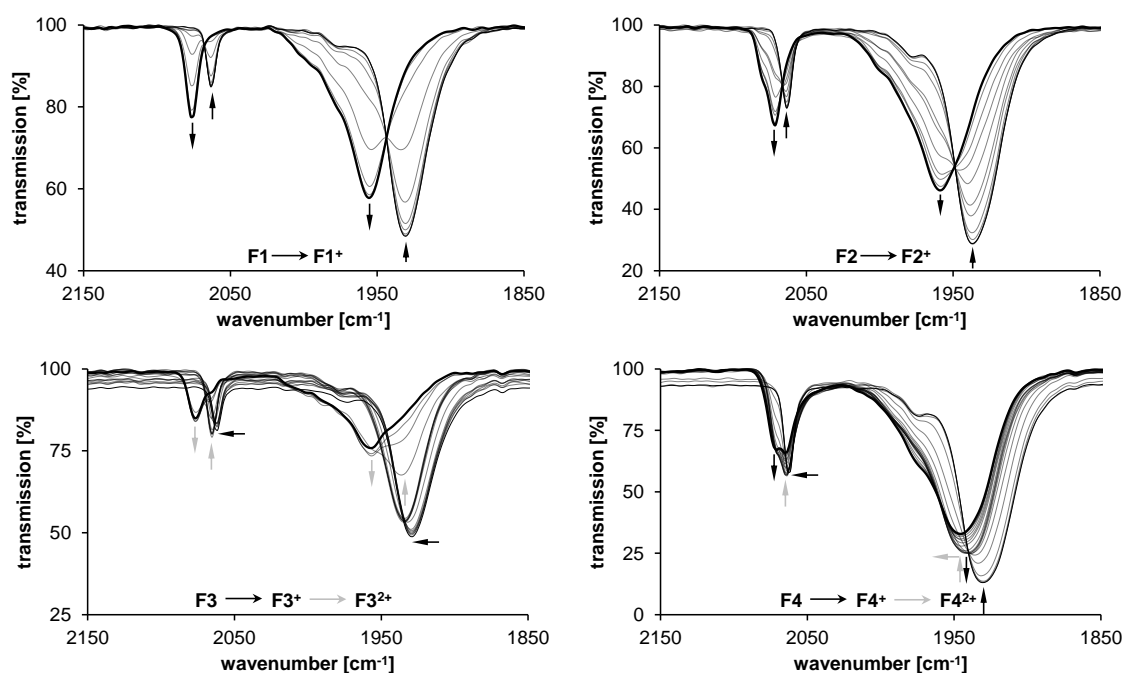


**Figure F5**. Infrared spectra of **F1** – **F4** at rising potentials (left top: –200 to 950 mV; right top: –200 to 1350 mV; left bottom: –100 to 1350 mV; right bottom: –100 to 1600 mV). All potentials *vs.* Ag/AgCl at 25 °C in dichloromethane on 5 mM analyte solutions, supporting electrolyte [N$^n$Bu$_4$][B(C$_6$F$_5$)$_4$] (0.1 M). Arrows indicate increasing or decreasing as well as shifting absorptions.

The absorption behavior of **F2$^+$** during the oxidation of molecule **F2** is similar to the corresponding Fischer monocarbene complex **F1** (Table F4, Figure F4). Absorptions at 3670 cm$^{-1}$ and 8000 cm$^{-1}$ could be noticed and are assigned to a ligand field transition and an electronic interaction between the tungsten carbene units and the iron center, too (MMCT, *vide supra*). The latter transition was observed as being more intense as the corresponding absorption for **F1$^+$**, due to the second Fischer carbene substituent on the

ferrocenyl moiety. During the infrared spectroelectrochemical investigations of **F2**, a band at 1959 cm$^{-1}$ as well as a broad absorption at 2071 cm$^{-1}$, the carbonyl stretching frequency (A1'', *vide supra*), could be found upon generation of **F2$^+$** (Figure F5, Table F4). However, the width of the latter band suggests a superposition of two absorptions close together and would be consistent with a class II electronic coupling behavior according to Robin and Day (*vide supra*).[68] A comparison between the observed ($\Delta\tilde{v}_{1/2}$) and the calculated band width at half height ($\Delta\tilde{v}_{1/2(theo)}$) of the MMCT absorption supports this classification (Table F4).[50,57]

An enhancement of ferrocenyl complex **F1** to a biferrocenyl Fischer carbene complex **F3** leads to an occurrence of two (Figure AF1-6) absorptions in the NIR range during the generation of cation **F3$^+$**. Characteristic for biferrocenyl systems is the observation of an intervalence charge transfer (IVCT) band close together with another absorption on the low energy side of the ICVT absorption (Table 4, Figure AF1-6). Tuczek *et al.* attributed this intra-biferrocenyl transition (IBT), around 3800 cm$^{-1}$ for **F3$^+$**, to a further intervalence charge transfer.[126,127] However, the latter absorption is very narrow compared to the corresponding value of $\Delta\tilde{v}_{1/2(theo)}$ (Table F4, Figure AF1-6). An assignment to a LMCT or a charge transfer assisted ligand field transition is also not uncommon.[239,265,288,387,388] Furthermore, a similar absorption band, which was found for **F1$^+$** and **F2$^+$**, attributed to an electronic interaction between the tungsten carbonyl moiety and the iron center, is observed as an ill-pronounced shoulder (very weak) that could be resolved into a separate peak via deconvolution (Figure AF1-6, Table F4). The infrared spectroelectrochemical investigations of **F3** support this observation, since upon formation of **F3$^+$** the initial $v$(CO) frequencies (Table F4) shift by only a few wavenumbers to higher energies (1935 cm$^{-1}$ and 2065 cm$^{-1}$, Figure F5). Thus, in combination with the electrochemical results, the first oxidation in **F3** takes primarily place at the terminal ferrocenyl unit. During the generation of **F3$^{2+}$** the low energy absorptions in the NIR range disappear and further transitions could be detected at 3510 cm$^{-1}$ (LF) and around 8200 cm$^{-1}$ (Table F4, Figure AF1-6, Appendix Section). The latter transition is also associated to a metal-metal charge transfer between the tungsten increment and the Bfc unit. The corresponding infrared absorption behavior during the formation of **F3$^{2+}$** verifies this conclusion, similar as observed for **F1$^+$** (*vide supra*, Figure F5).

A second tungsten Fischer complex fragment on the biferrocenyl building block leads to three NIR absorptions for monocationic **F4$^+$** (Table F4, Figure F6). The two transitions at lower energies are typical for such mixed-valent biferrocenyl species (*vide supra*). The

intensities are higher as observed for **F3⁺** but weaker than for symmetrical electron donor substituted biferrocenyl systems.[389] The third absorption around 8900 cm⁻¹ can be assigned again to a MMCT transition, caused by an electronic interaction of the tungsten units with the biferrocenyl group in **F4⁺**.
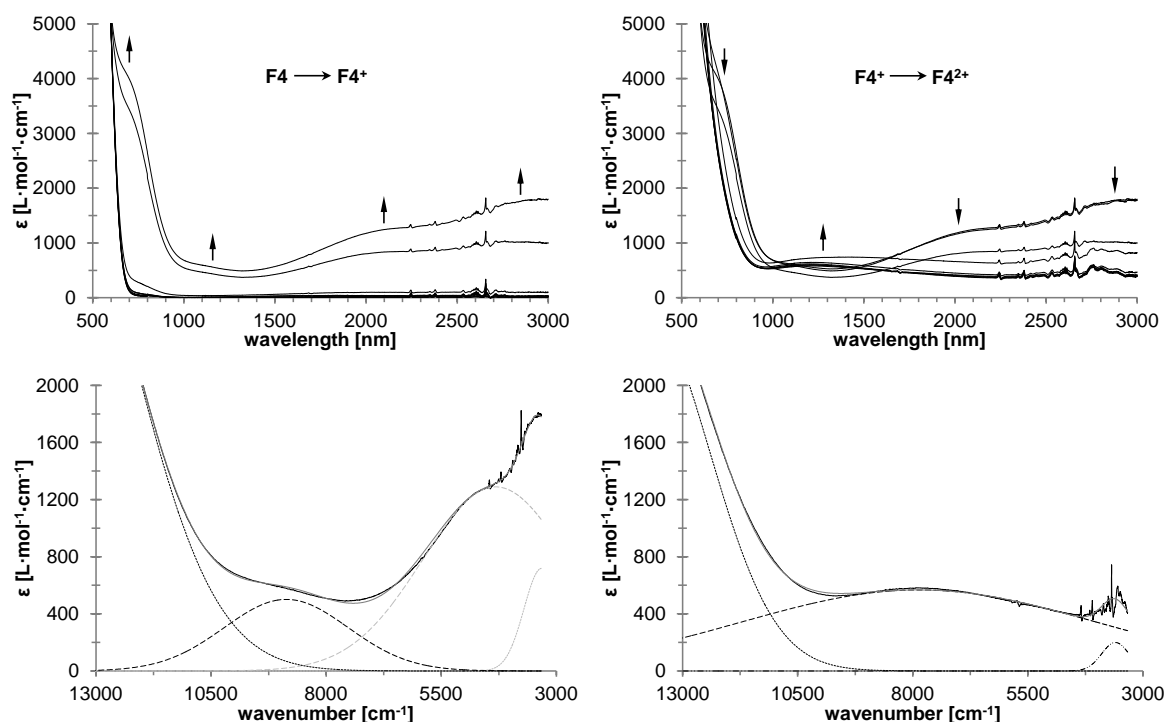


**Figure F6**. UV-Vis-NIR spectra of **F4** at rising potentials (left top: –100 to 600 mV; right top: 600 to 1050 mV). Bottom (left): deconvolution of NIR absorptions at 600 mV using four distinct overlapping transitions with Gaussian shapes. Bottom (right): deconvolution of NIR absorptions at 1050 mV, using three distinct overlapping transitions with Gaussian shapes (dashed line indicates IVCT (grey) or MMCT (black) absorptions, dotted line corresponds to absorptions caused by interactions between ligand and metal (black) as well as intra-biferrocenyl transitions (IBT, grey), dotted-dashed line represents ligand field transitions). All potentials *vs.* Ag/AgCl at 25 °C in dichloromethane, supporting electrolyte [N$^n$Bu$_4$][B(C$_6$F$_5$)$_4$] (0.1 M). Arrows indicate increasing or decreasing as well as shifting absorptions.

Within the infrared spectroelectrochemical studies of **F4**, a shifting of the initial $v$(CO) stretching frequencies from 1930 cm⁻¹ and 2063 cm⁻¹ to formal 1941 cm⁻¹ and 2065 cm⁻¹ is characteristic, whereas an increase of a shoulder at 2071 cm⁻¹ could be observed (Figure F5). This suggests a main localization of positive charge in the biferrocenyl fragment within the infrared timescale corresponding to a weakly coupled class II system according to Robin and Day.[68] Further oxidation to the dicationic **F4²⁺** leads to absorptions at 1945 cm⁻¹ and an increasing band at 2071cm⁻¹ (A1''), and thus the small magnitude of carbonyl band shift indicates again a limited delocalization of the positive charge between tungsten moieties and the iron centers (*vide supra*). This is consistent with the detection of an increasing NIR absorption at 7870 cm⁻¹ (MMCT) upon decreasing of the low energy transitions, caused from intra-biferrocenyl electronic interactions, during the formation of **F4²⁺** (Table F4, Figure F6). Finally, a very weak ligand field transition could be observed

at 3600 cm⁻¹, similar as described previously (*vide supra*, Table F4 and Figure F6).[210,242–244,253]

**Crystallography.** The molecular structures of **F1**[239,360–370,387,388] and **F2** – **F4** in the solid state have been determined by single-crystal X-ray diffraction analysis. Suitable single crystals of **F1** – **F4** were obtained by slow evaporation of a saturated dichloromethane solution of the respective complex layered with *n*-hexane at –5 °C. The *ORTEP* diagrams with selected bond lengths (Å), bond angles (°), and torsion angles (°) are shown in Figures F7 and F8. The appropriate complexes crystallize in the orthorhombic space groups *Pca*2₁ (**F1**) and *Pbcn* (**F2**), the triclinic space group *P*–1 (**F3**) and the monoclinic space group *P*2₁/*n* (**F4**) with one (**F1**), a half (**F2**, **F4**) and four (**F3**) molecules in the asymmetric unit. Among the numerous solid state structures of Fischer carbene complexes, only six group VI alkoxyferrocenyl-substituted derivatives have been reported so far, whereby just one contains tungsten.[373,376,390]
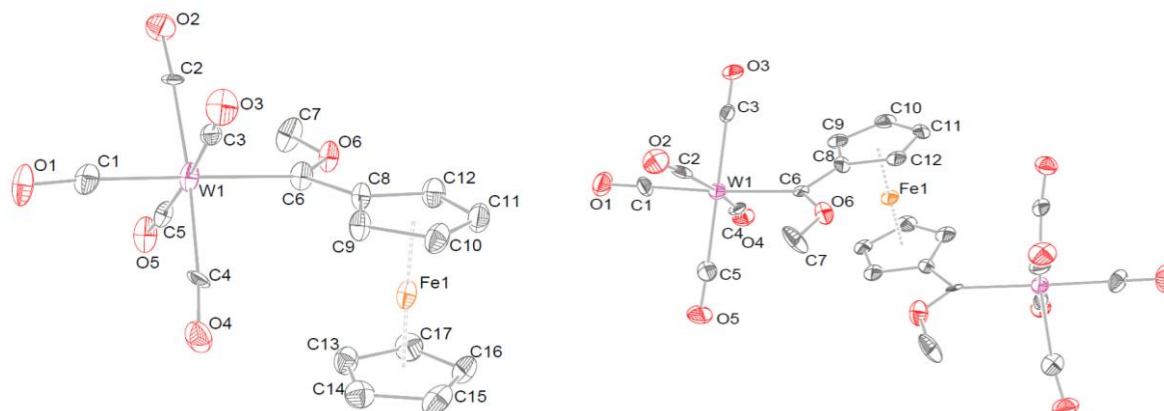


**Figure F7**. Single crystal X-ray structure analysis of **F1** and **F2** with the atom numbering scheme (**F2**: equivalent atoms are generated by the following symmetry operation: –x+1, y, –z+3/2). Ellipsoids represent 50 % probability levels. Disordered and hydrogen atoms are omitted for clarity. Selected bond lengths (Å), angles (°), and torsion angles (°). **F1**: W1–C1 1.981(14), W1-C6 2.211(13), C6-O6 1.339(15), C6-C8 1.458(19), D1–Fe1 1.652(19), D2–Fe1 1.656(17), O6-C6-W1 128.33(92), C8-C6-W1 126.39(93), O6-C6-C8 105.24(11), D1–Fe1–D2 176.77(18), C8–D1–D2–C13 –13.31(10), W1–C6–O6–C7 –1.67(19), C8–C6–O6–C7 –179.67(12), O6–C6–W1–C2 –46.63(13), C8–C6–W1–C2 –130.97(12), O6–C6–C8–C9 –178.96(14), W1–C6–C8–C9 3.00(21). D1: C8–C9–C10–C11–C12, D2: C13–C14–C15–C16–C17. **F2**: W1–C1 1.987(11), W1-C6 2.204(99), C6-O6 1.353(12), C6-C8 1.443(12), D1–Fe1 1.657, O6-C6-W1 127.84(57), C8-C6-W1 125.54(61), O6-C6-C8 106.49(81), D1–Fe1–D1_$1 176.95(12), C8–D1–D1_$1–C12_$1 3.69(63), W1–C6–O6–C7 –4.45(12), C8–C6–O6–C7 171.66(95), O6–C6–W1–C2 44.08(61), C8–C6–W1–C2 –131.33(54), O6–C6–C8–C9 174.36(61), W1–C6–C8–C9 –9.41(91). D1: C8–C9–C10–C11–C12.

In a comparison of the angles and bond distances (Figures F7 and F8) at the trigonal-planar carbene carbon, no further differences, not for the ferrocenyl unit nor for the biferrocenyls can be identified. W1–C1 distances are equal for all four complexes and coincide with the corresponding ethoxy-substituted derivative of **F1**.[390] The lone pairs at O6 are always directed towards the ferrocenyl moiety of the molecules, due to the electronic interaction with the carbonyl groups.[391] Thus, to avoid electronic interactions, the bonded methyl

group C6 shields the oxygen atom O6. The carbene carbon and the $C_5H_4$ plane of the ferrocenyl moieties extend their $\pi$-system by arranging almost coplanar to each other. The highest deviations of the corresponding O6–C6–C8–C9 torsion angles can be found for one molecule in the asymmetric unit of **F3** (10.99(39) °). Additionally, this plane shows a staggered orientation related to the carbonyl groups. The highest deviations from an ideally assumed angle (45 °) can be found in carbene **F3**, which shows differences of 5.43(40) ° and 10.37(38) ° for the representing torsion angle O6–C6–W1–C2.
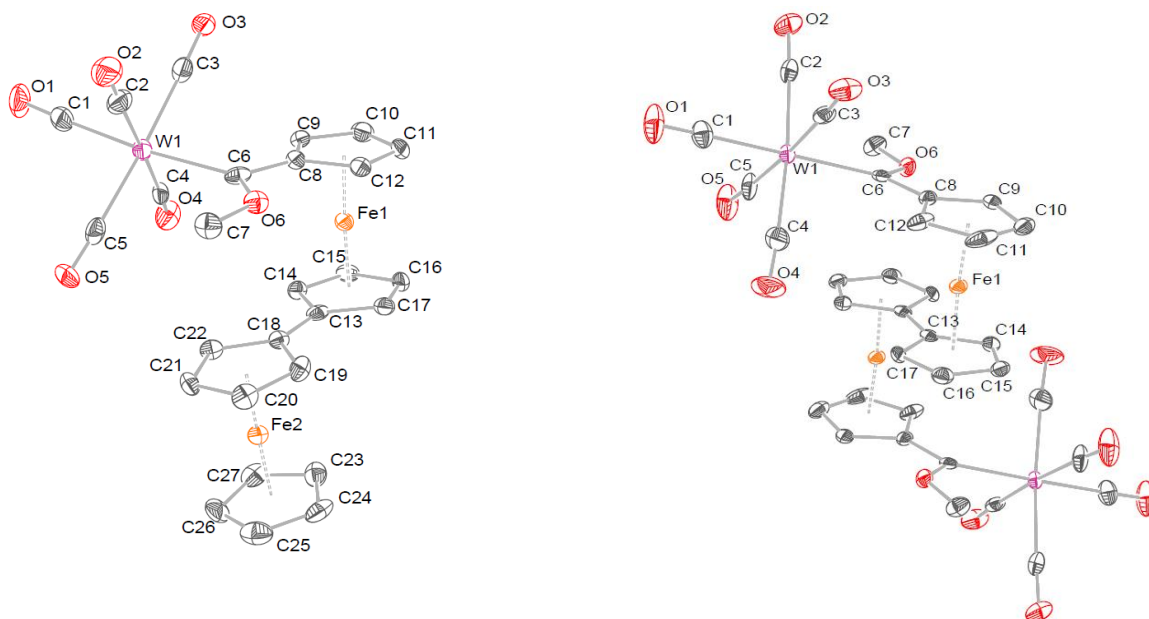


**Figure F8**. Single crystal X-ray structure analysis of **F3** and **F4** with the atom numbering scheme (**F4**: equivalent atoms are generated by the following symmetry operation: –x+2, –y, –z). Ellipsoids represent 50 % probability levels. Hydrogen atoms are omitted for clarity. Selected bond lengths (Å), angles (°), and torsion angles (°). **F3**: W1–C1 2.034(56), W1-C6 2.207(49), C6-O6 1.335(51), C6-C8 1.457(71), D1–Fe1 1.653(7), D2–Fe1 1.662(7), O6-C6-W1 129.14(37), C8-C6-W1 123.69(31), O6-C6-C8 106.83(41), D1–Fe1–D2 176.25(5), C8–D1–D2–C13 –21.58(31), C18–D3–D4–C23 –0.27(33), D3–Fe2 1.6426(7), D4–Fe2 1.695(7), D3–Fe2–D4 166.47(5), W1–C6–O6–C7 6.92(58), C8–C6–O6–C7 –179.65(37), O6–C6–W1–C2 47.81(40), C8–C6–W1–C2 –124.63(38), O6–C6–C8–C9 172.42(41), W1–C6–C8–C9 –13.70(65), D1: C8–C9–C10–C11–C12, D2: C13–C14–C15–C16–C17, D3: C18–C19–C20–C21–C22, D4: C23–C24–C25–C26–C27. **F4**: W1–C1 2.022(37), W1-C6 2.217(31), C6-O6 1.317(38), C6-C8 1.456(44), D1–Fe1 1.649(5), D2–Fe1 1.658(5), O6-C6-W1 128.60(22), C8-C6-W1 123.87(23), O6-C6-C8 107.22(27), D1–Fe1–D2 175.72(4), C8–D1–D2–C13 22.60(22), W1–C6–O6–C7 –5.69(40), C8–C6–O6–C7 –179.39(26), O6–C6–W1–C2 –44.36(28), C8–C6–W1–C2 128.38(25), O6–C6–C8–C9 6.14(41), W1–C6–C8–C9 –167.93(23), D1: C8–C9–C10–C11–C12, D2: C13–C14–C15–C16–C17.

For the biferrocenyl complexes **F3** and **F4**, both ferrocenyl units are oriented in an antiparallel fashion with nearly or exactly coplanar $C_5H_4$ rings (highest deviation: 17.73(25) ° for **F3** and 0.00(24) ° for **F4**, respectively). Interestingly, carbene fragments are disposed synclinal and synperiplanar to the ferrocenyl substituent. This conformation depends strongly on the rotation of the cyclopentadienyl rings. Fischer carbenes **F1** and **F4** exhibit rather eclipsed than staggered torsion angles (–13.31(101) ° for **F1** and 22.60(22) ° for **F4**). In contrast, complex **F2** with two tungsten carbene building blocks nearly shows an eclipsed conformation (3.69(63) °) for both $C_5H_4$ rings, whereby both fragments show

synclinal orientation. The same conformation can also be found for the corresponding chromium complex with $^n$propoxy substituents.[371–374] Torsion angles of both entities in the biferrocenyl unit of complex **F3** are summarized in Table F5 showing great differences between the molecules (Table F5, A – D) of the asymmetric unit for the 1,1'-disubstituted moiety.

**Table F5. Torsion angles** (°) **for F3.**

| Molecule | C8–CT1–CT2–C13 | C18–CT3–CT4–C23 |
|---|---|---|
| A | –21.61(29) | –0.70(31) |
| B | 62.44(34) | –14.08(42) |
| C | –61.49(32) | –4.27(39) |
| D | 15.65(29) | –16.22(29) |

Molecules B and C exhibit a nearly synclinal orientation, while A and D are rather arranged synperiplanar. However, all mono-substituted ferrocenyl fragments are synperiplanar oriented with small deviations for molecule B and D (Table F5).

CONCLUSION

Within this study, a series of ferrocenyl (Fc = ferrocenyl; fc = ferrocen-1,1'-diyl) and biferrocenyl (Bfc = 1',1''-biferrocenyl; bfc = 1',1''-biferrocen-1,1'''diyl) tungsten Fischer carbene complexes, of type [(CO)$_5$W=C(OMe)R] (**F1**, R = Fc; **F3**, R = Bfc) and [(CO)$_5$W=C(OMe)-R'-(OMe)C=W(CO)$_5$] (**F2**, R' = fc; **F4**, R' = bfc), is reported with the aim of investigating low energy charge transfer between the transition metal carbonyl fragment and the (oxidized) carbene substituents. For this reason, ferrocenyl and biferrocenyl mono- and bismethoxycarbene tungsten(0) complexes **F1** – **F4** were prepared and characterized spectroscopically in solution. Furthermore, the structural properties of **F1** – **F4** in the solid state were investigated by single-crystal X-ray diffraction studies whereby the biferrocenyl derivatives **F3** and **F4** exhibit a *syn*-conformation of ferrocenyl and carbene moiety. The results reveal no substituent effects in the bond-lengths and angles.

The electrochemical studies of **F1** – **F4** reveal reversible one-electron redox events for the ferrocenyl/biferrocenyl moieties. Moreover, an electrochemical one electron transfer reaction could be found for the reduction of the Fischer carbene units. For the tungsten carbonyl moieties, irreversible oxidation processes could be detected. During the UV-Vis-NIR spectroelectrochemical investigations typical low energy absorptions for the mixed-valent biferrocenyl units were found. A further observed high energy NIR absorption was

attributed to a metal-metal charge transfer transition between the tungsten carbonyl increment and the ferrocenyl/biferrocenyl unit in the corresponding oxidized state and is reported herein for the first time. Finally, a verification was made within infrared spectroelectrochemical studies by which the electronic interactions in the corresponding cationic species can be described as weakly coupled class II systems according to Robin and Day.

EXPERIMENTAL SECTION

**General Informations**. All operations were carried out under an inert atmosphere of nitrogen or argon gas using standard Schlenk techniques. Solvents were dried by refluxing over sodium metal (*n*-hexane and tetrahydrofuran) or phosphorous pentoxide (dichloromethane) and were distilled under nitrogen prior to use. Chemicals were used without further purification unless stated elsewhere. Dibromobiferrocene was synthesized according to a literature procedure.[379] Tetra-*n*-butylammonium tetrakis(pentafluoro-phenyl)borate was prepared by metathesis of lithium tetrakis(pentafluorophenyl)borate etherate (Boulder Scientific) with tetra-*n*-butylammonium bromide according the a published procedure.[90,100,101] Purification with column chromatography was done using Silica gel 60 (0.0063 – 0.200mm) as stationary phase. A Bruker AVANCE 500 spectrometer was used for NMR recordings. $^1$H NMR spectra were recorded at 500.30 MHz and $^{13}$C{$^1$H} NMR spectra at 125.80 MHz. The signal of the solvent was used as reference: $^1$H, CDCl$_3$ at 7.26 ppm and $^{13}$C{$^1$H}, CDCl$_3$ at 77.16 ppm. Infrared spectra were obtained with a Thermo Nicolet 200 FT-IR spectrometer using a NaCl cell and dichloromethane as solvent. Only the vibration bands in the carbonyl stretching region (1600 – 2200 cm$^{-1}$) were recorded. The melting points were determined using a Gallenkamp MFB 595 010 M melting point apparatus. Microanalyses were performed by using a Thermo FLASHEA 1112 Series instrument. High-resolution mass spectra were recorded with a Bruker micrOTOF QII with an Apollo II ESI source.

**Synthesis of Fischer carbene complexes F1 – F4. [(CO)$_5$W=C(OMe)Fc] (F1)**. Ferrocene (3.0 mmol, 0.56 g) was monolithiated according to a literature procedure in tetrahydrofuran (thf) with $^t$BuLi (3.2 mmol).[378] The solution was cooled to –80 °C and W(CO)$_6$ (3.0 mmol, 1.06 g) was added in a single portion. The color of the solution turned deep red upon addition. The reaction mixture was stirred isotherm for 30 min and then allowed to reach room temperature within 1 h. The solvent was changed to

dichloromethane ($CH_2Cl_2$), cooled to –50 $^oC$ and methyl trifluoromethanesulfonate (9.9 mmol, 1.09 mL) was added. The reaction mixture was removed from the cold bath and stirred overnight at ambient temperature. Purification of the product was performed by using column chromatography and *n*-hexane as initial eluent. The polarity of the eluent was increased by adding small portions of $CH_2Cl_2$. Yield 1.44g (87%), dark red crystals. Anal. Calcd. for $C_{17}H_{12}FeO_6W$ (551.98): C, 36.99; H, 2.20; found C, 36.94; H, 2.12. Mp: 153°C. NMR ($CDCl_3$) $^1H$: 4.99 (m, 2H, $H_\alpha$), 4.84 (m, 2H, $H_\beta$), 4.27 (s, 5H, Cp), 4.53 (s, 3H, $CH_3$). $^{13}C\{^1H\}$: 307.73($C_{carbene}$), 202.34($C_{trans}$), 198.03($C_{cis}$), 95.23($C_{ipso}$), 75.06($C_\alpha$), 73.25($C_\beta$), 70.80(Cp), 68.60($CH_3$). IR $v$(CO) (*n*-hexane): 2063 m ($A_1''$), 1974 w (B), 1946 s ($A_1'$), 1935 vs (E). FAB-MS [m/z]: 551.95 [$M^+$].

**[{$(CO)_5W=C(OMe)$}$_2$fc] (F2)**. Dilithiation of ferrocene (3.0 mmol, 0.56 g) was done according to methods previously reported with an 1:1 $^n$BuLi/TMEDA solution in *n*-hexane (6.5 mmol) overnight at ambient temperature. Afterward, the solvent was removed by filtration via cannula and the remaining dilithioferrocene was redissolved in tetrahydrofuran. The resulting solution was cooled to –60 $^oC$ and $W(CO)_6$ (6.0 mmol, 2.11 g) was added in a single portion. After 1 h of isothermal stirring the solution was warmed up to room temperature within 60 min. All volatiles were removed, the residue was redissolved in $CH_2Cl_2$ and methyl trifluoromethanesulfonate (20.0 mmol, 2.41 mL) was added at –30 $^oC$ after which the reaction solution darkened. The resulting mixture was stirred overnight at ambient temperature. Purification of the crude product was performed by column chromatography using *n*-hexane as initial eluent. The polarity of the eluent was increased by adding small portions of dichloromethane. Yield 1.51g (85%), dark purple solid. Anal. Calcd. for $C_{24}H_{14}FeO_{12}W_2$ (917.91): C, 31.40; H, 1.54; found C, 30.92; H, 1.42. Mp: 195°C. NMR ($CDCl_3$) $^1H$: 5.01 (m, 4H, $H_\alpha$), 4.82 (m, 4H, $H_\beta$), 4.54 (s, 6H, $CH_3$). $^{13}C\{^1H\}$: 310.72 ($C_{carbene}$), 202.07 ($C_{trans}$), 197.66 ($C_{cis}$), 96.07 ($C_{ipso}$), 76.58 ($C_\alpha$), 74.93 ($C_\beta$), 69.09 ($CH_3$). IR $v$(CO) (*n*-hexane): 2063 m ($A_1''$), 1974 w (B), 1940 vs ($A_1'$ overlap E). FAB-MS [m/z]: 917.89 [$M^+$].

**[$(CO)_5W=C(OMe)Bfc$] (F3) and [{$(CO)_5W=C(OMe)$}$_2$Bfc] (F4)**. Dibromo-biferrocene[378,379] (3.0 mmol, 1.58 g) was dissolved in 50 mL of tetrahydrofuran and $^n$BuLi (6.0 mmol) was added slowly at –40 $^oC$. After 30 min of isothermal stirring, $W(CO)_6$ (6.0 mmol, 2.11 g) was added in a single portion. The solution was kept at –40 °C for an additional hour and then allowed to reach room temperature within 1 h. Afterward, the solvent was changed to dichloromethane and methyl trifluoromethanesulfonate (20.0 mmol, 2.41 mL) was added at –30 $^oC$. The reaction mixture was removed from the cold

bath and stirred overnight at ambient temperature. Purification of the product was performed by column chromatography using *n*-hexane as initial eluent. The polarity of the eluent was increased by adding small portions of dichloromethane. Complexes **F3** and **F4** were purified and separated with column chromatography and gradient elution.

Compound **F3**: Yield 0.96g (40%), red brown crystals. Anal. Calcd. for $C_{27}H_{20}Fe_2O_6W$ (736.01): C, 44.06; H, 2.74; found C, 43.95; H, 2.68. Mp: 166°C. NMR (CDCl$_3$) $^1$H: 4.83 (m, 2H, H$_{ipso1\alpha}$), 4.64 (m, 2H, H$_{ipso1\beta}$), 4.47 (m, 2H, H$_{ipso2\alpha}$), 4.32 (m, 2H, H$_{ipso2\beta}$), 4.27 (m, 2H, H$_{ipso3\alpha}$), 4.26 (m, 2H, H$_{ipso3\beta}$), 3.97 (s, 5H, Cp), 4.24 (s, 3H, CH$_3$). $^{13}$C{$^1$H}: 307.36(C$_{carbene}$), 202.48(C$_{trans}$), 198.13(C$_{cis}$), 95.96(C$_{ipso1}$),88.24 (C$_{ipso2}$), 80.67 (C$_{ipso3}$), 75.06 (C$_{ipso1\alpha}$), 73.25(C$_{ipso1\beta}$), 70.17 (C$_{ipso2\alpha}$), 68.47(C$_{ipso2\beta}$), 68.12 (C$_{ipso3\alpha}$), 66.46(C$_{ipso3\beta}$), 69.43(Cp), 53.47(CH$_3$). IR $v$(CO) (*n*-hexane): 2062 m (A$_1$''), 1972 w (B), 1943 s (A$_1$'), 1932 vs (E). FAB-MS [m/z]: 735.95 [M$^+$].

Compound **F4**: Yield 0.99g (30%), dark brown crystals. Anal. Calcd. for $C_{36}H_{26}Fe_2O_{12}W_2$ (1101.94): C, 37.06; H, 2.02; found C, 37.08; H, 2.05. Mp: 232°C (decomp.). NMR (CDCl$_3$) $^1$H: 4.83 (m, 4H, H$_{ipso1\alpha}$), 4.62 (m, 4H, H$_{ipso1\beta}$), 4.44 (m, 4H, H$_{ipso2\alpha}$), 4.32 (m, 4H, H$_{ipso2\beta}$), 4.30 (s, 6H, CH$_3$). $^{13}$C{$^1$H}: 308.72(C$_{carbene}$), 202.29(C$_{trans}$), 198.03(C$_{cis}$), 96.05(C$_{ipso1}$),84.98 (C$_{ipso2}$), 75.98 (C$_{ipso1\alpha}$), 74.12(C$_{ipso1\beta}$), 70.70 (C$_{ipso2\alpha}$), 68.43(C$_{ipso2\beta}$), 67.97(CH$_3$). IR $v$(CO) (*n*-hexane): 2062 m (A$_1$''), 1972 w (B), 1943 s (A$_1$'), 1932 vs (E). FAB-MS [m/z]: 1101.88 [M$^+$].

**Electrochemistry.** The electrochemical measurements were carried out under an argon atmosphere on 1.0 mmol·L$^{-1}$ dichloromethane solutions containing 0.1 mol·L$^{-1}$ of [N$^n$Bu$_4$][B(C$_6$F$_5$)$_4$] as supporting electrolyte utilizing a Voltalab 10 electrochemical laboratory from Radiometer Analytical.[90,100,101] Furthermore, an OTTLE (= Optically Transparent Thin Layer Electrochemistry) cell placed in a Varian Cary 5000 UV-VIS-NIR absorption spectrometer or in a Thermo Nicolet 200 FT-IR spectrometer was used in spectroelectrochemical measurements.[238] For voltammetry, a three electrode cell with a platinum counter electrode, a glassy carbon working electrode and a Ag/Ag$^+$ reference electrode was used. The working electrode was prepared by polishing with a Buehler micro cloth using Buehler diamond pastes with decreasing sizes (1 to 0.25 μm). The Ag/Ag$^+$ reference electrode was constructed from a silver wire inserted into a Luggin capillary with a Vycor tip containing a solution of 0.01 mol·L$^{-1}$ AgNO$_3$ as well as 0.1 mol·L$^{-1}$ [N$^n$Bu$_4$][B(C$_6$F$_5$)$_4$] in acetonitrile. This Luggin capillary was inserted into a second Luggin capillary with Vycor tip filled with a 0.1 mol·L$^{-1}$ [N$^n$Bu$_4$][B(C$_6$F$_5$)$_4$] solution in dichloromethane. Successive experiments under the same experimental conditions showed

that all formal reduction and oxidation potentials were reproducible within 5 mV. Experimentally potentials were referenced against a Ag/Ag$^+$ reference electrode but the results are presented referenced against the FcH/FcH$^+$ couple ($E^{0'}$ = 0.0 V) as required by IUPAC.[249] When decamethylferrocene was used as an internal standard, the experimentally measured potential was converted in to $E$ *vs.* FcH/FcH$^+$ by addition of –0.61 V.[250] The cyclic voltammograms were taken after typical two scans and are considered to be steady state cyclic voltammograms, in which the signal pattern differs not from the initial sweep. Finally, the experimental data were processed on Microsoft Excel worksheets.

**Computational Details.** All quantum chemical calculations were performed with TURBOMOLE 6.3.1.[392–395] After the initial guess the Kohn-Sham equations were converged in the small def-SV(P)[396–398] basis set using a damping factor of 20 and Fermi smearing. After this step a geometry optimization was performed. Next the structures were optimized at the PB86/def2-TZVP[392–395,399,400] level of theory using the m5 grid. In all calculations density fitting was applied.[401–403] The final stationary points were characterized by analyzing the hessian matrix.[404,405] The final energy evaluations were performed with the B3LYP[396–398,406,407] hybrid functional in combination with the def2-TZVP basis set. To include the solvent effects the COSMO[408] solvation model with $\varepsilon = \infty$ was applied. The reported relative energies include the zero point energy correction from the gas phase at the BP86/def2-TZVP level of theory.

**Single-Crystal X-ray Diffraction Analysis.** Crystal data for **F1** – **F4** are summarized in Table AF1-1 (Appendix Section). Data were collected with an Oxford Gemini S diffractometer at 100 K using Mo-Kα (λ = 0.71073 Å) radiation. The structures were solved by direct methods using SHELXS-97 and refined by full matrix least-square procedures on F2 using SHELXL-97.[251,252] All non-hydrogen atoms were refined anisotropically and a riding model was employed in the refinement of the hydrogen atom positions. Crystallographic data (excluding structure factors) for the structures in this paper have been deposited with the Cambridge Crystallographic Data Centre, CCDC, 12 Union Road, Cambridge CB21EZ, UK. Copies of the data can be obtained free of charge on quoting the depository numbers CCDC-949877 (**F1**), 949876 (**F2**), 949878 (**F3**) and 949875 (**F4**) (Fax: +44-1223-336-033; E-Mail: deposit@ccdc.cam.ac.uk, http://www.ccdc.cam.ac.uk).

**Supporting Information.** UV-Vis-NIR spectra in dichloromethane and crystal structure details for **F1** – **F4** as well as calculated infrared spectra of **F1** and **F1**$^+$ are given. This material is available in the Appendix Section (Chapter AF1).

## F2 (SPECTRO)ELECTROCHEMICAL INVESTIGATIONS ON (FERROCENYL)-THIOPHENES MODIFIED BY TUNGSTEN FISCHER CARBENES

B. van der Westhuizen,[#] J. M. Speck, M. Korb, D. I. Bezuidenhout[#] and Heinrich Lang

*Section F2 was made in collaboration with D. I. Bezuidenhout (#) and co-worker from the University of Pretoria, Hatfield, ZA (synthesis and characterization, manuscript preparation). The author of the present doctoral thesis has carried out educt synthesis (1,1'-dibromoferrocene, compound F7) and all electrochemical and spectroelectrochemical investigations, discussion of the results and manuscript preparation, together with M. Korb (solid-state structure determination, discussion), in supervision of Prof. Dr. Heinrich Lang.*

INTRODUCTION

In recent years, the application of Fischer carbene complexes has expanded from catalysis, auxiliary ligands and application in template organic chemistry to electronic probes and potential molecular wires.[72,326–329,409] These applications have mostly evolved around the M=C carbene double bond, however, some wire-like and switching performance is shown in organometallic complexes containing $\sigma$-bonded redox-active moieties.[409] Interest in the electrochemical properties of carbene complexes was the prelude to new applications, especially in the field of catalysis.[410,411] Fischer carbene complexes are excellent candidates for electrochemical studies, as redox centers can be extended from mono- to polymetallic,[373] and organic or organometallic $\pi$-conjugated linkers can be used to separate transition metal moieties.[363,412–414] Combining the properties of Fischer carbenes with $\pi$-conjugated bridges could result in the design of new push-pull systems with novel non-linear optical (NLO) character. In our recent papers we paid attention to metal-metal interactions in Fischer carbenes on ferrocenyl and biferrocenyl tungsten alkylidene complexes.[287,415] UV-Vis-NIR spectroelectrochemical investigations revealed a high-energy NIR absorption which was attributed to a metal-metal charge transfer transition (MMCT) between the tungsten and ferrocenyl/biferrocenyl moieties. Within this context, the use of redox active metal-based termini offers the possibility to design new materials, such as semiconducting polymers and molecular wires.

In this study we describe synthesis and characterization of tungsten thienyl and 2,5-diferrocenylthiophenes mono- and biscarbene Fischer complexes (Scheme F2). Electrochemical and spectroelectrochemical properties were investigated.

RESULTS AND DISCUSSION

**Synthesis and Characterization**. The tungsten Fischer carbene complexes **F5**, **F6**, **F8** and **F9** were prepared employing the classical Fischer carbene synthesis: $W(CO)_6$ was reacted with relevant lithiated species of thiophene, 2,5-dibromo thiophene (2,5-ThBr$_2$) and 2,5-di(1'-bromoferrocenyl)thiophene (**F7**) to form the respective metal acylates. After alkylation with methyl trifluoromethanesulfonate (MeOTf), neutral complexes were isolated as red/purple – dark brown solids. Complex **F5** was previously synthesized and spectroscopically characterized, but single crystal X-ray diffraction data were not reported.[416] The ethoxy-analogue of compound **F5** has also recently been electrochemically characterized.[417]

**Scheme F2. Synthesis of F5 – F9.**[a]
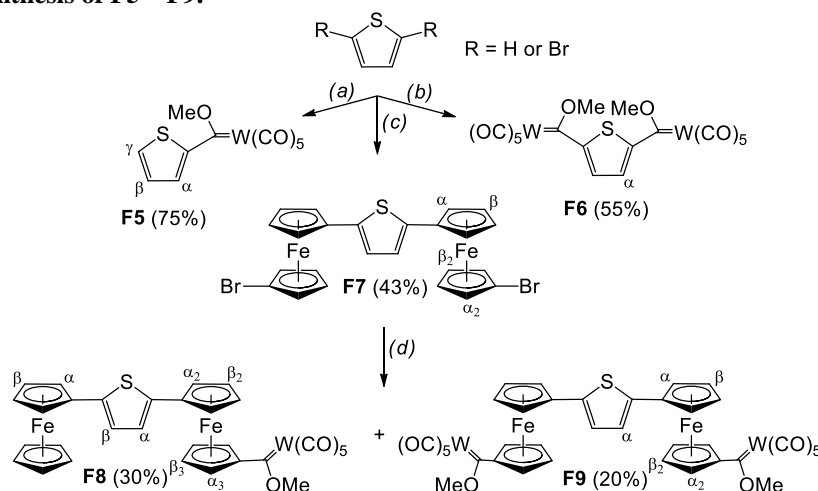


[a]Atom numbering scheme used for the series of complexes studied. Reaction conditions: (a) (i) R = H, thf, –80 °C, $^n$BuLi; (ii) $W(CO)_6$, –50 °C; (iii) $CH_2Cl_2$, –50 °C, MeOTf. (b) (i) R = Br, thf, –40 °C, $^n$BuLi; (ii) $W(CO)_6$, –40 °C; (iii) $CH_2Cl_2$, –30 °C, MeOTf. (c) (i) thf, FcBr$_2$, –100 °C, $^n$BuLi; (ii) [ZnCl$_2$·2thf], 0 °C; (iii) 2,5-ThBr$_2$, [Pd], 55 °C. (d) (i) thf, –40 °C, $^n$BuLi; (ii) $W(CO)_6$, –40 °C; (iii) $CH_2Cl_2$, –30 °C, MeOTf.

Lithiated thienyl/biferrocenylthiophenes were generated *in situ* from respective brominated precursors by lithiation or lithium-bromine exchange reactions according to literature procedures.[380] Purification of these complexes was done by column chromatography. Compounds **F5**, **F6**, **F8** and **F9** are stable toward moisture and air in the solid state and in solution. Compound **F7** was synthesized by employing the palladium-promoted Negishi *C,C* cross-coupling protocol[228] using 1,1'-dibromoferrocene and 2,5-dibromo thiophene, [Pd(CH$_2$CMe$_2$P$^t$Bu$_2$)($\mu$-Cl)] was applied as catalyst.[229,230]

The electronic effects of the carbene substituents in the named compounds can be followed in solution by both NMR and IR spectroscopy. The $\alpha$-proton relative to the carbene substituent in thienyl and ferrocenyl thiophenes experiences the greatest deshielding (Table F6) and corresponds well to the substituent effect of, for example, an ester functionality instead of a metal carbonyl fragment.[418]

**Table F6. Selected NMR data and the infrared $v$(CO) stretching frequencies ($A_1$'') of Fischer carbenes F5, F6, F8 and F9.**

| Compd. | $H_\alpha \delta^a$ $^1$H [ppm] | $C_{carbene} \delta^a$ $^{13}C\{^1H\}$ [ppm] | $A_1$'' $v$(CO)$^b$ [cm$^{-1}$] |
|--------|-----------|-----------|-----------|
| **F5** | 7.89 | 293.39 | 2069 |
| **F6** | 7.95 | 296.50 | 2062 |
| **F8** | 4.95 (α3) | 307.75 | 2062 |
| **F9** | 4.93 (α2) | 308.47 | 2060 |

$^a$ CDCl$_3$. $^b$ CH$_2$Cl$_2$.

Stabilization of the electrophilic carbene carbon also occurs in a similar way as with the ester analogues: via $\pi$-delocalization of the hetero-aryl ring. As expected, this effect is also seen in the $A_1$'' $v$(CO) stretching frequency which decreases as electron density donation from the heteroatom increases.[419,420] Due to the relative insensitivity of the carbonyl stretching frequencies toward the changes on the carbene substituents,[421] little difference is observed in the measured infrared frequencies for this series of complexes.

**Electrochemistry**. The electrochemical studies of complexes **F5**, **F6**, **F8** and **F9** were carried out under an argon atmosphere in dichloromethane solutions containing [N$^n$Bu$_4$][B(C$_6$F$_5$)$_4$] (0.1 M) as supporting electrolyte. An OTTLE[238] (= Optically Transparent Thin Layer Electrochemistry) cell was used during the spectroelectrochemical investigations (Experimental Section).

During the electrochemical study of **F5**, two significant redox events could be detected. A reduction process at $E_{pc}$ = –1745 mV, which is associated with the reduction of the carbene center itself, and a tungsten carbonyl oxidation reaction at $E_{pa}$ = 820 mV (Table F7 and Figure F9). Similar observations were made for other Fischer carbene complexes previously.[287,415–417] A second tungsten carbene moiety on the thiophene system (**F6**) results in a more anodic, irreversible tungsten oxidation process starting from $E_{pa}$ = 850 mV (Table F7 and Figure F9). In contrast, two reversible$^W$ one-electron reduction events could be detected for **F6** at $E^{0'}$ = –1320 mV and –1060 mV, wherein the generation of the mono-anion takes place around 600 mV more anodic as observed for **F5**. The corresponding redox separation $(\Delta E^{0'}$ = 260 mV) suggests an interaction of the Fischer carbene moieties in **F6**$^-$ over the thiophene bridge (*vide infra*).

A combination of the 2,5-diferrocenyl thiophene system with one carbene fragment (**F8**) results also in a significant anodic shift for the first ferrocenyl redox process compared to the 2,5-diferrocenyl thiophene.[253] The second iron-based oxidation process for **F8** could be

---

$^W$ A higher reversibility in reduction events has its origin probably in the ability of **F6** to stabilize negative charge better than **F5** or other more electron-rich Fischer carbene complexes in the corresponding redox active states (see ref. 287,415,417).

observed at $E^{0'}$ = 420 mV, further increasing of the potential leads to the typical irreversible tungsten carbonyl oxidation process around 1100 mV *vs.* FcH/FcH$^+$ (Table F7 and Figure F9).
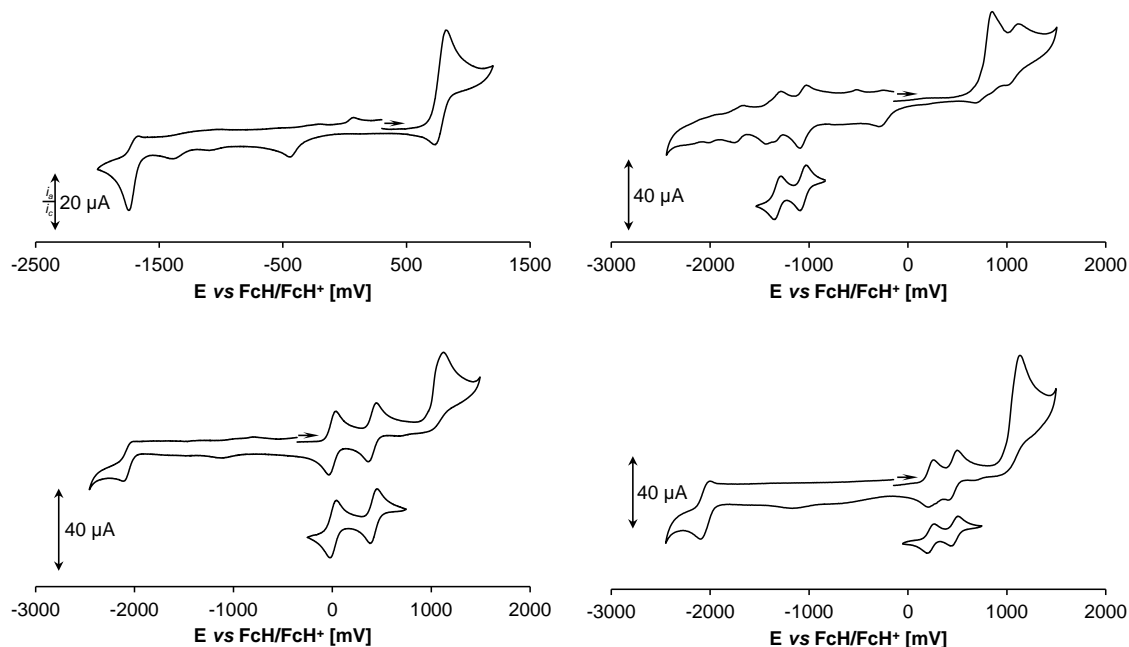


**Figure F9**. Cyclic voltammograms of Fischer type carbenes **F5** (left top), **F6** (right top), **F8** (left bottom) and **F9** (right bottom). Scan rate: 100 mVs$^{-1}$ (full range cyclic voltammograms of **F6** and **F9** at 300 mVs$^{-1}$) in dichloromethane solutions (1.0 mM) at 25 °C, supporting electrolyte [N$^n$Bu$_4$][B(C$_6$F$_5$)$_4$] (0.1 M). In case of the full range cyclic voltammograms the initial cycle is shown, arrows indicate the potential direction. For cyclic voltammetry data see Table F7.

The generation of **F8**$^-$ could be detected at $E_{pc} \approx$ –2100 mV. In case of the biscarbene **F9**, the first ferrocenyl-based redox event was observed at $E^{0'}$ = 230 mV, approximately 220 mV more anodic as detected for the corresponding **F8**/**F8**$^+$ redox event, but even slightly more cathodic as for the previously described ferrocenyl tungsten Fischer carbene system (*vide supra*).[287] The redox potential of the **F9**$^+$/**F9**$^{2+}$ process was determined to $E^{0'}$ = 475 mV *vs.* FcH/FcH$^+$. Hence, the corresponding redox separation is very similar as observed for the 2,5-diferrocenyl thiophene system ($\Delta E^{0'} \approx$ 250 mV) itself under comparable conditions (Table F7 and Figure F9).[253]

A partial reversible reduction event could be detected in the cathodic end of the electrochemical window with an $i_{pc}$ value nearly twice as large as observed for the **F9**/**F9**$^+$ process or the **F9**$^+$/**F9**$^{2+}$ respectively (Table F7, Figure F9 and AF2-1).[X] Thus, the reduction events of the Fischer carbene centers in **F9** occur very close together. This fact suggests only a very weak interaction between the Fischer carbene increments in **F9**$^-$.

---

[X] The partial reversibility is shown *inter alia* in the $i_{pa}/i_{pc}$ ratio and the occurrence of follow-up reactions during the carbene reductions, *e.g.* the oxidation process around 75 mV *vs* FcH/FcH$^+$ in Figure AF2-1 (Appendix Section).

**Table F7. Cyclic voltammetry data (potentials *vs.* FcH/FcH$^+$) of 1.0 mM solutions of F5, F6, F8 and F9 in dry dichloromethane containing [N$^n$Bu$_4$][B(C$_6$F$_5$)$_4$] (0.1 M) as supporting electrolyte at 25 °C.**

| Compd. | $E^{0'}/\Delta E_p/\Delta E^{0'}$ [mV]$^f$ Wave (no.) | | | | $K_C$ [$10^4$]$^g$ |
|---|---|---|---|---|---|
| | (1) | (2) | (3) | (4) | |
| **F5** | −1710/80 (0.33$^c$, −1665$^d$, −1745$^e$) | 775/95 (0.31$^b$, 820$^d$, 725$^e$) | | | |
| **F6** | −1320/65 (0.90$^b$) | −1060/60/260 (0.95$^b$) | 850$^{a,d}$/− | | 2.5 |
| **F8** | −2095$^{a,e}$/− (0.49$^{a,c}$) | 10/70 (1.00$^b$) | 420/70/410 (0.97$^b$) | 1135$^d$/− | 858.8 |
| **F9** | −2095$^{a,e}$/− (0.44$^{a,c}$) | 230/65 (0.97$^b$) | 475/70/245 (0.97$^b$) | 1135$^{a,d}$/− | 1.4 |

$^a$ 300 mVs$^{-1}$. $^b$ $i_{pc}/i_{pa}$. $^c$ $i_{pa}/i_{pc}$. $^d$ $E_{pa}$. $^e$ $E_{pc}$. $^f$ $E^{0'}$: Formal potential; $\Delta E_p$: Difference between the oxidation ($E_{pa}$) and reduction ($E_{pc}$) peak potential;[85,235] $\Delta E^{0'}$: Redox separation ($\Delta E^{0'} = E^{0'}(2) - E^{0'}(1)$). $^g$ $K_C$: Comproportionation constant $\left( K_C = \left( e^{\frac{\Delta E^{0'}F}{RT}} \right) \right)$.

Similar findings were made for ferrocenediyl and biferrocenediyl biscarbene complexes recently (*vide supra*).[287] The tungsten carbonyl oxidation electrode reactions of **F9** were detected in the same potential range as observed for ferrocenyl thiophene **F8** (Table F7 and Figure F9).

In order to get a closer insight into the oxidation process of **F5**, **F6**, **F8** and **F9** spectroelectrochemical studies were carried out by a stepwise increase of the potential *vs.* Ag/AgCl in an OTTLE[238] cell using a 0.1 M dichloromethane solution of [N$^n$Bu$_4$][B(C$_6$F$_5$)$_4$] as supporting electrolyte. This procedure allows for the *in situ* generation of intervalent species such as **F6$^{n-}$**, **F8$^{n+}$** and **F9$^{n+}$** (n = 1, 2). Within the deconvolution procedure of NIR absorptions, transitions with Gaussian shapes were taken to get fits good enough to allow an almost exact overlay of the sum of the spectral components with the experimental spectra. All neutral Fischer carbene complexes do not display, as expected, any absorptions in the NIR range (Figures F11, F12 and AF2-2). For calculation of the theoretical bandwidth at half height ($\Delta \tilde{v}_{1/2(theo)}$) in asymmetric systems, the energy gap between the diabatic states ($\Delta G^0$, *vide supra*) could be estimated, using the difference in oxidation potentials of the two redox sites.[49,57,61] Regarding this, the oxidation potential of (CO)$_5$W=C(OMe)Me[383] as well as the formal potential of the Fc/Fc$^+$ redox process of (CO)$_5$W=C(OMe)Fc[287] were used (Table F8). Within the UV-Vis-NIR spectroelectrochemical investigations of **F6** no noteworthy absorptions could be recorded in the NIR range (Figure AF2-2). However, the intense UV-Vis absorptions of **F6** around 340 nm (LF) and 550 nm (MLCT) decrease and shift formal to lower energies, if reduction takes place (Figure AF2-2). Within this context, two new absorption bands between 650 nm and 800 nm could be observed, which could offer an interaction between the tungsten

centers in **F6$^-$**. Further reduction to **F6$^{2-}$** leads to a decrease of these absorptions (Figure AF2-2). During the infrared spectroelectrochemistry of **F6**, significant changes in $v$(CO) stretching frequencies could be detected during the successive *in situ* generation of **F6$^-$** (Figure F10).
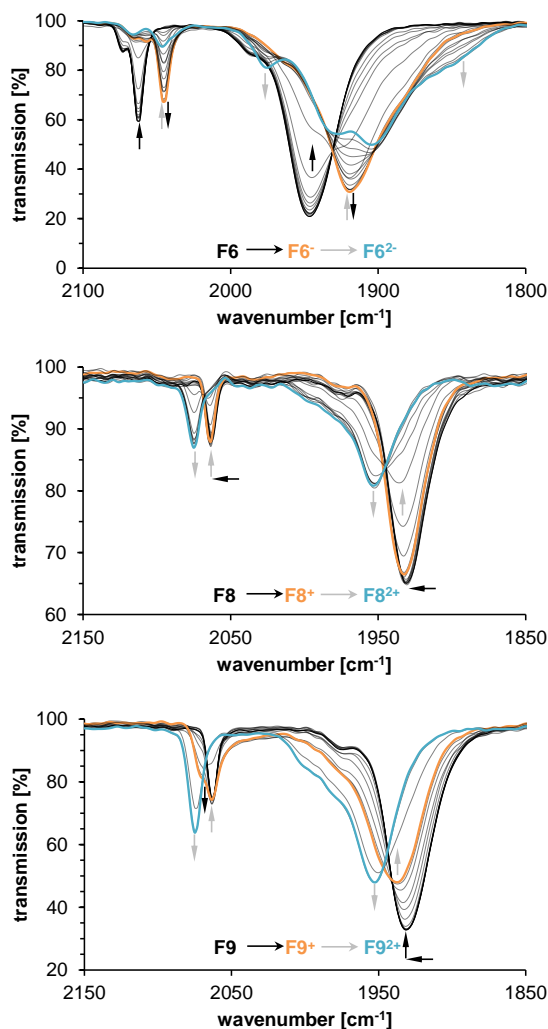


**Figure F10**. Infrared spectra of **F6**, **F8** and **F9** at rising potentials (top: –200 to –750 mV; middle: –100 to 650 mV; bottom: –100 to 710 mV). All potentials *vs*. Ag/AgCl at 25 °C in dichloromethane on 5 mM analyte solutions, supporting electrolyte [N$^n$Bu$_4$][B(C$_6$F$_5$)$_4$] (0.1 M). Arrows indicate increasing or decreasing as well as shifting absorptions.

Thus, the absorption of the original A$_1$'' mode at 2062 cm$^{-1}$ decreases together with an rising absorption band at 2045 cm$^{-1}$, with a comparable width at half height as the original band (Figure F10). This suggests a strong interaction between the two tungsten-based Fischer carbene increments over the thiophene connectivity and hence a high degree of charge delocalization within the infrared timescale. The $v$(CO) stretching frequencies of **F6** at 1947 cm$^{-1}$ shift formal to 1920 cm$^{-1}$ upon generation of the monoanion (Figure F10).

Further reduction to **F6$^{2-}$** leads to a decrease of the A$_1$'' $v$(CO) stretching frequencies in combination with a formal splitting of the band at 1920 cm$^{-1}$ to 1928 cm$^{-1}$ and 1905 cm$^{-1}$.

However, under our conditions a slow decomposition process could be observed during the generation of $F6^{2-}$ (see also Figure AF2-2) and hence the corresponding absorption behavior should be handled with caution.

During the infrared spectroelectrochemical study of ferrocenyl thiophene **F8**, $v$(CO) stretching frequencies were observed at 2063 $cm^{-1}$ and 1930 $cm^{-1}$ (Figure F10). Upon increasing the potential, the original absorptions shift only slightly to higher wavenumbers during the generation of $F8^{+}$ (2064 $cm^{-1}$ and 1932 $cm^{-1}$). This observation reveals that the first oxidation is mostly based on the non-substituted ferrocenyl unit and the interaction with the Fischer carbene moiety is very weak. Further increasing the potential leads to a decrease of the latter bands and $v$(CO) stretching frequencies at 2075 $cm^{-1}$ and 1953 $cm^{-1}$ could be found for $F8^{2+}$.

**Table F8. NIR data of F8 and F9 (2 mM) in dry dichloromethane containing $[N^{n}Bu_4][B(C_6F_5)_4]$ (0.1 M) as supporting electrolyte at 25 °C.**

| Compd. | Transition | $\tilde{v}_{max}$ [$cm^{-1}$] | $\Delta\tilde{v}_{1/2}$ [$cm^{-1}$] | $\Delta\tilde{v}_{1/2(theo)}$ [$cm^{-1}$][a] |
|---|---|---|---|---|
| $F8^{+}$ | LMCT | 10460 | 3280 | |
| | IVCT | 6600 | 3220 | $3100^{b,e}$ |
| | LF | 5140 | 720 | |
| | | 4080 | 730 | |
| $F8^{2+}$ | LMCT | 10800 | n. a. | |
| | MMCT | 7220 | 3130 | $1750^{b,d}$ |
| | LF | 3950 | 1240 | |
| $F9^{+}$ | LMCT/MMCT | 9170 | 2920 | $2750^{b,d}$ |
| | IVCT | 4660 | 4200 | $3280^{c}$ |
| | | 3610 | 900 | |
| $F9^{2+}$ | LMCT | 10200 | n. a. | |
| | MMCT | 6970 | 3800 | $1572^{b,d}$ |
| | LF | 4000 | 1000 | |

$^{a}$ $\Delta\tilde{v}_{1/2(theo)} = (2310\lambda)^{1/2}$. $^{b}$ $\lambda = \tilde{v}_{max} - \Delta G^{0}$. $^{c}$ $\lambda = \tilde{v}_{max}$. $^{d}$ $\Delta G^{0} = 5900$ $cm^{-1}$. $^{e}$ $\Delta G^{0} = 2420$ $cm^{-1}$

Within this regard, the shift in $v$(CO) stretching frequencies upon generation of $F8^{2+}$ is comparable with the corresponding behavior of the ferrocenyl tungsten Fischer carbene complex, $(CO)_5W=C(OMe)Fc$, itself during the $Fc/Fc^{+}$ redox process.[287] Thus, the interaction between the ferrocenyl unit and its Fischer carbene moiety should be very similar in both cases.[287] Within the UV-Vis-NIR spectroelectrochemical studies of **F8** typical absorptions in the UV-Vis region of inner ferrocenyl transitions ($\pi$-$\pi$* and MLCT/d-d) were observed (Table F8 and Figure 11).[239,387,388]

During the generation of $F8^{+}$ three main absorptions could be detected in the NIR range. A high energy near infrared absorption was observed around 10500 $cm^{-1}$ which is assigned to a ligand to metal charge transfer (LMCT) transition, similar as observed for the monocationic intermediate of 2,5-diferrocenyl thiophene as well as for other ferrocenyl-substituted heterocycles.[31,173,179,180,183,210,253,273,274]
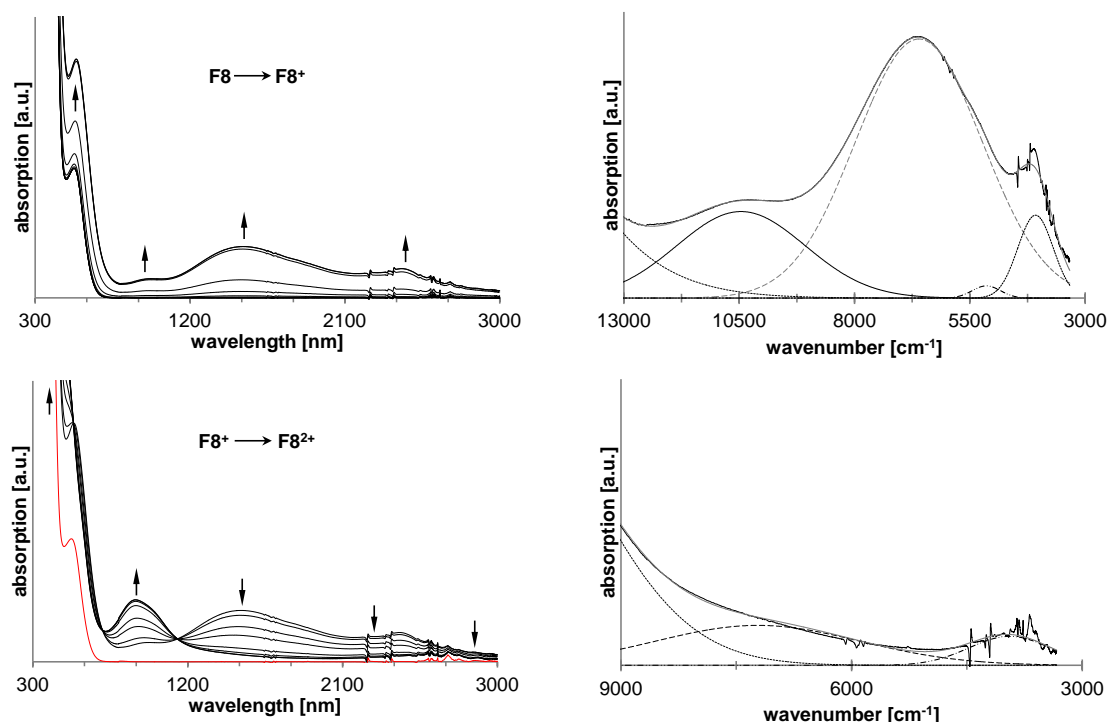
**Figure F11**. UV-Vis-NIR spectra of **F8** (2 mM) at rising potentials. Left top: –100 to 390 mV. Left bottom: 390 to 525 mV (red line represents rereduction to the neutral species). Right top: deconvolution of NIR absorptions at 390 mV, using five distinct overlapping transitions with Gaussian shapes (dashed line indicates IVCT absorptions, dotted line corresponds to absorptions caused by interactions between ligand and metal, dotted dashed line represents ligand field transitions).Right bottom: deconvolution of NIR absorptions at 525 mV, using three distinct overlapping transitions with Gaussian shapes (dashed line indicates MMCT absorptions, dotted line corresponds to absorptions caused by interactions between ligand and metal, dotted dashed line represents ligand field transitions). All potentials *vs.* Ag/AgCl at 25 °C in dichloromethane, supporting electrolyte [N$^{n}$Bu$_4$][B(C$_6$F$_5$)$_4$] (0.1 M). Arrows indicate increasing or decreasing as well as shifting absorptions.

An observation of an absorption caused by an ferrocenyl-tungsten interaction (MMCT) is not expected for **F8**$^+$ due to a very small shift in $v$(CO) stretching frequencies (*vide supra*) and thus a very weak electronic coupling between the corresponding redox increments.[287] Furthermore, the relative strong absorption at 6600 cm$^{-1}$ is assigned to an intervalence charge transfer (IVCT) between the iron centers in **F8**$^+$ (Table F8). The significant blue shift of the latter transition together with the smaller bandwidth at half height ($\Delta\tilde{v}_{1/2}$) compared with the corresponding absorption of the monocationic 2,5-diferrocenyl thiophene,[253] as we would observe for a symmetrical system in the same energy range, is caused by the asymmetry in **F8**/**F8**$^+$ (Table F8). Due to the fact that delocalization is not favored in asymmetrical systems and together with a good accordance of the corresponding theoretical bandwidth at half height for such species, the metal-metal interactions in **F8**$^+$ can be described with weakly (Fe-Fe) and very weakly (Fe-W) coupled class II systems according to Robin and Day.[68] A further low-energy absorption at 4080 cm$^{-1}$ which is too intense for a ligand field transition is ascribed to a further IC$^Y$ absorption,[289] since the

---

$^Y$ Interconfigurational (IC) transition.

experimentally determined bandwidth at half height would be too small as expected from the Hush theory. However, Tuczek *et al.* have proposed an IVCT character for such absorptions in intervalent non-bridged biferrocene species, which is commonly accepted for bisfulvalene diiron systems (Table F8 and Figure F11).[70,115,116,126,127] Further increasing of the potential leads to a decrease of the low energy absorptions upon generation of $\mathbf{F8^{2+}}$ together with an increasing LMCT absorption band around 11000 cm$^{-1}$. An absorption band at 7220 cm$^{-1}$ could be assigned to a MMCT interaction between ferrocenyl unit and its tungsten Fischer carbene substituent, similar as observed for the corresponding ferrocenyl and biferrocenyl systems previously.[287] The weak absorption at ca. 4000 cm$^{-1}$ is ascribed to formal forbidden ligand field (LF) transitions.[173,179,180,183,210,242–244,253,273,274]
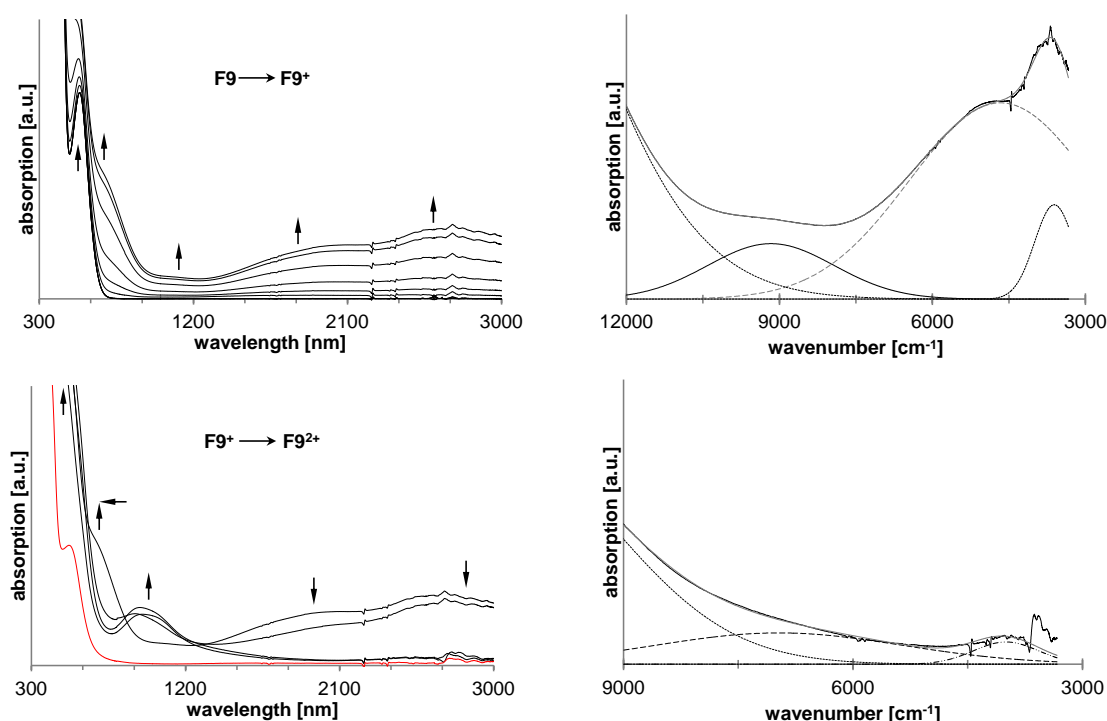


**Figure F12**. UV-Vis-NIR spectra of **F9** (2 mM) at rising potentials. Left top: –100 to 670 mV. Left bottom: 670 to 710 mV (red line represents rereduction to the neutral species). Right top: deconvolution of NIR absorptions at 670 mV, using four distinct overlapping transitions with Gaussian shapes (dashed line indicates IVCT absorptions, dotted line corresponds to absorptions caused by interactions between ligand and metal).Right bottom: deconvolution of NIR absorptions at 710 mV, using three distinct overlapping transitions with Gaussian shapes (dashed line indicates MMCT absorptions, dotted line corresponds to absorptions caused by interactions between ligand and metal, dotted dashed line represents ligand field transitions). All potentials *vs.* Ag/AgCl at 25 °C in dichloromethane, supporting electrolyte [N$^n$Bu$_4$][B(C$_6$F$_5$)$_4$] (0.1 M). Arrows indicate increasing or decreasing as well as shifting absorptions.

A second tungsten Fischer complex fragment on the $\alpha,\alpha$'-diferrocenyl thiophene building block (**F9**) leads to three NIR absorptions for **F9$^+$** at 9170 cm$^{-1}$, around 4700 cm$^{-1}$ and at 3610 cm$^{-1}$ (Table F8, Figure F12). The latter transition can be assigned again to a low-energy IC (*vide supra*). The more intense absorption at 4660 cm$^{-1}$ is well-described with a formal iron-iron inter valence charge transfer, slightly more bathochromically shifted as observed for monocationic 2,5-diferrocenyl thiophene previously.[171,253] A comparison of

the corresponding bandwidth at half height with the theoretical value suggests also a class II assignment, according to Robin and Day (Table F8, Figure F12).[68] The third near infrared transition around 9200 cm$^{-1}$ for **F9$^+$** could be ascribed with an LMCT transition (*vide supra*) between the thiophene core and the ferrocenyls,[253] however it can also be an combination together with a ferrocenyl-tungsten MMCT transition (Table F8 and Figure F12).

During the successive generation of monocationic **F9** the $v$(CO) stretching frequencies at 1931 cm$^{-1}$ shifts formally to higher energy (1937 cm$^{-1}$) together with an occurrence of a double band for the A$_1$'' $v$(CO) stretching frequencies (2070 cm$^{-1}$ and 2063 cm$^{-1}$), verifying the valence-trapped situation in **F9$^+$** and hence a class II coupling regime (*vide supra*, Figure F10). Upon oxidation of **F9$^+$**, the low-energy NIR absorptions decreases and near infrared absorption bands at higher energies, around 1000 nm, become more intense (Table F8, Figure F12). Furthermore, absorption bands at 6970 cm$^{-1}$ (MMCT) and at around 4000 cm$^{-1}$ (LF) could be detected. However, a slow decomposition of **F9$^{2+}$** was observed during the spectroelectrochemical measurements, thus the corresponding absorption behavior should be handled with care.

In the infrared range, the $v$(CO) stretching frequencies at 2070 cm$^{-1}$, 2063 cm$^{-1}$ and 1937 cm$^{-1}$ decrease upon generation of **F9$^{2+}$** together with increasing absorptions at 2075 cm$^{-1}$ and 1953 cm$^{-1}$, very similar as observed during the generation of mono-cationic (CO)$_5$W=C(OMe)Fc.[287] Hence, a class II assignment according to Robin and Day should also be valid.[68]

**Crystallography**. The molecular structures of **F5**, **F8** and **F9** in the solid state have been determined by single-crystal X-ray diffraction analysis. Suitable single crystals of **F5**, **F8** and **F9** were obtained by slow evaporation of a saturated dichloromethane solution of the respective complex layered with *n*-hexane at –5 $^o$C. The *ORTEP* diagrams with selected bond lengths (Å), bond angles (°), and torsion angles (°) are shown in Figures F13 – F14. Compounds **F5**, **F8** and **F9** crystallize in the triclinic space group *P*–1 (**F9**) or in the monoclinic space group *P*2$_1$/*n* (**F8**, **F5**) with one (**F8**, **F5**) or a half molecule (**F9**) in the asymmetric unit. The thiophene heterocycle in **F9** is refined disordered on two positions with an occupation of 50 % for each orientation and is omitted for clarity in Figure F13. The ferrocenyl containing derivatives **F8** and **F9** show an almost planar conformation between the thiophene and the cyclopentadienyl cycles (**F9**: C14–C13–C18–C19 –16(3) °, **F8**: C14–C13–C18–C19 176.6(5) ° and C20–C21–C22–C26 1.1(8) °) and also to the planar carbene substituent (**F9**: O6–C6–C8–C9 1.3(9) °, **F8**: O6–C6–C8–C9 –0.2(6) °). A

directly bonded heterocycle (**F5**) also obtains a planar conformation between the carbene and the thiophene $\pi$-system (O6–C6–C8–C9 –170.9(4) °).
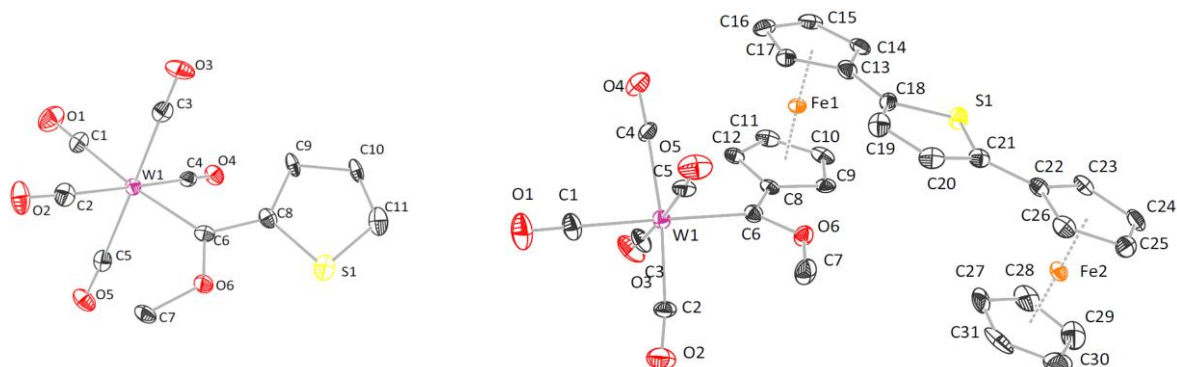


**Figure F13**. ORTEP diagrams (50% probability level) of the molecular structures of **F5** and **F8** with the atom-numbering scheme. All hydrogen atoms have been omitted for clarity. Selected bond distances (Å), angles (°), and torsion angles (°). **F5**: C1−O1 1.140(6), C1–W1 2.030(5), C6–O6 1.330(5), C6–C8 1.461(6), C6–W1 2.180(5), O6–C7 1.449(5), C8–C9 1.476(6), C9–C10 1.436(6), C10–C11 1.354(5), C11–S1 1.678(5), C8–S1 1.725(5), O1–C1–W1 177.8(4), O6–C6–C8 105.1(4), O6–C6–W1 130.1(3), C8–C6–W1 124.8(3), C11–S1–C8 92.1(2), O6–C6–C8–C9 –170.9(4), W1–C6–C8–C9 11.6(6), C8–C6–O6–C7 179.3(3), O6–C6–W1–C5 –49.7(4) **F8**: C1−O1 1.129(6), C1–W1 2.046(5), C6–W1 2.202(4), C6–O6 1.334(5), O6–C7 1.436(6), C6–C8 1.453(6), C13–C18 1.458(7), C18–C19 1.361(7), C19–C20 1.417(7), C20–C21 1.357(7), C18–S1 1.725(5), C21–S1 1.741(4), C21–C22 1.446(6), D1–Fe1 1.6467(7), D2–Fe1 1.6558(7), D3–Fe2 1.6328(7), D4–Fe2 1.6425(7), O1–C1–W1 176.6(4), O6–C6–C8 105.6(4), O6–C6–W1 128.9(3), C8–C6–W1 125.4(3), C18–S1–C21 92.4(2), D1–Fe1–D2 177.17(5), D3–Fe2–D4 179.00(5), O6–C6–C8–C9 –0.2(6), W1–C6–O6–C7 1.0(6), C14–C13–C18–C19 176.6(5), C20–C21–C22–C26 1.1(8), O6–C6–W1–C2 –41.3(4), C8–D1–D2–C17 –16.8(3), C8–D1–D2–C13 55.2(3), C22–D3–D4–C27 3.8(4), Fe–Fe 7.4837(10) (D denote the centroids of: D1: C8–C12, D2 C13–C17, D3 C22–C26, D4 C27–C31).
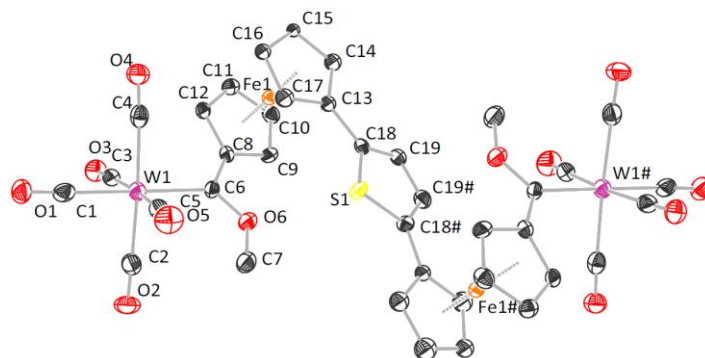


**Figure F14**. ORTEP diagram (50% probability level) of the molecular structure of **F9** with the atom-numbering scheme. All hydrogen atoms have been omitted for clarity. Selected bond distances (Å), angles (°), and torsion angles (°): C1−O1 1.139(9), C1–W1 2.030(8), C6–W1 2.222(7), C6–O6 1.328(8), C6–C8 1.461(9), O6–C7 1.425(8), C13–C18 1.45(2), C18–C19 1.406(19), C18–S1 1.707(13), C19–C19# 1.367(19), D1–Fe1 1.6552(9), D2–Fe1 1.6990(9), O1–C1–W1 177.0(6), C18–S1–C18# 93.3(7), C8–C6–W1 124.9(5), O6–C6–W1 128.5(5), O6–C6–C8 106.3(6), D1–Fe1–D2 178.76(7), C8–D1–D2–C17 –4(1), C8–D1–D2–C13 67.2(8), C8–C6–O6–C7 178.2(6), O6–C6–W1–C2 –41.5(6), O6–C6–C8–C9 1.3(9), C14–C13–C18–C19 – 16(3), Fe1–Fe1# 8.4367(2) (D1 denotes the centroid of C8–C12; D2 denotes the centroid of C13–C17). Symmetry operation for the generation of equivalent atoms: –x–1, –y, –z.

The ferrocenyls themselves are almost eclipsed (**F9**: C8–D1–D2–C17 –4(1) °, **F8**: C22–D3–D4–C27 3.8(4) °) or between eclipsed and staggered (**F8**: C8–D1–D2–C17 –16.8(3) °) with a synclinal conformation for 1,1'-substituted ferrocenyl fragments. Nevertheless, the substituents at the carbene carbon C6 influence the W1–C6 distance. The Electron rich

126

metallocenyl moieties lead to an extension of the formal double bond to a maximum of 2.222(7) Å (**F9**), whereas the thiophene derivative **F5** significantly shortens the bond to 2.180(5) Å. In **F8** the distances are averaged to 2.202(4) Å. A further influence to the W1–C1 distance is not detectable. Regarding the bond lengths in the thiophene core for unsymmetrical **F5**, the carbene carbon influences the C–S bonds. The bond length from S1 to C8 is 1.725(5) Å, whereas to the non-substituted bond to C11 is shortened to 1.678(5) Å. The free electron pairs of O6 are oriented away from the carbonyls for all three compounds to avoid an electronic interaction. The steric interaction of the methyl group at C7 to the W(CO)$_5$ fragment is prevented by a staggered conformation between two carbonyls (**F9**: O6–C6–W1–C2 –41.5(6) °, **F8**: O6–C6–W1–C2 –41.3(4) °, **F5**: O6–C6–W1–C5 –49.7(4) °). Nevertheless, the W(CO)$_5$ fragment decreases the O6–C6–C8 angle from ideal 120 ° to 106.3(6) (**F9**), 105.6(4) (**F8**) and 105.1(4) (**F5**).

CONCLUSION

Within this study, a series of thiophene tungsten Fischer carbene complexes of type [(CO)$_5$W=C(OMe)R] (**F5**, R = 2-thienyl; **F8**, R = fcthFc; th = 2,5-thiendiyl; Fc = ferrocenyl; fc = 1,1'-ferrocenediyl) and [(CO)$_5$W=C(OMe)-R'-(OMe)C=W(CO)$_5$] (**F6**, R' = th; **F9**, R' = fcthfc) is reported with the aim of investigating low-energy charge transfer transitions between the carbene substituents and the transition metal carbonyl fragment, incorporating the thiophene system. For this reason, tungsten Fischer carbene functionalized thiophenes and α,α'-diferrocenyl thiophene complexes **F5**, **F6**, **F8** and **F9** were prepared and characterized spectroscopically in solution. The structural properties of **F5**, **F8** and **F9** in the solid state were investigated by single-crystal X-ray diffraction studies.

The electrochemical studies reveal reversible one-electron redox events for the ferrocenyl moieties (**F8**, **F9**). Moreover, typical electrode reactions could be found for the carbene reductions itself and for the tungsten carbonyl oxidation processes. However, for biscarbene **F6** two well-separated reversible one-electron reduction events could be found suggesting a significant electronic coupling in **F6**$^-$. During the UV-Vis-NIR spectroelectrochemical investigations typical low-energy absorptions for the mixed-valent α,α'-diferrocenyl thiophene increment were found, as well as high-energy NIR absorptions which were attributed to metal-metal charge transfer transition between the tungsten carbonyl increment and the ferrocenyl units in the corresponding species. Further infrared spectroelectrochemical studies reveal, in accordance with the NIR experiments, that the

electronic interactions in the corresponding cationic species can be described with class II systems according to Robin and Day. The corresponding infrared spectroelectrochemical investigations on biscarbene **F6** reveal a high degree of charge delocalization in the formal mixed valent **F6⁻**.

EXPERIMENTAL SECTION

**General procedures**. Inert Schlenk techniques were employed in all operations and syntheses were done under argon or nitrogen. Solvents were distilled over sodium/benzophenone (*n*-hexane, tetrahydrofuran (thf)) or phosphorpentoxide (dichloromethane ($CH_2Cl_2$)) and collected under nitrogen or argon gas. Chemicals were used as purchased without any further purification unless stated otherwise. Purification with column chromatography was done using silica gel 60 (0.0063–0.200 mm) as stationary phase. A Bruker AVANCE 500 spectrometer was used for NMR recordings. $^1$H NMR spectra were recorded at 500.139 MHz and $^{13}$C{$^1$H} NMR spectra at 125.75 MHz. The signal of the solvent was used as reference: $^1$H CDCl$_3$ at 7.26 ppm and $^{13}$C{$^1$H} CDCl$_3$ at 77.16 ppm. IR spectra were recorded on a Perkin-Elmer Spectrum RXI FT-IR spectrophotometer in solvent as specified. Only the vibration bands in the carbonyl-stretching region (1600 – 2200 cm$^{-1}$) were recorded.

**Synthesis of complex F5**.[416] To a thf solution of thiophene (3.0 mmol, 0.24 mL), $^n$BuLi (3.3 mmol) was slowly added at –80 $^o$C. After 1 h the cold bath was removed and the reaction mixture allowed to reach room temperature for ca. 20 min. It was cooled to –50 $^o$C and W(CO)$_6$ (3.0 mmol, 1.06g) was added in a single portion. The color of the solution turned red upon addition. The reaction mixture was stirred isotherm for 30 min after which it was stirred for an additional hour at rt. Volatiles were removed by reduced pressure and the residue redissolved in dichloromethane. Afterwards, the reaction mixture was cooled to –50 $^o$C and methyl trifluorosulfonate (9.9 mmol, 1.09 mL) was added. The resulting dark mixture was stirred overnight at ambient temperature. Purification of the crude product was performed by using column chromatography and *n*-hexane as initial eluent. The polarity of the eluent was increased by adding small portions of dichloromethane. Yield 1.23 g (88 %), red crystals. Anal. Calcd. for C$_{11}$H$_6$O$_6$SW (450.08): C: 29.35 %; H: 1.35 %. Found: C: 29.11 %; H: 1.20 %. Mp: 102 $^o$C. NMR (CDCl$_3$) $^1$H: 7.89 (d, $J$ = 1.0 Hz, 1H, H$_\alpha$), 7.22-7.08 (m, 2H), 6.63 (dd, $J$ = 3.7, 1.7 Hz, 1H, H$_ß$), 4.64 (s, 3H, CH$_3$). $^{13}$C{$^1$H}: 293.39 (C$_{carbene}$), 202.63 (C$_{trans}$), 197.80 (C$_{cis}$), 158.45 (C$_{ipso}$), 141.90 (C$_\alpha$), 136.33 (C$_\gamma$),

129.20 ($C_\text{ß}$), 68.93 ($CH_3$). IR ($CH_2Cl_2$) $v$($cm^{-1}$): 2069 (m), 1988 (w), 1963 (m), 1948 (vs). Suitable single crystals of **F5** were obtained from a solution of **F5** at ambient temperature.

**Synthesis of complex F6**. 2,5-Dibromo thiophene (3.0 mmol, 0.34 mL) was added to 50 mL of thf, followed by a slow addition of $^n$BuLi (7.0 mmol) at –40 $^o$C. After 30 min of isothermal stirring, W($CO$)$_6$ (6.0 mmol, 2.11 g) was added to the reaction mixture in a single portion. The resulting solution was stirred isotherm for an additional hour and then allowed to reach room temperature within 60 min. Afterwards, solvent was changed to dichloromethane and methyl trifluorosulfonate (20.0 mmol, 2.41 mL) was added at –30 $^o$C in a single portion. The dark mixture was removed from the cold bath and stirred overnight at ambient temperature. Purification of the crude product was performed by column chromatography and *n*-hexane as initial eluent. The polarity of the eluent was increased by adding small portions of $CH_2Cl_2$. Yield 1.51 g (55 %), purple solid. Anal. Calcd. for $C_{18}H_8O_{12}SW_2$ (816.05): C: 26.49 %; H: 0.99 %. Found: C: 29.43 %; H: 0.93 %. Mp: 264 $^o$C (decomp.). NMR ($CDCl_3$) $^1$H: 7.95 (s, 2H, $H_\alpha$), 4.67 (s, 6H, $CH_3$). $^{13}$C{$^1$H}: 296.50 ($C_\text{carbene}$), 202.64 ($C_\text{trans}$), 196.92 ($C_\text{cis}$), 162.53 ($C_\text{ipso}$), 137.26 ($C_\alpha$), 69.09 ($CH_3$). IR ($CH_2Cl_2$) $v$($cm^{-1}$): 2062 (m), 1974 (w), 1948 (vs), 1935 (s).

**Synthesis of 2,5-di-(1'-bromoferrocenyl)thiophene (F7)**. 1,1'-Dibromoferrocene (5.1 g, 14.8 mmol) was dissolved in 50 mL of thf and cooled to –100 $^o$C. $^n$BuLi (6 mL, 14.8 mmol) was slowly added and the reaction mixture left to stir at this temperature for 45 min. Dry [$ZnCl_2$·2thf] (4.2 g, 15.0 mmol) was added in a single portion and the resulting preparation was kept at 0$^o$C for 30 min. Afterward, 2,5-dibromo thiophene (0.83 mL, 6.45 mmol) and [Pd($CH_2CMe_2P^tBu_2$)($\mu$-Cl)]$_2$[229,230] (0.025 g, 36.4 µmol) were added to the solution. The reaction mixture was heated to 55$^o$C and stirred for 36 h at this temperature. After cooling to ambient temperature, the crude product was adsorbed on alumina and purified by column chromatography on alumina, using a *n*-hexane/toluene mixture of ratio 4:1 (v:v) as eluent. Yield 1.60 g (43 %), dark orange solid. Anal. Calcd. for $C_{24}H_{18}Br_2Fe_2S$ (609.98): C:47.24 %; H:2.98 %; Found: C:47.16 %; H: 2.99 %. Mp: 220 $^o$C. NMR ($CDCl_3$) $^1$H: 6.90 (s, 2H, $Th_\alpha$), 4.98 (m, 4H, $H_\alpha$), 4.35 (m, 4H, $H_\text{ß}$), 4.30 (m, 4H, $H_{\alpha2}$), 4.06 (m, 4H, $H_{\text{ß}2}$). $^{13}$C{$^1$H}: 139.49 ($Th_\text{ipso}$), 123.42 ($Th_\alpha$), 82.52 ($Fc_\text{ipso2}$), 78.97 ($Fc_\text{ipso}$), 72.22 ($Fc_{\alpha2}$), 71.28 ($Fc_{\text{ß}2}$), 69.23 ($Fc_\alpha$), 68.97 ($Fc_\text{ß}$).

**Synthesis of Complexes F8 and F9**. Compound **F7** (3.0 mmol, 0.34 mL) was dissolved in 50 mL of thf and $^n$BuLi (7 mmol) was slowly added at –40 $^o$C. The reaction mixture was stirred isotherm for 30 min after which W($CO$)$_6$ (6.0 mmol, 2.11 g) was added in a single

portion. The solution was kept at –40 °C for 1 h and then allowed to reach ambient temperature within 60 min. All volatiles were removed and the residue was redissolved in $CH_2Cl_2$. Methyl trifluorosulfonate (20.0 mmol, 2.41 mL) was added at –30°C after which the solution darkened. The mixture was removed from the cold bath and stirred overnight at room temperature. Purification of the product was performed by using column chromatography and *n*-hexane as initial eluent. The polarity of the eluent was increased by adding small portions of dichloromethane. Compound **F8** eluted first as a dark-red fraction followed by compound **F9** (brown-red).

Compound **F8**: Yield 0.96 g (40 %), red brown crystals. Anal. Calcd. for $C_{31}H_{22}Fe_2O_6SW$ (818.1): C, 45.51 %; H, 2.72 %; found C, 45.59 %; H, 2.79 %. Mp: 237 °C (decomp.). NMR ($CDCl_3$) $^1H$: 6.84 (m, 2H, Th), 4.95 (m, 2H, $H_{\alpha 3}$), 4.93 (m, 2H, $H_{\beta 3}$), 4.72 (m, 2H, $H_{\alpha 2}$), 4.67 (m, 2H, $H_{\beta 2}$), 4.66 (m, 5H, Cp), 4.43 (m, 2H, $H_{\alpha}$), 4.40 (m, 2H, $H_{\beta}$), 4.32 (s, 3H, $CH_3$). $^{13}C\{^1H\}$: 307.75 ($C_{carbene}$), 202.59 ($C_{trans}$), 198.18 ($C_{cis}$), 142.40 ($Th_{ipso}$), 137.54 ($Th_{\alpha'}$), 96.18 ($Fc_{ipso3}$), 83.77 ($Fc_{ipso2}$), 80.07 ($Fc_{ipso}$), 77.36 ($C_{\alpha 3}$), 76.92 ($C_{\beta 3}$), 74.8 5($C_{\alpha 2}$), 71.20 ($C_{\beta 2}$), 70.15 ($C_{\alpha}$), 68.93 ($CH_3$), 68.67 ($C_{\beta}$), 66.83 (Cp). IR ($CH_2Cl_2$) $v(cm^{-1})$: 2062 (m), 1971 (w), 1929 (vs, br). Suitable single crystals of **F8** were obtained from a solution of **F8** at ambient temperature.

Compound **F9**: Yield 0.99 g (30 %), dark brown crystals. Anal. Calcd. for $C_{38}H_{24}Fe_2O_{12}SW_2$ (1184.0): C, 38.54 %; H, 2.05 %; found C, 38.57 %; H, 2.06 %. Mp: 248 °C (decomp.). NMR ($CDCl_3$) $^1H$: 6.85 (s, 2H, $Th_{\alpha}$), 4.93 (m, 4H, $H_{\alpha 2}$), 4.72 (m, 4H, $H_{\beta 2}$), 4.67 (m, 4H, $H_{\alpha}$), 4.40 (m, 4H, $H_{\beta}$), 4.32 (s, 6H, $CH_3$). $^{13}C\{^1H\}$: 308.47 ($C_{carbene}$), 202.42 ($C_{trans}$), 198.14 ($C_{cis}$), 139.16 ($Th_{ipso}$), 123.97 ($Th_{\alpha}$), 96.15 ($Fc_{ipso2}$), 82.99 ($Fc_{ipso}$), 77.34 ($C_{\alpha 2}$), 76.86 ($C_{\beta 2}$), 74.78 ($C_{\alpha}$), 71.65 ($C_{\beta}$), 68.68 ($CH_3$). IR ($CH_2Cl_2$) $v(cm^{-1})$: 2060 (m), 1972 (w), 1929 (vs, br). Suitable single crystals of **F9** were obtained from a solution of **F9** at ambient temperature.

**Electrochemistry**. The electrochemical measurements were carried out under an argon atmosphere on 1.0 mM dichloromethane solutions containing $[N^nBu_4][B(C_6F_5)_4]$ (0.1 M) as supporting electrolyte utilizing a Voltalab 10 electrochemical laboratory from Radiometer Analytical.[90,100,101] An OTTLE cell placed in a Varian Cary 5000 UV-VIS-NIR absorption spectrometer or in a Thermo Nicolet 200 FT-IR spectrometer was used in spectroelectrochemical measurements.[238] For voltammetry, a three electrode cell with a platinum wire counter electrode, a glassy carbon working electrode and a $Ag/Ag^+$ reference electrode was used. The working electrode was prepared by polishing with a Buehler micro cloth using Buehler diamond pastes with decreasing sizes (1 to 0.25 μm). The $Ag/Ag^+$

reference electrode was constructed from a silver wire inserted into a Luggin capillary with a Vycor tip containing a solution of 0.01 mol·L$^{-1}$ $AgNO_3$ as well as 0.1 mol·L$^{-1}$ [N$^n$Bu$_4$][B(C$_6$F$_5$)$_4$] in acetonitrile. This Luggin capillary was inserted into a second Luggin capillary with Vycor tip filled with a 0.1 mol·L$^{-1}$ [N$^n$Bu$_4$][B(C$_6$F$_5$)$_4$] solution in dichloromethane. Cyclic voltammetry was carried out using a scan rate of 100 mVs$^{-1}$. If irreversible redox processes were investigated, a scan rate of 300 mVs$^{-1}$ was also applied. Successive experiments under the same experimental conditions showed that all formal reduction and oxidation potentials were reproducible within 5 mV. Experimentally potentials were referenced against a Ag/Ag$^+$ reference electrode but the results are presented referenced against the FcH/FcH$^+$ couple ($E^{0'}$ = 0.0 mV) as required by IUPAC.[249] When decamethylferrocene was used as an internal standard, the experimentally measured potential was converted in to $E$ $vs.$ FcH/FcH$^+$ by addition of –0.61 V.[250] Cyclic voltammograms were taken after typical two scans and are considered to be steady state cyclic voltammograms, in which the signal pattern differs not from the initial sweep. Finally, the experimental data were processed on Microsoft Excel worksheets.

**Single-Crystal X-ray Diffraction Analysis**. Data were collected with an Oxford Gemini S diffractometer at 100 K using Mo K$\alpha$ ($\lambda$ = 0.71073 Å) radiation. The structures were solved by direct methods using SHELXS-97 and refined by full matrix least-square procedures on F$^2$ using SHELXL-97.[251,252] All non-hydrogen atoms were refined anisotropically and a riding model was employed in the refinement of the hydrogen atom positions. Copies of the data can be obtained free of charge on quoting the depository numbers CCDC-969409 (**F5**), 969408 (**F8**) and 969407 (**F9**) (http://www.ccdc.cam.ac.uk)

**Supporting Information**. The UV-Vis-NIR spectra of **F6**, **F8** and **F9** in dichloromethane as well as a table of crystal data (Table AF2-1) are available in the Appendix Section (Chapter AF2).

# G ELECTROCHEMICAL STUDIES ON RUTHENIUM CYCLOPENTADIENYLS STABILIZED BY FERROCENYL-SUBSTITUTED THIOPHENES

J. M. Speck, M. Korb and Heinrich Lang

*Manuscript,* for publishing in Organometallics

*Section G was made by the author of the present doctoral thesis (synthesis, characterization, electrochemistry, interpretation of results and manuscript preparation) together with M. Korb (solid-state structure determination, discussion), in supervision of Prof. Dr. Heinrich Lang.*

## INTRODUCTION

The understanding of charge transfer phenomena and electrochemical processes represent main interests of current research activities in organic and organometallic chemistry.[37,47,49,74,77] For instance, examinations on heterocyclic intrinsically conducting polymers (ICP) are crucial for the development of new flexible electroactive materials, pliable conducting materials or antistatic coatings.[12–14,19–21,29] Regarding this, the appropriate $\pi$-conjugated material is often reduced to a smaller system, *inter alia* modified with redox-active entities, to get a deeper insight into observable charge transfer processes.[29,31,63,190,422,423] Suitable redox probes should own a high stability in both, the oxidized and reduced states. Thus, triaryl amine building blocks represent prime examples in organic chemistry for this purpose.[37,63,154,318,321,424–426] In the field of organometallic chemistry foremost ferrocene derivatives are applied as redox-active increments.[166,171–173,178–180,183,184,210,223,224,232,253,271,273,274] Electrochemical investigations were carried out on a wealth of ferrocenylated aromatics, including benzenes[163,166,223] and heterocycles[48,167,169,172,176–178,181,182,184] as well as on ferrocenyl-substituted transition metal complexes.[186–188,232,427–429] In general, the magnitude of electronic coupling in mixed-valence complexes depends strongly on the electronic structure of the respective species in combination with the environmental conditions.[37,47] On the basis of 2,5-diferrocenyl thiophene, a strong variation of the electronic metal-metal interaction could be demonstrated by changing the electronic properties of the bridging unit and the ferrocenyl moieties by the way of introduction of electron-donating or electron-withdrawing functionalities.[253,271,320,430] Regarding an evaluation of electronic influences of $\pi$-bonded transition metal fragments, ruthenium cyclopentadienyls represent prime candidates due to their toleration of a diversity of different aromatic substrates and (thus) the high stability of the desired arene complexes.[38,427,431–439]

In continuation of our recently reported work, we report herein a study on thia-heterobi- and termetallocenes – $\eta^5$-thiophene Ru($\eta^5$-C$_5$H$_5$)/Ru($\eta^5$-C$_5$Me$_5$) complexes of a series of ferrocenyl-substituted thiophenes (Figure G1).



M = Ru($\eta^5$-C$_5$H$_5$)[PF$_6$]  (**G2**)
  Ru($\eta^5$-C$_5$Me$_5$)[PF$_6$] (**G7**)

M = Ru($\eta^5$-C$_5$H$_5$)[PF$_6$]  (**G3**)
  Ru($\eta^5$-C$_5$Me$_5$)[PF$_6$] (**G8**)

M = Ru($\eta^5$-C$_5$H$_5$)[PF$_6$]  (**G4**)
  Ru($\eta^5$-C$_5$Me$_5$)[PF$_6$] (**G9**)

M = Ru($\eta^5$-C$_5$H$_5$)[PF$_6$]  (**G5**)
  Ru($\eta^5$-C$_5$Me$_5$)[PF$_6$] (**G10**)

M = Ru($\eta^5$-C$_5$H$_5$)[PF$_6$]  (**G6**)
  Ru($\eta^5$-C$_5$Me$_5$)[PF$_6$] (**G11**)
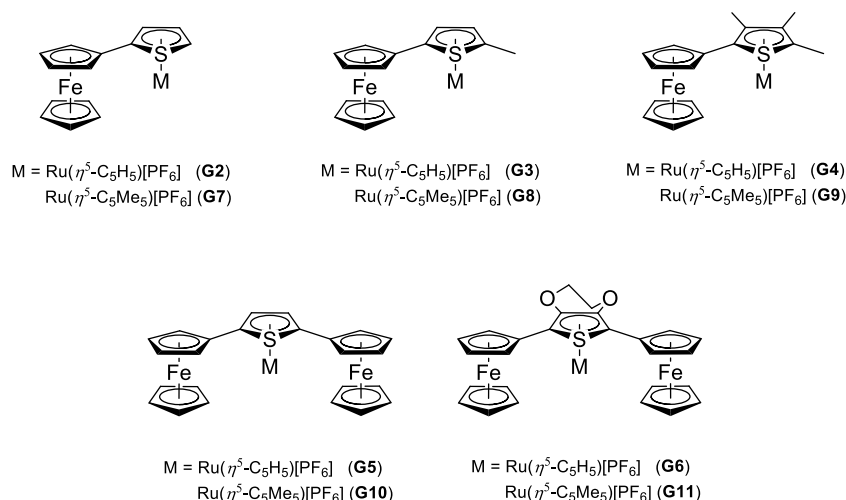
**Figure G1**. Ruthenium complexes **G2** – **G11**.

Their electronic properties were studied within electrochemical investigations, supported by UV-Vis-NIR spectroelectrochemical measurements, with the aim to get a better understanding of the influence of $\pi$-thiophene-bonded transition metal moieties on the thermodynamic stability and charge transfer of the resulting complexes as well as in their oxidized states.

RESULTS AND DISCUSSION

**Synthesis and Characterization.** The synthesis of Ru-complexes **G2** – **G11** is based on literature-known synthesis methodologies, by merging one equivalent of [Ru($\eta^5$-C$_5$H$_5$)(CH$_3$CN)$_3$]PF$_6$ or [Ru($\eta^5$-C$_5$Me$_5$)(CH$_3$CN)$_3$]PF$_6$ with the corresponding thiophene in abs. 1,2-dichloropropane or dichloromethane (*vide infra*, Experimental Section).[253,271,427,429,432,440,441,Z] The resulting reaction mixtures were warmed to 90 °C (1,2-dichloropropane) or 50 °C (dichloromethane) for 12 h. After cooling to ambient temperature 100 mL of *n*-hexane were added and the supernatant solution was removed. The remaining residue was washed with *n*-hexane and/or diethyl ether until the solution becomes colorless. The obtained crude product was finally filtered through a pad of celite, using dichloromethane as solvent. Compounds **G2** – **G11** were obtained as orange or red solids (Experimental Section). For the syntheses of Ru-compounds **G4** and **G9**, the required 2-ferrocenyl-3,4,5-trimethylthiophene (**G1**) was obtained in a Pd-promoted

---

[Z] $\eta^5$-C$_5$H$_5$ = Cp, $\eta^5$-C$_5$Me$_5$ = Cp*

Negishi *C,C* cross-coupling of 2-bromo-3,4,5-trimethylthiophene[442,443] with *in situ* generated ferrocenyl zinc chloride (FcZnCl).[210,247,253,271] Moreover, the utilized RuCp/Cp* transfer reagents [CpRu(CH$_3$CN)$_3$]PF$_6$ and [Cp*Ru(CH$_3$CN)$_3$]PF$_6$ were prepared according to literature-known synthesis procedures.[440,441,AA] However by use of published amounts of NaPF$_6$ during the preparation of [Cp*Ru(CH$_3$CN)$_3$]PF$_6$,[BB] no complete formation of the desired PF$_6$-salt was found. Thus from the crude product of **G9** *inter alia* [Cp*Ru($\eta^5$-2-Fc-3,4,5-(CH$_3$)$_3$-C$_4$S)]$_2$[Zn$_2$Cl$_6$] instead of pure [Cp*Ru($\eta^5$-2-Fc-3,4,5-(CH$_3$)$_3$-C$_4$S)]PF$_6$ was obtained (solid state structure analysis, *vide infra*).[441,CC] This issue can be circumvented by using a fivefold excess of the PF$_6^-$-source.

Compounds **G1** – **G11** are soluble in most common organic solvents including dichloromethane, acetone and tetrahydrofuran. All Ru-complexes are stable in the solid state as well as in solution, under "non-coordinating" conditions. They were identified by elemental analysis, high resolution ESI-TOF mass spectrometry as well as IR and NMR ($^1$H, $^{13}$C{$^1$H}) spectroscopy. The molecular structures of **G3**, **G5**, **G7**, **G9** and **G11** in the solid state were determined by single X-ray structure analysis. All compounds were electrochemically investigated by cyclic (CV) and square wave voltammetry (SWV), in combination with *in situ* UV-Vis-NIR spectroelectrochemical measurements.

For compounds **G1** – **G11**, the anticipated absorptions in the infrared range could be observed, the $^1$H and $^{13}$C{$^1$H} NMR spectra show the expected signal patterns in the predicted ranges (Experimental Section). Moreover, the complexation of [RuCp]$^+$/[RuCp*]$^+$ fragments on the thiophene core can be verified through an observation of significant up-field shifts of proton and carbon resonances (foremost of the thiophene, but also for the ferrocenyls), in combination with a widening of the signal pattern (the occurrence of diastereotopic/heterotopic protons/carbons for the ferrocenyl and ethylenedioxy functionalities) (Experimental Section).

**Solid state structures**. The molecular structures of **G3**, **G5**, **G7**, **G9** and **G11** in the solid state were determined by single crystal X-ray diffraction analysis (Figures G2 and G3, Table AG-1) at 110 K. Crystal and structure refinement data are displayed in the Experimental Section (*vide infra*). The compounds crystallize in triclinic (*P*–1: **G3**, **G7**, **G9**, **G11**) and monoclinic (*P*2$_1$/*n*: **G5**) space groups with one (**G9**, **G11**), two (**G3**, **G7**) or the half of three (**G5**) crystallographically independent molecules in the asymmetric unit.

---

[AA] Potassium hexafluorophosphate can be also used instead of NH$_4$PF$_6$ or NaPF$_6$.
[BB] Zinc dust was used for the reduction of [($\eta^5$-C$_5$Me$_5$)RuCl$_2$]$_n$ in acetonitrile, in presence of NaPF$_6$.
[CC] This is may be one reason for the deviant published elemental analysis of [Cp*Ru(CH$_3$CN)$_3$][PF$_6$].

The compounds crystallize with $PF_6^-$ (**G3**, **G5**, **G7**, **G11**; omitted in Figures G2 and G3) or 0.5 $[Zn_2Cl_6]^{2-}$ counter ions, and $CH_2Cl_2$ (**G5**, **G7**, **G9**, **G11**) as the packing solvent.
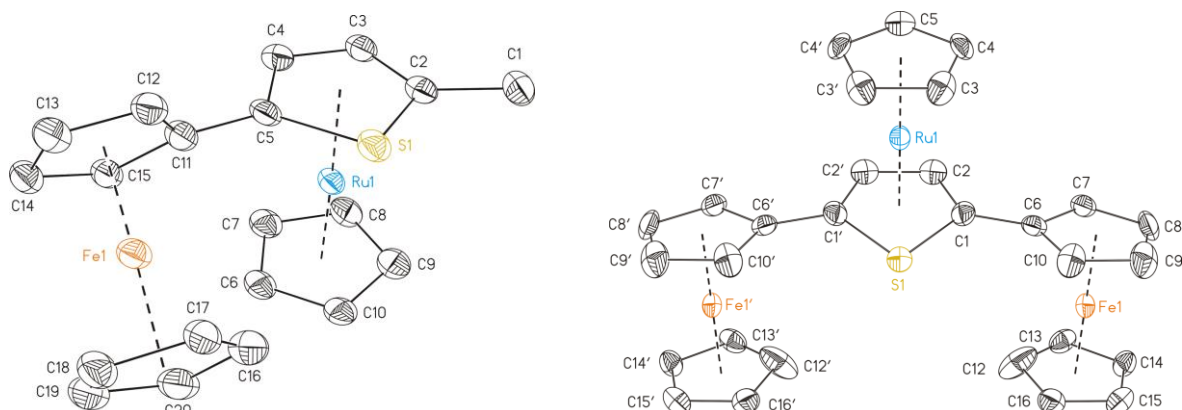


**Figure G2**. ORTEP diagrams (50 % probability level) of the molecular structures of **G3** (left) and **G5** (right) with the atom-numbering scheme. The $PF_6^-$ counter ions, H atoms, solvent molecules (one molecule of $CH_2Cl_2$ in **G5**) and a second molecule of the asymmetric unit in **G5** have been omitted for clarity. (Symmetry operation ('): x, –y+3/2, z).

The cyclopentadienyls of the ferrocenyl backbones adopt ecliptic conformations, *e.g.* 0.4(5) ° (**G5**). For the thia-ruthenocenyl moieties, eclipsed (**G3**, 3.7(12); **G11**, 4.4(2) °) and conformations between eclipsed and staggered (between 14.22(19) ° (9) and 19.3(3) °) are observed for **G3**, **G7** and **G9**. In compound **G5**, mirror planes are present through the sulfur in the thiophene ring, one carbon of the $C_5H_5$ cycles and the Ru atoms, resulting in torsions of 0.00(0) ° or 36.1(3)/36.6(4) °.
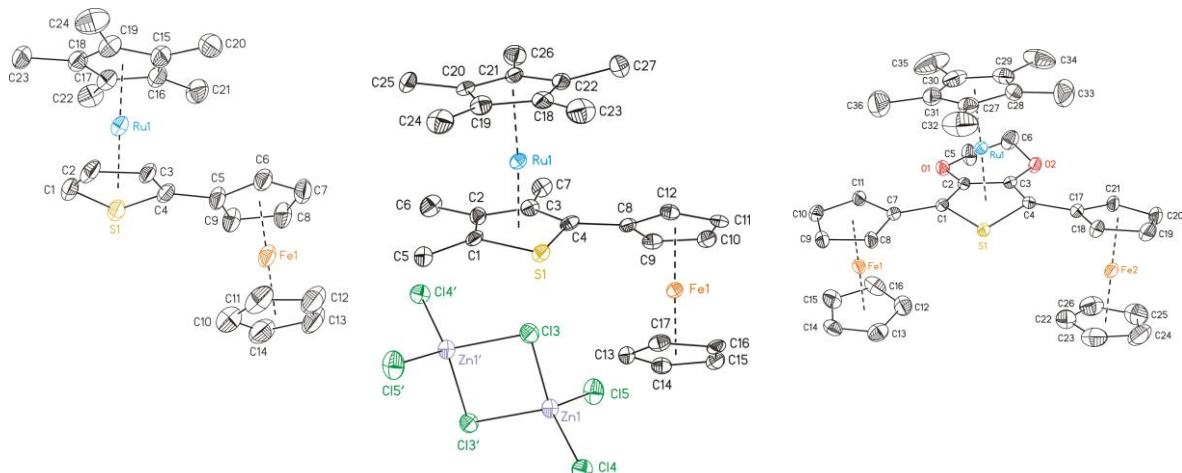


**Figure G3**. ORTEP diagrams (50 % probability level) of the molecular structures of **G7** (left), **G9** (middle) and **G11** (right) with the atom-numbering scheme. $PF_6^-$ counter ions ($PF_6^-$ in **G7** and **G11**), H atoms, $CH_2Cl_2$ solvent molecules (one in **G7**, **G9**; two in **G11**) and a second molecule of the asymmetric unit in **G7** as well as the disordering of the ethylene bridge in **G11** have been omitted for clarity. The $[Zn_2Cl_6]_2^-$ counter ion in **G9** has been completed by using the symmetry operation (') –x+2, –y+2, –z.

Furthermore, in 2,5-diferrocenyl substituted **G5** and **G11** both metallocenyl fragments are oriented *syn* towards each other and are almost coplanar with the thiophene core (**G11**, 1.52(16) – **G5**, 32.52(19) °). Coplanarity between the ferrocenyls and the thiophene cycle is also observed for monoferrocenyl compound **G7**, whereas **G3** and **G9** are twisted by

44.06(15) (**G9**) and 55.0(9)/59.4(9) ° (**G3**). The rotation in **G3** can be explained by a steric interaction of the *syn*-ruthenocenyl fragment, in contrast to an *anti*-arrangement as observed for **G5**, **G7**, **G9** and **G11**.

To the best of our knowledge solid state structure analyses of thia-ruthenocene derivatives are not known in the literature. Nevertheless, an 1,1'-dithia-ruthenocene representative ([Ru($\eta^5$-$C_4(CH_3)_4S$)$_2$][$BF_4$]$_2$) was reported by Lockemeyer *et al.* with Ru-centroid (Ct) distances of 1.819(7)/1.825(7) Å, very similar to those found for ruthenocene itself.[444,445] The corresponding Ru-Ct distances in **G3**, **G5**, **G7**, **G9** and **G11** range between 1.7949(5) (**G7**) and 1.830(5) (**G7**) Å, with a predominantly longer Ru–$C_4S$ compared to the Ru–$C_5$ bonds, except for **G11** and one molecule of **G7** (Table AG-1, Appendix Section).

The Ct–M–Ct (M = Fe, Ru) angles decrease from M = Fe (179.79(6) – 175.2(10) °) to M = Ru (175.60(4) – 171.68(17) °) in each compound. By the complexation of the thiophene to a ruthenium sandwich unit, the $^cC_4S$ C–C single bonds are shortened while enlarged C=C double bonds can be observed, resulting in equal distances. The C–S bonds are enlarged, which can be verified by comparing **G11** (1.765(4), 1.776(4) Å) with its uncomplexed precursor (1.7299(17), 1.7342(17) Å).[271]

The complexation of the $C_4S$ cycle by a metal-containing fragment also has an immense influence on the planarity of the thiophene core, thus, a bending of the sulfur atom out of the dienic $C_4$-plane occurs, in an opposite direction to the complexed metal atom. This can be clarified by a decrease from 0.0428 – 0.0133 of the rms deviations of the planes to 0.0149 – 0, calculated without the sulfur atom (Table AG-1). The shift of the sulfur atom out of the dienic $C_4$-plane reaches 0.175(6) Å in compound **G11**, which reveals a bending of the thiophene of 8.26(5) °. For other uncomplexed thiophenes, *e.g.* 1'-modified 2,5-diferrocenyl thiophenes and 2,5-diferrocenyl ethylenedioxy thiophenes, rms deviations of the $C_4S$ core between 0.0007 – 0.0080 were observed.[271] Heterocycles bearing nitro and amino substituents in the 3,4-position exhibit rms deviations between 0.0038 and 0.0073. Solely an electronic interaction between the lone pairs of two amino nitrogen's distorts the core (rms = 0.0123).[430]

Regarding the complex anion [$Zn_2Cl_6$]$^{2-}$ in compound **G9**, a significant increase of the Zn–Cl distances from the non-bridging chlorides of 2.2112(11) and 2.2079(11) Å to 2.3544(10) and 2.3573(11) Å for the chlorine atoms, involved in the 3-center 4-electron bond. This results in a distortion of the tetrahedral geometry at the Zn atom, clarified by a decrease of the Cl–Zn–Cl angle from 114.26(4) (Cl4–Zn1–Cl5) to 93.25(5) ° (Cl3–Zn1–Cl3'). Intermolecular interactions in the crystal packing are present in compounds **G3** and

**G11** occurring as a *T*-shaped $\pi$-interaction in **G3** (Figure AG-1) or one-dimensional parallel-displaced $\pi$-$\pi$ interactions along the *a*-axis in **G11** (Figure AG-2).

**Electrochemistry**. The electrochemical studies on **G1** – **G11** were carried out under an argon atmosphere on solutions containing $[N^nBu_4][B(C_6F_5)_4]$ (0.1 M) as supporting electrolyte (Experimental Section). The corresponding electrochemical data are presented in Table G1 and the cyclic voltammograms (CV) are shown in Figure G4. Under our conditions, monoferrocenyl compounds **G1** – **G4** and **G7** – **G9** show reversible ferrocenyl-based redox events with small $\varDelta E_p$ values and $i_{pc}/i_{pa}$ ratios close to unity (Table G1, Figure G4).[85,234,235] With regard to 2-ferrocenyl thiophene ($E^{0'}$ = 16 mV *vs.* FcH/FcH$^+$)[253], a successive methylation of the thiophene core leads, as expected, to a decreasing potential for the appropriate Fc/Fc$^+$ redox processes (Table G1).

**Table G1. Cyclic voltammetry data (potentials *vs.* FcH/FcH$^+$) of 1.0 mM solutions of G1 – G11, 2-Fc-C$_4$H$_3$S (C1), 2-Fc-5-CH$_3$-C$_4$H$_2$S, 2,5-Fc$_2$-C$_4$H$_2$S (C3) and 2,5-Fc$_2$-EDOT (E4) measured in dichloromethane containing $[N^nBu_4][B(C_6F_5)_4]$ (0.1 M) as supporting electrolyte at 25 °C.**

| Compd. | $E^{0'}/\Delta E_p$ [mV]$^a$ Wave (no.) (1) | (2) | (3) | $\Delta E^{0'}$ [mV]$^b$ | $K_C$ [10$^3$]$^c$ |
|---|---|---|---|---|---|
| **G1** | –51/64 | - | - | - | - |
| **G2** | –1694$^d$/ - | 420/66 | - | - | - |
| **G3** | –1778$^d$/ - | 402/68 | - | - | - |
| **G4** | –1972$^d$/ - | 411/62 | - | - | - |
| **G5**$^f$ | –1763$^d$/ - | 343$^d$/ - {275/56}$^g$ | 425$^e$/ - {360/54}$^g$ | - {85}$^g$ | - {0.04}$^g$ |
| **G6**$^f$ | –1758$^d$/ - | 313$^d$/ - {246/63}$^g$ | 376$^e$/ - {335/62}$^g$ | - {89}$^g$ | - {0.04}$^g$ |
| **G7** | –2008$^d$/ - | 381/66 | - | - | - |
| **G8** | –2117$^d$/ - | 361/62 | - | - | - |
| **G9** | –2202$^d$/ - | 355/66 | - | - | - |
| **G10**$^f$ | –2024$^d$/ - | 323$^d$/ - {246/56}$^g$ | 422$^e$/ - {344/56}$^g$ | - {98}$^g$ | - {0.06}$^g$ |
| **G11**$^f$ | –2028$^d$/ - | 267$^d$/ - {213/56}$^g$ | 370$^e$/ - {313/56}$^g$ | - {100}$^g$ | - {0.07}$^g$ |
| **2-Fc-C$_4$H$_3$S (C1)** | 16/60$^g$ | - | - | - | - |
| **2-Fc-5-CH$_3$-C$_4$H$_2$S** | –19/62 | - | - | - | - |
| **2,5-Fc$_2$-C$_4$H$_2$S (C3)** | –53/60$^h$ {–8/55}$^{f,g}$ | 195/62$^h$ {165/55}$^{f,g}$ | | 248$^h$ {173}$^{f,g}$ | 15.6$^h$ {1.6}$^{f,g}$ |
| **2,5-Fc$_2$-EDOT (E4)** | –160/64$^h$ {–92/55}$^{f,g}$ | 153/66$^h$ {131/55}$^{f,g}$ | | 313$^h$ {223}$^{f,g}$ | 195.3$^h$ {13.0}$^{f,g}$ |

$^a$ Formal potential ($E^{0'}$). Difference between the oxidation ($E_{pa}$) and reduction ($E_{pc}$) peak potential ($\Delta E_p$).[85,235] $^b$ Redox separation between the formal iron-based redox events ($\Delta E^{0'}$ = $E^{0'}(n)$ – $E^{0'}(n–1)$). $^c$ Comproportionation constant $\left(K_C = e^{\frac{\Delta E^{0'} F}{RT}}\right)$. $^d$ $E_{pc}$. $^e$ $E_{pa}$. $^f$ 0.5 mM analyte. $^g$ Measured in CH$_2$Cl$_2$/CH$_3$CN of ratio 1:1 (*v:v*) at 0 °C. $^h$ Data from ref. 253,271.

Thus a consequent $\alpha$-methylation (2-Fc-5-CH$_3$-C$_4$H$_2$S) results in a 35 mV cathodic shift. For 2-ferrocenyl-3,4,5-trimethylthiophene (**G1**) the corresponding wave was detected at $E^{0'}$ = –51 mV *vs.* FcH/FcH$^+$, similar as observed for the first iron-based redox event of 2,5-diferrocenyl thiophene.[253] In contrast, a large anodic shifting for the ferrocenyl-based

electrode reactions were found when $[Ru(\eta^5\text{-}C_5R_5)]^+$ is formal attached on the thiophene $\pi$-system. For thia-heterobimetallocene **G2** the latter redox process was observed at $E^{0'} = 420$ mV $vs.$ FcH/FcH$^+$, approx. 0.4 V more anodic as reported for 2-Fc-C$_4$H$_3$S itself (Table G1 and Figure G4).[253] Such an anodic shift highlights the electronic interaction between the electron withdrawing Ru-moiety and the ferrocenyl thiophene unit, $i.e.$ at least an indirect Fc-Ru electronic interaction ($vide$ $infra$). Similar observations were reported for other ferrocenyl modified $\eta^6$-arene Ru($\eta^5$-C$_5$H$_5$)/Ru($\eta^5$-C$_5$Me$_5$) systems, in dependency of the distance between the redox centers as well as the nature of interconnecting bridging units.[427,429,432]
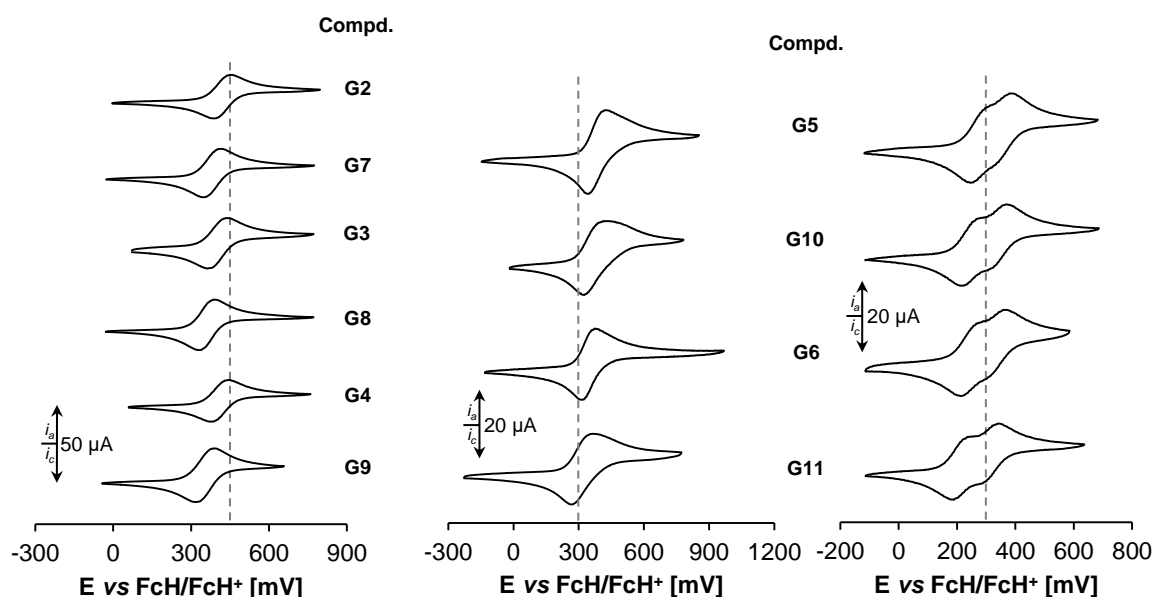


**Figure G4**. Cyclic voltammograms of **G2** – **G11**. Left: 1 mM analyte in dichloromethane at 25 °C. Middle: 0.5 mM analyte in dichloromethane at 25°C. Right: 0.5 mM analyte in a CH$_2$Cl$_2$/CH$_3$CN mixture of ratio 1:1 ($v$:$v$) at 0 °C. Scan rate: 100 mVs$^{-1}$, supporting electrolyte [N$^n$Bu$_4$][B(C$_6$F$_5$)$_4$] (0.1 M).

The latter electrode reaction is very sensitive against electronic modifications on the thiophene $\pi$-system. Thus, by introducing methyl groups on the thiophene building block the appropriate RuCp-reduction was shifted to more cathodic potentials (Table G1). A further cathodic shift of 0.2 to 0.3 V can be forced out by permethylation of the cyclopentadienyl ring in complexes **G7** – **G9** (RuCp*). The accompanying ferrocenyl redox events could be found at ca. 40 mV (**G7** and **G8**) or 55 mV (**G9**) more cathodic, when compared with its RuCp-derivatives (Table G1 and Figure G4). In the case of diferrocenyl complexes **G5**, **G6 G10** and **G11** the current response from the appropriate potential sweep offers formal only an one-electron redox process with an additional anodic current "shoulder" (Figure G4 middle) under comparable experimental conditions. The determined oxidation/ reduction peak currents are proportional to the square root of scan rate (diffusion controlled, $vide$ $supra$).

138

Similar results were obtained within electrochemical studies at lower temperatures (–20 °C) as well as by the use of $[N^n Bu_4][B(C_6H_3(CF_3)_2)_4]$ as supporting electrolyte (Figure G5, left top). Thus, an observation of electrochemically hindered second Fc-based electrode reactions can be assumed. A simulation of cyclic voltammetric data in Figure G5 (left bottom), by varying the heterogenic charge transfer coefficient $\alpha$ as well as the related rate constant $k_s$, represents a qualitative explanation (see also Chapter B, *vide supra*). An addition of small amounts of a polar solvent (MeCN) has no significant influence on the current response (Figure G5 left top, red curve). By the use of larger amounts of more polar propylene carbonate (PC), a clearly "broader" cyclic voltammogram was recorded (Figure G5 left, blue curve).
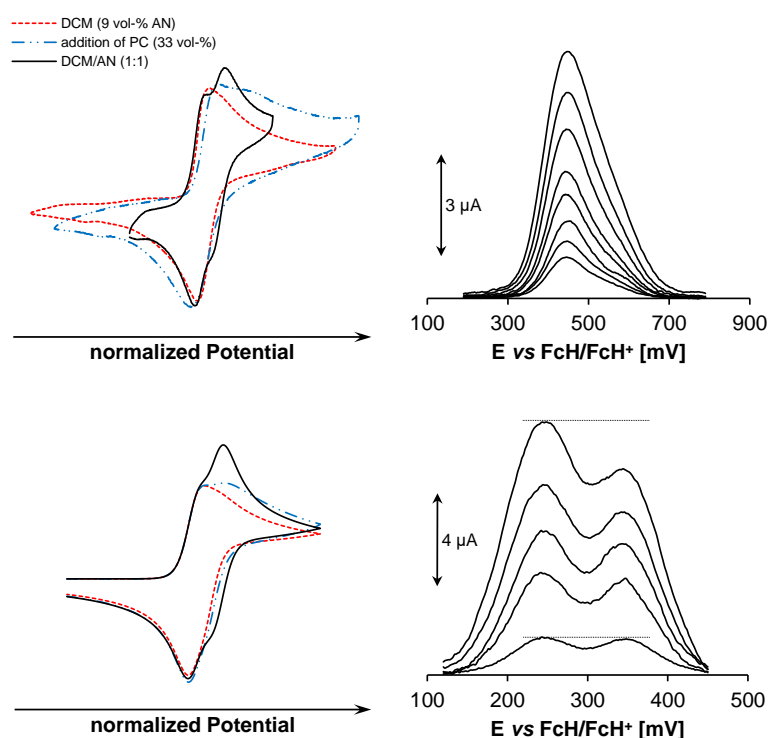


**Figure G5**. Left top: cyclic voltammograms of **G11** in different media, using $[N^n Bu_4][B(C_6H_3(CF_3)_2)_4]$ as supporting electrolyte at 25 °C, scan rate: 100 mVs$^{-1}$. Left bottom: simulated cyclic voltammograms of **G11** at 25 °C ($\Delta E^{0'}$ = 100 mV); 1$^{st}$ redox process: $\alpha$ = 0.5 and $k_s$ = 1 cm/s; 2$^{nd}$ redox process: $\alpha$ = 0.01 and $k_s$ = 0.002 cm/s (red line), $\alpha$ = 0.15 and $k_s$ = 0.003 cm/s (blue line), $\alpha$ = 0.5 and $k_s$ = 1 cm/s (black line). Right top: square wave voltammogram of **G10** (0.5 mM) at different frequencies (0.5, 1, 2, 4, 6.25, 12.5, 25 and 50 Hz) in $CH_2Cl_2$ at 25 °C, supporting electrolyte $[N^n Bu_4][B(C_6F_5)_4]$ (0.1 M). Right bottom: square wave voltammogram of **G10** (0.5 mM) at different frequencies (0.5, 5, 10, 25 and 50 Hz) in a $CH_2Cl_2/CH_3CN$ mixture of ratio 1:1 (*v:v*) at 0 °C, supporting electrolyte $[N^n Bu_4][B(C_6F_5)_4]$ (0.1 M).

No considerable changes were detected by using larger amounts of PC. However, when a dichloromethane/acetonitrile mixture of ratio 1:1 (*v:v*) is applied, two separated and reversible Fc/Fc$^+$ redox events could be observed (Figure G5 left and Figure G4 right).[DD]

---

[DD] An analogous effect could be detected by applying an electrolyte with a stronger coordinating anion (PF$_6^-$) in dichloromethane. Thus for **G10** two poorly resolved Fc/Fc$^+$ redox processes were found ($\Delta E^{0'} \approx$ 75 mV, determined by deconvolution of the corresponding square wave voltammogram) (Figure AG-3, Appendix Section).

Nevertheless, a decomposition of the original complexes (**G5**, **G6**, **G10** and **G11**) as well as their oxidized species was observed under these conditions, yielding the corresponding diferrocenyl thiophene. This issue isn't reported for arene-rutheniumcyclopentadienyls in recent publications, despite electrochemical data measured in acetonitrile-containing solutions.[432] Hence, further electrochemical investigations were carried out at reduced temperatures (0 °C). Moreover, a further qualitative indication for slower heterogenic charge transfer processes during the second Fc/Fc$^+$ electrode reaction represents an increasing current difference by an increasing scan rate (frequencies, Figure G5), during square wave voltammetry experiments.[80,88,250] Thus, for compound **G10** at low frequencies (small currents) two well-separated current peaks with equal heights were found (Figure G5 right). Within increasing the scan rate a successive decreasing of the second peak current relative to the 1$^{st}$ peak can be seen (also pronounced in CH$_2$Cl$_2$ at 25 °C, Figure G5 right).

As results from the electrochemical investigations on diferrocenyl complexes **G5**, **G6**, **G10** and **G11** carried out at 0 °C, the individual two Fc/Fc$^+$ redox processes were observed as shifted towards cathodic potentials as the electron density of thiophene increases together with a decreasing electrophilicity of the ruthenium cyclopentadienyl increment, similar as described for monoferrocenyl complexes (*vide supra*).[429] Thus, the first Fc/Fc$^+$ events of the respective RuCp* derivatives **G6** and **G11** are observed as 30 mV more cathodic shifted as found for **G5** and **G10** (Table G1 and Figure G4). The corresponding redox process of **G10** itself was detected at $E^{0'}$ = 246 mV *vs.* FcH/FcH$^+$, 30 mV more cathodic shifted as for compound **G5**. Moreover, a distinct decrease of the redox separation ($\Delta E^{0'} \approx$ 90 mV for **G5** and **G6**, $\Delta E^{0'} \approx$ 100 mV for **G10** and **G11**) could be observed, due to the electron-withdrawing properties of the Ru-fragments, with regard to 2,5-Fc$_2$-C$_4$H$_2$S ($\Delta E^{0'}$ = 173 mV) and 2,5-Fc$_2$-EDOT ($\Delta E^{0'}$ = 223 mV) (Table G1). Thus, the thermodynamic stability of the appropriate dicationic (mixed-valent) species falls significantly if a transition metal fragment (RuCp/RuCp*) is $\pi$-bonded to the thiophene aromatic core, whereby the nature of the cyclopentadienyl ring should not have a major impact (Table G1 and Figure G4).

For a better understanding of the electronic coupling between the Ru-centers and the ferrocenyl thiophene unit, *in situ* spectroelectrochemical studies on **G1**, **G9** and **G11** were carried out by an stepwise increase of the potential (varying step heights: 5 – 100 mV) *vs.* Ag/AgCl in an OTTLE[238] (= Optically Transparent Thin Layer Electrochemistry) cell using a 0.1 M dichloromethane solution of [N$^n$Bu$_4$][B(C$_6$F$_5$)$_4$] as supporting electrolyte.

**Table G2. NIR data of G1, G9 and G11 measured in CH$_2$Cl$_2$ containing [N$^n$Bu$_4$][B(C$_6$F$_5$)$_4$] (0.1 M) as supporting electrolyte at 25 °C.**

| Compd. | Transition | $\tilde{v}_{max}$ [cm$^{-1}$] ($\varepsilon_{max}$ [Lmol$^{-1}$cm$^{-1}$])$^a$ | $\varDelta\tilde{v}_{1/2}$ [cm$^{-1}$]$^b$ | $\varDelta\tilde{v}_{1/2(theo)}$ [cm$^{-1}$]$^c$ |
|---|---|---|---|---|
| **G1$^+$** | LMCT | 8950 (2370) | 2690$^d$ | |
| | LF | 4400 (180) | 950 | |
| **G9$^+$** | LMCT | 12170 (770) | 2950 | |
| | LF | 3970 (80) | 970 | |
| **G11$^+$** | LMCT | 12260 (710) | 3330 | |
| | IVCT | 7230 (140) | 6420 | 4090 |
| | LF | 4100 (50) | 1100 | |

$^a$ Wavenumber of the bands maximum intensity ($\tilde{v}_{max}$), extinction coefficient at $\tilde{v}_{max}$ ($\varepsilon_{max}$). $^b$ Bandwidth at half height ($\varDelta\tilde{v}_{1/2}$). $^c$ Bandwidth at half height expected from the Hush theory ($\varDelta\tilde{v}_{1/2(theo)} = (2310\tilde{v}_{max})^{1/2}$). $^d$ asymmetric band.

If deconvolution of NIR absorptions was applied, two or three Gaussian-shaped transitions were used to get simulated spectra with an almost exact overlay with the experimental data (Table G2). The corresponding spectra are presented in Figures G6 and G7.

All monocationic thiophene complexes do not display any absorptions in the NIR range. During the oxidation of **G1**, **G9** and **G11** typical absorptions in the UV-Vis (inner ferrocenyl related $\pi$-$\pi^*$ and MLCT/d-d transitions) and NIR region were observed (*vide infra*).[31,239,240,253]
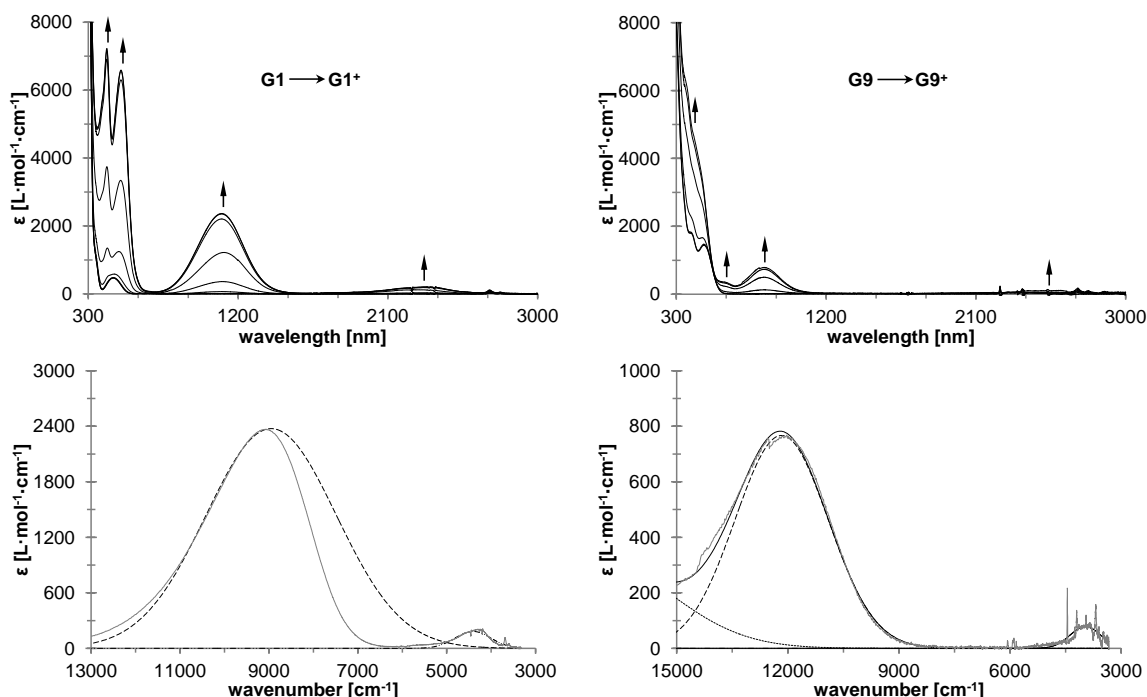


**Figure G6**. Left: UV-Vis-NIR spectra of **G1** at rising potentials (–300 to 550 mV), bottom: deconvolution of NIR absorptions at 550 mV using two distinct overlapping transitions with Gaussian shapes (dashed line indicates LMCT absorptions, dotted-dashed line indicates LF transitions). Right: UV-Vis-NIR spectra of **G9** at rising potentials (–300 to 900 mV), bottom: deconvolution of NIR absorptions at 900 mV using three distinct overlapping transitions with Gaussian shapes (dashed line indicates LMCT absorptions, dotted line corresponds to high-energy absorptions caused by inner-ferrocenium interactions, dotted-dashed line indicates LF transitions). All potentials *vs.* Ag/AgCl, measured in dichloromethane containing [N$^n$Bu$_4$][B(C$_6$F$_5$)$_4$] (0.1 M) as supporting electrolyte at 25 °C. Arrows indicate increasing or decreasing as well as shifting absorptions.

For **G1$^+$** an asymmetric absorption band could be observed in the crossing section between visible- and NIR-range around 9000 cm$^{-1}$ (Figure G6, dashed Gaussian transition for comparison). The higher intensity ($\varepsilon_{max} \approx 2400$ Lmol$^{-1}$cm$^{-1}$) of the latter thiophene-to-ferrocenium ligand metal charge transfer (LMCT), compared to the 2-ferrocenyl thiophene monocation (**C1$^+$**, $\varepsilon_{max} \approx 1300$ Lmol$^{-1}$cm$^{-1}$), has its origin presumably in the reduced ionization potential of the trimethylthienyl moiety and hence a larger donor-acceptor electronic interaction (Table G2, *vide supra*).[31,253] These observations are in good accordance with published results on similar ferrocenyl-functionalized thiophene systems.[31,446] Moreover, an additional observed low-energy NIR absorption at $\tilde{v}_{max} = 4400$ cm$^{-1}$, which is caused by formal forbidden ligand field transitions (LF) of the (partial) oxidized ferrocenyl unit (typical for a 17 valence electron (VE) species), supports this conclusion.[166,210,244,253,319,430] However, a large hypsochromic and hypochromic shifting of the above addressed LMCT absorption could be detected due to coordination on a [Ru($\eta^5$-C$_5$Me$_5$)]$^+$ fragment (formation of **G9$^+$**) (Table G2 and Figure G6). This charge transfer band was, in comparison to **G1$^+$**, detected as almost Gaussian-shaped, which might be a confirmation for the significantly reduced electronic thiophene-ferrocenyl coupling in **G9$^+$** (Table G2 and Figure G6).
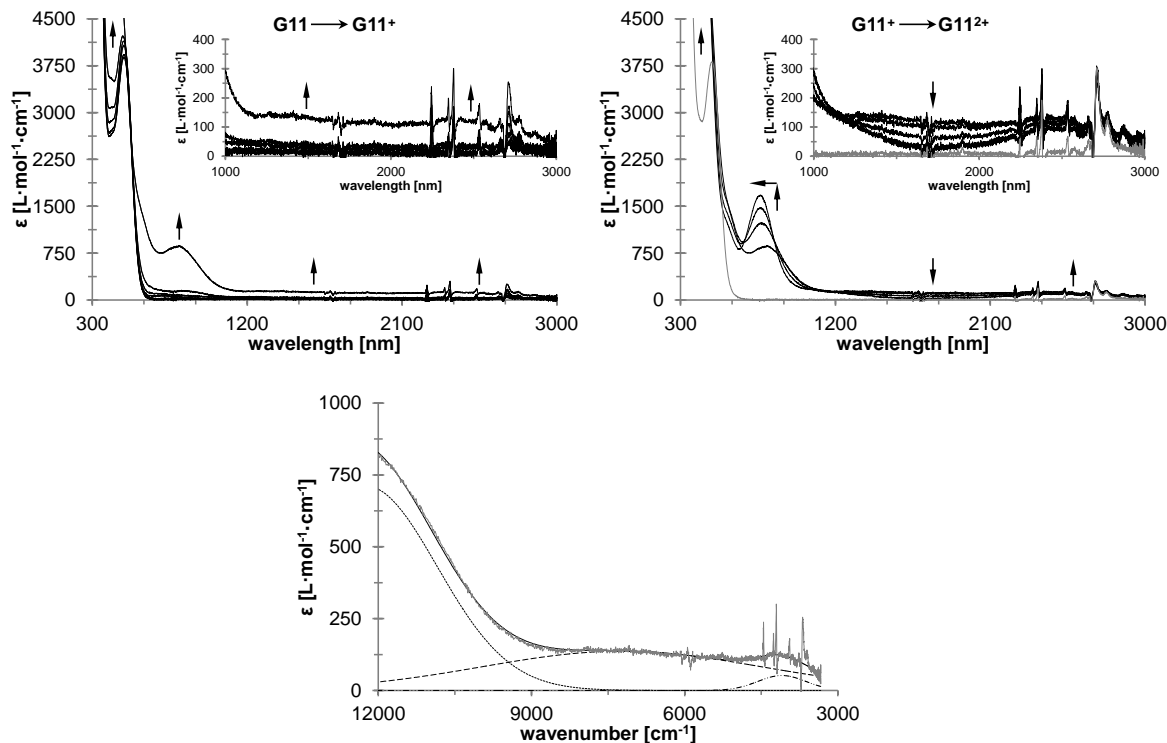


**Figure G7**. UV-Vis-NIR spectra of **G11** at rising potentials. Left: –300 to 700 mV. Right: 700 to 900mV (grey line represents re-reduction to the neutral species). Bottom: deconvolution of NIR absorptions at 700 mV using three distinct overlapping transitions with Gaussian shapes (dashed line indicates IVCT absorption, dotted line corresponds to absorptions caused by interactions between ligand and metal, solid line indicates LF transitions). All potentials *vs.* Ag/AgCl, measured in dichloromethane containing [N$^n$Bu$_4$][B(C$_6$F$_5$)$_4$] (0.1 M) as supporting electrolyte at 25 °C. Arrows indicate increasing or decreasing as well as shifting absorptions.

The smaller extinction coefficient of the related LF transition verifies this conclusion.[49,271,289,319,430]

As exemplary for the diferrocenyl Ru-complexes (*vide supra*), UV-Vis-NIR spectroelectrochemistry was carried out on dichloromethane solutions of ethylenedioxy thiophene derivative **G11**. During the successive oxidation process a very weak and broad NIR IVCT absorption band at around 7200 cm$^{-1}$, which is accompanied by a narrow and also weak ligand field transition, could be detected during the generation of mixed-valent **G11$^+$** (Table F2 and Figure G7). This kind of a NIR absorption behavior is characteristic for very weakly coupled class II systems and verifies the electrochemical results, *i.e.* an IVCT absorption band with a bandwidth at half height ($\Delta\tilde{v}_{1/2}$) more than 1.5 times larger as predicted from the Hush theory ($\Delta\tilde{v}_{1/2(theo)}$), together with an occurrence of such weak ligand field transitions.[49,60,68,166,253,430] Upon generation of tricationic **G11$^{2+}$** a decrease of the absorption near 7200 cm$^{-1}$ (IVCT) was found, in combination with a formal hyperchromic and hypsochromic shift of the ligand to metal charge transfer band around 12000 cm$^{-1}$ (Table G2 and Figure G7).

CONCLUSION

Within this study the synthesis of a series of $\eta^5$-thiophene Ru($\eta^5$-C$_5$H$_5$)/Ru($\eta^5$-C$_5$Me$_5$) complexes on the basis of ferrocenyl-substituted thiophenes is reported with the aim for a better understanding of the influence of $\pi$-thiophene-bonded transition metal moieties onto the thermodynamic stability and charge transfer interactions of the resulting complexes and their oxidized intermediates. The synthesis of the title compounds was carried out in a metathesis reaction procedure using [Ru($\eta^5$-C$_5$H$_5$)(CH$_3$CN)$_3$]PF$_6$ or [Ru($\eta^5$-C$_5$Me$_5$)(CH$_3$CN)$_3$]PF$_6$ and the appropriate ferrocenyl thiophene. The obtained molecules **G1** – **G11** (Figure G1) were identified by elemental analysis, high resolution ESI-TOF mass spectrometry as well as IR and NMR ($^1$H, $^{13}$C{$^1$H}) spectroscopy. As supplementing of the spectroscopic characterization, the first crystal structures for thia-heterooligometallocenes are described. The related molecular structures of **G3**, **G5**, **G7**, **G9**, and **G11** in the solid state reveal a bending of the thiophene core as a consequence of the complexation of [Ru($\eta^5$-C$_5$H$_5$)]$^+$ or [Ru($\eta^5$-C$_5$Me$_5$)]$^+$ respectively.

Within the electrochemical investigations, reversible one-electron and iron-based redox events were found for the mono-ferrocenyl Ru-complexes, whereby the corresponding Fc/Fc$^+$ redox potential increases as the degree of methylation of the thiophene core and the RuCp moiety decreases. Moreover, for diferrocenyl compounds **G5**, **G6**, **G10** and **G11** a

hindered $2^{nd}$ ferrocenyl-based electrode reaction was observed under "weakly-coordinating" conditions. Thus, two well-separated Fc/Fc$^+$ redox events could be detected by the use of "more" solvating solvents or (smaller) anions. With regard to the uncomplexed diferrocenyl thiophenes, the thermodynamic stability of the appropriate mixed-valent species decreases clearly when a [RuCp]$^+$/[RuCp*]$^+$ fragment is bonded on the thiophene aromatic system, whereby the nature of the cyclopentadienyl ring should not have a major impact. The related decrease of electronic coupling between the ferrocenyl units and the thiophene in the corresponding oxidized states could be verified during UV-Vis-NIR spectroelectrochemical measurements.

EXPERIMENTAL SECTION

**General Procedures**. All reactions were carried out under an atmosphere of argon using standard Schlenk techniques. Tetrahydrofuran was purified by distillation from sodium/benzophenone ketyl. Toluene, *n*-hexane and diethyl ether were purified with a MBRAUN SPS-800 purification system. Dichloromethane and 1,2-dichloropropane were purified by distillation from CaH$_2$. For electrochemical usage acetonitrile (analytical grade, Acros Organics) and dichloromethane were stored over molecular sieve (4 Å).

**Reagents.** 2-Ferrocenyl thiophene[226,253] could be synthesized within a Suzuki-Miyaura reaction of ferroceneboronic acid[247,322,430] and 1 eq of 2-bromo thiophene in dioxane (90 °C, 12 h, yield: 71 %), using Pd(dppf)Cl$_2$ (2 mol-%) and [$^n$Bu$_4$N]OH (aq.). 2-Ferrocenyl-5-methyl thiophene[447] was prepared by treating 2-ferrocenyl thiophene with 1.1 eq of $^n$BuLi (1.6 M, hexane) in tetrahydrofuran (–80 °C, 45 min) followed by an addition of methyl iodide (1.5 eq), the crude product was purified throughout filtration over alumina with *n*-hexane (yield: 95 % based on 2-ferrocenyl thiophene). Tetra-*n*-butylammonium tetrakis(pentafluorophenyl)borate was prepared by metathesis of lithium tetrakis(pentafluorophenyl)borate etherate (Boulder Scientific) with tetra-*n*-butylammonium bromide, according to a published procedure.[101] It was enhanced by a filtration step of the crude product through a pad of silica using dichloromethane as solvent. All other chemicals were synthesized according to published procedures or purchased from commercial suppliers and used as received.

**Instruments.** Infrared spectra were recorded with a Thermo Nicolet 200 FT-IR spectrometer using KBr press techniques for sample preparation. NMR spectra were recorded using an Bruker Avance III 500 FT-NMR spectrometer ($^1$H NMR at 500.303

MHz, $^{13}C\{^1H\}$ NMR at 125.813 MHz) at ambient temperature, unless otherwise noted. Chemical shifts ($\delta$) are reported in parts per million (ppm) relative to tetramethylsilane using the solvent as internal reference (CDCl$_3$: $^1H$ NMR $\delta$ = 7.26 ppm, $^{13}C\{^1H\}$ NMR $\delta$ = 77.16 ppm; acetone-$D_6$ (CH$_3$): $^1H$ NMR $\delta$ = 2.05 ppm, $^{13}C\{^1H\}$ NMR $\delta$ = 29.84 ppm)[246]. Coupling constants ($J$) are reported in Hertz (Hz) and integrations are reported in number of protons. The following abbreviations are used to describe peak patterns: s = singlet, d = doublet, dd = doublet of doublets, pt = pseudotriplet, m = multiplet. Resonance assignments were made using HSQC and HMBC NMR experiments. The melting points were determined using a Gallenkamp MFB 595 010 M melting point apparatus. Microanalyses were performed with a Thermo FLASHEA 1112 Series instrument. High resolution mass spectra were recorded with a Bruker micrOTOF QII with an Apollo II ESI-source.

**Synthesis of 2-ferrocenyl-3,4,5-trimethylthiophene (G1)**. Ferrocene (2.53 g, 13.6 mmol) and 0.125 eq of KO$^t$Bu (191 mg) were dissolved in 50 mL of tetrahydrofuran. The resulting solution was cooled to –90 °C and was then treated with 2 eq (14.3 mL) of a 1.9 M *tert*-butyllithium solution (*n*-pentane) within 5 min. After 60 min of isothermal stirring, one eq (3.81 g) of [ZnCl$_2$·2thf] was added in a single portion and the obtained reaction mixture was stirred at 0 °C for 30 min. Afterwards, 0.57 eq (1.59 g) of 2-bromo-3,4,5-trimethylthiophene[442,443] and 33.5 µmol (23 mg) of [Pd(CH$_2$CMe$_2$P$^t$Bu$_2$)(µ-Cl)]$_2$[229,230] were added to the reaction mixture. This reaction mixture was stirred at 55 °C for 18 h. After cooling to ambient temperature, the reaction mixture was hydrolyzed with water, the organic layer was separated and the aqueous phase was extracted exhaustively with diethyl ether. The combined organic phases were dried over MgSO$_4$ and the resulting crude product was adsorbed on silica and purified by column chromatography (column size: 20 x 3 cm, silica) using *n*-hexane as eluent. Thiophene **G1** was obtained as bright orange solid. Yield: 1.05 g (3.38 mmol, 44 % based on 2-bromo-3,4,5-trimethylthiophene). Anal. Calcd. for C$_{17}$H$_{18}$FeS (310.2 gmol$^{-1}$): C, 65.82; H, 5.85. Found; C, 65.82; H, 5.82. Mp.: 129 °C. IR data (KBr) [cm$^{-1}$]: 3101 w, 3083 w, 2935 w, 2854 w, 1443 m, 1412 w, 1106 s, 1002 m, 823 s, 809 s, 549 m, 504 s. $^1H$ NMR (CDCl$_3$)[$\delta$]: 4.45 (pt, $J_{HH}$ = 1.9 Hz, 2H, C$_5$H$_4$), 4.24 (pt, $J_{HH}$ = 1.9 Hz, 2H, C$_5$H$_4$), 4.17 (s, 5H, C$_5$H$_5$), 2.31 (m, 3H, CH$_3$), 2.11 (s, 3H, CH$_3$), 2.01 (m, 3H, CH$_3$). $^{13}C\{^1H\}$ NMR (CDCl$_3$)[$\delta$]: 133.8 (C$_i$-C$_4$S), 133.8 (C$_i$-C$_4$S), 131.6 (C$_i$-C$_4$S), 129.7 (C$_i$-C$_4$S), 81.6 (C$_i$-C$_5$H$_4$), 69.8 (C$_5$H$_5$), 69.0 (C$_5$H$_4$), 68.0 (C$_5$H$_4$), 14.2 (CH$_3$), 13.4 (CH$_3$), 12.8 (CH$_3$). HR-ESI MS (calc) [m/z]: 310.0459 (310.0473) [M]$^+$.

**General procedure for the synthesis of [CpRu($\eta^5$-ferrocenyl thiophene)]PF$_6$ (G2 – G6)**. A solution of [CpRu(CH$_3$CN)$_3$]PF$_6$[440] in 5 mL of 1,2-dichloropropane was treated with the corresponding ferrocenyl thiophene dissolved in 1,2-dichloropropane (5 mL). The resulting reaction mixture was warmed to 90 °C for 12 h. After cooling to ambient temperature, 100 mL of *n*-hexane were added, the supernatant solution was removed and the remaining residue was washed with *n*-hexane or diethyl ether until the solution becomes colorless. The crude product was filtered with dichloromethane through a pad of celite and finally crystallized as described below (*vide infra*).

**[CpRu($\eta^5$-2-Fc-C$_4$H$_3$S)]PF$_6$ (G2)**: [CpRu(CH$_3$CN)$_3$]PF$_6$[440] (100 mg, 0.23 mmol), 1 eq of 2-ferrocenyl thiophene[226,253] (62 mg). Compound **G2** was crystallized by diffusion of *n*-hexane into a dichloromethane solution at –35 °C affording a red-orange solid. Yield: 108 mg (0.19 mmol, 81 %). Anal. Calcd. for C$_{19}$H$_{17}$F$_6$FePRuS (579.3 gmol$^{-1}$): C, 39.39; H, 2.96. Found; C, 39.35; H, 3.10. Mp.: 107 °C. IR data (KBr) [cm$^{-1}$]: 3111 w, 3100 w, 3081 w, 1506 m, 1413 w, 1105 m, 1010 w, 843 s, 823 s, 809 s, 557 s, 505 m. $^1$H NMR (CDCl$_3$)[$\delta$]: 6.45 (dd, $J_{HH}$ = 3.2 Hz, 0.5 Hz, 1H, C$_4$H$_3$S), 6.31 (pt, $J_{HH}$ = 3.1 Hz, 1H, C$_4$H$_3$S), 6.14 (dd, $J_{HH}$ = 3.0 Hz, 0.5 Hz, 1H, C$_4$H$_3$S), 5.29 (s, 5H, Ru($\eta^5$-C$_5$H$_5$)), 4.62 (m, 1H, C$_5$H$_4$), 4.42 (m, 1H, C$_5$H$_4$), 4.40 (m, 1H, C$_5$H$_4$), 4.36 (m, 1H, C$_5$H$_4$), 4.18 (s, 5H, C$_5$H$_5$). $^{13}$C{$^1$H} NMR (CDCl$_3$)[$\delta$]: 102.9 (C$_i$-C$_4$H$_3$S), 86.1 (C$_4$H$_3$S), 83.3 (C$_4$H$_3$S), 81.1 (Ru($\eta^5$-C$_5$H$_5$)), 76.8 (C$_4$H$_3$S), 74.4 (C$_i$-C$_5$H$_4$), 71.0 (C$_5$H$_4$), 71.0 (C$_5$H$_4$), 70.9 (C$_5$H$_5$), 69.6 (C$_5$H$_4$), 68.9 (C$_5$H$_4$). HR-ESI MS (calc) [m/z]: 434.9494 (434.9445) [CpRu($\eta^5$-2-Fc-C$_4$H$_3$S)]$^+$.

**[CpRu($\eta^5$-2-Fc-5-CH$_3$-C$_4$H$_2$S)]PF$_6$ (G3)**: [CpRu(CH$_3$CN)$_3$]PF$_6$[440] (290 mg, 0.67 mmol), 1.06 eq 2-ferrocenyl-5-methyl thiophene[447] (200 mg). Compound **G3** was crystallized from dichloromethane/diethyl ether (1:1, v:v) at –35 °C affording an orange solid. Yield: 297 mg (0.50 mmol, 75 % based on [CpRu(CH$_3$CN)$_3$]PF$_6$). Anal. Calcd. for C$_{20}$H$_{19}$F$_6$FePRuS (593.3 gmol$^{-1}$): C, 40.49; H, 3.23. Found; C, 40.24; H, 3.30. Mp.: 145 °C. IR data (KBr) [cm$^{-1}$]: 3102 m, 2926 w, 1555 s, 1507 w, 1413 m, 1167 m, 1109 m, 1002 m, 852 s, 836 s, 824 s, 557 s. $^1$H NMR (CDCl$_3$)[$\delta$]: 6.34 (m, 1H, C$_4$H$_2$S), 6.26 (m, 1H, C$_4$H$_2$S), 5.24 (s, 5H, Ru($\eta^5$-C$_5$H$_5$)), 4.58 (m, 1H, C$_5$H$_4$), 4.38 (m, 1H, C$_5$H$_4$), 4.37 (m, 1H, C$_5$H$_4$), 4.32 (m, 1H, C$_5$H$_4$), 4.19 (s, 5H, C$_5$H$_5$), 2.39 (s, 3H, CH$_3$). $^{13}$C{$^1$H} NMR (CDCl$_3$)[$\delta$]: 101.7 (C$_i$-C$_4$H$_2$S), 96.7 (C$_i$-C$_4$H$_2$S), 86.8 (C$_4$H$_2$S), 83.5 (C$_4$H$_2$S), 81.2 (Ru($\eta^5$-C$_5$H$_5$)), 74.8 (C$_i$-C$_5$H$_4$), 70.8 (C$_5$H$_4$), 70.8 (C$_5$H$_4$), 70.8 (C$_5$H$_5$), 69.5 (C$_5$H$_4$), 68.9 (C$_5$H$_4$), 16.0 (CH$_3$). HR-ESI MS (calc) [m/z]: 448.9649 (448.9601) [CpRu($\eta^5$-2-Fc-5-CH$_3$-C$_4$H$_2$S)]$^+$.

**Crystal data for G3**: $C_{20}H_{19}F_6FePRuS$, $M_r$ = 593.3 g·mol$^{-1}$, monoclinic, $P$–1, $\lambda$ = 1.54184 Å, $a$ = 10.4886(6) Å, $b$ = 11.3604(7) Å, $c$ = 17.1022(12) Å, $\alpha$ = 88.858(5)° , $\beta$ = 83.887(5)°, $\gamma$ = 88.039(5)°, $V$ = 2024.8(2) Å$^3$, Z = 4, $\rho_{calcd}$ = 1.946 g·cm$^{-3}$, $\mu$ = 14.055 mm$^{-1}$, $T$ = 110.00(10) K, $\Theta$ range = 3.8940 – 64.991 °, reflections collected: 12435, independent: 6850 ($R_{int}$ = 0.0619), $R_1$ = 0.1559, w$R_2$ = 0.4167 [$I$> 2$\sigma(I)$].

**[CpRu($\eta^5$-2-Fc-3,4,5-(CH₃)₃-C₄S)]PF₆  (G4)**:  [CpRu(CH₃CN)₃]PF₆[440] (74 mg, 0.17 mmol), 1 eq **G1** (53 mg). Compound **G4** was crystallized from dichloromethane/diethyl ether (1:1, v:v) at –35 °C as an orange solid. Yield: 96 mg (0.15 mmol, 90 %). Anal. Calcd. for $C_{22}H_{23}F_6FePRuS$ (621.4 gmol$^{-1}$): C, 42.53; H, 3.73. Found; C, 42.22; H, 3.55. Mp.: 159 °C. IR data (KBr) [cm$^{-1}$]: 3126 w, 2968 w, 2926 w, 1413 w, 1369 w, 1107 m, 1030 w, 1001 w, 841 s, 825 s, 558 s. $^1$H NMR (CDCl₃)[$\delta$]: 5.18 (s, 5H, Ru($\eta^5$-C₅H₅)), 4.50 (m, 1H, C₅H₄), 4.37 (m, 2H, C₅H₄), 4.27 (m, 1H, C₅H₄), 4.27 (s, 5H, C₅H₅), 2.35 (s, 3H, CH₃), 2.35 (s, 3H, CH₃), 2.24 (s, 3H, CH₃). $^{13}$C{$^1$H} NMR (CDCl₃)[$\delta$]: 103.4 ($C_i$-C₄S), 102.9 ($C_i$-C₄S), 99.1 ($C_i$-C₄S), 94.2 ($C_i$-C₄S), 81.5 (Ru($\eta^5$-C₅H₅)), 75.1 ($C_i$-C₅H₄), 72.7 (C₅H₄), 72.0 (C₅H₄), 70.6 (C₅H₄), 70.4 (C₅H₅), 70.1 (C₅H₄), 14.6 (CH₃), 14.5 (CH₃), 13.7 (CH₃). HR-ESI MS (calc) [m/z]: 476.9937 (476.9915) [CpRu($\eta^5$-2-Fc-3,4,5-(CH₃)₃-C₄S)]$^+$.

**[CpRu($\eta^5$-2,5-Fc₂-C₄H₂S)]PF₆ (G5)**: [CpRu(CH₃CN)₃]PF₆[440] (600 mg, 1.38 mmol) in 10 mL of 1,2-dichloropropane, 0.8 eq of 2,5-diferrocenyl thiophene[167,253] (2,5-Fc₂-C₄H₂S) (500 mg) in 15 mL 1,2-dichloropropane. Compound **G5** was crystallized from dichloromethane/ diethyl ether (2:1, v:v) at –35 °C as a red solid. Yield: 320 mg (0.42 mmol, 38 % based on 2,5-diferrocenyl thiophene). Anal. Calcd. for $C_{29}H_{25}F_6Fe_2PRuS$ (763.3 gmol$^{-1}$): C, 45.63; H, 3.30. Found; C, 45.61; H, 3.38. Mp.: 206 °C. IR data (KBr) [cm$^{-1}$]: 3104 w, 1499 m, 1415 w, 1269 w, 1106 m, 1102 w, 851 s, 825 s, 558 s, 511 m. $^1$H NMR (CDCl₃)[$\delta$]: 6.56 (s, 2H, C₄H₂S), 5.16 (s, 5H, Ru($\eta^5$-C₅H₅)), 4.64 (m, 2H, C₅H₄), 4.42 (m, 2H, C₅H₄), 4.41 (m, 2H, C₅H₄), 4.39 (m, 2H, C₅H₄), 4.22 (s, 10H, C₅H₅). $^{13}$C{$^1$H} NMR (CDCl₃)[$\delta$]: 100.6 ($C_i$-C₄H₂S), 83.7 (C₄H₂S), 81.4 (Ru($\eta^5$-C₅H₅)), 74.8 ($C_i$-C₅H₄), 71.0 (C₅H₄), 71.0 (C₅H₄), 70.8 (C₅H₅), 69.6 (C₅H₄), 68.7 (C₅H₄). HR-ESI MS (calc) [m/z]: 618.9503 (618.9424) [CpRu($\eta^5$-2,5-Fc₂-C₄H₂S)]$^+$.

**Crystal data for G5**: $C_{29}H_{25}F_6Fe_2PRuS$·1/3(CH₂Cl₂), $M_r$ = 791.6 g·mol$^{-1}$, monoclinic, $P2_1/m$, $\lambda$ = 1.54184 Å, $a$ = 12.5542(5) Å, $b$ = 18.1037(5) Å, $c$ = 19.0147(7) Å, $\beta$ = 1006.157(4) °, $V$ = 4150.9(3) Å$^3$, Z = 6, $\rho_{calcd}$ = 1.900 g·cm$^{-3}$, $\mu$ = 15.055 mm$^{-1}$, $T$ = 104.9(3) K, $\Theta$ range = 3.437 – 65.841 °, reflections collected: 16756, independent: 7305 ($R_{int}$ = 0.0424), $R_1$ = 0.0604, w$R_2$ = 0.1596 [$I$> 2$\sigma(I)$].

**[CpRu($\eta^5$-2,5-Fc$_2$-EDOT)]PF$_6$ (G6)**: [CpRu(CH$_3$CN)$_3$]PF$_6$[440] (106 mg, 0.24 mmol), 1 eq of 2,5-diferrocenyl-3,4-ethylenedioxy thiophene[271] (2,5-Fc$_2$-EDOT) (125 mg). Compound **G6** was crystallized by diffusion of *n*-hexane into a dichloromethane solution at –35 °C as a red solid. Yield: 142 mg (0.17 mmol, 71 %). Anal. Calcd. for C$_{31}$H$_{27}$F$_6$Fe$_2$O$_2$PRuS (821.3 gmol$^{-1}$): C, 45.33; H, 3.31. Found; C, 45.16; H, 3.35. Mp.: 235 °C (dec.). IR data (KBr) [cm$^{-1}$]: 3117 w, 3104 w, 2990 w, 2965 w, 1517 w, 1474 m, 1372 m, 1070 m, 852 s, 831 s, 558 s, 504 m. $^1$H NMR (acetone-*D$_6$*)[$\delta$]: 5.51 (s, 5H, Ru($\eta^5$-C$_5$H$_5$)), 4.81 (m, 2H, C$_5$H$_4$), 4.73 (m, 2H, OCH$_2$CH$_2$O) 4.62 (m, 2H, C$_5$H$_4$), 4.53 (m, 2H, OCH$_2$CH$_2$O) 4.50 (m, 2H, C$_5$H$_4$), 4.48 (m, 2H, C$_5$H$_4$), 4.34 (s, 10H, C$_5$H$_5$). $^{13}$C{$^1$H} NMR (acetone-*D$_6$*)[$\delta$]: 121.4 (C$_i$-C$_4$S), 84.2 (C$_i$-C$_4$S), 82.5 (Ru($\eta^5$-C$_5$H$_5$)), 74.5 (C$_i$-C$_5$H$_4$), 71.6 (C$_5$H$_4$), 71.3 (C$_5$H$_4$), 71.1 (C$_5$H$_5$), 71.1 (C$_5$H$_4$), 71.0 (C$_5$H$_4$), 66.8 (OCH$_2$CH$_2$O). HR-ESI MS (calc) [m/z]: 676.9494 (676.9480) [CpRu($\eta^5$-2,5-Fc$_2$-EDOT)]$^+$.

**General procedure for the synthesis of [Cp\*Ru($\eta^5$-ferrocenyl thiophene)]PF$_6$ (G7 – G11)**. [Cp\*Ru(CH$_3$CN)$_3$]PF$_6$[441] was dissolved in 5 mL of dichloromethane and the thus obtained solution was treated with the corresponding ferrocenyl thiophene dissolved in dichloromethane (10 mL). The resulting reaction mixture was warmed to 50 °C for 12 h. After cooling it to ambient temperature, 100 mL *n*-hexane were added, the supernatant solution was removed and the remaining residue was washed with *n*-hexane until the solution becomes colorless. The crude product was filtered through a pad of celite, using dichloromethane, and crystallized finally as described below (*vide infra*).

**[Cp\*Ru($\eta^5$-2-Fc-C$_4$H$_3$S)]PF$_6$ (G7)**: [Cp\*Ru(CH$_3$CN)$_3$]PF$_6$[441] (100 mg, 0.20 mmol), 1 eq of 2-ferrocenyl thiophene[226,253] (53 mg). Compound **G7** was crystallized from dichloromethane/*n*-hexane (2:1, v:v) at –35 °C as an orange solid. Yield: 122 mg (0.19 mmol, 95 %). Anal. Calcd. for C$_{24}$H$_{27}$F$_6$FePRuS (649.4 gmol$^{-1}$): C, 44.39; H, 4.19. Found; C, 44.49; H, 4.42. Mp.: 185 °C. IR data (KBr) [cm$^{-1}$]: 3109 w, 2971 w, 2910 w, 1507 w 1474 w, 1387 w, 1032 w, 840 s, 558 m, 506 w. $^1$H NMR (CDCl$_3$)[$\delta$]: 5.98 (m, 2H, C$_4$H$_3$S), 5.93 (dd, $J_{HH}$ = 2.8 Hz, 0.7 Hz, 1H, C$_4$H$_3$S), 4.62 (m, 1H, C$_5$H$_4$), 4.44 (m, 1H, C$_5$H$_4$), 4.42 (m, 1H, C$_5$H$_4$), 4.21 (m, 1H, C$_5$H$_4$), 4.14 (s, 5H, C$_5$H$_5$), 1.82 (s, 15H, RuCp\*). $^{13}$C{$^1$H} NMR (CDCl$_3$)[$\delta$]: 100.1 (C$_i$-C$_4$H$_3$S), 96.2 (C$_i$-RuCp\*), 88.3 (C$_4$H$_3$S), 83.8 (C$_4$H$_3$S), 77.4 (C$_4$H$_3$S), 73.8 (C$_i$-C$_5$H$_4$), 70.9 (C$_5$H$_4$), 70.8 (C$_5$H$_5$), 70.7 (C$_5$H$_4$), 67.6 (C$_5$H$_4$), 66.7 (C$_5$H$_4$), 10.8 (C$_H$-RuCp). HR-ESI MS (calc) [m/z]: 505.0289 (505.0229) [Cp\*Ru($\eta^5$-2-Fc-C$_4$H$_3$S)]$^+$.

**Crystal data for G7**: C$_{24}$H$_{27}$F$_6$FePRuS·1/2(CH$_2$Cl$_2$), M$_r$ = 691.9 g·mol$^{-1}$, monoclinic, P–1, $\lambda$ = 0.71073 Å, *a* = 10.9251(12) Å, *b* = 13.0127(6) Å, *c* = 19.4261(8) Å, $\alpha$ = 99.898(4)° ,

$\beta$ = 105.238(3)°, $\gamma$ = 91.142(3)°, $V$ = 2618.79(19) Å$^3$, Z = 4, $\rho_{calcd}$ = 1.755 g·cm$^{-3}$, $\mu$ = 1.429 mm$^{-1}$, $T$ = 110(2) K, $\Theta$ range = 2.953 – 25.999 °, reflections collected: 29564, independent: 10255 ($R_{int}$ = 0.0731), $R_1$ = 0.0568, w$R_2$ = 0.1347 [$I > 2\sigma(I)$].

**[Cp\*Ru($\eta^5$-2-Fc-5-CH$_3$-C$_4$H$_2$S)]PF$_6$ (G8)**: [Cp\*Ru(CH$_3$CN)$_3$]PF$_6$[441] (72 mg, 0.14 mmol), 1 eq of 2-ferrocenyl-5-methyl thiophene[447] (40 mg). Compound **G8** was crystallized from dichloromethane/$n$-hexane (2:1, v:v) at –35 °C as an orange solid. Yield: 87 mg (0.13 mmol, 92 %). Anal. Calcd. for C$_{25}$H$_{29}$F$_6$FePRuS (663.4 gmol$^{-1}$): C, 45.26; H, 4.41. Found; C, 45.12; H, 4.55. Mp.: 196 °C. IR data (KBr) [cm$^{-1}$]: 3112 w, 2965 w, 2915 w, 1507 w, 1476 w, 1458 w, 1390 m, 1106 m, 1032 m, 839 s, 558 s. $^1$H NMR (CDCl$_3$)[$\delta$]: 5.93 (d, $J_{HH}$ = 3.2 Hz, 1H, C$_4$H$_2$S), 5.83 (d, $J_{HH}$ = 3.2 Hz, 1H, C$_4$H$_2$S), 4.61 (m, 1H, C$_5$H$_4$), 4.41 (m, 2H, C$_5$H$_4$), 4.16 (m, 1H, C$_5$H$_4$), 4.16 (s, 5H, C$_5$H$_5$), 2.22 (s, 3H, CH$_3$), 1.78 (s, 15H, RuCp\*). $^{13}$C{$^1$H} NMR (CDCl$_3$)[$\delta$]: 100.0 (C$_i$-C$_4$H$_2$S), 95.5 (C$_i$-RuCp\*), 94.2 (C$_i$-C$_4$H$_2$S), 89.3 (C$_4$H$_2$S), 84.6 (C$_4$H$_2$S), 74.1 (C$_i$-C$_5$H$_4$), 70.8 (C$_5$H$_5$), 70.7 (C$_5$H$_4$), 70.7 (C$_5$H$_4$), 67.5 (C$_5$H$_4$), 66.5 (C$_5$H$_4$), 14.2 (CH$_3$), 10.6 (C$_H$-RuCp). HR-ESI MS (calc) [m/z]: 519.0437 (519.0385) [Cp\*Ru($\eta^5$-2-Fc-5-CH$_3$-C$_4$H$_2$S)]$^+$.

**[Cp\*Ru($\eta^5$-2-Fc-3,4,5-(CH$_3$)$_3$-C$_4$S)]PF$_6$ (G9)**: [Cp\*Ru(CH$_3$CN)$_3$]PF$_6$[441] (70 mg, 0.14 mmol), 1 eq of **G1** (45 mg). Compound **G9** was crystallized from dichloromethane/$n$-hexane (2:1, v:v) at –35 °C as an orange solid. Yield: 83 mg (0.12 mmol, 86 %). Anal. Calcd. for C$_{27}$H$_{33}$F$_6$FePRuS (691.5 gmol$^{-1}$): C, 46.90; H, 4.81. Found; C, 47.12; H, 5.04. Mp.: 230 °C (dec.). IR data (KBr) [cm$^{-1}$]: 3114 w, 3091 w, 2961 w, 2921 w, 2864 w, 1498 w, 1474 w, 1386 m, 1271 w, 1105 m, 1029 m, 839 s, 558 s, 508 w. $^1$H NMR (CDCl$_3$)[$\delta$]: 4.59 (m, 1H, C$_5$H$_4$), 4.40 (m, 1H, C$_5$H$_4$), 4.37 (m, 1H, C$_5$H$_4$), 4.25 (m, 1H, C$_5$H$_4$), 4.21 (s, 5H, C$_5$H$_5$), 2.13 (s, 3H, CH$_3$), 2.12 (s, 3H, CH$_3$), 2.06 (s, 3H, CH$_3$), 1.71 (s, 15H, RuCp\*). $^{13}$C{$^1$H} NMR (CDCl$_3$)[$\delta$]: 101.5 (C$_i$-C$_4$S), 98.8 (C$_i$-C$_4$S), 98.4 (C$_i$-C$_4$S), 93.9 (C$_i$-RuCp\*), 92.4 (C$_i$-C$_4$S), 74.7 (C$_i$-C$_5$H$_4$), 70.8 (C$_5$H$_5$), 70.3 (C$_5$H$_4$), 70.0 (C$_5$H$_4$), 69.2 (C$_5$H$_4$), 68.7 (C$_5$H$_4$), 12.7 (CH$_3$), 12.5 (CH$_3$), 10.9 (CH$_3$), 10.1 (C$_H$-RuCp\*). HR-ESI MS (calc) [m/z]: 547.0685 (547.0699) [Cp\*Ru($\eta^5$-2-Fc-3,4,5-(CH$_3$)$_3$-C$_4$S)]$^+$.

**Crystal data for G9**: C$_{28}$H$_{35}$Cl$_5$FeRuSZn, $M_r$ = 803.16 g·mol$^{-1}$, monoclinic, $P$–1, $\lambda$ = 0.71073 Å, $a$ = 10.1842(5) Å, $b$ = 11.8628(5) Å, $c$ = 13.2955(6) Å, $\alpha$ = 81.054(4)° , $\beta$ = 75.337(4)°, $\gamma$ = 87.205(4)°, $V$ = 1534.98(13) Å$^3$, Z = 2, $\rho_{calcd}$ = 1.738 g·cm$^{-3}$, $\mu$ = 2.248 mm$^{-1}$, $T$ = 110.05(10) K, $\Theta$ range = 3.018 – 25.998 °, reflections collected: 10701, independent: 5997 ($R_{int}$ = 0.0382), $R_1$ = 0.0391, w$R_2$ = 0.0775 [$I > 2\sigma(I)$].

**[Cp\*Ru($\eta^5$-2,5-Fc$_2$-C$_4$H$_2$S)]PF$_6$ (G10)**: [Cp\*Ru(CH$_3$CN)$_3$]PF$_6$[441] (112 mg, 0.22 mmol), 1 eq of 2,5-diferrocenyl thiophene[167,253] (100 mg). Compound **G10** was crystallized from dichloromethane/*n*-hexane (2:1, v:v) at –35 °C as a red solid. Yield: 164 mg (0.20 mmol, 89 %). Anal. Calcd. for C$_{34}$H$_{35}$F$_6$Fe$_2$PRuS (833.4 gmol$^{-1}$): C, 49.00; H, 4.23. Found; C, 48.89; H, 4.42. Mp.: 240 °C (dec.). IR data (KBr) [cm$^{-1}$]: 3102 w, 3078 w, 2974 w, 2961 w, 2911 w, 1507 w, 1457 w, 1411 w, 1382 w, 1108 m, 1030 m, 839 s, 830 s, 557 m, 507 m. $^1$H NMR (CDCl$_3$)[$\delta$]: 6.13 (s, 2H, C$_4$H$_2$S) 4.70 (m, 2H, C$_5$H$_4$), 4.44 (m, 2H, C$_5$H$_4$), 4.43 (m, 2H, C$_5$H$_4$), 4.22 (m, 2H, C$_5$H$_4$), 4.21 (s, 10H, C$_5$H$_5$), 1.62 (s, 15H, RuCp\*). $^{13}$C{$^1$H} NMR (CDCl$_3$)[$\delta$]: 98.8 (C$_i$-C$_4$H$_2$S), 95.5 (C$_i$-RuCp\*), 84.6 (C$_4$H$_2$S), 74.4 (C$_i$-C$_5$H$_4$), 70.9 (C$_5$H$_5$), 70.8 (C$_5$H$_4$), 70.8 (C$_5$H$_4$), 67.9 (C$_5$H$_4$), 66.4 (C$_5$H$_4$), 10.4 (C$_H$-RuCp\*). HR-ESI MS (calc) [m/z]: 689.0249 (689.0208) [Cp\*Ru($\eta^5$-2,5-Fc$_2$-C$_4$H$_2$S)]$^+$.

**[Cp\*Ru($\eta^5$-2,5-Fc$_2$-EDOT)]PF$_6$ (G11)**: [Cp\*Ru(CH$_3$CN)$_3$]PF$_6$[441] (75 mg, 0.15 mmol), 1 eq of 2,5-diferrocenyl-3,4-ethylenedioxy thiophene[271] (75 mg). Compound **G11** was crystallized from dichloromethane/*n*-hexane (2:1, v:v) at –35 °C as a red solid. Yield: 121 mg (0.14 mmol, 92 %). Anal. Calcd. for C$_{36}$H$_{37}$F$_6$Fe$_2$O$_2$PRuS (891.5 gmol$^{-1}$): C, 48.50; H, 4.18. Found; C, 48.42; H, 4.45. Mp.: 255 °C (dec.). IR data (KBr) [cm$^{-1}$]: 3120 w, 3085 w, 2974 w, 2958 w, 2919 w, 1520 w, 1473 m, 1368 m, 1241 w, 1218 w, 1070 m, 1030 w, 842 s, 558 m, 504 w. $^1$H NMR (CDCl$_3$)[$\delta$]: 4.90 (m, 2H, C$_5$H$_4$), 4.68 (m, 2H, OCH$_2$CH$_2$O), 4.44 (m, 2H, C$_5$H$_4$), 4.42 (m, 2H, C$_5$H$_4$), 4.39 (m, 2H, OCH$_2$CH$_2$O), 4.24 (m, 2H, C$_5$H$_4$), 4.23 (s, 10H, C$_5$H$_5$), 1.56 (s, 15H, RuCp\*). $^{13}$C{$^1$H} NMR (CDCl$_3$)[$\delta$]: 118.1 (C$_i$-C$_4$S), 95.0 (C$_i$-RuCp\*), 82.2 (C$_i$-C$_4$S), 73.4 (C$_i$-C$_5$H$_4$), 70.7 (C$_5$H$_5$), 70.7 (C$_5$H$_4$), 70.1 (C$_5$H$_4$), 68.5 (C$_5$H$_4$), 65.8 (C$_5$H$_4$), 65.7 (OCH$_2$CH$_2$O), 10.0 (C$_H$-RuCp\*). HR-ESI MS (calc) [m/z]: 747.0265 (747.0264) [Cp\*Ru($\eta^5$-2,5-Fc$_2$-EDOT)]$^+$.

**Crystal data for G11**: C$_{36}$H$_{37}$F$_6$Fe$_2$O$_2$PRuS·2(CH$_2$Cl$_2$), M$_r$ = 1061.31 g·mol$^{-1}$, monoclinic, *P*–1, $\lambda$ = 0.71073 Å, *a* = 10.7634(6) Å, *b* = 11.5208(7) Å, *c* = 17.7464(10) Å, $\alpha$ = 82.466(5)° , $\beta$ = 82.928(5)°, $\gamma$ = 69.054(5)°, *V* = 2030.5(2) Å$^3$, Z = 2, $\rho_{calcd}$ = 1.736 g·cm$^{-3}$, $\mu$ = 1.488 mm$^{-1}$, *T* = 110(2) K, $\Theta$ range = 2.976 – 25.998 °, reflections collected: 16904, independent: 7976 ($R_{int}$ = 0.0365), $R_1$ = 0.0455, w$R_2$ = 0.1017 [*I*> 2$\sigma$(*I*)].

**Electrochemistry.** For electrochemical measurements, a Voltalab 10 electrochemical laboratory from Radiometer Analytical was used. All experiments were carried out under an atmosphere of argon on dichloromethane, acetonitrile and propylene carbonate solutions of the analyte, containing 0.1 mol·L$^{-1}$ of [N$^n$Bu$_4$][B(C$_6$F$_5$)$_4$] or [N$^n$Bu$_4$][PF$_6$] as supporting electrolyte, otherwise noted.[90,100] For spectroelectrochemical measuements, an OTTLE cell

(= Optically Transparent Thin Layer Electrochemistry) placed in a Varian Cary 5000 UV-VIS-NIR absorption spectrometer was used.[238] A verification of the obtained extinction coefficients was made within additional UV-Vis spectroscopic measurements. For voltammetry, a three electrode cell with a platinum auxiliary electrode, a glassy carbon working electrode (3.0 mm dia.) and a $Ag/Ag^+$ reference electrode were used. The working electrode was prepared by polishing with Buehler MicroFloc using Buehler diamond suspensions with decreasing sizes (1 to 0.25 μm). The $Ag/Ag^+$ reference electrode was constructed from a silver wire inserted into a Luggin capillary with a CoralPor/Vycor tip containing a solution of 0.01 $mol·L^{-1}$ [AgNO$_3$] and 0.1 $mol·L^{-1}$ of the supporting electrolyte in acetonitrile. This Luggin capillary was inserted into a second Luggin capillary with CoralPor/Vycor tip filled with a 0.1 $mol·L^{-1}$ supporting electrolyte solution in the corresponding solvent. Alternatively, a silver wire as quasi-reference electrode was applied. Successive experiments under the same experimental conditions showed that all formal reduction and oxidation potentials were reproducible within ±5 mV. Experimentally potentials were referenced against a $Ag/Ag^+$ reference electrode but the results are presented referenced against the FcH/FcH$^+$ couple ($E^{0'}$ = 0.0 V) as required by IUPAC.[249] Within this context, decamethylferrocene was used as an internal standard and the experimentally measured potentials were converted in to $E$ vs. FcH/FcH$^+$ by addition of -0.61 V.[250,272] The cyclic voltammograms were taken after typical two scans and are considered to be steady state cyclic voltammograms in which the signal pattern differs not from the initial sweep. Cyclic voltammetry simulations were carried out with DigiSim 3.03b from Bioanalytical Systems, using the Butler-Volmer (BV) kinetic model ($R_u$ = 0 Ohms). Finally, the experimental data were processed on Microsoft Excel worksheets.

**Crystallography**. Data were collected with an Oxford Gemini S diffractometer at 100 K using Mo K$\alpha$ ($\lambda$ = 0.71073 Å) for **G7**, **G9** and **G11** or Cu K$\alpha$ ($\lambda$ = 1.54184 Å) radiation for **G3** and **G5**. The structures were solved by direct methods using SHELXS-13 and refined by full matrix least-square procedures on F$^2$ using SHELXL-13.[251,252,324,448]

Crystallographic data (Experimental Section) for the structures of **G3**, **G5**, **G7**, **G9** and **G11** have been deposited with the Cambridge Crystallographic Data Centre, CCDC, 12 Union Road, Cambridge CB21EZ, UK. Copies of the data can be obtained free of charge on quoting the depository numbers CCDC-1446380 (**G3**), 1446381 (**G5**), 1446382 (**G7**), 1446383 (**G9**), 1446384 (**G11**), (Fax: +44-1223-336-033; e-mail: deposit@ccdc.cam.ac.uk, http://www.ccdc.cam.ac.uk).

**Supporting Information**. Additional crystallographic data Table AG-1 as well as Figures AG-1 and AG-2 are available in the Appendix Section (Chapter AG).

# H      SUMMARY

SUMMARY

This PhD thesis deals with a study concerning the electrochemical behavior of various ferrocenyl-substituted thiophene systems. Additional investigations regarding possible charge transfer interactions between the ferrocenyls with a direct or indirect involvement of the thiophene aromatic system in the individual redox states are discussed. The dependence of the latter properties on numeric and/or electronic variations of the redox centers itself, on a functionalization of the bridging unit and the introduction of further $\sigma$- or $\pi$-bonded transition metal complex fragments is illuminated.

Within this regard, the corresponding results are presented in 5 Chapters:

| | |
|---|---|
| **Chapter C** | ELECTRON TRANSFER STUDIES ON FERROCENYL THIOPHENES – SYNTHESIS, PROPERTIES AND ELECTROCHEMISTRY |
| **Chapter D** | ATROPISOMERIC 3,3',4,4',5,5'-HEXAFERROCENYL-2,2'-BITHIOPHENE: SYNTHESIS, SOLID-STATE STRUCTURE AND ELECTROCHEMISTRY |
| **Chapter E** | FUNCTIONALIZATIONS ON 2,5-DIFERROCENYLTHIOPHENES AND THEIR IMPLICATIONS ONTO ELECTRONIC PROPERTIES |
| **Chapter F** | ELECTROCHEMICAL EXAMINATIONS OF FERROCENES MODIFIED BY TUNGSTEN ALKYLIDENE COMPLEXES AND THEIR ELECTRONIC INTERACTION WITH THIOPHENE |
| **Chapter G** | ELECTROCHEMICAL STUDIES ON RUTHENIUM CYCLOPENTADIENYLS STABILIZED BY FERROCENYL-SUBSTITUTED THIOPHENES |

**Chapter C**

Chapter C deals with an electrochemical study on the ferrocenyl thiophene series (number of ferrocenyls n = 1 – 4) (Figure H1). These metallocenyl heterocycles were synthesized by palladium-promoted Negishi *C,C* coupling reactions of the corresponding bromo thiophenes and ferrocenyl zinc chloride.

The redox properties of **C1** – **C4** and **C9** – **C13**[183] were studied by cyclic (CV) and square wave voltammetry (SWV) in combination with UV-Vis-NIR spectroelectrochemistry. For the considered ferrocenyl thiophenes one (**C1**, **C2**), two (**C3**, **C4**, **C9**, **C10**), three (**C11**, **C12**) or four (**C13**) well-resolved electrochemically reversible Fc/Fc$^+$ electrode reactions were found. During the spectroelectrochemical studies of ferrocenyl thiophenes **C1** and **C2** a ligand-to-metal charge transfer (LMCT, thiophene-to-ferrocenyl) absorption for **C2**$^+$ at

around 12000 cm$^{-1}$ was observed as less intense than for **C1**$^+$ suggesting a lower degree of electronic interaction between the thiophene core and the ferrocenyl unit (in *β*-position).



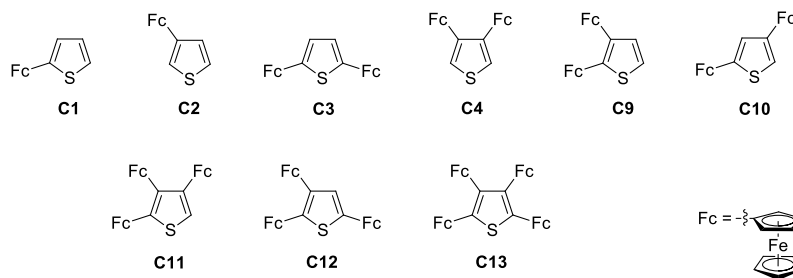**Figure H1**. Ferrocenyl thiophenes **C1 – C4** and **C9 – C13**.

Further spectroelectrochemical studies on the oligoferrocenyl molecules reveal weak metal-metal interactions in the corresponding mixed-valent species, *i.e.* in the series of diferrocenyl thiophenes the interaction between the iron centers in the monooxidized compounds decreases in the series **C3**$^+$ > **C9**$^+$ > **C10**$^+$ > **C4**$^+$. A comparison between the peak width at half-height $\Delta\tilde{v}_{1/2}$ (IVCT) and the Hush prediction $\Delta\tilde{v}_{1/2(theo)}$ (of **C3**$^+$, **C4**$^+$, **C9**$^+$, **C10**$^+$, **C11**$^+$, **C11**$^{2+}$, **C12**$^+$ and **C12**$^{2+}$) is clearly consistent with the identification of the low-energy absorptions of this class of compounds as class II according to Robin and Day.[68] Generally, the ferrocenyl units placed in *α*-position of the thiophene, interact more strongly with the five-membered heterocycle, *i.e.* larger extinction coefficients can be detected for the corresponding ligand-to-metal and intervalence charge transfer absorptions of the individual cationic species.

**Chapter D**

In this section the perferrocenylated 3,3',4,4',5,5'-hexaferrocenyl-2,2'-bithiophene (**D3**), as formal combination of two units of **C11**, is electrochemically investigated (Figure H2).



**Figure H2**. 3,3',4,4',5,5'-Hexaferrocenyl-2,2'-bithiophene (**D3**).
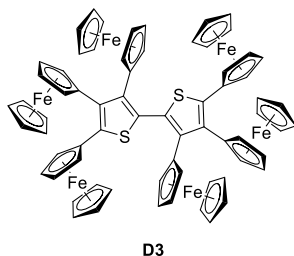
Consequences regarding increasing electrosteric repulsions in such systems and the effect of possible highly charged species are discussed. The title compound is accessible in a Pd-promoted Negishi *C,C* coupling of 2-bromo-3,4,5-triferrocenyl thiophene (**D1**) and 2,3,4-triferrocenyl thiophene zinc chloride (**D2**). The solid state structure determination reveals

the steric demand of the six ferrocenyl termini at the bithiophene core. The atropisomerism of **D3**, as a consequence of a hampered rotation along the thiophene-thiophene bond, could be verified by dynamic $^1$H NMR spectroscopy.

Electrochemical as well as spectroelectrochemical studies on the starting material **D1** indicate a weak electronic coupling between the three partially oxidized ferrocenyl termini, as evidenced by the appearance of IVCT transitions in the NIR region. However, for the hexaferrocenyl bithiophene (**D3**) another electrochemical behavior is characteristic. Due to the low solubility of this compound in dichloromethane, as well as the even lower solubility of the oligo-cationic species, the respective electrochemical measurements had to be carried out in anisole. In the latter case four reversible redox events at $E^{0'} = -131$, 260, 471 and 569 mV $vs.$ FcH/FcH$^+$ were observed at ambient temperature. The formal lack of the sixth redox process is probably caused by a strong adsorption of the appropriate pentacation onto the electrode. However, when the electrochemical experiments were run at 100 °C a total number of five redox processes were observed. However, no IVCT absorptions could be detected in the NIR range during the spectroelectrochemical examination of **D3**.

**Chapter E**

In advance of illuminations on functionalized 2,5-diferrocenyl thiophenes, the influence of electrolyte anion's coordination/pairing properties on the electronic coupling in cationic mixed valent species is investigated, on biferrocene as model system (Subchapter E1). The dependency on the solvent polarity was determined by using dichloromethane, acetonitrile and propylene carbonate. Within the UV-Vis-NIR spectroelectrochemical investigations, significant differences in the NIR absorption behavior could be detected for [BfcH][B(C$_6$F$_5$)$_4$] in comparison with the hexafluorophosphate derivative, when the solvent polarity is decreased (dichloromethane). Thus, an increasing thermodynamic stability ($K_C$) of cationic mixed-valent species by weakly-coordinating anions instead of traditional anions has its origin not only in Coulomb interactions, as usually assumed.

In Subchapter E2 a series of $\alpha,\alpha'$-diferrocenyl thiophenes and ethylenedioxy thiophenes, with electron withdrawing functionalities on the ferrocenyls, is reported with the aim of investigating the electronic influence of functional groups at the ferrocenyl entities and the heterocyclic bridging unit on low-energy charge transfer transitions (Figure H3).
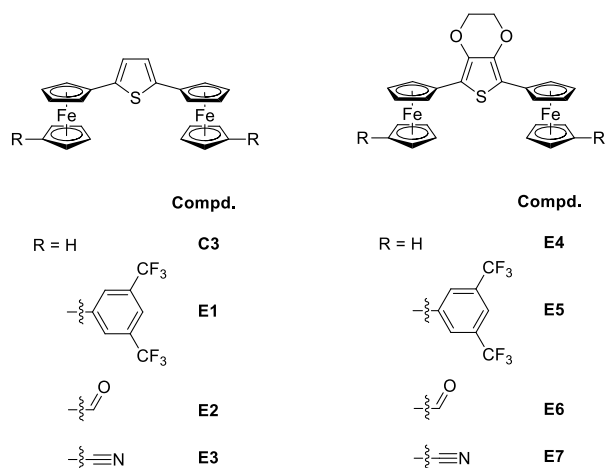
**Figure H3**. *α,α'*-Diferrocenyl thiophenes and ethylenedioxy thiophenes **C3** and **E1** – **E7**.

The electrochemical studies on thiophenes **E1** – **E7** exhibit an increasing redox separation/thermodynamic stability of the mixed-valent species in the series **C3** < **E2** < **E4** < **E3** ≈ **E1** < **E5** < **E6** < **E7**. Further UV-Vis-NIR and infrared spectroelectrochemical studies verified these observations. Thus electron-withdrawing groups at the ferrocenyls in combination with the electron-donating ethylenedioxy unit at the thiophene building block enforce the electronic coupling between the iron-based redox centers in the corresponding mixed-valent state.

Continuing electrochemistry (Subchapter E3) on a series of 3,4-di-*N*-substituted 2,5-diferrocenyl thiophenes reveals an increasing thermodynamic stability of the mixed-valent species ($K_C$) in the order **E12** < **E13** ≈ **E14** < **E15** (Figure H4).
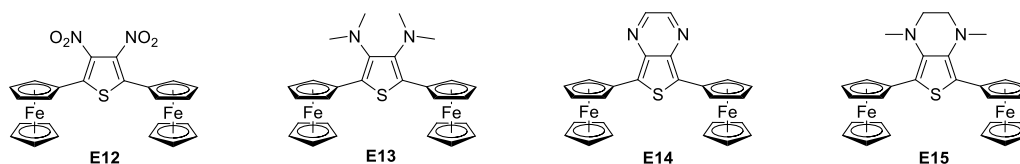


**Figure H4**. 3,4-Di-*N*-substituted 2,5-diferrocenyl thiophenes **E12** – **E15**.

Moreover, the NIR absorptions of the corresponding mixed-valent species become more intense and less solvatochromic as the electron-donating effect and the extension of the electronic π-system of the bridging unit increases. Hence, electronic coupling between the iron-based redox centers over the thiophene-based core increases in this direction (**E12** < **E13** ≈ **E14** < **E15**).

With regard to the whole series of thiophene-bridged biferrocenes, a decreasing solvatochromic shift of inter valence charge transfer absorptions was found as the redox separation/thermodynamic stability of a mono-cationic species ($K_C$) increases. By the fact that a smaller solvatochromism could represent a stronger electronic interaction,[57,70,123] an evaluation of the electronic coupling by using the solvatochromic shift should be a

powerful tool for a characterization of such biferrocenes – a more general alternative compared to the absorption intensity. Furthermore, due to the application of benchmark systems with a known "communication behavior" a distinct classification should be possible. Thus, by the use of biferrocene (BfcH$^+$), with a solvatochromic shift of $\Delta\tilde{v}_{max-IVCT}$ = 1100 cm$^{-1}$ (Chapter E1), the above named species with a less pronounced solvatochromism can be clearly classified as strongly-coupled class II/borderline systems according to Robin and Day.[68]

Moreover, for charge transfer processes via a super exchange (tunneling) mechanism, as proposed for organic mixed-valence complexes, an exponential decay of electronic coupling with the charge transfer distance is expected.[63,75,76,426]
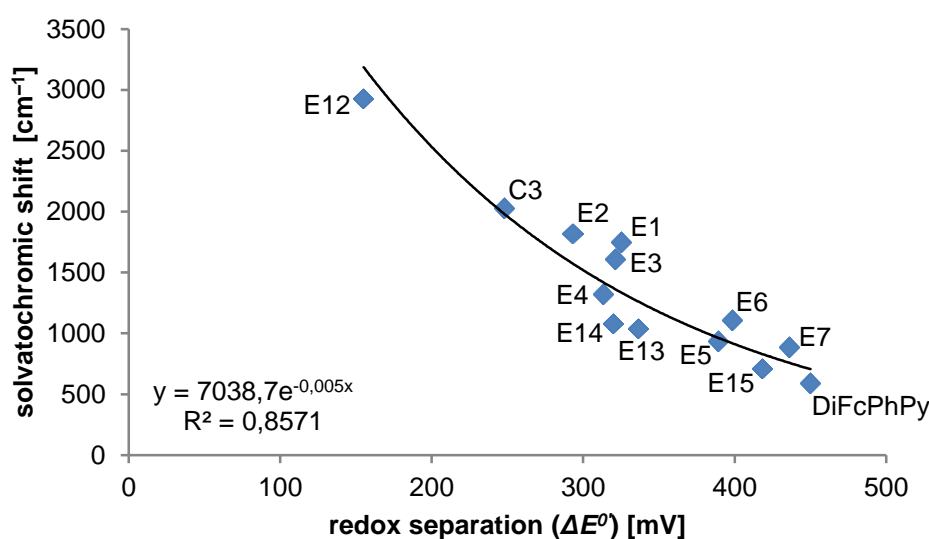


**Figure H5**. Correlation between the solvatochromic shift of IVCT absorption band (for the related mixed-valent species) and the redox separation of the corresponding diferrocenyl heterocycle. (DiFcPhPy denotes 2,5-diferrocenyl-*N*-phenylpyrrole (**B18**)).

Thus, by plotting the solvatochromic shift over the redox separation (Figure H5), the individual datapoints follow roughly an exponential function with a negative argument. This finding would imply a charge transfer in these systems, which is dominated by a superexchange mechanism (*vide supra*, Chapter B). Nevertheless, future works on strong-coupled (class III) derivatives of this type of compounds would be suitable for a verification of this relationship.

**Chapter F**

In Chapter F the influence of further $\sigma$-bonded transition metal fragments (Fischer carbenes) on the electronic properties of the ferrocenyl unit and the thiophene itself as well as the biferrocene system (with or without thiophene bridge) is discussed.

A series of ferrocenyl (Fc = ferrocenyl; fc = ferrocen-1,1'-diyl) and biferrocenyl (Bfc = 1',1''-biferrocenyl; bfc = 1',1''-biferrocen-1,1'''diyl) tungsten Fischer carbene complexes is reported in Section F1 with the aim of investigating low-energy charge transfer between the transition metal carbonyl fragment, over the carbene carbon, and the (oxidized) metallocenyl substituents (Figure H6).
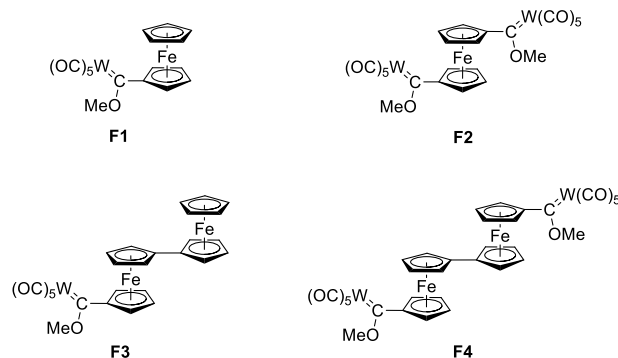


**Figure H6**. Tungsten Fischer carbene complexes **F1** – **F4**.

The electrochemical studies of **F1** – **F4** reveal reversible one-electron redox events for the ferrocenyl/biferrocenyl moieties. Moreover, an electrochemical one electron transfer reaction could be found for the reduction of the Fischer carbene units. For the tungsten carbonyl moieties, irreversible oxidation processes could be detected. During the UV-Vis-NIR spectroelectrochemical investigations typical low energy absorptions for the mixed-valent biferrocenyl units were found. A further observed high energy NIR absorption was attributed to a metal-metal charge transfer transition between the tungsten carbonyl increment and the ferrocenyl/biferrocenyl unit in the corresponding oxidized state and is reported herein for the first time.

In Subchapter F2 a series of thiophene tungsten Fischer carbene complexes of type $[(CO)_5W=C(OMe)R]$ (**F5**, R = 2-thienyl; **F8**, R = fcthFc; th = 2,5-thiendiyl; Fc = ferrocenyl; fc = 1,1'-ferrocenediyl) and $[(CO)_5W=C(OMe)-R'-(OMe)C=W(CO)_5]$ (**F6**, R' = th; **F9**, R' = fcthfc) is reported with the aim of investigating low-energy charge transfer transitions between the carbene substituents and the transition metal carbonyl fragment, incorporating the thiophene system. Reversible one-electron redox events could be found for the ferrocenyl moieties (**F8**, **F9**). Moreover, typical electrode reactions could be found for the carbene reductions and the tungsten carbonyl oxidation processes as previously reported (*vide supra*). However, for biscarbene **F6** two well-separated reversible one-electron reduction events could be found suggesting a significant electronic coupling in **F6**⁻. The corresponding infrared spectroelectrochemical investigations on biscarbene **F6** reveal a high degree of charge delocalization in the formal mixed valent **F6**⁻.

**Chapter G**

Within this Chapter the synthesis of a series of $\eta^5$-thiophene Ru($\eta^5$-C$_5$H$_5$)/Ru($\eta^5$-C$_5$Me$_5$) complexes, on the basis of ferrocenyl-substituted thiophenes, is reported with the aim of a better understanding of the influence of $\pi$-thiophene-bonded transition metal moieties onto the thermodynamic stability and charge transfer interactions of the resulting complexes and their oxidized intermediates (Figure H7). Within the electrochemical investigations, reversible one-electron and iron-based redox events were found for the mono-ferrocenyl Ru-complexes, whereby the corresponding Fc/Fc$^+$ redox potential increases as the degree of methylation of the thiophene core and the Ru($\eta^5$-C$_5$H$_5$) moiety decreases. Moreover for diferrocenyl compounds **G5**, **G6**, **G10** and **G11** a hindered 2$^{nd}$ ferrocenyl-based electrode reaction was observed under "weak-coordinating" conditions.



M = Ru($\eta^5$-C$_5$H$_5$)[PF$_6$] (**G2**)      M = Ru($\eta^5$-C$_5$H$_5$)[PF$_6$] (**G3**)     M = Ru($\eta^5$-C$_5$H$_5$)[PF$_6$] (**G4**)
Ru($\eta^5$-C$_5$Me$_5$)[PF$_6$] (**G7**)     Ru($\eta^5$-C$_5$Me$_5$)[PF$_6$] (**G8**)     Ru($\eta^5$-C$_5$Me$_5$)[PF$_6$] (**G9**)

M = Ru($\eta^5$-C$_5$H$_5$)[PF$_6$] (**G5**)     M = Ru($\eta^5$-C$_5$H$_5$)[PF$_6$] (**G6**)
Ru($\eta^5$-C$_5$Me$_5$)[PF$_6$] (**G10**)     Ru($\eta^5$-C$_5$Me$_5$)[PF$_6$] (**G11**)
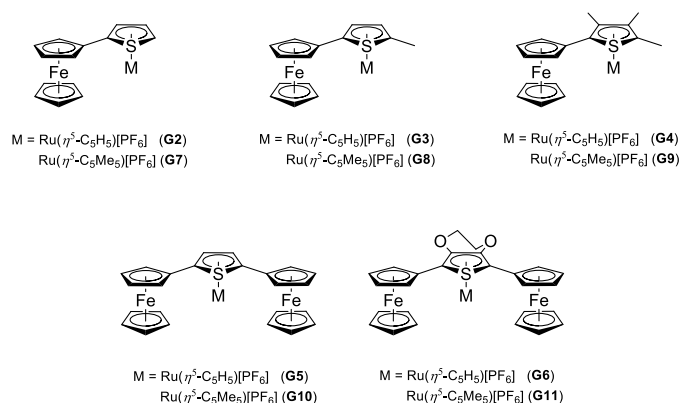
**Figure H7**. Ruthenium complexes **G2** – **G11**.

Thus, two well-separated Fc/Fc$^+$ redox events could be detected by the use of "more" solvating solvents or (smaller) anions. With regard to the uncomplexed diferrocenyl thiophenes, the thermodynamic stability of the appropriate mixed-valent species decreases clearly when a [Ru($\eta^5$-C$_5$H$_5$)]$^+$/[Ru($\eta^5$-C$_5$Me$_5$)]$^+$ fragment is bonded on the thiophene aromatic system. The nature of the cyclopentadienyl ring should not have a major impact. The related decrease of electronic coupling between ferrocenyl unit and thiophene or a second Fc-moiety, in the corresponding oxidized states, could be verified during UV-Vis-NIR spectroelectrochemical measurements.

ZUSAMMENFASSUNG

Die vorliegende Dissertation beschäftigt sich mit dem elektrochemischen Verhalten verschiedener, Ferrocenyl-substituierter Thiophene. In diesem Zusammenhang werden mögliche Ladungstransferprozesse zwischen den Ferrocenyleinheiten, in den

verschiedenen Redoxzuständen und unter Beeinflussung durch den Thiophen-Brückenliganden, diskutiert. Dabei wird die Abhängigkeit dieser Ladungstransfer-wechselwirkungen von numerischen, konstitutionellen und elektronischen Veränderungen der redox-aktiven Ferrocenyleinheiten, von Modifikationen an der Brückeneinheit sowie von der Einführung zusätzlicher $\sigma$- oder $\pi$-gebundener Übergangsmetall-komplexfragmente beleuchtet. Die entsprechenden Ergebnisse werden in 5 Kapiteln (Chapters) aufgezeigt:

**Chapter C**     ELECTRON TRANSFER STUDIES ON FERROCENYL THIOPHENES – SYNTHESIS, PROPERTIES AND ELECTROCHEMISTRY

**Chapter D**     ATROPISOMERIC 3,3',4,4',5,5'-HEXAFERROCENYL-2,2'-BITHIOPHENE: SYNTHESIS, SOLID-STATE STRUCTURE AND ELECTROCHEMISTRY

**Chapter E**     FUNCTIONALIZATIONS ON 2,5-DIFERROCENYLTHIOPHENES AND THEIR IMPLICATIONS ONTO ELECTRONIC PROPERTIES

**Chapter F**     ELECTROCHEMICAL EXAMINATIONS OF FERROCENES MODIFIED BY TUNGSTEN ALKYLIDENE COMPLEXES AND THEIR ELECTRONIC INTERACTION WITH THIOPHENE

**Chapter G**     ELECTROCHEMICAL STUDIES ON RUTHENIUM CYCLOPENTADIENYLS STABILIZED BY FERROCENYL-SUBSTITUTED THIOPHENES

**Chapter C**

Kapitel C beschäftigt sich mit dem elektrochemischen Verhalten der Serie der Ferrocenylthiophene, dabei variiert die Anzahl der redox-aktiven (Ferrocenyl) Gruppen von n = 1 – 4 (Abbildung H1). Die Synthese dieser heterozyklischen Systeme erfolgte im Rahmen Pd-vermittelter Negishi-Kreuzkupplungsreaktionen der entsprechenden Bromthiophene mit Ferrocenylzinkchlorid.

Die elektrochemischen Eigenschaften von **C1** – **C4** und **C9** – **C13**[183] wurden mittels Cyclovoltammetrie, Square-Wave-Voltammetrie untersucht, ergänzt durch UV-Vis-NIR-spektroelektrochemische Studien. Die betrachteten Verbindungen zeigen ein (**C1**, **C2**), zwei (**C3**, **C4**, **C9**, **C10**), drei (**C11**, **C12**) bzw. vier (**C13**) elektrochemisch reversible Fc/Fc$^+$-Elektrodenreaktionen. In spektroelektrochemischen (SEC) Untersuchungen an **C1** und **C2** konnten Ligand-zu-Metall Ladungstransfer Absorptionsbanden (LMCT, Thiophen-zu-Ferrocenyl) beobachtet werden. Dabei zeigte sich, dass im Vergleich zu **C1**$^+$ die entsprechenden Absorptionen für **C2**$^+$ hypsochrom und hyphochrom verschoben sind, und

somit auf eine geringere elektronische Wechselwirkung zwischen der Ferrocenyleinheit (in *β*-Position) und dem Thiophen-Heterozyklus hindeuten.
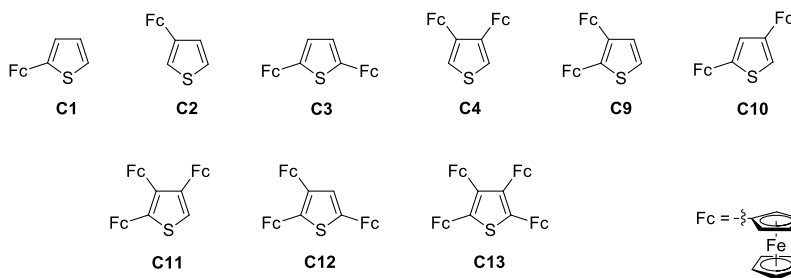


**Abbildung H1**. Ferrocenylthiophene **C1** – **C4** und **C9** – **C13**.

Die SEC-Untersuchungen der Oligoferrocenyl-Derivate offenbaren schwache Metall-Metall-Wechselwirkungen in den gemischtvalenten Verbindungen, wobei in der Serie der monokationischen Diferrocenylthiophene die elektronische Wechselwirkung (Kommunikation) zwischen den Eisen-Zentren in der Reihe $C3^+ > C9^+ > C10^+ > C4^+$ abnimmt. Ein Vergleich der experimentellen Halbwertsbreiten der Intervalenz-Ladungstransfer-Absorptionsbanden $\Delta\tilde{v}_{1/2}$ (IVCT) mit der Vorhersage der Hush-Theorie $\Delta\tilde{v}_{1/2(theo)}$ (von $C3^+$, $C4^+$, $C9^+$, $C10^+$, $C11^+$, $C11^{2+}$, $C12^+$ sowie $C12^{2+}$) verifiziert die Einordnung dieser Gemischtvalenzkomplexe als Klasse-II-Systeme nach Robin und Day.[68] Zusammenfassend konnte festgestellt werden, dass redox-aktive (Ferrocenyl) Einheiten in der *α*-Position des Thiophens stärker (als in *β*-Position) mit dem Heterozyklus in elektronische Wechselwirkung treten.

## Chapter D

Dieser Abschnitt widmet sich dem perferrocenyliertem 3,3',4,4',5,5'-Hexaferrocenyl-2,2'-bithiophen (**D3**) als formales Dimer des Triferrocenylthiophens **C11** (Abbildung H2).



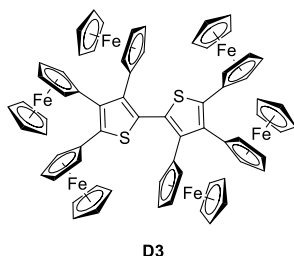**Abbildung H2**. 3,3',4,4',5,5'-Hexaferrocenyl-2,2'-bithiophen (**D3**).

In diesem Zusammenhang werden Konsequenzen infolge elektronischer/räumlicher Abstoßung und der Einfluss hochgeladener Intermediate auf die elektrochemische Charakterisierung und die Metall-Metall-Kommunikation diskutiert. Die Darstellung von Verbindung **D3** erfolgte in einer Palladium-vermittelten Negishi-Kreuzkupplung von 2-

Brom-3,4,5-triferrocenyl-thiophen (**D1**) mit 2,3,4-Triferrocenylthiophen-Zinkchlorid (**D2**). Die Bestimmung der molekularen Struktur im Festkörper zeigt die strukturelle Penetration der 2,2'-Bithiophen-Grundstruktur durch den räumlichen Anspruch der Ferrocenyl-Substituenten auf. Das, infolge der gehinderten Rotation um die Inner-Bithiophenbindung, atropisomere Verhalten von **D3** konnte durch temperaturabhängige ^{1}H-NMR-Spektroskopie verifiziert werden.

Die Daten der elektrochemischen Untersuchungen an Thiophen **D1** weisen, nicht zuletzt aufgrund beobachteter IVCT-Banden, auf schwach-elektronische Wechselwirkungen zwischen den Fc-Einheiten in **D1**$^+$ bzw. **D1**$^{2+}$ hin. Auf Grund der geringen Löslichkeit von Bithiophen **D3**, und der (partiell) oxidierten Spezies, in Dichlormethan wurden weitere elektrochemische Untersuchungen in Anisol durchgeführt. Bei Raumtemperatur wurden so vier Redoxwellen bei $E^{0'}$ = –131, 260, 471 und 569 mV *vs.* FcH/FcH$^+$ detektiert. Im Rahmen von anschließenden Hochtemperatur-cyclovoltammetrischen Experimenten (100 °C) konnten fünf separierte, reversible und Ferrocenyl-basierende Redoxprozesse beobachtet werden, wobei die erste Welle formal aus zwei sich überlagernden Ein-Elektroden-Reaktionen zusammengesetzt ist. Allerdings konnten in abschließenden spektroelektrochemischen Untersuchungen an **D3** keine Absorptionen registriert werden, welche Intervalenz-Ladungstransfer-Wechselwirkungen zugeordnet werden können.

**Chapter E**

In Kontext der Weiterführung von Ladungstransferuntersuchungen am 2,5-Diferrocenylthiophen-Motiv wurde zunächst in Unterkapitel E1 eine Evaluierung des Einflusses des Anions auf die elektronische Kopplung in kationischen Gemischtvalenzsystemen, am Beispiel von Biferrocen als Modelsystem, durchgeführt. Dabei wurde der Einfluss des Lösungsmittels unter Verwendung von Dichlormethan, Acetonitril und Propylencarbonat untersucht. Während der UV-Vis-NIR-Spektroelektrochemie konnten deutliche Unterschiede im Absorptionsverhalten von [BfcH][B(C$_6$F$_5$)$_4$] im Vergleich zu [BfcH][PF$_6$] festgestellt werden, vor allem in Medien geringer Polarität (Dichlormethan). Folglich sollte die Ursache der höheren thermodynamischen Stabilität ($K_C$) kationischer Gemischtvalenz-Systeme, wie oftmals angenommen, nicht nur in elektrostatischen Wechselwirkungen begründet sein.

Im folgenden Unterkapitel E2 wird sich einer Serie von $\alpha,\alpha'$-Diferrocenylthiophenen und Ethylendioxythiophenen zugewandt, wobei der Einfluss elektronenziehender

Funktionalitäten an den Ferrocenyleinheiten (in 1'-Position) sowie die Auswirkungen des Ethylendioxy-Substituenten auf Ladungstransfer-Wechselwirkungen beleuchtet werden (Abbildung H3).
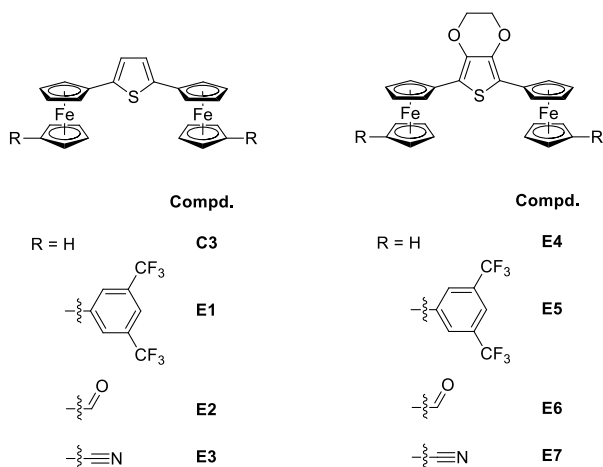


**Abbildung H3**. *α,α'*-Diferrocenylthiophene und Ethylendioxythiophene **C3** und **E1** – **E7**.

Die elektrochemischen Untersuchungen an **E1** – **E7** ergeben eine Vergrößerung der Redoxseparation bzw. eine Zunahme der thermodynamischen Stabilität der gemischtvalenten Spezies in der Reihe **C3** < **E2** < **E4** < **E3** ≈ **E1** < **E5** < **E6** < **E7**. Zusätzliche UV-Vis-NIR- und Infrarot-spektroelektrochemische Studien bestätigen diese Beobachtungen, d. h. Elektronakzeptor-Gruppen an den Ferrocenyleinheiten in Kombination mit Etylendioxy-Substituenten am Thiophen-Brückensystem führen zu einer Steigerung der formalen Eisen-Eisen-Kommunikation in den entsprechenden Gemischtvalenz-Verbindungen.

Darüber hinausgehende elektrochemische Studien (Unterkapitel E3) an einer Serie 3,4-di-*N*-substituierter 2,5-Diferrocenylthiophene (**E12** – **E15**, Abbildung H4) offenbaren eine ebenfalls ansteigende thermodynamische Stabilität der mono-kationischen Verbindungen in der Reihe **E12** < **E13** ≈ **E14** < **E15**.
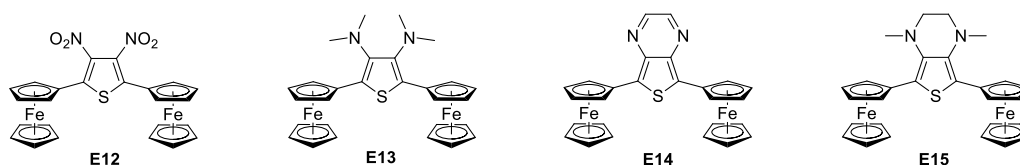


**Abbildung H4**. 3,4-Di-*N*-substituierte 2,5-Diferrocenylthiophene **E12** – **E15**.

Die während der Spektroelektrochemie detektierten NIR-Absorptionen der Gemischtvalenz-Komplexe zeigen eine höhere Intensität und geringere Lösungsmittelunabhängigkeit (steigende elektronische Kopplung) in gleicher Reihenfolge.

Zusammenfassend über alle in Kapitel E betrachteten Thiophen-verbrückten Biferrocenderivate konnte mit einer steigenden thermodynamischen Stabilität der

Gemischtvalenz-Verbindungen eine geringere Solvatochromie ihrer Intervalenz-Ladungstransfer-Absorptionsbanden festgestellt werden. Für gewöhnlich geht eine steigende Lösungsmittelunabhängigkeit mit einer stärkeren elektronischen Kopplung einher,[57,70,123] folglich sollte eine Evaluierung der elektronischen Kopplung unter Zuhilfenahme des solvatochromen Verhaltens derartiger Biferrocene eine Alternative zur Intensitäts-basierenden Charakterisierung darstellen. In diesem Zusammenhang müsste auch eine genauere Klassifizierung durch die Verwendung von gut-charakterisierten Referenzsystemen möglich sein. So können durch einen Vergleich mit Biferrocen (BfcH$^+$), mit $\Delta\tilde{\nu}_{max\text{-}IVCT}$ = 1100 cm$^{-1}$ (Unterkapitel E1), die oben betrachteten Systeme mit einer deutlich geringeren Lösungsmittelabhängigkeit ohne Weiteres als stark-gekoppelte Klasse-II bzw. als sogenannte Borderline-Systeme nach Robin und Day angesehen werden.[68]

In Allgemeinen wird für organische (metallorganische) Gemischtvalenz-Verbindungen eine elektronische Kopplung über einen Superaustausch (Tunnelmechanismus) erwartet, und somit ein exponentieller Abfall der elektronischen Kopplung mit zunehmenden Abstand der Redoxzentren.[63,75,76,426]
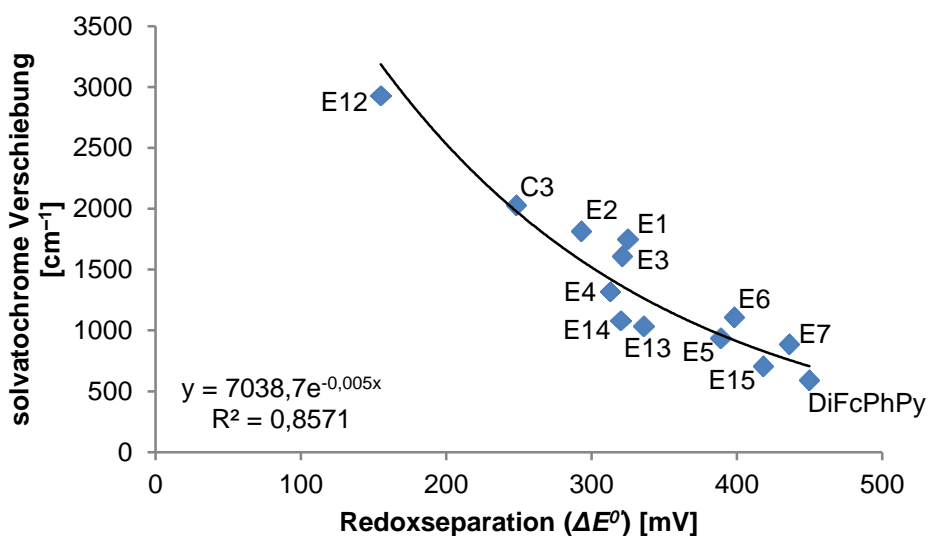


**Abbildung H5**. Korrelation zwischen der solvatochromen Verschiebung der IVCT-Absorptionsbanden (der Gemischtvalenzkomplexe) und der Redoxseparation der entsprechenden Diferrocenylheterozyklen. (DiFcPhPy entspricht 2,5-Diferrocenyl-*N*-phenylpyrrol (**B18**)).

In diesem Zusammenhang kann bei Auftragung der solvatochromen Verschiebung über die Redoxseparation (Abbildung H5) ungefähr der Verlauf einer reziproken Exponentialfunktion (negatives Argument) beschrieben werden. Letzterer Befund würde Ladungstransferprozesse dominiert über einen Superaustausch-Mechanismus nahe legen. Diesbezüglich sollten zukünftige Arbeiten, an stark-gekoppelten (Klasse-III) Systemen dieser Verbindungsklasse, Aufschluss über die Richtigkeit dieser Beziehung geben.

**Chapter F**

In Kapitel F wird der Einfluss von zusätzlichen σ-gebundenen Übergangsmetall-komplexfragmenten (Fischercarbene) auf die elektronischen Eigenschaften des 2,5-Diferrocenylthiophen-Motivs untersucht.

Am Beispiel einer Serie von Ferrocenyl- (Fc = Ferrocenyl; fc = Ferrocen-1,1'-diyl) und Biferrocenyl- (Bfc = 1',1''-Biferrocenyl; bfc = 1',1''-Biferrocen-1,1'''diyl) Wolfram-Fischercarben-Komplexen werden zunächst Ladungstransferprozesse zwischen dem Metallcarbonyl-Inkrement und dem Metallocen, über den Carben-Kohlenstoff, studiert (Unterkapitel F1, Abbildung H6).
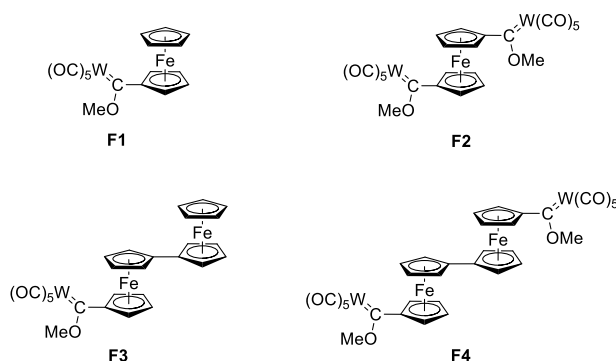


**Abbildung H6**. Wolfram-Fischercarbene **F1** – **F4**.

Im Rahmen der elektrochemischen Charakterisierung von **F1** – **F4** konnten reversible Ein-Elektronen-Redoxprozesse für die Ferrocenyl- und Biferrocenyleinheiten beobachtet werden. Darüber hinaus wurden Ein-Elektronen-Reduktionen für die Carben-Zentren sowie elektrochemisch irreversible Wolframcarbonyl-basierte Oxidationsprozesse detektiert. Während der dazugehörigen spektroelektrochemischen Untersuchungen wurden im niederenergetischen Nahinfrarotbereich typische Absorptionen für gemischtvalente Biferrocene beobachtet. Des Weiteren wurden im Grenzgebiet zum schichtbaren Spektralbereich Hochenergie-NIR-Absorptionsbanden, basierend auf Metall-Metall-Ladungstransfer-Wechselwirkungen zwischen Wolframcarbonyl und Ferrocenium, zum ersten Mal beobachtet.

Das anschließende Unterkapitel F2 widmet auf der Basis einer Serie von Thiophen-haltigen Wolfram-Fischercarbenen, des Typs $[(CO)_5W=C(OMe)R]$ (**F5**, R = 2-Thienyl; **F8**, R = fcthFc; th = 2,5-Thiendiyl; Fc = Ferrocenyl; fc = 1,1'-Ferrocenediyl) und $[(CO)_5W=C(OMe)-R'-(OMe)C=W(CO)_5]$ (**F6**, R' = th; **F9**, R' = fcthfc), Ladungstransfer-Wechselwirkungen unter Integration eines Thiophen(brücken)liganden. Für Verbindungen **F8** und **F9** konnten reversible Ferrocenyl-Redoxprozesse detektiert werden. In diesem Zusammenhang wurden auch typische Reduktions- und Oxidationsreaktionen des Carbens

und des Wolframcarbonyl-Fragmentes beobachtet (siehe Unterkapitel F1). Darüber hinaus verweisen für Biscarben **F6** zwei reversible Ein-Elektronen-Reduktionsprozesse auf eine signifikante thermodynamische Stabilität von **F6**⁻. Abschließende Infrarot-spektroelektrochemische Untersuchungen offenbaren ein hohes Maß an Ladungsdelokalisation in dieser gemischtvalenten Spezies.

## Chapter G

Kapitel G beschäftigt sich mit einer Serie $\eta^5$-Thiophen-Ru($\eta^5$-C$_5$H$_5$)/Ru($\eta^5$-C$_5$Me$_5$)-Komplexen, basierend auf verschiedenen ferrocenyl-substituierten Thiophenen, zum Zwecke eines besseren Verständnisses des Einflusses $\pi$-Thiophen-gebundener Übergangsmetallkomplex-Fragmente auf die elektronischen Eigenschaften der Ferrocenylthiophen-Grundmotive (Abbildung H7). Während der elektrochemischen Charakterisierung der Monoferrocenyl-Komplexe wurden reversible Fc/Fc⁺-Redoxprozesse beobachtet, wobei Letztere mit sinkendem Methylierungsgrad des Thiophenrings und der Ru($\eta^5$-C$_5$H$_5$)-Einheit mehr zu anodischen Potentialen verschoben sind. Für die Diferrocenylverbindungen **G5**, **G6**, **G10** und **G11** wurde unter den gewählten Bedingungen zusätzlich eine zweite, gehinderte Ferrocenyl-basierte Elektrodenreaktion gefunden.
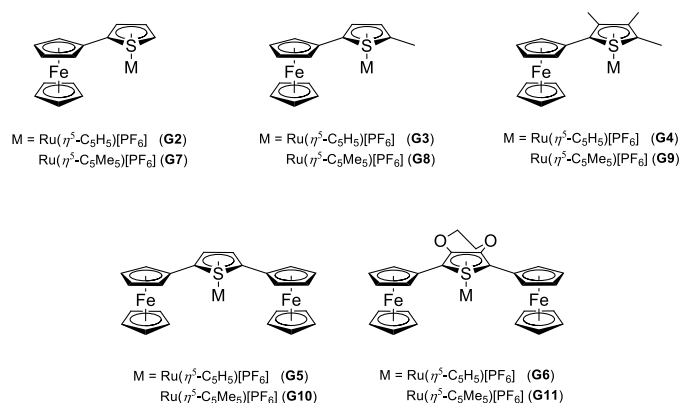


M = Ru($\eta^5$-C$_5$H$_5$)[PF$_6$]  (**G2**)
      Ru($\eta^5$-C$_5$Me$_5$)[PF$_6$] (**G7**)

M = Ru($\eta^5$-C$_5$H$_5$)[PF$_6$]  (**G3**)
      Ru($\eta^5$-C$_5$Me$_5$)[PF$_6$] (**G8**)

M = Ru($\eta^5$-C$_5$H$_5$)[PF$_6$]  (**G4**)
      Ru($\eta^5$-C$_5$Me$_5$)[PF$_6$] (**G9**)

M = Ru($\eta^5$-C$_5$H$_5$)[PF$_6$]  (**G5**)
      Ru($\eta^5$-C$_5$Me$_5$)[PF$_6$] (**G10**)

M = Ru($\eta^5$-C$_5$H$_5$)[PF$_6$]  (**G6**)
      Ru($\eta^5$-C$_5$Me$_5$)[PF$_6$] (**G11**)

**Abbildung H7**. Rutheniumkomplexe **G2** – **G11**.

Dieser Umstand kann durch die Anwendung stärker solvatisierender Lösungsmittel und (kleiner) Anionen umgangen werden. In diesem Zusammenhang konnte nun gezeigt werden, dass die thermodynamische Stabilität der gemischtvalenten Diferrocenylthiophen-Kationen durch eine Komplexierung von [Ru($\eta^5$-C$_5$H$_5$)]⁺/[Ru($\eta^5$-C$_5$Me$_5$)]⁺-Fragmenten abnimmt, wobei die Methylierung des Cyclopentadienyl-Liganden diesbezüglich keinen wesentlichen Einfluss hat. Die Abnahme der elektronischen Kopplung konnte in UV-Vis-NIR-spektroelektrochemischen Untersuchungen verifiziert werden.

## DANKSAGUNG

# REFERENCES

(1)     Van Delft, D.; Kes, P. *Phys. Today* **2010**, *63*, 38–43.

(2)     Imada, M.; Fujimori, A.; Tokura, Y. *Rev. Mod. Phys.* **1998**, *70*, 1039–1263.

(3)     Hilgenkamp, H.; Mannhart, J. *Rev. Mod. Phys.* **2002**, *74*, 485–549.

(4)     *http://commons.wikimedia.org/wiki/File%3ACERN-cables-p1030764.jpg, by Rama (Own work) [CC BY-SA 2.0 fr (http://creativecommons.org/licenses/by-sa/2.0/fr/deed.en)], via Wikimedia Commons from Wikimedia Commons.*

(5)     Farinola, G. M.; Ragni, R. *Chem. Soc. Rev.* **2011**, *40*, 3467–3482.

(6)     Natta, G.; Mazzanti, G.; Corradini, P. *Atti. accad. Naz. Lincei, Rend. Sc. fis. mat. e nat.* **1958**, *25*, 3–12.

(7)     Shirakawa, H. *Synth. Met.* **1995**, *69*, 3–8.

(8)     Ito, T.; Shirakawa, H.; Ikeda, S. *J. Polym. Sci. - Polym. Chem. Ed.* **1974**, *12*, 11–20.

(9)     Shirakawa, H.; Louis, E. J.; MacDiarmid, A. G.; Chiang, C. K.; Heeger, A. J. *J. Chem. Soc. Chem. Commun.* **1977**, 578–580.

(10)    Chiang, C. K.; Fincher, C. R.; Park, Y. W.; Heeger, a. J.; Shirakawa, H.; Louis, E. J.; Gau, S. C.; MacDiarmid, A. G. *Phys. Rev. Lett.* **1977**, *39*, 1098–1101.

(11)    Chiang, C. K.; Druy, M. A.; Gau, S. C.; Heeger, A. J.; Louis, E. J.; MacDiarmid, A. G.; Park, Y. W.; Shirakawa, H. *J. Am. Chem. Soc.* **1978**, *100*, 1013–1015.

(12)    MacDiarmid, A. G. *Synth. Met.* **1997**, *84*, 27–34.

(13)    Heeger, A. J. *Angew. Chem. Int. Ed.* **2001**, *40*, 2591–2611.

(14)    MacDiarmid, A. G. *Angew. Chem. Int. Ed.* **2001**, *40*, 2581–2590.

(15)    Jonas, F.; Heywang, G.; Schmidtberg, W. Preparation of (alkylenedioxy)thiophene polymers for use as antistatic agents. DE 3813589 A1 19891102, 1989.

(16)    Jonas, F.; Heywang, G. *Electrochim. Acta* **1994**, *39*, 1345–1347.

(17)    Jonas, F.; Morrison, J. T. *Synth. Met.* **1997**, *85*, 1397–1398.

(18)    Groenendaal, L.; Jonas, F.; Freitag, D.; Pielartzik, H.; Reynolds, J. R. *Adv. Mater.* **2000**, *12*, 481–494.

(19)    Zhang, D.; Ryu, K.; Liu, X.; Polikarpov, E.; Ly, J.; Tompson, M. E.; Zhou, C. *Nano Lett.* **2006**, *6*, 1880–1886.

(20)    Kim, Y. H.; Lee, J.; Hofmann, S.; Gather, M. C.; Müller-Meskamp, L.; Leo, K. *Adv. Funct. Mater.* **2013**, *23*, 3763–3769.

(21)    Roncali, J.; Blanchard, P.; Frère, P. *J. Mater. Chem.* **2005**, *15*, 1589–1610.

(22)    Ohtsuka, T. *Int. J. Corros.* **2012**, *2012*, 1–7.

(23)    Tan, C. K.; Blackwood, D. J. *Corros. Sci.* **2003**, *45*, 545–557.

(24)    Ocón, P.; Cristobal, a. B.; Herrasti, P.; Fatas, E. *Corros. Sci.* **2005**, *47*, 649–662.

(25)    Roncali, J. *Chem. Rev.* **1992**, *92*, 711–738.

(26)    Roncali, J. *Chem. Rev.* **1997**, *97*, 173–206.

(27)    Zhang, L.; Li, M.; Wang, C.; Lai, G.; Shen, Y. *Polym. Bull.* **2012**, *70*, 353–369.

(28)   Heywang, G.; Jonas, F. *Adv. Mater.* **1992**, *4*, 116–118.

(29)   Holliday, B. J.; Swager, T. M. *Chem. Commun.* **2005**, 23–36.

(30)   Zhu, Y.; Wolf, M. O. *Chem. Mater.* **1999**, *11*, 2995–3001.

(31)   Zhu, Y.; Wolf, M. O. *J. Am. Chem. Soc.* **2000**, *122*, 10121–10125.

(32)   Apperloo, J. J.; Groenendaal, L. B.; Verheyen, H.; Jayakannan, M.; Janssen, R. A. J.; Dkhissi, A.; Beljonne, D.; Lazzaroni, R.; Brédas, J.-L. *Chem. - A Eur. J.* **2002**, *8*, 2384–2396.

(33)   Kishida, M.; Muratsugu, S.; Sakamoto, R.; Kusamoto, T.; Nishihara, H. *Chem. Lett.* **2013**, *42*, 361–362.

(34)   Thomas, K. R. J.; Lin, J. T.; Wen, Y. S. *Organometallics* **2000**, *19*, 1008–1012.

(35)   Thomas, K. R. J.; Lin, J. T. *J. Organomet. Chem.* **2001**, *637-639*, 139–144.

(36)   Brisset, H.; Navarro, A.-E.; Moggia, F.; Jousselme, B.; Blanchard, P.; Roncali, J. *J. Electroanal. Chem.* **2007**, *603*, 149–154.

(37)   Heckmann, A.; Lambert, C. *Angew. Chem. Int. Ed.* **2012**, *51*, 326–392.

(38)   Ceccon, A.; Santi, S.; Orian, L.; Bisello, A. *Coord. Chem. Rev.* **2004**, *248*, 683–724.

(39)   Mishra, A.; Ma, C.-Q.; Bäuerle, P. *Chem. Rev.* **2009**, *109*, 1141–1276.

(40)   Tour, J. M. *Acc. Chem. Res.* **2000**, *33*, 791–804.

(41)   Debroy, P.; Roy, S. *Coord. Chem. Rev.* **2007**, *251*, 203–221.

(42)   Coletti, C.; Marrone, A.; Re, N. *Acc. Chem. Res.* **2012**, *45*, 139–149.

(43)   Paul, F.; Lapinte, C. *Coord. Chem. Rev.* **1998**, *178-180*, 431–509.

(44)   Ward, M. D. *Chem. Soc. Rev.* **1995**, *24*, 121–134.

(45)   Akita, M.; Koike, T. *Dalt. Trans.* **2008**, *9226*, 3523–3530.

(46)   Barigelletti, F.; Flamigni, L. *Chem. Soc. Rev.* **2000**, *29*, 1–12.

(47)   Barlow, S.; O'Hare, D. *Chem. Rev.* **1997**, *97*, 637–670.

(48)   Hildebrandt, A.; Lang, H. *Organometallics* **2013**, *32*, 5640–5653.

(49)   Demadis, K. D.; Hartshorn, C. M.; Meyer, T. J. *Chem. Rev.* **2001**, *101*, 2655–2686.

(50)   Brunschwig, B. S.; Creutz, C.; Sutin, N. *Chem. Soc. Rev.* **2002**, *31*, 168–184.

(51)   Aguirre-Etcheverry, P.; O'Hare, D. *Chem. Rev.* **2010**, *110*, 4839–4864.

(52)   Holleman, A. F.; Wiberg, N.; Wiberg, E.; Fischer, G. *Lehrbuch der Anorganischen Chemie*; Walter de Gruyter: Berlin, New York, 2007.

(53)   Huheey, J. E.; Keiter, E. A.; Keiter, R. L. *Anorganische Chemie*; DE GRUYTER: Berlin, Boston, 2012.

(54)   Marcus, R. A. *J. Chem. Phys.* **1956**, *24*, 966–978.

(55)   Marcus, R. A. *Rev. Mod. Phys.* **1993**, *65*, 599–610.

(56)   Creutz, C. In *Progress in Inorganic Chemistry*; 1983; pp. 1–73.

(57)   D'Alessandro, D. M.; Keene, F. R. *Chem. Soc. Rev.* **2006**, *35*, 424–440.

(58)   Blackbourn, R. L.; Hupp, J. T. *J. Phys. Chem.* **1990**, *94*, 1788–1793.

(59)   Reimers, J. R.; Hush, N. S. *Inorg. Chem.* **1990**, *29*, 4510–4513.

(60)   Hush, N. S. *Electrochim. Acta* **1968**, *13*, 1005–1023.

(61)   Barlow, S. *Inorg. Chem.* **2001**, *40*, 7047–7053.

(62)   Nelsen, S. F.; Ismagilov, R. F.; Trieber II, D. A. *Science* **1997**, *278*, 846–849.

(63)   Lambert, C.; Nöll, G. *J. Am. Chem. Soc.* **1999**, *121*, 8434–8442.

(64)   Creutz, C.; Newton, M. D.; Sutin, N. *J. Photochem. Photobiol. A Chem.* **1994**, *82*, 47–59.

(65)   Piepho, S. B.; Krausz, E. R.; Schatz, P. N. *J. Am. Chem. Soc.* **1978**, *100*, 2996–3005.

(66)   Piepho, S. B. *J. Am. Chem. Soc.* **1990**, *112*, 4197–4206.

(67)   Talham, D. R.; Cowan, D. O. *Organometallics* **1984**, *3*, 1712–1715.

(68)   Robin, M. B.; Day, P. *Adv. Inorg. Chem. Radiochem.* **1968**, *10*, 247–422.

(69)   Keene, R. F. *Coord. Chem. Rev.* **1999**, *187*, 121–149.

(70)   Breuer, R.; Schmittel, M. *Organometallics* **2013**, *32*, 5980–5987.

(71)   Badger, B.; Brocklehurst, B. *Trans. Faraday Soc.* **1969**, *65*, 2576–2581.

(72)   Astruc, D. *Electron Transfer and Radical Processes in Transition-Metal Chemistry*; John Wiley & Sons Inc.: New York, 1995.

(73)   Brunschwig, B. S.; Sutin, N. *Coord. Chem. Rev.* **1999**, *187*, 233–254.

(74)   Winter, R. F. *Organometallics* **2014**, *33*, 4517–4536.

(75)   Kosloff, R.; Ratner, M. A. *Isr. J. Chem.* **1990**, *30*, 45–58.

(76)   Ratner, M. A. *J. Phys. Chem.* **1990**, *94*, 4877–4883.

(77)   Geiger, W. E. *Organometallics* **2007**, *26*, 5738–5765.

(78)   Connelly, N. G.; Geiger, W. E. *Chem. Rev.* **1996**, *96*, 877–910.

(79)   Kolbe, H. *Justus Liebigs Ann. Chem.* **1848**, *64*, 339–341.

(80)   Bard, A. J.; Faulkner, L. R. *Electrochemical Methods: Fundamentals and Applications*; 2nd ed.; John Wiley & Sons, Inc.: New York, 2001.

(81)   Wang, J. *Analytical Electrochemistry*; 3rd ed.; John Wiley & Sons Inc.: New York, 2006.

(82)   Cottrell, F. G. *Zeitschrift für Phys. Chemie* **1903**, *42*, 385–431.

(83)   Maloy, J. T. *J. Chem. Educ.* **1983**, *60*, 285–288.

(84)   Meites, L.; Zuman, P.; Nürnberg, H. W. *Pure Appl. Chem.* **1985**, *57*, 1491–1505.

(85)   Mabbott, G. A. *J. Chem. Educ.* **1983**, *60*, 697–701.

(86)   Evans, D. H.; O'Connell, K. M.; Petersen, R. A.; Kelly, M. J.; Kissinger, P. T.; Heineman, W. R. *J. Chem. Educ.* **1983**, *60*, 702–706.

(87)   Parsons, R. *Pure Appl. Chem.* **1974**, *37*, 499–516.

(88)   Osteryoung, J. G.; Osteryoung, R. A. *Anal. Chem.* **1985**, *57*, 101A – 110A.

(89) LeSuer, R. J.; Geiger, W. E. *Angew. Chem. Int. Ed.* **2000**, *39*, 248–250.

(90) Barrière, F.; Camire, N.; Geiger, W. E.; Mueller-Westerhoff, U. T.; Sanders, R. *J. Am. Chem. Soc.* **2002**, *124*, 7262–7263.

(91) Krossing, I.; Raabe, I. *Angew. Chem. Int. Ed.* **2004**, *43*, 2066–2090.

(92) Seppelt, K. *Angew. Chem. Int. Ed. Engl.* **1993**, *32*, 1025–1027.

(93) Yoshida, J.-I.; Sugawara, M.; Tatsumi, M.; Kise, N. *J. Org. Chem.* **1998**, *63*, 5950–5961.

(94) Brandl, M.; Ebner, A.; Kubicki, M. M.; Mugnier, Y.; Wachter, J.; Vigier-Juteau, E.; Zabel, M. *Eur. J. Inorg. Chem.* **2007**, 994–1003.

(95) Geiger, W. E. In *Electroanalytical Chemistry: A Series of Advances*; Bard, A. J.; Zoski, C. G., Eds.; CRC Press: New York, 2013; pp. 179–222.

(96) Bochmann, M. *Angew. Chem. Int. Ed. Engl.* **1992**, *31*, 1181–1182.

(97) Pal, P. K.; Chowdhury, S.; Drew, M. G. B.; Datta, D. *New J. Chem.* **2002**, *26*, 367–371.

(98) Camire, N.; Mueller-Westerhoff, U. T.; Geiger, W. E. *J. Organomet. Chem.* **2001**, *637-639*, 823–826.

(99) Nafady, A.; Chin, T. T.; Geiger, W. E. *Organometallics* **2006**, *25*, 1654–1663.

(100) Barrière, F.; Geiger, W. E. *J. Am. Chem. Soc.* **2006**, *128*, 3980–3989.

(101) LeSuer, R. J.; Buttolph, C.; Geiger, W. E. *Anal. Chem.* **2004**, *76*, 6395–6401.

(102) Strauss, S. H. *Chem. Rev.* **1993**, *93*, 927–942.

(103) Ceroni, P.; Paolucci, F.; Paradisi, C.; Juris, A.; Roffia, S.; Serroni, S.; Campagna, S.; Bard, A. J. *J. Am. Chem. Soc.* **1998**, *120*, 5480–5487.

(104) Garcia, E.; Kwak, J.; Bard, A. J. *Inorg. Chem.* **1988**, *27*, 4377–4382.

(105) Geiger, W. E.; Barrière, F. *Acc. Chem. Res.* **2010**, *43*, 1030–1039.

(106) Stewart, M. P.; Paradee, L. M.; Raabe, I.; Trapp, N.; Slattery, J. S.; Krossing, I.; Geiger, W. E. *J. Fluor. Chem.* **2010**, *131*, 1091–1095.

(107) Yakelis, N. A.; Bergman, R. G. *Organometallics* **2005**, *24*, 3579–3581.

(108) Cameron, T. S.; Decken, A.; Dionne, I.; Fang, M.; Krossing, I.; Passmore, J. *Chem. Eur. J.* **2002**, *8*, 3386–3401.

(109) Raabe, I.; Wagner, K.; Guttsche, K.; Wang, M.; Grätzel, M.; Santiso-Quiñones, G.; Krossing, I. *Chem. Eur. J.* **2009**, *15*, 1966–1976.

(110) Krossing, I. *Chem. Eur. J.* **2001**, *7*, 490–502.

(111) Klotz, I. M.; Czerlinski, G. H.; Fiess, H. A. *J. Am. Chem. Soc.* **1958**, *80*, 2920–2923.

(112) Powell, H. M. *Proc. Chem. Soc.* **1959**, 73–75.

(113) Wurster, C.; Morley, H. F. *Berichte der Dtsch. Chem. Gesellschaft* **1879**, *12*, 1814–1815.

(114) Creutz, C.; Taube, H. *J. Am. Chem. Soc.* **1969**, *91*, 3988–3989.

(115) Cowan, D. O.; Kaufman, F. *J. Am. Chem. Soc.* **1970**, *92*, 6198–6204.

(116) Levanda, C.; Bechgaard, K.; Cowan, D. O. *J. Org. Chem.* **1976**, *41*, 2700–2704.

(117) Cowan, D. O.; Levanda, C. *J. Am. Chem. Soc.* **1972**, *94*, 9271–9272.

(118) Reimers, J. R.; Cai, Z.-L.; Hush, N. S. *Chem. Phys.* **2005**, *319*, 39–51.

(119) Kaim, W.; Sarkar, B. *Coord. Chem. Rev.* **2007**, *251*, 584–594.

(120) LeVanda, C.; Bechgaard, K.; Cowan, D. O.; Mueller-Westerhoff, U. T.; Eilbracht, P.; Candela, G. A.; Collins, R. L. *J. Am. Chem. Soc.* **1976**, *98*, 3181–3187.

(121) Dong, T.-Y.; Schei, C.-C. *J. Organomet. Chem.* **1993**, *447*, 107–111.

(122) Powers, M. J.; Meyer, T. J. *J. Am. Chem. Soc.* **1978**.

(123) Chen, P.; Meyer, T. J. *Chem. Rev.* **1998**, *98*, 1439–1478.

(124) Blackbourn, R. L.; Hupp, J. T. *Chem. Phys. Lett.* **1988**, *150*, 399–405.

(125) Lowery, M. D.; Hammack, W. S.; Drickamer, H. G.; Hendrickson, D. N. *J. Am. Chem. Soc.* **1987**, *109*, 8019–8024.

(126) Warratz, R.; Aboulfadl, H.; Bally, T.; Tuczek, F. *Chem. - A Eur. J.* **2009**, *15*, 1604–1617.

(127) Warratz, R.; Tuczek, F. *Inorg. Chem.* **2009**, *48*, 3591–3607.

(128) Bell, F. A.; Ledwith, A.; Sherrington, D. C. *J. Chem. Soc. C* **1969**, 2719–2720.

(129) Ambrose, J. F.; C., L. L.; Nelson, R. F. *J. Electrochem. Soc.* **1975**, *122*, 876–894.

(130) Wu, X.; Davis, A. P.; Lambert, P. C.; Steffen, L. K.; Toy, O.; Fry, A. J. *Tetrahedron* **2009**, *65*, 2408–2414.

(131) Lambert, C.; Nöll, G. *Angew. Chem. Int. Ed.* **1998**, *37*, 2107–2110.

(132) Amthor, S.; Lambert, C. *J. Phys. Chem. A* **2006**, *110*, 1177–1189.

(133) Stoll, M. E.; Lovelace, S. R.; Geiger, W. E.; Schimanke, H.; Hyla-Kryspin, I.; Gleiter, R. *J. Am. Chem. Soc.* **1999**, *121*, 9343–9351.

(134) Kasahara, A.; Izumi, T.; Yoshida, Y.; Shimizu, I. *Bull. Chem. Soc. Jpn.* **1982**, *55*, 1901–1906.

(135) Lee, M. T.; Foxman, B. M.; Rosenblum, M. *Organometallics* **1985**, *4*, 539–547.

(136) Mücke, P.; Winter, R. F.; Novak, I.; Kowalski, K. *J. Organomet. Chem.* **2012**, *717*, 14–22.

(137) Mücke, P.; Winter, R. F.; Kowalski, K. *J. Organomet. Chem.* **2013**, *735*, 10–14.

(138) Lyssenko, K. A.; Antipin, M. Y.; Antonov, D. Y. *ChemPhysChem* **2003**, *4*, 817–823.

(139) Caramori, G. F.; Galembeck, S. E. *J. Phys. Chem. A* **2007**, *111*, 1705–1712.

(140) Lin, H.-C.; Jin, B.-Y. *J. Phys. Chem. A* **2008**, *112*, 2948–2954.

(141) Grimme, S. *Chem. Eur. J.* **2004**, *10*, 3423–3429.

(142) Kattnig, D. R.; Mladenova, B.; Grampp, G.; Kaiser, C.; Heckmann, A.; Lambert, C. *J. Phys. Chem. C* **2009**, *113*, 2983–2995.

(143) Foxman, B. M.; Rosenblum, M.; Sokolov, V.; Khrushchova, N. *Organometallics* **1993**, *12*, 4805–4809.

(144) Atzkern, H.; Huber, B.; Köhler, F. H.; Müller, G.; Müller, R. *Organometallics* **1991**, *10*, 238–244.

(145) Morrison, W. H.; Krogsrud, S.; Hendrickson, D. N. *Inorg. Chem.* **1973**, *12*, 1998–2004.

(146) Ferguson, G.; Glidewell, C.; Opromolla, G.; Zakaria, C. M.; Zanello, P. *J. Organomet. Chem.* **1996**, *517*, 183–190.

(147) Jones, S. C.; Barlow, S.; O'Hare, D. *Chem. Eur. J.* **2005**, *11*, 4473–4481.

(148) Nowicka, A. M.; Stojek, Z.; Ciszkowska, M. *Anal. Lett.* **2005**, *37*, 979–994.

(149) Delgado-Pena, F.; Talham, D. R.; Cowan, D. O. *J. Organomet. Chem.* **1983**, *253*, C43–C46.

(150) Chen, Y. J.; Pan, D.-S.; Chiu, C.-F.; Su, J.-X.; Lin, S. J.; Kwan, K. S. *Inorg. Chem.* **2000**, *39*, 953–958.

(151) Son, K.-I.; Kang, S.-Y.; Oh, Y. E.; Noh, D.-Y. *J. Korean Chem. Soc.* **2009**, *53*, 79–83.

(152) Poppitz, E. A.; Hildebrandt, A.; Korb, M.; Lang, H. *J. Organomet. Chem.* **2014**, *752*, 133–140.

(153) Ribou, A.-C.; Launay, J.-P.; Sachtleben, M. L.; Li, H.; Spangler, C. W. *Inorg. Chem.* **1996**, *35*, 3735–3740.

(154) Barlow, S.; Risko, C.; Coropceanu, V.; Tucker, N. M.; Jones, S. C.; Levi, Z.; Khrustalev, V. N.; Antipin, M. Y.; Kinnibrugh, T. L.; Timofeeva, T.; Marder, S. R.; Brédas, J.-L. *Chem. Commun.* **2005**, *377*, 764–766.

(155) Barlow, S.; Risko, C.; Chung, S.-J.; Tucker, N. M.; Coropceanu, V.; Jones, S. C.; Levi, Z.; Brédas, J.-L.; Marder, S. R. *J. Am. Chem. Soc.* **2005**, *127*, 16900–16911.

(156) Dong, T. Y.; Ke, T. J.; Peng, S. M.; Yeh, S. K. *Inorg. Chem.* **1989**, *28*, 2103–2106.

(157) Bildstein, B.; Schweiger, M.; Kopacka, H.; Wurst, K. *J. Organomet. Chem.* **1998**, *553*, 73–81.

(158) Bildstein, B.; Loza, O.; Chizhov, Y. *Organometallics* **2004**, *23*, 1825–1835.

(159) Skibar, W.; Kopacka, H.; Wurst, K.; Salzmann, C.; Ongania, K. H.; De Biani, F. F.; Zanello, P.; Bildstein, B. *Organometallics* **2004**, *23*, 1024–1041.

(160) Bildstein, B.; Kopacka, H.; Schweiger, M.; Ellmerer-Müller, E.; Ongania, K.-H.; Wurst, K. *Organometallics* **1996**, *15*, 4398–4406.

(161) Bildstein, B.; Schweiger, M.; Angleitner, H.; Kopacka, H.; Wurst, K.; Ongania, K.-H.; Fontani, M.; Zanello, P. *Organometallics* **1999**, *18*, 4286–4295.

(162) Bildstein, B. *Coord. Chem. Rev.* **2000**, *206-207*, 369–394.

(163) Jin, B.; Tao, F.; Liu, P. *J. Electroanal. Chem.* **2008**, *624*, 179–185.

(164) Patoux, C.; Coudret, C.; Launay, J.-P.; Joachim, C.; Gourdon, A. *Inorg. Chem.* **1997**, *36*, 5037–5049.

(165) Hollis Jr., W. G.; Bonsall, T. F.; Cuba, V. L.; Deck, P. A.; Fronczek, F. R. *Transit. Met. Chem.* **2006**, *31*, 246–249.

(166) Pfaff, U.; Hildebrandt, A.; Schaarschmidt, D.; Hahn, T.; Liebing, S.; Kortus, J.;

Lang, H. *Organometallics* **2012**, *31*, 6761–6771.

(167) Iyoda, M.; Kondo, T.; Okabe, T.; Matsuyama, H.; Sasaki, S.; Kuwatani, Y. *Chem. Lett.* **1997**, *26*, 35–36.

(168) Wang, Y.-Q.; Han, L.-M.; Suo, Q.-L.; Zhu, N.; Hao, J.-M.; Xie, R.-J. *Polyhedron* **2013**, *54*, 221–227.

(169) Braunschweig, H.; Breher, F.; Chiu, C.-W.; Gamon, D.; Nied, D.; Radacki, K. *Angew. Chem. Int. Ed.* **2010**, *49*, 8975–8978.

(170) Braunschweig, H.; Chiu, C.-W.; Gamon, D.; Kaupp, M.; Krummenacher, I.; Kupfer, T.; Müller, R.; Radacki, K. *Chem. Eur. J.* **2012**, *18*, 11732–11746.

(171) Hildebrandt, A.; Schaarschmidt, D.; Claus, R.; Lang, H. *Inorg. Chem.* **2011**, *50*, 10623–10632.

(172) Gidron, O.; Diskin-Posner, Y.; Bendikov, M. *Chem. Eur. J.* **2013**, *19*, 13140–13150.

(173) Miesel, D.; Hildebrandt, A.; Korb, M.; Low, P. J.; Lang, H. *Organometallics* **2013**, *32*, 2993–3002.

(174) Miesel, D.; Hildebrandt, A.; Korb, M.; Wild, D. A.; Low, P. J.; Lang, H. *Chem. Eur. J.* **2015**, *21*, 11545–11559.

(175) Miesel, D.; Hildebrandt, A.; Korb, M.; Schaarschmidt, D.; Lang, H. *Organometallics* **2015**, *34*, 4293–4304.

(176) Lehrich, S. W.; Hildebrandt, A.; Korb, M.; Lang, H. *J. Organomet. Chem.* **2015**, *792*, 37–45.

(177) Korb, M.; Pfaff, U.; Hildebrandt, A.; Rüffer, T.; Lang, H. *Eur. J. Inorg. Chem.* **2014**, *2014*, 1051–1061.

(178) Pfaff, U.; Hildebrandt, A.; Schaarschmidt, D.; Rüffer, T.; Low, P. J.; Lang, H. *Organometallics* **2013**, *32*, 6106–6117.

(179) Hildebrandt, A.; Schaarschmidt, D.; Lang, H. *Organometallics* **2011**, *30*, 556–563.

(180) Hildebrandt, A.; Lang, H. *Dalt. Trans.* **2011**, *40*, 11831–11837.

(181) Goetsch, W. R.; Solntsev, P. V.; Van Stappen, C.; Purchel, A. A.; Dudkin, S. V.; Nemykin, V. N. *Organometallics* **2014**, *33*, 145–157.

(182) Lehrich, S. W.; Hildebrandt, A.; Rüffer, T.; Korb, M.; Low, P. J.; Lang, H. *Organometallics* **2014**, *33*, 4836–4845.

(183) Hildebrandt, A.; Rüffer, T.; Erasmus, E.; Swarts, J. C.; Lang, H. *Organometallics* **2010**, *29*, 4900–4905.

(184) Kowalski, K.; Winter, R. F. *J. Organomet. Chem.* **2009**, *694*, 1041–1048.

(185) Pfaff, U.; Hildebrandt, A.; Korb, M.; Lang, H. *Polyhedron* **2015**, *86*, 2–9.

(186) Kaleta, K.; Hildebrandt, A.; Strehler, F.; Arndt, P.; Jiao, H.; Spannenberg, A.; Lang, H.; Rosenthal, U. *Angew. Chem. Int. Ed.* **2011**, *50*, 11248–11252.

(187) Kaleta, K.; Strehler, F.; Hildebrandt, A.; Beweries, T.; Rüffer, T.; Spannenberg, A.; Lang, H.; Rosenthal, U. *Chem. Eur. J.* **2012**, *18*, 12672–12680.

(188) Becker, L.; Strehler, F.; Korb, M.; Arndt, P.; Spannenberg, A.; Baumann, W.; Lang, H.; Rosenthal, U. *Chem. Eur. J.* **2014**, *20*, 3061–3068.

(189) Hildebrandt, A.; Pfaff, U.; Lang, H. *Rev. Inorg. Chem.* **2011**, *31*, 111–141.

(190) Sato, M.; Arita, S.; Kawajiri, K.; Isayama, A. *Chem. Lett.* **2013**, *42*, 1571–1573.

(191) Sato, M.; Fukui, K. *Synth. Met.* **2007**, *157*, 619–626.

(192) Sato, M.; Fukui, K.; Kashiwagi, S.; Hiroi, M. *Jpn. J. Appl. Phys.* **2000**, *39*, L939–L941.

(193) Sato, M.; Fukui, K.; Sakamoto, M.; Kashiwagi, S.; Hiroi, M. *Thin Solid Films* **2001**, *393*, 210–216.

(194) Sato, M.; Sakamoto, M.; Sugano, Y.; Hiroi, M. *Synth. Met.* **2001**, *121*, 1285–1286.

(195) Ogawa, S.; Kikuta, K.; Muraoka, H.; Saito, F.; Sato, R. *Tetrahedron Lett.* **2006**, *47*, 2887–2891.

(196) Ogawa, S.; Muraoka, H.; Kikuta, K.; Saito, F.; Sato, R. *J. Organomet. Chem.* **2007**, *692*, 60–69.

(197) Nishikawa, H.; Ogawa, S. Organic compounds or organometallic compounds for semiconductor devices. JP20070139624 20070525, 2008.

(198) Paul, F.; Goeb, S.; Justaud, F.; Argouarch, G.; Toupet, L.; Ziessel, R. F.; Lapinte, C. *Inorg. Chem.* **2007**, *46*, 9036–9038.

(199) Bildstein, B.; Malaun, M.; Kopacka, H.; Fontani, M.; Zanello, P. *Inorg. Chim. Acta* **2000**, *300-302*, 16–22.

(200) Mathur, P.; Chatterjee, S.; Das, A.; Lahiri, G. K.; Maji, S.; Mobin, S. M. *J. Organomet. Chem.* **2007**, *692*, 1601–1607.

(201) Packheiser, R.; Lohan, M.; Bräuer, B.; Justaud, F.; Lapinte, C.; Lang, H. *J. Organomet. Chem.* **2008**, *693*, 2898–2902.

(202) Packheiser, R.; Ecorchard, P.; Walfort, B.; Lang, H. *J. Organomet. Chem.* **2008**, *693*, 933–946.

(203) Richardson, D. E.; Taube, H. *Coord. Chem. Rev.* **1984**, *60*, 107–129.

(204) Bruce, M. I. *Coord. Chem. Rev.* **1997**, *166*, 91–119.

(205) Ratner, M. A.; Jortner, J. *Molecular Electronics*; Chemistry for the 21st century; Blackwell Science: Malden, MA, 1997.

(206) Collier, C. P.; Wong, E. W.; Belohradský, M.; Raymo, F. M.; Stoddart, J. F.; Kuekes, P. J.; Williams, R. S.; Heath, J. R. *Science* **1999**, *285*, 391–394.

(207) Carroll, R. L.; Gorman, C. B. *Angew. Chem. Int. Ed.* **2002**, *41*, 4378–4400.

(208) Robertson, N.; McGowan, C. A. *Chem. Soc. Rev.* **2003**, *32*, 96–103.

(209) Hildebrandt, A.; Schaarschmidt, D.; van As, L.; Swarts, J. C.; Lang, H. *Inorg. Chim. Acta* **2011**, *374*, 112–118.

(210) Speck, J. M.; Schaarschmidt, D.; Lang, H. *Organometallics* **2012**, *31*, 1975–1982.

(211) Auger, A.; Muller, A. J.; Swarts, J. C. *Dalt. Trans.* **2007**, 3623–3633.

(212) Swarts, J. C.; Swarts, D. M.; Maree, D. M.; Neuse, E. W.; La Madeleine, C.; Van Lier, J. E. *Anticancer Res.* **2001**, *21*, 2033–2037.

(213) Swarts, J. C.; Vosloo, T. G.; Cronje, S. J.; Du Plessis, W. C.; Van Rensburg, C. E.

J.; Kreft, E.; Van Lier, J. E. *Anticancer Res.* **2008**, *28*, 2781–2784.

(214) Weber, B.; Serafin, A.; Michie, J.; Van Rensburg, C. E. J.; Swarts, J. C.; Bohm, L. *Anticancer Res.* **2004**, *24*, 763–770.

(215) Fourie, E.; Erasmus, E.; Swarts, J. C.; Jakob, A.; Lang, H.; Joone, G. K.; Van Rensburg, C. E. J. *Anticancer Res.* **2011**, *31*, 825–829.

(216) Klapars, A.; Campos, K. R.; Chen, C.-Y.; Volante, R. P. *Org. Lett.* **2005**, *7*, 1185–1188.

(217) Shen, Q.; Shekhar, S.; Stambuli, J. P.; Hartwig, J. F. *Angew. Chem. Int. Ed.* **2005**, *44*, 1371–1375.

(218) Percec, V.; Bae, J.-Y.; Hill, D. H. *J. Org. Chem.* **1995**, *60*, 1060–1065.

(219) Conradie, J.; Lamprecht, G. J.; Roodt, A.; Swarts, J. C. *Polyhedron* **2007**, *26*, 5075–5087.

(220) Conradie, J.; Swarts, J. C. *Organometallics* **2009**, *28*, 1018–1026.

(221) Swarts, P. J.; Immelman, M.; Lamprecht, G. J.; Greyling, S. E.; Swarts, J. C. *South African J. Chem.* **1997**, *50*, 208–216.

(222) Spänig, F.; Kovacs, C.; Hauke, F.; Ohkubo, K.; Fukuzumi, S.; Guldi, D. M.; Hirsch, A. *J. Am. Chem. Soc.* **2009**, *131*, 8180–8195.

(223) Yu, Y.; Bond, A. D.; Leonard, P. W.; Lorenz, U. J.; Timofeeva, T. V.; Vollhardt, K. P. C.; Whitener, G. D.; Yakovenko, A. A. *Chem. Commun.* **2006**, 2572–2574.

(224) Diallo, A. K.; Daran, J.-C.; Varret, F.; Ruiz, J.; Astruc, D. *Angew. Chem. Int. Ed.* **2009**, *48*, 3141–3145.

(225) Kowalski, K.; Winter, R. F. *J. Organomet. Chem.* **2008**, *693*, 2181–2187.

(226) Nesmeyanov, A. N.; Sazonova, V. A.; Drozd, V. N. *Dokl. Akad. Nauk SSSR* **1964**, *154*, 158.

(227) Liu, C.-M.; Chen, B.-H.; Liu, W.-Y.; Wu, X.-L.; Ma, Y.-X. *J. Organomet. Chem.* **2000**, *598*, 348–352.

(228) Negishi, E.; King, A. O.; Okukado, N. *J. Org. Chem.* **1977**, *42*, 1821–1823.

(229) Clark, H. C.; Goel, A. B.; Goel, R. G.; Goel, S.; Ogini, W. O. *Inorg. Chim. Acta* **1978**, *31*, L441–L442.

(230) Goel, A. B.; Goel, S. *Inorg. Chim. Acta* **1985**, *98*, 67–70.

(231) Mathur, P.; Singh, A. K.; Singh, V. K.; Singh, P.; Rahul, R.; Mobin, S. M.; Thöne, C. *Organometallics* **2005**, *24*, 4793–4798.

(232) Yu, Y.; Bond, A. D.; Leonard, P. W.; Vollhardt, K. P. C.; Whitener, G. D. *Angew. Chem. Int. Ed.* **2006**, *45*, 1794–1799.

(233) Smith, M. B.; March, J. *March's Advanced Organic Chemistry: Reactions, Mechanisms, and Structure*; 5th ed.; John Wiley & Sons Inc.: New York, 2001.

(234) Evans, D. H.; O'Connell, K. M.; Petersen, R. A.; Kelly, M. J. *J. Chem. Educ.* **1983**, *60*, 290–293.

(235) Kissinger, P. T.; Heineman, W. R. *J. Chem. Educ.* **1983**, *60*, 702–706.

(236) Van Benschoten, J.; Lewis, J. Y.; Heineman, W. R.; Roston, D. A.; Kissinger, P. T.

*J. Chem. Educ.* **1983**, *60*, 772–775.

(237) Gericke, H. J.; Barnard, N. I.; Erasmus, E.; Swarts, J. C.; Cook, M. J.; Aquino, M. A. S. *Inorg. Chim. Acta* **2010**, *363*, 2222–2232.

(238) Krejčik, M.; Daněk, M.; Hartl, F. *J. Electroanal. Chem.* **1991**, *317*, 179–187.

(239) Sohn, Y. S.; Hendrickson, D. N.; Gray, H. B. *J. Am. Chem. Soc.* **1971**, *93*, 3603–3612.

(240) Duggan, D. M.; Hendrickson, D. N. *Inorg. Chem.* **1975**, *14*, 955–970.

(241) Zanello, P.; Opromolla, G.; Fabrizi de Biani, F.; Ceccanti, A.; Giorgi, G. *Inorg. Chim. Acta* **1997**, *255*, 47–52.

(242) Lohan, M.; Ecorchard, P.; Rüffer, T.; Justaud, F.; Lapinte, C.; Lang, H. *Organometallics* **2009**, *28*, 1878–1890.

(243) Paul, F.; Toupet, L.; Thépot, J.-Y.; Costuas, K.; Halet, J.-F.; Lapinte, C. *Organometallics* **2005**, *24*, 5464–5478.

(244) Atwood, C. G.; Geiger, W. E. *J. Am. Chem. Soc.* **1994**, *116*, 10849–10850.

(245) Caballero, A.; García, R.; Espinosa, A.; Tárraga, A.; Molina, P. *J. Org. Chem.* **2007**, *72*, 1161–1173.

(246) Fulmer, G. R.; Miller, A. J. M.; Sherden, N. H.; Gottlieb, H. E.; Nudelman, A.; Stoltz, B. M.; Bercaw, J. E.; Goldberg, K. I. *Organometallics* **2010**, *29*, 2176–2179.

(247) Sanders, R.; Mueller-Westerhoff, U. T. *J. Organomet. Chem.* **1996**, *512*, 219–224.

(248) Xie, Y.; Wu, B.-M.; Xue, F.; Ng, S.-C.; Mak, T. C. W.; Hor, T. S. A. *Organometallics* **1998**, *17*, 3988–3995.

(249) Gritzner, G.; Kuta, J. *Pure Appl. Chem.* **1984**, *56*, 461–466.

(250) Nafady, A.; Geiger, W. E. *Organometallics* **2008**, *27*, 5624–5631.

(251) Sheldrick, G. M. *Acta Crystallogr. Sect. A Found. Crystallogr.* **1990**, *46*, 467–473.

(252) Sheldrick, G. M. *SHELXL-97, Progr. Cryst. Struct. Refinement* **1997**.

(253) Speck, J. M.; Claus, R.; Hildebrandt, A.; Rüffer, T.; Erasmus, E.; van As, L.; Swarts, J. C.; Lang, H. *Organometallics* **2012**, *31*, 6373–6380.

(254) Stephenson, D. G.; Binsch, G. DNMR5 - Quantum Chemistry Program Exchange.

(255) Günther, H. *NMR Spectroscopy: Basic Principles, Concepts, and Applications in Chemistry*; 2nd ed.; John Wiley & Sons, Inc.: New York, 1996.

(256) Wong, W.-Y.; Lu, G.-L.; Ng, K.-F.; Choi, K.-H.; Lin, Z. *J. Chem. Soc. Dalt. Trans.* **2001**, 3250–3260.

(257) Morgan, I. S.; D'Aleo, D. N.; Hudolin, M. L.; Chen, A.; Assoud, A.; Jenkins, H. A.; MacKinnon, C. D. *J. Mater. Chem.* **2009**, *19*, 8162–8168.

(258) Imrie, C.; Engelbrecht, P.; Loubser, C.; McCleland, C. W.; Nyamori, V. O.; Bogardi, R.; Levendis, D. C.; Tolom, N.; van Rooyen, J.; Williams, N. *J. Organomet. Chem.* **2002**, *645*, 65–81.

(259) Swarts, J. C.; Nafady, A.; Roudebush, J. H.; Trupia, S.; Geiger, W. E. *Inorg. Chem.* **2009**, *48*, 2156–2165.

(260) Chong, D.; Slote, J.; Geiger, W. E. *J. Electroanal. Chem.* **2009**, *630*, 28–34.

(261) Nielson, R. M.; McManis, G. E.; Weaver, M. J. *J. Phys. Chem.* **1989**, *93*, 4703–4706.

(262) Fellows, E. a; Keene, F. R. *J. Phys. Chem. B* **2007**, *111*, 6667–6675.

(263) Masuda, A.; Masuda, Y.; Fukuda, T. *J. Mol. Liq.* **1995**, *65-66*, 397–400.

(264) Cowan, D. O.; Colins, R. L.; Kaufman, F. *J. Phys. Chem.* **1971**, *76*, 2025–2030.

(265) Lohan, M.; Justaud, F.; Roisnel, T.; Ecorchard, P.; Lang, H.; Lapinte, C. *Organometallics* **2010**, *29*, 4804–4817.

(266) Barrière, F. *Organometallics* **2014**, *33*, 5046–5048.

(267) Tahara, K.; Terashita, N.; Akita, T.; Katao, S.; Kikuchi, J.; Tokunaga, K. *Organometallics* **2015**, *34*, 299–308.

(268) Talham, D. R.; Cowan, D. O. *Organometallics* **1987**, *6*, 932–937.

(269) Hupp, J. T. *Inorg. Chem.* **1990**, *29*, 5010–5012.

(270) *CRC Handbook of Chemistry and Physics*; 82nd ed.; Taylor & Francis Ltd.: Boca Raton, FL 33431, 2002.

(271) Speck, J. M.; Korb, M.; Rüffer, T.; Hildebrandt, A.; Lang, H. *Organometallics* **2014**, *33*, 4813–4823.

(272) Noviandri, I.; Brown, K. N.; Fleming, D. S.; Gulyas, P. T.; Lay, P. A.; Masters, A. F.; Phillips, L. *J. Phys. Chem. B* **1999**, *103*, 6713–6722.

(273) Hildebrandt, A.; Lehrich, S. W.; Schaarschmidt, D.; Jaeschke, R.; Schreiter, K.; Spange, S.; Lang, H. *Eur. J. Inorg. Chem.* **2012**, *2012*, 1114–1121.

(274) Taher, D.; Awwadi, F. F.; Pfaff, U.; Speck, J. M.; Rüffer, T.; Lang, H. *J. Organomet. Chem.* **2013**, *736*, 9–18.

(275) Shearer, J.; Neupane, K. P.; Callan, P. E. *Inorg. Chem.* **2009**, *48*, 10560–10571.

(276) Tran-Van, F.; Garreau, S.; Louarn, G.; Froyer, G.; Chevrot, C. *J. Mater. Chem.* **2001**, *11*, 1378–1382.

(277) Dong, T.-Y.; Lai, L.-L. *J. Organomet. Chem.* **1996**, *509*, 131–134.

(278) Vowinkel, E.; Bartel, J. *Chem. Ber.* **1974**, *107*, 1221–1227.

(279) Scholz, S.; Scheibitz, M.; Schödel, F.; Bolte, M.; Wagner, M.; Lerner, H.-W. *Inorg. Chim. Acta* **2007**, *360*, 3323–3329.

(280) Webb, R. J.; Lowery, M. D.; Shiomi, Y.; Sorai, M.; Wittebort, R. J.; Hendrickson, D. N. *Inorg. Chem.* **1992**, *31*, 5211–5219.

(281) O'Connor, A. R.; Nataro, C.; Golen, J. A.; Rheingold, A. L. *J. Organomet. Chem.* **2004**, *689*, 2411–2414.

(282) Hanisch, C.; Leo, A.; Taft, R. W. *Chem. Rev.* **1991**, *91*, 165–195.

(283) Groenendaal, L.; Zotti, G.; Jonas, F. *Synth. Met.* **2001**, *118*, 105–109.

(284) Tourillon, G.; Garnier, F. *J. Electroanal. Chem. Interfacial Electrochem.* **1982**, *135*, 173–178.

(285) Sato, M.; Kubota, Y.; Tanemura, A.; Maruyama, G.; Fujihara, T.; Nakayama, J.;

Takayanagi, T.; Takahashi, K.; Unoura, K. *Eur. J. Inorg. Chem.* **2006**, 4577–4588.

(286) Wolf, M. O.; Zhu, Y. *Adv. Mater.* **2000**, *12*, 599–601.

(287) van der Westhuizen, B.; Speck, J. M.; Korb, M.; Friedrich, J.; Bezuidenhout, D. I.; Lang, H. *Inorg. Chem.* **2013**, *52*, 14253–14263.

(288) Siebler, D.; Förster, C.; Gasi, T.; Heinze, K. *Organometallics* **2011**, *30*, 313–327.

(289) Li, Y.; Josowicz, M.; Tolbert, L. M. *J. Am. Chem. Soc.* **2010**, *132*, 10374–10382.

(290) Kuprat, M.; Lehmann, M.; Schulz, A.; Villinger, A. *Organometallics* **2010**, *29*, 1421–1427.

(291) Thomas, K. R. J.; Lin, J. T.; Tao, Y.-T.; Chuen, C.-H. *Adv. Mater.* **2002**, *14*, 822–826.

(292) Kenning, D. D.; Mitchell, K. A.; Calhoun, T. R.; Funfar, M. R.; Sattler, D. J.; Rasmussen, S. C. *J. Org. Chem.* **2002**, *67*, 9073–9076.

(293) Li, Q.; Li, J.; Deng, L.; Wang, Q.; Gao, Z.; Liu, D. *Chem. Lett.* **2011**, *40*, 417–419.

(294) Kondo, Y.; Tanabe, H.; Kudo, H.; Nakano, K.; Otake, T. *Materials* **2011**, *4*, 2171–2182.

(295) Lee, C. W.; Lee, J. Y. *Chem. Commun.* **2013**, *49*, 1446–1448.

(296) Fan, C.; Miao, J.; Jiang, B.; Yang, C.; Wu, H.; Qin, J.; Cao, Y. *Org. Electron.* **2013**, *14*, 3392–3398.

(297) Fujisaki, Y.; Nakajima, Y.; Takei, T.; Fukagawa, H.; Yamamoto, T.; Fujikake, H. *IEEE Trans. Electron Devices* **2012**, *59*, 3442–3449.

(298) Sun, F.; Jin, R. *J. Lumin.* **2014**, *149*, 125–132.

(299) Cheng, H.; Djukic, B.; Jenkins, H. A.; Gorelsky, S. I.; Lemaire, M. T. *Can. J. Chem.* **2010**, *88*, 954–963.

(300) Marcus, Y. *Chem. Soc. Rev.* **1993**, *22*, 409–416.

(301) Yokoyama, T.; Taft, R. W.; Kamlet, M. J. *J. Am. Chem. Soc.* **1976**, *98*, 3233–3237.

(302) Kamlet, M. J.; Abboud, J. L. M.; Abraham, M. H.; Taft, R. W. *J. Org. Chem.* **1983**, *48*, 2877–2887.

(303) Kamlet, M. J.; Abboud, J. L.; Taft, R. W. *J. Am. Chem. Soc.* **1977**, *99*, 6027–6038.

(304) Kamlet, M. J.; Hall, T. N.; Boykin, J.; Taft, R. W. *J. Org. Chem.* **1979**, *44*, 2599–2604.

(305) Kamlet, M. J.; Taft, R. W. *J. Am. Chem. Soc.* **1976**, *98*, 377–383.

(306) Catalán, J. *J. Phys. Chem. B* **2009**, *113*, 5951–5960.

(307) Catalán, J. *J. Org. Chem.* **1997**, *62*, 8231–8234.

(308) Catalán, J.; Díaz, C. *Eur. J. Org. Chem.* **1999**, *1999*, 885–891.

(309) Catalán, J.; Díaz, C.; López, V.; Pérez, P.; De Paz, J. L. G.; Rodríguez, J. G. *Liebigs Ann.* **1996**, *1996*, 1785–1794.

(310) Catalán, J.; López, V.; Pérez, P. *Liebigs Ann.* **1995**, *1995*, 793–795.

(311) Catalán, J.; Palomar, J.; Díaz, C.; de Paz, J. L. G. *J. Phys. Chem. A* **1997**, *101*,

5183–5189.

(312) Catalán, J.; Hopf, H. *Eur. J. Org. Chem.* **2004**, 4694–4702.

(313) Reichardt, C.; Welton, T. *Solvents and Solvent Effects in Organic Chemistry*; 4<sup>th</sup> ed.; Wiley-VCH Verlag GmbH & Co. KGaA: Weinheim, Germany, 2010.

(314) Wen, L.; Heth, C. L.; Rasmussen, S. C. *Phys. Chem. Chem. Phys.* **2014**, *16*, 7231–7240.

(315) Heth, C. L.; Tallman, D. E.; Rasmussen, S. C. *J. Phys. Chem. B* **2010**, *114*, 5275–5282.

(316) Dietrich, M.; Heinze, J.; Heywang, G.; Jonas, F. *J. Electroanal. Chem.* **1994**, *369*, 87–92.

(317) Lin, B. C.; Cheng, C. P.; Lao, Z. P. M. *J. Phys. Chem. A* **2003**, *107*, 5241–5251.

(318) Amthor, S.; Noller, B.; Lambert, C. *Chem. Phys.* **2005**, *316*, 141–152.

(319) Tagg, T.; Kjaergaard, H. G.; Lane, J. R.; McAdam, C. J.; Robinson, B. H.; Simpson, J. *Organometallics* **2015**, *34*, 2662–2666.

(320) van der Westhuizen, B.; Speck, J. M.; Korb, M.; Bezuidenhout, D. I.; Lang, H. *J. Organomet. Chem.* **2014**, *772-773*, 18–26.

(321) Reuter, L. G.; Bonn, A. G.; Stückl, A. C.; He, B.; Pati, P. B.; Zade, S. S.; Wenger, O. S. *J. Phys. Chem. A* **2012**, *116*, 7345–7352.

(322) Nesmejanow, A. N.; Ssasonowa, W. A.; Drosd, V. N. *Chem. Ber.* **1960**, *93*, 2717–2729.

(323) Flack, H. D. *Acta Crystallogr. Sect. A Found. Crystallogr.* **1983**, *39*, 876–881.

(324) Farrugia, L. J. *J. Appl. Crystallogr.* **2012**, *45*, 849–854.

(325) Fischer, E. O.; Maasböl, A. *Angew. Chem. Int. Ed. Engl.* **1964**, *3*, 580–581.

(326) Bezuidenhout, D. I.; Lotz, S.; Liles, D. C.; van der Westhuizen, B. *Coord. Chem. Rev.* **2012**, *256*, 479–524.

(327) Astruc, D. *Acc. Chem. Res.* **1997**, *30*, 383–391.

(328) Long, N. J. *Angew. Chem. Int. Ed. Engl.* **1995**, *34*, 21–38.

(329) Behrens, U.; Brussaard, H.; Hagenau, U.; Heck, J.; Hendrickx, E.; Körnich, J.; van Der Linden, J. G. M.; Persoons, A.; Spek, A. L.; Veldman, N.; Voss, B.; Wong, H. *Chem. Eur. J.* **1996**, *2*, 98–103.

(330) Dötz, K. H. *Angew. Chem. Int. Ed. Engl.* **1975**, *14*, 644–645.

(331) Aumann, R.; Heinen, H. *Chem. Ber.* **1987**, *120*, 537–540.

(332) Pike, A. R.; Ryder, L. C.; Horrocks, B. R.; Clegg, W.; Connolly, B. A.; Houlton, A. *Chem. - A Eur. J.* **2005**, *11*, 344–353.

(333) Shago, R. F.; Swarts, J. C.; Kreft, E.; Van Rensburg, C. E. J. *Anticancer Res.* **2007**, *27*, 3431–3433.

(334) Van Rensburg, C. E. J.; Kreft, E.; Swarts, J. C.; Dalrymple, S. R. Macdonald, D. M.; Cooke, M. W.; Aquino, M. A. S. *Anticancer Res.* **2002**, *22*, 889–892.

(335) Gross, A.; Hüsken, N.; Schur, J.; Raszeja, Ł.; Ott, I.; Metzler-Nolte, N. *Bioconjug.*

*Chem.* **2012**, *23*, 1764–1774.

(336) Ott, I.; Kowalski, K.; Gust, R.; Maurer, J.; Mücke, P.; Winter, R. F. *Bioorg. Med. Chem. Lett.* **2010**, *20*, 866–869.

(337) Herndon, J. W. *Coord. Chem. Rev.* **2009**, *253*, 86–179.

(338) Herndon, J. W. *Coord. Chem. Rev.* **2002**, *227*, 1–58.

(339) Herndon, J. W. *Coord. Chem. Rev.* **2006**, *250*, 1889–1964.

(340) Herndon, J. W. *Coord. Chem. Rev.* **2004**, *248*, 3–79.

(341) Herndon, J. W. *Coord. Chem. Rev.* **2003**, *243*, 3–81.

(342) Herndon, J. W. *Coord. Chem. Rev.* **2011**, *255*, 3–100.

(343) Herndon, J. W. *Coord. Chem. Rev.* **2009**, *253*, 1517–1595.

(344) Herndon, J. W. *Coord. Chem. Rev.* **2007**, *251*, 1158–1258.

(345) Herndon, J. W. *Coord. Chem. Rev.* **2005**, *249*, 999–1084.

(346) Herndon, J. W. *Coord. Chem. Rev.* **2012**, *256*, 1281–1376.

(347) Herndon, J. W. *Coord. Chem. Rev.* **2010**, *254*, 103–194.

(348) Wulff, W. D. *Advances in Metal-Organic Chemistry*; Lanny S. Liebeskind, Ed.; Vol. 1.; JAI Press Inc.: Greenwich, CT, 1989.

(349) Wulff, W. D. *Comprehensive Organic Synthesis*; Trost, B. M.; Fleming, I., Eds.; Vol. 5.; Pergamon Press: Oxford, U. K., 1990.

(350) Wulff, W. D. *Comprehensive Organometallic Chemistry II*; Abel, E. W.; Stone, R. G. A.; Wilkinson, G., Eds.; Vol. 12.; Pergamon Press, 1995.

(351) Wulff, W. D. *Organometallics* **1998**, *17*, 3116–3134.

(352) Leroux, F.; Stumpf, R.; Fischer, H. *Eur. J. Inorg. Chem.* **1998**, 1225–1234.

(353) Licandro, E.; Maiorana, S.; Papagni, A.; Hellier, P.; Capella, L.; Persoons, A.; Houbrechts, S. *J. Organomet. Chem.* **1999**, *583*, 111–119.

(354) Robin-Le Guen, F.; Le Poul, P.; Caro, B.; Pichon, R.; Kervarec, N. *J. Organomet. Chem.* **2001**, *626*, 37–42.

(355) Faux, N.; Caro, B.; Robin-Le Guen, F.; Le Poul, P.; Nakatani, K.; Ishow, E. *J. Organomet. Chem.* **2005**, *690*, 4982–4988.

(356) Baldoli, C.; Cerea, P.; Falciola, L.; Giannini, C.; Licandro, E.; Maiorana, S.; Mussini, P.; Perdicchia, D. *J. Organomet. Chem.* **2005**, *690*, 5777–5787.

(357) Chandrasekhar, V.; Thirumoorthi, R. *Organometallics* **2007**, *26*, 5415–5422.

(358) *Ferrocenes: Ligands, Materials and Biomolecules*; Štěpnička, P., Ed.; John Wiley & Sons Inc.: New York, 2008.

(359) Ludvik, J.; Stepnicka, P. In *ECS Transactions*; ECS, 2007; Vol. 2, pp. 17–25.

(360) Connor, J. A.; Jones, E. M.; Lloyd, J. P. *J. Organomet. Chem.* **1970**, *24*, C20–C22.

(361) Lloyd, M. K.; McCleverty, J. A.; Orchard, D. G.; Connor, J. A.; Hall, M. B.; Hillier, I. H.; Jones, E. M.; McEwen, G. K. *J. Chem. Soc. Dalt. Trans.* **1973**, 1743–1747.

(362) Casey, C. P.; Albin, L. D.; Saeman, M. C.; Evans, D. H. *J. Organomet. Chem.* **1978**,

*155*, C37–C40.

(363) Limberg, A.; Lemos, M. A. N. D. A.; Pombeiro, A. J. L.; Maiorana, S.; Papagni, A.; Licandro, E. *Port. Electrochim. Acta* **1995**, *13*, 319–323.

(364) Pombeiro, A. J. L. *New J. Chem.* **1997**, *21*, 649–660.

(365) Fernández, I.; Mancheño, M. J.; Gómez-Gallego, M.; Sierra, M. A. *Org. Lett.* **2003**, *5*, 1237–1240.

(366) Martínez-Álvarez, R.; Gómez-Gallego, M.; Fernández, I.; Mancheño, M. J.; Sierra, M. A. *Organometallics* **2004**, *23*, 4647–4654.

(367) Wulff, W. D.; Korthals, K. A.; Martínez-Álvarez, R.; Gómez-Gallego, M.; Fernández, I.; Sierra, M. A. *J. Org. Chem.* **2005**, *70*, 5269–5277.

(368) López-Alberca, M. P.; Mancheño, M. J.; Fernández, I.; Gómez-Gallego, M.; Sierra, M. A.; Hemmert, C.; Gornitzka, H. *Eur. J. Inorg. Chem.* **2011**, *2011*, 842–849.

(369) van der Westhuizen, B.; Swarts, P. J.; Strydom, I.; Liles, D. C.; Fernández, I.; Swarts, J. C.; Bezuidenhout, D. I. *Dalt. Trans.* **2013**, *42*, 5367–5378.

(370) van der Westhuizen, B.; Swarts, P. J.; van Jaarsveld, L. M.; Liles, D. C.; Siegert, U.; Swarts, J. C.; Fernández, I.; Bezuidenhout, D. I. *Inorg. Chem.* **2013**, *52*, 6674–6684.

(371) Bezuidenhout, D. I.; Lotz, S.; Landman, M.; Liles, D. C. *Inorg. Chem.* **2011**, *50*, 1521–1533.

(372) Helten, H.; Beckmann, M.; Schnakenburg, G.; Streubel, R. *Eur. J. Inorg. Chem.* **2010**, 2337–2341.

(373) Bezuidenhout, D. I.; van der Watt, E.; Liles, D. C.; Landman, M.; Lotz, S. *Organometallics* **2008**, *27*, 2447–2456.

(374) Fischer, E. O.; Postnov, V. N.; Kreissl, F. R. *J. Organomet. Chem.* **1982**, *231*, C73–C77.

(375) Meca, L.; Dvořák, D.; Ludvík, J.; Císařová, I.; Štěpnička, P. *Organometallics* **2004**, *23*, 2541–2551.

(376) Butler, I. R.; Cullen, W. R.; Einstein, F. W. B.; Willis, A. C. *Organometallics* **1985**, *4*, 603–604.

(377) Fischer, E. O.; Gammel, F. J.; Besenhard, J. O.; Frank, A.; Neugebauer, D. *J. Organomet. Chem.* **1980**, *191*, 261–282.

(378) Schobert, R.; Kempe, R.; Schmalz, T.; Gmeiner, A. *J. Organomet. Chem.* **2006**, *691*, 859–868.

(379) Sünkel, K.; Bernhartzeder, S. *J. Organomet. Chem.* **2011**, *696*, 1536–1540.

(380) Dong, T.-Y.; Chang, C.-K.; Lee, S.-H.; Lai, L.-L.; Chiang, M. Y.-N.; Lin, K.-J. *Organometallics* **1997**, *16*, 5816–5825.

(381) *Spectral Database for Organic Compounds (SDBS); 1H NMR spectrum (No. 6650HPM-00-130); SDBS No.: 6650; RN: 102-54-5; http://riodb01.ibase.aist.go.jp/sdbs/.*

(382) Cardona, C. M.; Li, W.; Kaifer, A. E.; Stockdale, D.; Bazan, G. C. *Adv. Mater.* **2011**, *23*, 2367–2371.

(383) Baldoli, C.; Cerea, P.; Falciola, L.; Giannini, C.; Licandro, E.; Maiorana, S.;

Mussini, P.; Perdicchia, D. *J. Organomet. Chem.* **2005**, *690*, 5777–5787.

(384) Bott, A. W.; Heineman, W. R. *Curr. Sep.* **2004**, *20*, 121–126.

(385) Anson, F. C.; Christie, J. H.; Osteryoung, R. A. *J. Electroanal. Chem.* **1967**, *13*, 343–353.

(386) Bezuidenhout, D. I.; Barnard, W.; van der Westhuizen, B.; van der Watt, E.; Liles, D. C. *Dalt. Trans.* **2011**, *40*, 6711–6721.

(387) Connor, J. A.; Lloyd, J. P. *J. Chem. Soc. Dalt. Trans.* **1972**, 1470–1476.

(388) Rosenblum, M.; Santer, J. O.; Howells, W. G. *J. Am. Chem. Soc.* **1963**, *85*, 1450–1458.

(389) Dong, T.-Y.; Lee, T.-Y.; Lee, S.-H.; Lee, G.-H.; Peng, S.-M. *Organometallics* **1994**, *13*, 2337–2348.

(390) López-Cortés, J. G.; Contreras de la Cruz, L. F.; Ortega-Alfaro, M. C.; Toscano, R. A.; Alvarez-Toledano, C.; Rudler, H. *J. Organomet. Chem.* **2005**, *690*, 2229–2237.

(391) Fernández, I.; Cossío, F. P.; Arrieta, A.; Lecea, B.; Mancheño, M. J.; Sierra, M. A. *Organometallics* **2004**, *23*, 1065–1071.

(392) TURBOMOLE V6.3 2011, a development of University of Karlsruhe and Forschungszentrum Karlsruhe GmbH, since 2007; available from http://www.turbomole.com.

(393) Häser, M.; Ahlrichs, R. *J. Comput. Chem.* **1989**, *10*, 104–111.

(394) Deglmann, P.; Furche, F.; Ahlrichs, R. *Chem. Phys. Lett.* **2002**, *362*, 511–518.

(395) van Wüllen, C. *J. Comput. Chem.* **2011**, *32*, 1195–1201.

(396) Weigend, F.; Ahlrichs, R. *Phys. Chem. Chem. Phys.* **2005**, *7*, 3297–3305.

(397) Weigend, F.; Häser, M.; Patzelt, H.; Ahlrichs, R. *Chem. Phys. Lett.* **1998**, *294*, 143–152.

(398) Schäfer, A.; Horn, H.; Ahlrichs, R. *J. Chem. Phys.* **1992**, *97*, 2571–2577.

(399) Becke, A. D. *Phys. Rev. A* **1988**, *38*, 3098–3100.

(400) Perdew, J. P. *Phys. Rev. B* **1986**, *33*, 8822–8824.

(401) Weigend, F. *Phys. Chem. Chem. Phys.* **2006**, *8*, 1057.

(402) Eichkorn, K.; Treutler, O.; Öhm, H.; Häser, M.; Ahlrichs, R. *Chem. Phys. Lett.* **1995**, *240*, 283–290.

(403) Eichkorn, K.; Weigend, F.; Treutler, O.; Ahlrichs, R. *Theor. Chem. Accounts Theory, Comput. Model. (Theoretica Chim. Acta)* **1997**, *97*, 119–124.

(404) Treutler, O.; Ahlrichs, R. *J. Chem. Phys.* **1995**, *102*, 346–354.

(405) von Arnim, M.; Ahlrichs, R. *J. Chem. Phys.* **1999**, *111*, 9183–9190.

(406) Lee, C.; Yang, W.; Parr, R. G. *Phys. Rev. B* **1988**, *37*, 785–789.

(407) Becke, A. D. *J. Chem. Phys.* **1993**, *98*, 5648–5652.

(408) Klamt, A.; Schüürmann, G. *J. Chem. Soc. Perkin Trans. 2* **1993**, 799–805.

(409) Motoyama, K.; Li, H.; Koike, T.; Hatakeyama, M.; Yokojima, S.; Nakamura, S.;

Akita, M. *Dalt. Trans.* **2011**, *40*, 10643–10657.

(410) Watanuki, S.; Ochifuji, N.; Mori, M. *Organometallics* **1995**, *14*, 5062–5067.

(411) Fernández-Rodríguez, M. Á.; García-García, P.; Aguilar, E. *Chem. Commun.* **2010**, *46*, 7670–7687.

(412) Lage, M. L.; Curiel, D.; Fernández, I.; Mancheño, M. J.; Gómez-Gallego, M.; Molina, P.; Sierra, M. A. *Organometallics* **2011**, *30*, 1794–1803.

(413) Crause, C.; Görls, H.; Lotz, S. *Dalt. Trans.* **2005**, 1649–1657.

(414) Terblans, Y. M.; Marita Roos, H.; Lotz, S. *J. Organomet. Chem.* **1998**, *566*, 133–142.

(415) Bezuidenhout, D. I.; Fernández, I.; van der Westhuizen, B.; Swarts, P. J.; Swarts, J. C. *Organometallics* **2013**, *32*, 7334–7344.

(416) Fischer, E. O.; Held, W.; Kreißl, F. R.; Frank, A.; Huttner, G. *Chem. Ber.* **1977**, *110*, 656–666.

(417) Landman, M.; Pretorius, R.; Buitendach, B. E.; van Rooyen, P. H.; Conradie, J. *Organometallics* **2013**, *32*, 5491–5503.

(418) Pickett, T. E.; Richards, C. J. *Tetrahedron Lett.* **1999**, *40*, 5251–5254.

(419) Braterman, P. S. *Metal Carbonyl Spectra*; Organometallic chemistry; Academic Press: London ; New York, 1975.

(420) Adams, D. M. *Metal-ligand and Related Vibrations*; Edward Arnold Publishers Ltd: London, U.K., 1967.

(421) McIver, J. W.; Komornicki, A. *J. Am. Chem. Soc.* **1972**, *94*, 2625–2633.

(422) Rodríguez González, S.; Aragó, J.; Viruela, P. M.; Ortí, E.; López Navarrete, J. T.; Sato, M.; Casado, J. *J. Chem. Phys.* **2011**, *135*, 234705.

(423) Kingsborough, R. P.; Swager, T. M. *Adv. Mater.* **1998**, *10*, 1100–1104.

(424) Lambert, C.; Schelter, J.; Fiebig, T.; Mank, D.; Trifonov, A. *J. Am. Chem. Soc.* **2005**, *127*, 10600–10610.

(425) Coropceanu, V.; Gruhn, N. E.; Barlow, S.; Lambert, C.; Durivage, J. C.; Bill, T. G.; Nöll, G.; Marder, S. R.; Brédas, J.-L. *J. Am. Chem. Soc.* **2004**, *126*, 2727–2731.

(426) Nelsen, S. F.; Tran, H. Q.; Nagy, M. A. *J. Am. Chem. Soc.* **1998**, *120*, 298–304.

(427) Steffens, S.; Prosenc, M. H.; Heck, J.; Asselberghs, I.; Clays, K. *Eur. J. Inorg. Chem.* **2008**, *2008*, 1999–2006.

(428) Astruc, D. *Anal. Bioanal. Chem.* **2011**, *399*, 1811–1814.

(429) Schulz, J.; Uhlík, F.; Speck, J. M.; Císařová, I.; Lang, H.; Štěpnička, P. *Organometallics* **2014**, *33*, 5020–5032.

(430) Speck, J. M.; Korb, M.; Schade, A.; Spange, S.; Lang, H. *Organometallics* **2015**, *34*, 3788–3798.

(431) Slugovc, C.; Rüba, E.; Schmid, R.; Kirchner, K.; Mereiter, K. *Monatsh. Chem.* **2000**, *131*, 1241–1251.

(432) Ziemann, E. A.; Baljak, S.; Steffens, S.; Stein, T.; Van Steerteghem, N.; Asselberghs, I.; Clays, K.; Heck, J. *Organometallics* **2015**, *34*, 1692–1700.

(433) Ueda, T.; Mochida, T. *Organometallics* **2015**, *34*, 1279–1286.

(434) Wong, H.; Meyer-Friedrichsen, T.; Farrell, T.; Mecker, C.; Heck, J. *Eur. J. Inorg. Chem.* **2000**, *2000*, 631–646.

(435) Cuesta, L.; Karnas, E.; Lynch, V. M.; Sessler, J. L.; Kajonkijya, W.; Zhu, W.; Zhang, M.; Ou, Z.; Kadish, K. M.; Ohkubo, K.; Fukuzumi, S. *Chem. Eur. J.* **2008**, *14*, 10206–10210.

(436) Kündig, P. E. *Transition Metal Arene p-Complexes in Organic Synthesis and Catalysis - Topics in Organometallic Chemistry*; Kündig, P. E., Ed.; Vol. 7.; Springer Berlin Heidelberg: Berlin, Heidelberg, 2004.

(437) Mercier, A.; Yeo, W. C.; Chou, J.; Chaudhuri, P. D.; Bernardinelli, G.; Kündig, E. P. *Chem. Commun.* **2009**, 5227–5229.

(438) Ruiz, J.; Ogliaro, F.; Saillard, J.-Y.; Halet, J.-F.; Varret, F.; Astruc, D. *J. Am. Chem. Soc.* **1998**, *120*, 11693–11705.

(439) Jones, C. L.; Higgins, S. J. *J. Mater. Chem.* **1999**, *9*, 865–874.

(440) Trost, B. M.; Older, C. M. *Organometallics* **2002**, *21*, 2544–2546.

(441) Steinmetz, B.; Schenk, W. A. *Organometallics* **1999**, *18*, 943–946.

(442) Engelmann, G.; Kossmehl, G.; Heinze, J.; Tschuncky, P.; Jugelt, W.; Welzel, H.-P. *J. Chem. Soc. Perkin Trans. 2* **1998**, 169–176.

(443) Engelmann, G.; Jugelt, W.; Kossmehl, G.; Welzel, H.-P.; Tschuncky, P.; Heinze, J. *Macromolecules* **1996**, *29*, 3370–3375.

(444) Lockemeyer, J. R.; Rauchfuss, T. B.; Rheingold, A. L.; Wilson, S. R. *J. Am. Chem. Soc.* **1989**, *111*, 8828–8834.

(445) Seiler, P.; Dunitz, J. D. *Acta Crystallogr. Sect. B Struct. Crystallogr. Cryst. Chem.* **1980**, *36*, 2946–2950.

(446) Poppitz, E. A.; Hildebrandt, A.; Korb, M.; Schaarschmidt, D.; Lang, H. *Z. Anorg. Allg. Chem.* **2014**, *640*, 2809–2816.

(447) Egger, H.; Schlögl, K. *Monatsh. Chem.* **1964**, *95*, 1750–1758.

(448) Sheldrick, G. M. *Acta Crystallogr. Sect. A Found. Crystallogr.* **2008**, *64*, 112–122.

(449) Inkpen, M. S.; Du, S.; Driver, M.; Albrecht, T.; Long, N. J. *Dalt. Trans.* **2013**, *42*, 2813–2816.
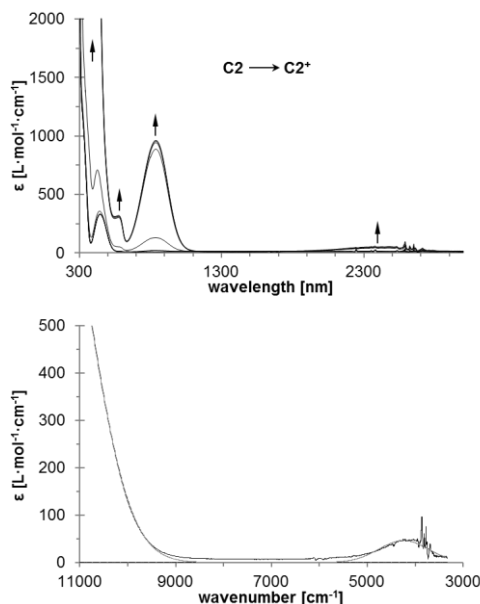
# APPENDIX

## APPENDIX AC



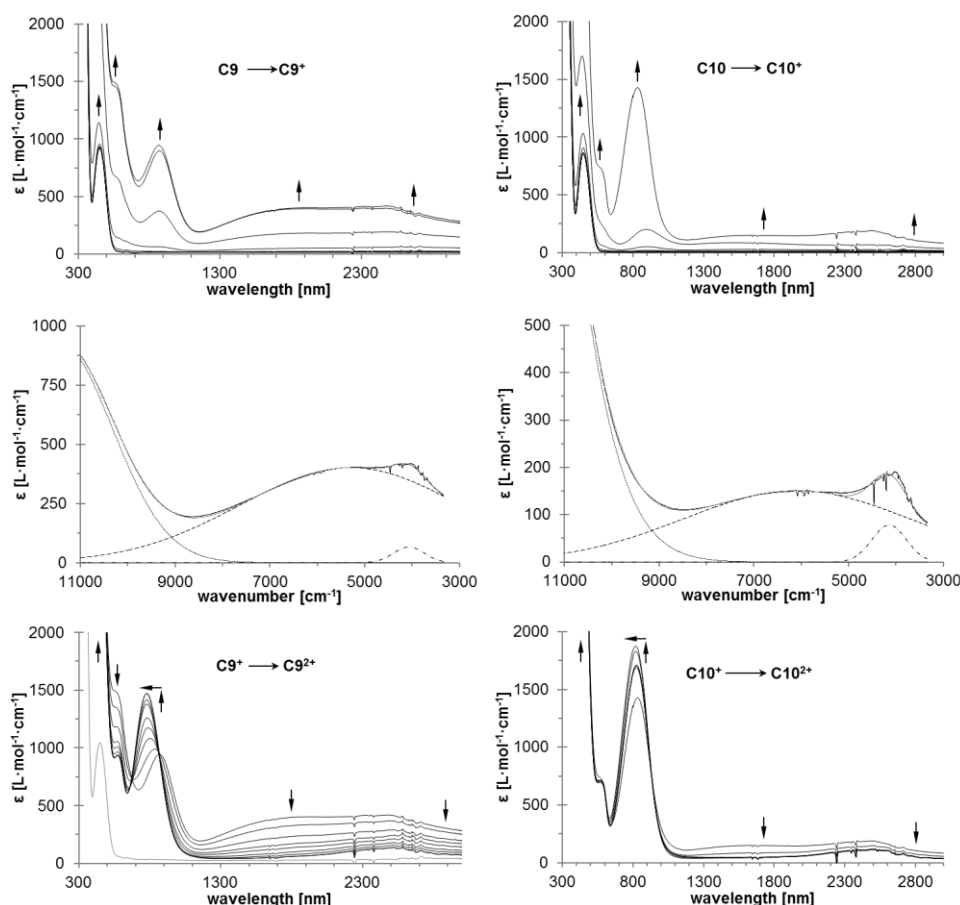**Figure AC-1**. UV-Vis-NIR spectra of **C2** at rising potentials. Top: –500 to 300 mV. Bottom: deconvolution of NIR absorptions at 300 mV, using transitions with Gaussian shapes (dotted line corresponds to absorptions caused by interactions between ligand and metal, dotted dashed line represents ligand field transitions). All potentials *vs.* Ag/AgCl at 25 °C in dichloromethane, supporting electrolyte $[N^nBu_4][B(C_6F_5)_4]$ (0.1 M). Arrows indicate increasing or decreasing absorptions.
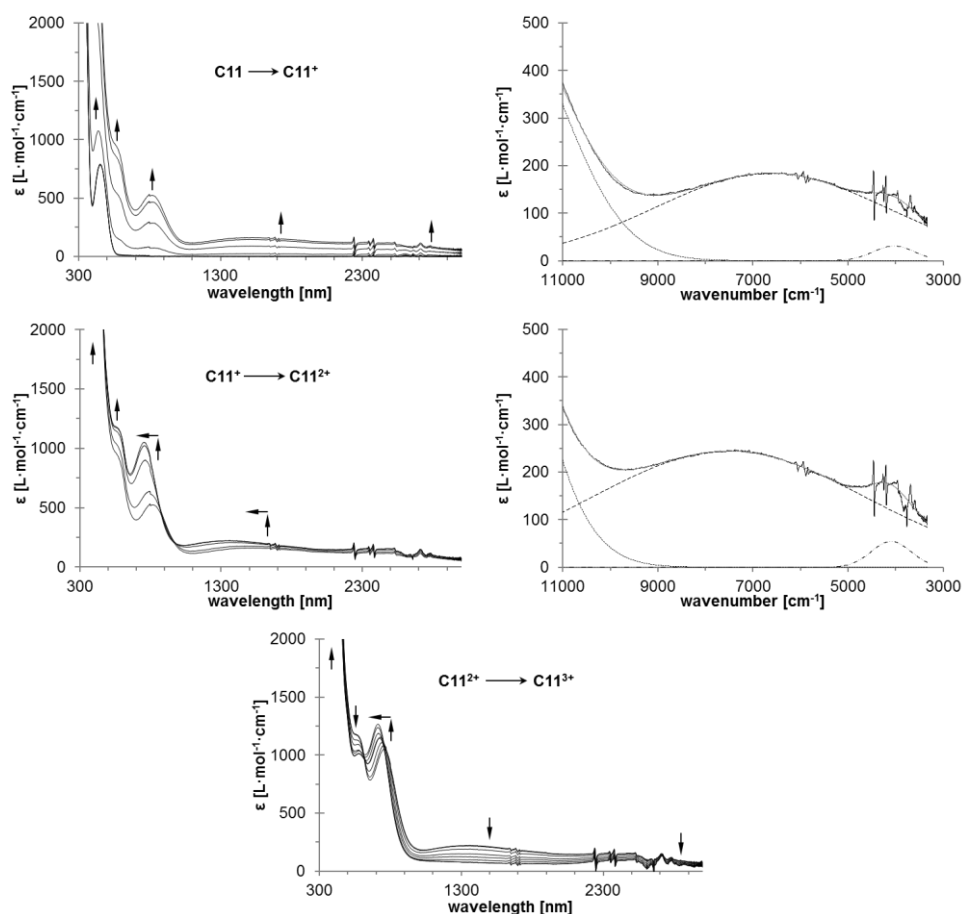


**Figure AC-2**. Left: UV-Vis-NIR spectra of **C9** at rising potentials. Top: –500 to 250 mV. Middle: deconvolution of NIR absorptions at 250 mV, using three distinct overlapping transitions with Gaussian

shapes (dashed line indicates IVCT absorption, dotted line corresponds to absorptions caused by interactions between ligand and metal, dotted dashed line represents ligand field transitions). Bottom: 250 to 900 mV and –500 mV (grey line). Right: UV-Vis-NIR spectra of **C10** at rising potentials. Top: –200 to 425 mV. Middle: deconvolution of NIR absorptions at 425 mV, using three distinct overlapping transitions with Gaussian shapes (dashed line indicates IVCT absorption, dotted line corresponds to absorptions caused by interactions between ligand and metal, dotted dashed line represents ligand field transitions). Bottom: 425 to 700 mV. All potentials *vs.* Ag/AgCl at 25 °C in dichloromethane, supporting electrolyte $[N^nBu_4][B(C_6F_5)_4]$ (0.1 M). Arrows indicate increasing or decreasing as well as shifting absorptions.
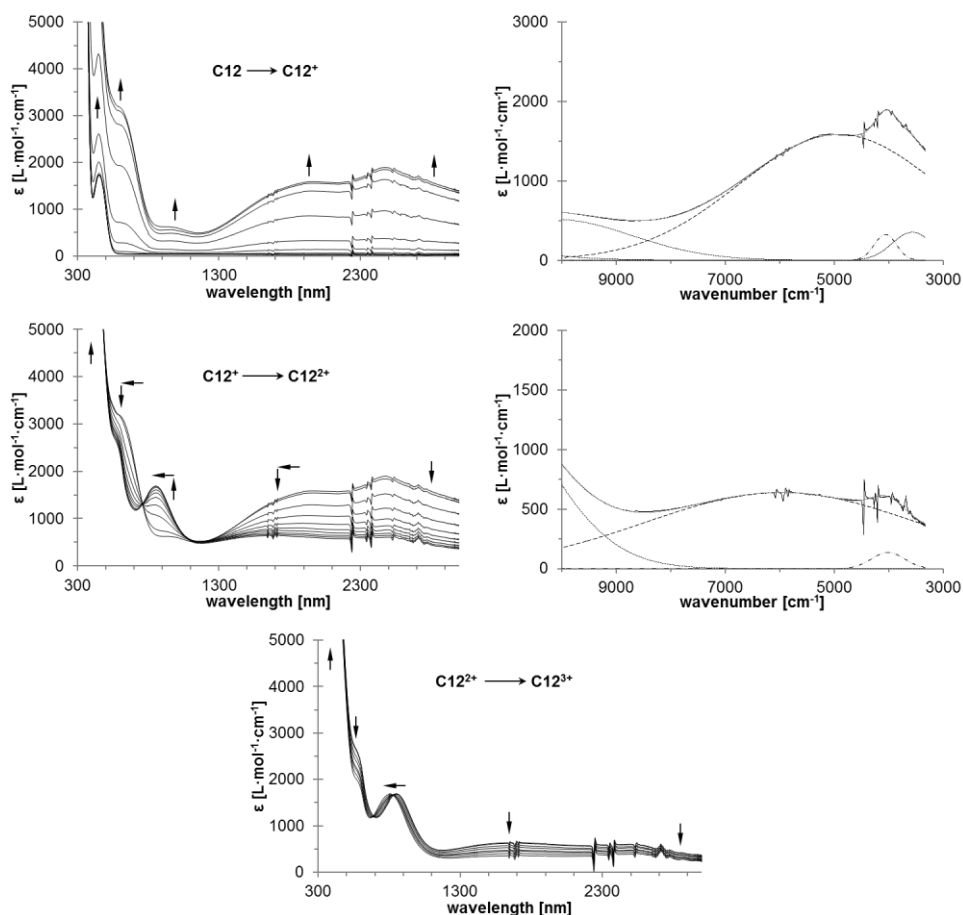


**Figure AC-3**. UV-Vis-NIR spectra of **C11** at rising potentials. Top (left): –200 to 250 mV. Top (right): deconvolution of NIR absorptions at 250 mV, using three distinct overlapping transitions with Gaussian shapes (dashed line indicates IVCT absorption, dotted line corresponds to absorptions caused by interactions between ligand and metal, dotted dashed line represents ligand field transitions). Middle (left): 250 to 450 mV. Middle (right): deconvolution of NIR absorptions at 450 mV, using three distinct overlapping transitions with Gaussian shapes. Bottom: 450 to 1100 mV. All potentials *vs.* Ag/AgCl at 25 °C in dichloromethane, supporting electrolyte $[N^nBu_4][B(C_6F_5)_4]$ (0.1 M). Arrows indicate increasing or decreasing as well as shifting absorptions.

**Figure AC-4**. UV-Vis/NIR spectra of **C12** at rising potentials. Top (left): –500 to 275 mV. Top (right): deconvolution of NIR absorptions at 275 mV, using five distinct overlapping transitions with Gaussian shapes (dashed line indicates IVCT absorption, dotted line corresponds to absorptions caused by interactions between ligand and metal, dotted dashed line represents ligand field transitions). Middle (left): 275 to 525 mV. Middle (right): deconvolution of NIR absorptions at 525 mV, using three distinct overlapping transitions with Gaussian shapes. Bottom: 525 to 1100 mV. All potentials *vs.* Ag/AgCl at 25 °C in dichloromethane, supporting electrolyte [N$^n$Bu$_4$][B(C$_6$F$_5$)$_4$] (0.1 M). Arrows indicate increasing or decreasing as well as shifting absorptions.
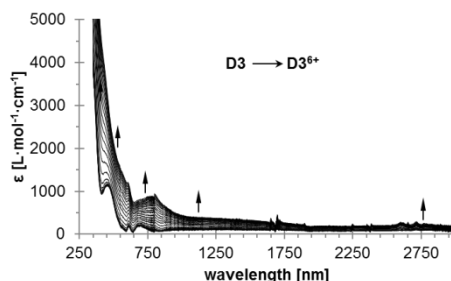
# APPENDIX AD



**Figure AD-1**. UV-Vis-NIR spectra of **D3** at rising potentials (–500 to 1200 mV) *vs.* Ag/AgCl at 25 °C in dichloromethane, supporting electrolyte [N$^n$Bu$_4$][B(C$_6$F$_5$)$_4$] (0.1 M).
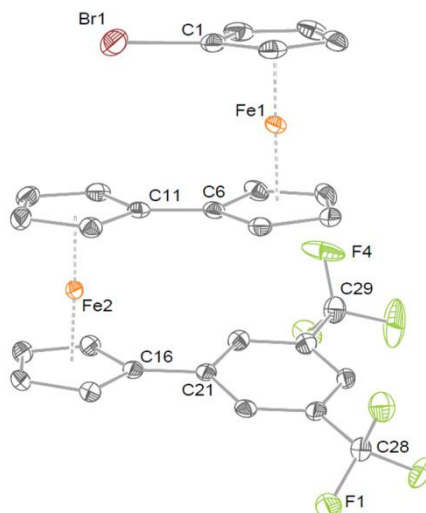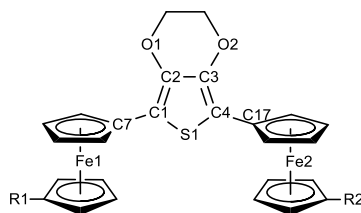
**Solid state structure analysis of E10.**



**Figure AE2-1.** Single crystal X-ray structure analyses of **E10** with atom numbering schemes. Ellipsoids represent 50 % probability levels. Hydrogen atoms are omitted for clarity. Selected bond lengths (Å), angles (°), torsion angles (°), and plain intersections (P/°) for **E10**: C1–Br1 1.881(3), D1–Fe1 1.6436(4), D2–Fe1 1.6516(4), D3–Fe2 1.6580(4), D4–Fe2 (1.6486(4), D1–Fe1–D2 177.11(3), D3–Fe2–D4 177.93(2), C1–D1–D2–C6 14.12(18), C11–D3–D4–C16 –3.82(17), $P_{D2}$-$P_{D3}$ 3.2(2), $P_{D4}$-$P_{Ph}$ 11.01(16) (Centroids are represented by D: D1 = $C_5H_4$–Br, D2/D3 = $C_5H_4$–$C_5H_4$, D4 = $C_5H_4$–$C_6H_3(CF_3)_2$.)

Compound **E10** is formed during the synthesis of **E8** (Experimental Section). It crystallizes in the monoclinic space group $P2_1/n$ with one molecule in the asymmetric unit (Figure AE1-1). The orientation of the ferrocenyls to each other and the plane intersections with the ArF (=3,5-bis(trifluoromethyl)phenyl) substituent is similar to compound **E1** and **E5** and results in a "S"-shaped conformation. The distances between the phenyl and the cyclopentadienyl cycles exhibit a minimum for C10–C27 (3.301(4) Å), which is in the range of the sum of the Van der Waals radii. However, the slight rotation of the phenyl ring in respect to the cyclopentadienyl ring ($P_{D4}$-$P_{Ph}$ 11.01(16) °) and the increasing distance between the two stacked aromatic moieties (D3–Fe2–D4 177.93(2) °), exclude $\pi$-$\pi$ interactions.

**Table AE2-1. Selected bond lengths (Å), angles (°), torsion angles (°), and plain intersections* (°) for E1 – E4, [E4][B(C$_6$F$_5$)$_4$], E5 and E7.**



| | Thiophene | | | Ethylendioxythiophene | | | |
|---|---|---|---|---|---|---|---|
| | **E1** | **E2** | **E3** | **E4** | **[E4][B(C$_6$F$_5$)$_4$]** | **E5** | **E7** |
| R = | C$_6$H$_3$(CF$_3$)$_2$ | CHO | C≡N | H | H | C$_6$H$_3$(CF$_3$)$_2$ | C≡N |
| Fe1–D1 | 1.6569(3) | 1.6550(5) | 1.6507(2) | 1.6484(5) | 1.6571(4) | 1.6542(3) | 1.6460(9) |
| Fe2–D3 | 1.6472(3) | 1.6560(5) | 1.6538(2) | 1.6520(5) | 1.6636(4) | 1.6567(3) | 1.6574(9) |
| Fe1–D2 | 1.6509(3) | 1.6600(5) | 1.6415(2) | 1.6604(5) | 1.6668(4) | 1.6508(3) | 1.6498(9) |
| Fe2-D4 | 1.6514(3) | 1.6439(5) | 1.6551(2) | 1.6516(5) | 1.6840(4) | 1.6508(3) | 1.6483(9) |
| D1–Fe1–D2[a] | 177.99(2) | 176.86(4) | 177.09(2) | 177.33(3) | 176.27(3) | 177.43(2) | 177.57(6) |
| D3–Fe2–D4[a] | 177.04(2) | 175.68(3) | 178.19(2) | 178.85(3) | 174.95(3) | 178.34(2) | 179.17(6) |
| P$_{Tp}$–P$_{D1}$* | 12.49(12) | 11.9(3) | 6.57(13) | 11.5(2) | 2.7(8) | 6.23(13) | 7.3(4) |
| P$_{Tp}$–P$_{D3}$* | 17.37(12) | 11.8(3) | 7.1(2) | 20.33(19) | 14.78(5) | 11.34(12) | 7.2(4) |
| Tors$_{Cp–Cp}$$^a$ | 7.93(15) | 5.9(2) | −2.81(13) | −9.6(2) | 9.3(2) | 2.78(12) | −1.6(4) |
| Tors$_{Cp–Cp}$$^a$ | 2.94(16) | −0.6(2) | 4.21(12) | 10.9(2) | −16.2(2) | −16.71(16) | −8.1(4) |
| S1–C1 | 1.738(2) | 1.742(3) | 1.7299(17) | 1.738(3) | 1.729(3) | 1.743(2) | 1.733(6) |
| S1–C4 | 1.731(2) | 1.738(4) | 1.7342(17) | 1.739(3) | 1.734(3) | 1.737(2) | 1.741(6) |
| C1–C2 | 1.360(3) | 1.364(5) | 1.362(2) | 1.362(5) | 1.383(4) | 1.364(3) | 1.362(8) |
| C2–C3 | 1.412(3) | 1.423(5) | 1.411(2) | 1.434(5) | 1.403(4) | 1.427(3) | 1.412(7) |
| C3–C4 | 1.365(3) | 1.352(5) | 1.363(2) | 1.358(5) | 1.380(4) | 1.358(3) | 1.373(8) |
| C2–O1 | – | – | – | 1.370(4) | 1.354(3) | 1.371(3) | 1.363(7) |
| C3–O2 | – | – | – | 1.378(4) | 1.359(3) | 1.377(3) | 1.367(7) |
| C1–C7 | 1.454(3) | 1.454(5) | 1.457(2) | 1.460(5) | 1.434(4) | 1.449(3) | 1.462(8) |
| C4–C17 | 1.459(3) | 1.450(5) | 1.460(2) | 1.448(5) | 1.432(4) | 1.455(3) | 1.443(7) |

[a] Torsion angles. Tp = Thiphene cycle. D1 = C$_5$H$_4$ centroid bonded to C1. D2 = C$_5$H$_4$ centroid bonded to R1. D3 = C$_5$H$_4$ centroid bonded to C4. D4 = C$_5$H$_4$ centroid bonded to R2.

**Table AE2-2. Cyclic voltammetry data (potentials *vs*. FcH/FcH$^+$) of 1.0 mmol·L$^{-1}$ solutions of E9, formylferrocene and cyanoferrocene in dichloromethane containing [N$^n$Bu$_4$] [B(C$_6$F$_5$)$_4$] (0.1 M) as supporting electrolyte at 25 °C.**

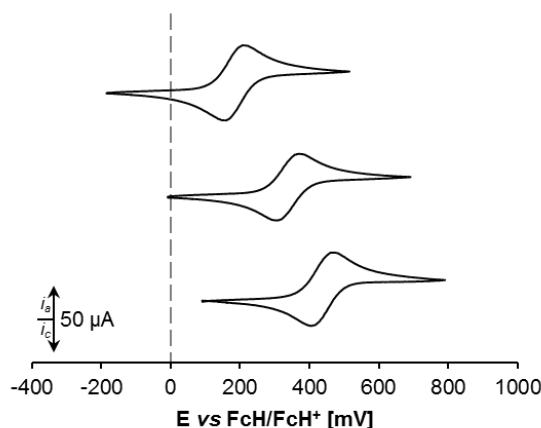| Compd. | $E^{0'}/\Delta E_p$ [mV] Wave |
|---|---|
| **E9** | 183/62 |
| **FcCHO** | 338/69 |
| **FcCN** | 439/66 |

**Figure AE2-2**. Cyclic voltammograms (CV) of **E9** (top), formylferrocene (middle) and cyanoferrocene (bottom), scan rate: 100 mVs$^{-1}$ in dichloromethane solutions (1.0 mM) at 25 °C, supporting electrolyte [N$^n$Bu$_4$][B(C$_6$F$_5$)$_4$] (0.1 M).

**Table AE2-3. Hammett correlation data.**[282] **Formal potentials ($E^{0'}$) were determined in dichloromethane solutions (1.0 mM) at 25 °C, scan rate: 100 mVs$^{-1}$, supporting electrolyte [N$^n$Bu$_4$][B(C$_6$F$_5$)$_4$] (0.1 M).**

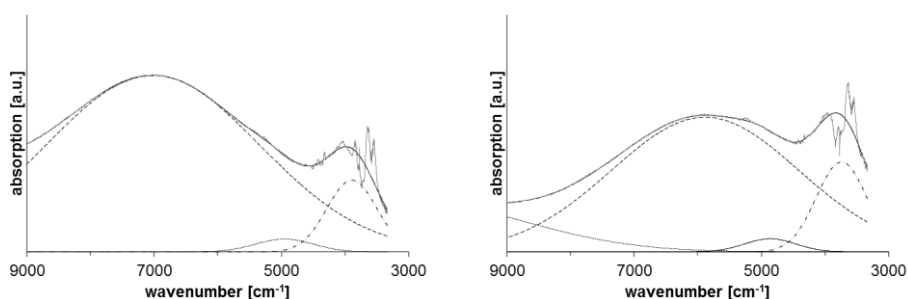| Compd. | $E^{0'}$ [mV] | $\sigma_P$ |
|---|---|---|
| FcCH$_2$CH$_2$Ph | −55 | −0.12 |
| FcCHCHPh | −17 | −0.07 |
| 3-ferrocenyl-thiophene | −9 | −0.02 |
| FcH | 0 | 0.0 |
| 2-ferrocenyl-thiophene | 16 | 0.05 |
| FcC≡CPh | 101 | 0.16 |
| FcAc | 280 | 0.5 |
| FcCHO | 338 | 0.42 |
| FcC≡N | 439 | 0.66 |



**Figure AE2-3**. Left: Deconvolution of NIR absorptions (at 450 mV) for **C3$^+$** (1 mM) using four distinct overlapping transitions with Gaussian shapes (dashed line indicates IVCT transitions). Right: Deconvolution of NIR absorptions (at 550 mV) for **E1$^+$** (1 mM) using four distinct overlapping transitions with Gaussian shapes (dashed line indicates IVCT transitions). All potentials *vs.* Ag/AgCl at 25 °C in propylene carbonate, supporting electrolyte [N$^n$Bu$_4$][B(C$_6$F$_5$)$_4$] (0.1 M).
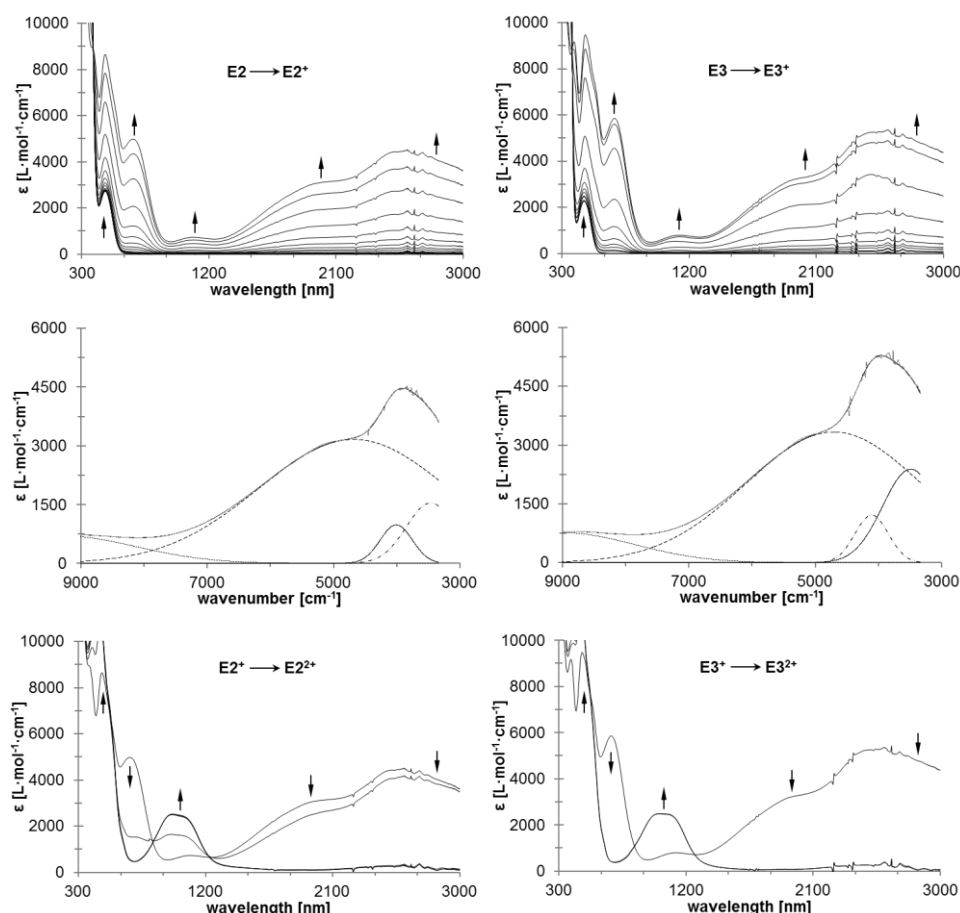
191

**Figure AE2-4**. Left: UV-Vis-NIR spectra of **E2** at rising potentials. Top: –100 to 615 mV. Middle: deconvolution of NIR absorptions at 615 mV using four distinct overlapping transitions with Gaussian shapes (dashed line indicates IVCT absorption, dotted line corresponds to absorptions caused by interactions between ligand and metal). Bottom: 615 to 700 mV. Right: UV-Vis-NIR spectra of **E3** at rising potentials. Top: –100 to 675 mV. Middle: deconvolution of NIR absorptions at 675 mV using four distinct overlapping transitions with Gaussian shapes (dashed line indicates IVCT absorption, dotted line corresponds to absorptions caused by interactions between ligand and metal). Bottom: 675 to 700 mV. All potentials *vs.* Ag/AgCl at 25 °C in dichloromethane, supporting electrolyte [N$^n$Bu$_4$][B(C$_6$F$_5$)$_4$] (0.1 M). Arrows indicate increasing or decreasing as well as shifting absorptions.
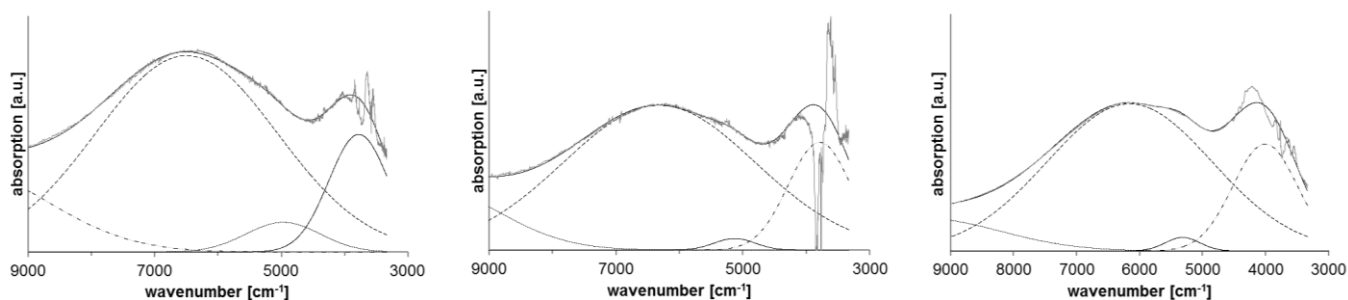


**Figure AE2-5**. Left: Deconvolution of NIR absorptions (at 550 mV) for **E2**$^+$ (1 mM) using four distinct overlapping transitions with Gaussian shapes (dashed line indicates IVCT transitions). Middle: Deconvolution of NIR absorptions (at 900 mV) for **E3**$^+$ (1 mM) using four distinct overlapping transitions with Gaussian shapes (dashed line indicates IVCT transitions). Right: Deconvolution of NIR absorptions (at 530 mV) for **E4**$^+$ (1 mM) using four distinct overlapping transitions with Gaussian shapes (dashed line indicates IVCT transitions). All potentials *vs.* Ag/AgCl at 25 °C in propylene carbonate, supporting electrolyte [N$^n$Bu$_4$][B(C$_6$F$_5$)$_4$] (0.1 M).
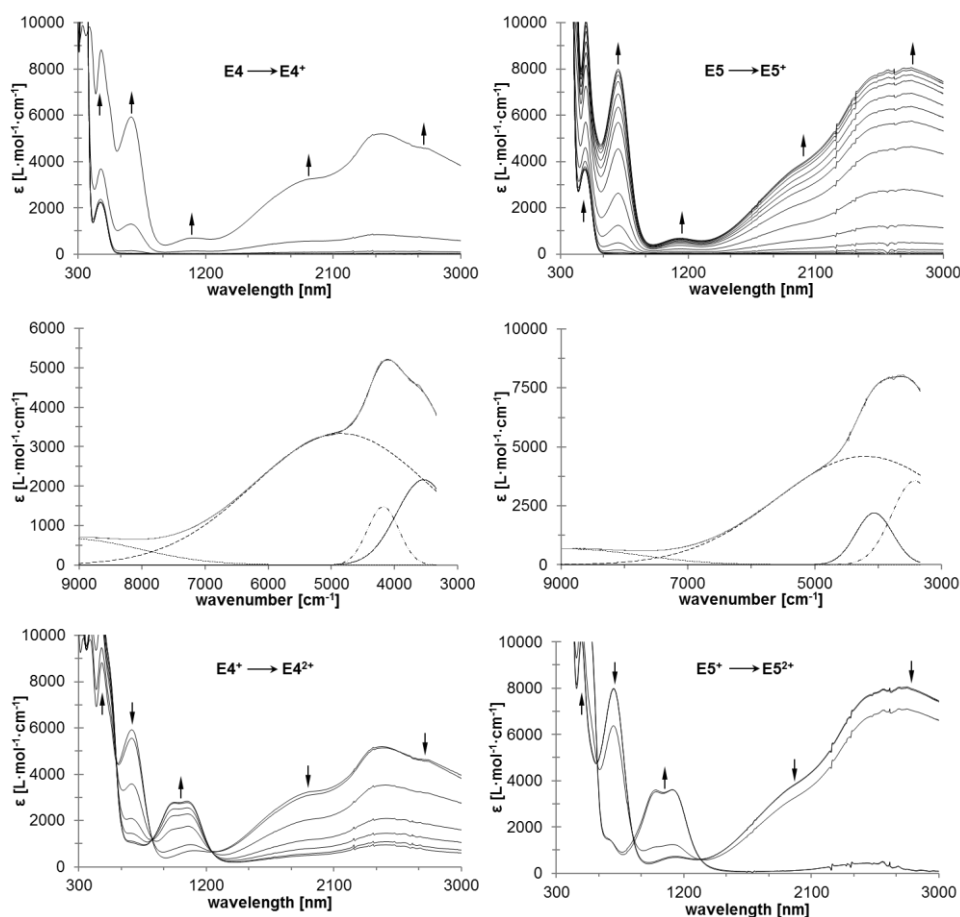
**Figure AE2-6**. Left: UV-Vis-NIR spectra of **E4** at rising potentials. Top: –200 to 300 mV. Middle: deconvolution of NIR absorptions at 300 mV using four distinct overlapping transitions with Gaussian shapes (dashed line indicates IVCT absorption, dotted line corresponds to absorptions caused by interactions between ligand and metal). Bottom: 300 to 900 mV. Right: UV-Vis-NIR spectra of **E5** at rising potentials. Top: 0 to 575 mV. Middle: deconvolution of NIR absorptions at 575 mV using four distinct overlapping transitions with Gaussian shapes (dashed line indicates IVCT absorption, dotted line corresponds to absorptions caused by interactions between ligand and metal). Bottom: 575 to 900 mV. All potentials *vs.* Ag/AgCl at 25 °C in dichloromethane, supporting electrolyte [N$^n$Bu$_4$][B(C$_6$F$_5$)$_4$] (0.1 M). Arrows indicate increasing or decreasing as well as shifting absorptions.
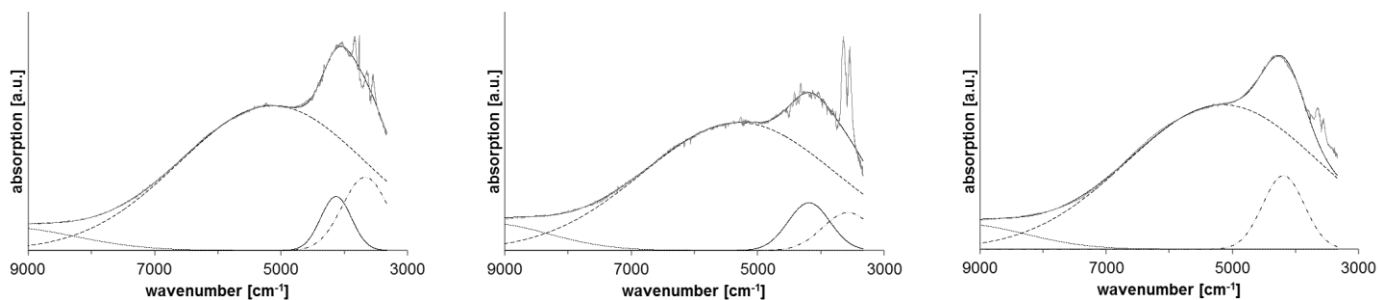


**Figure AE2-7**. Left: Deconvolution of NIR absorptions (at 520 mV) for **E5**$^+$ (1 mM) using four distinct overlapping transitions with Gaussian shapes (dashed line indicates IVCT transitions). Middle: Deconvolution of NIR absorptions (at 640 mV) for **E6**$^+$ (1 mM) using four distinct overlapping transitions with Gaussian shapes (dashed line indicates IVCT transitions). Right: Deconvolution of NIR absorptions (at 875 mV) for **E7**$^+$ (1 mM) using four distinct overlapping transitions with Gaussian shapes (dashed line indicates IVCT transitions). All potentials *vs.* Ag/AgCl at 25 °C in propylene carbonate, supporting electrolyte [N$^n$Bu$_4$][B(C$_6$F$_5$)$_4$] (0.1 M).
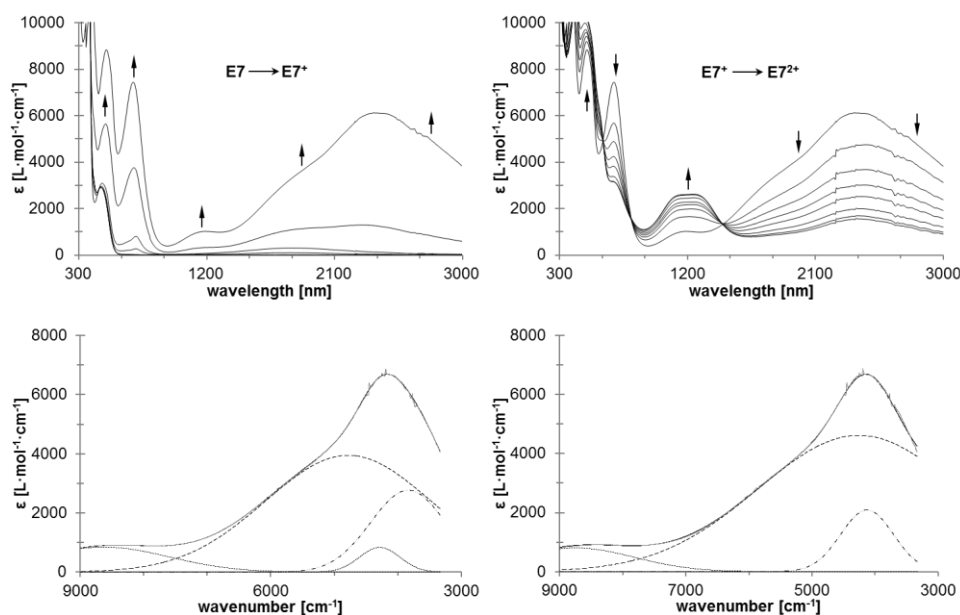
**Figure AE2-8**. UV-Vis/NIR spectra of **E7** at rising potentials. Left top: 0 to 525 mV. Left bottom: deconvolution of NIR absorptions at 525 mV using four distinct overlapping transitions with Gaussian shapes (dashed line indicates IVCT absorption, dotted line corresponds to absorptions caused by interactions between ligand and metal). Right top: 525 to 1100 mV. Right bottom: deconvolution of NIR absorptions at 525 mV using three distinct overlapping transitions with Gaussian shapes. All potentials *vs.* Ag/AgCl at 25 °C in dichloromethane, supporting electrolyte $[N^nBu_4][B(C_6F_5)_4]$ (0.1 M). Arrows indicate increasing or decreasing as well as shifting absorptions.

**Synthesis of 1-bromo-1'-(3,5-bis(trifluoromethyl)phenyl)-ferrocene (E8), 3,5-bis(trifluoromethyl)phenylferrocene (E9) and 1-bromo-1'''-(3,5-bis(trifluoromethyl)phenyl)-1',1''-bi-ferrocene (E10)**. A solution of 1,1'-dibromoferrocene[449] (4.0 g, 11.6 mmol) in 100 mL of tetrahydrofuran was cooled to –90 °C and 1.05 eq (4.9 mL) of 2.5 M *n*-butyllithium (*n*-hexane) were added within 5 min. After 45 min of isothermal stirring, 1.05 eq (3.41 g) of [ZnCl$_2$·2thf] were added in a single portion and the resulting reaction mixture was stirred for 30 min at 0 °C. Afterward, 2 eq (4.0 mL) of 1-bromo-3,5-bis(trifluoromethyl)benzene and 40.8 µmol (28 mg) of [Pd(CH$_2$CMe$_2$P$^t$Bu$_2$)(µ-Cl)]$_2$[229,230] were added and the reaction mixture was warmed to 30 °C for 25 h. After cooling to ambient temperature, the mixture was hydrolyzed with water, the aqueous layer was separated and extracted with dichloromethane (100 mL). The combined organic layers were dried over MgSO$_4$. After evaporation of all volatiles, the crude product was purified by column chromatography (column size: 20 x 3 cm, alumina) using *n*-hexane as eluent. After recrystallization from methanol, compound **E8** was obtained as an orange solid. Yield: 4.03 g (8.45 mmol, 73 % based on 1,1'-dibromoferrocene). From the supernatant solution, 3,5-bis(trifluoromethyl)phenylferrocene (**E9**) could be obtained as an orange solid (0.2 g, 0.50 mmol, 4 % based on 1,1'-dibromoferrocene). By the use of an *n*-hexane/diethylether mixture of ratio 5:1 (v/v) as eluent, 1-bromo-1'''-(3,5-

bis(trifluoromethyl)phenyl)-1',1''-biferrocene (**E10**) could be collected from a small band on the column and after crystallization from methanol as a red solid material (0.19 g, 0.29 mmol, 3 % based on 1,1'-dibromoferrocene).

**E8**: Mp: 55 °C. IR data (KBr)[cm$^{-1}$]: 3103 w, 3091 w, 1620 w, 1613 w, 1499 w, 1489 w, 1360 m, 1278 s, 1126 s, 890 m, 828 m, 698 m, 681 m. $^1$H NMR (CDCl$_3$)[$\delta$]: 7.86 (m, 2H, C$_6$H$_3$), 7.70 (m, 1H, C$_6$H$_3$), 4.72 (pt, $J_{HH}$ = 1.9 Hz, 2H, C$_5$H$_4$), 4.51 (pt, $J_{HH}$ = 1.9 Hz, 2H, C$_5$H$_4$), 4.25 (pt, $J_{HH}$ = 1.9 Hz, 2H, C$_5$H$_4$), 4.05 (pt, $J_{HH}$ = 1.9 Hz, 2H, C$_5$H$_4$). $^{13}$C{$^1$H} NMR (CDCl$_3$)[$\delta$]: 141.2 (C$_i$-C$_6$H$_3$), 131.9 (q, $J_{CF}$ = 33 Hz, C$_i$-C$_6$H$_3$), 126.1 (m, C$_6$H$_3$), 123.6 (q, $J_{CF}$ = 273 Hz, CF$_3$), 119.8 (m, C$_6$H$_3$), 84.0 (C$_i$-C$_5$H$_4$), 78.6 (C$_i$-C$_5$H$_4$), 72.5 (C$_5$H$_4$), 72.2 (C$_5$H$_4$), 69.4 (C$_5$H$_4$), 68.9 (C$_5$H$_4$). HR-ESI-MS (calc) {int} [m/z]: 475.9315 (475.9294) {100} [M]$^+$, 477.9289 (477.9273) {98} [M]$^+$.

**E9**: Anal. Calcd for C$_{18}$H$_{12}$F$_6$Fe (398.1): C, 54.30; H, 3.04. Found: C, 53.94; H, 3.26. Mp: 102 °C. IR data (KBr)[cm$^{-1}$]: 3089 w, 1623 w, 1499 m, 1363 s, 1271 s, 1128 s, 892 m, 829 m, 814 m, 702 s, 681 s. $^1$H NMR (CDCl$_3$)[$\delta$]: 7.84 (m, 2H, C$_6$H$_3$), 7.67 (m, 1H, C$_6$H$_3$), 4.71 (pt, $J_{HH}$ = 1.9 Hz, 2H, C$_5$H$_4$), 4.44 (pt, $J_{HH}$ = 1.9 Hz, 2H, C$_5$H$_4$), 4.08 (s, 5H, C$_5$H$_5$). $^{13}$C{$^1$H} NMR (CDCl$_3$)[$\delta$]: 143.0 (C$_i$-C$_6$H$_3$), 131.8 (q, $J_{CF}$ = 33 Hz, C$_i$-C$_6$H$_3$), 125.8 (m, C$_6$H$_3$), 123.6 (q, $J_{CF}$ = 273 Hz, CF$_3$), 119.4 (m, C$_6$H$_3$), 82.1 (C$_i$-C$_5$H$_4$), 70.3 (C$_5$H$_4$), 70.1 (C$_5$H$_5$), 67.1 (C$_5$H$_4$). HR-ESI-MS (calc) [m/z]: 398.0242 (398.0187) [M]$^+$.

**E10**: Anal. Calcd for C$_{28}$H$_{19}$BrF$_6$Fe$_2$ (661.0): C, 50.87; H, 2.90. Found: C, 51.13; H, 3.10. Mp: 128 °C. IR data (KBr)[cm$^{-1}$]: 3115 w, 3096 w, 3084 w, 1613 w, 1501 w, 1356 m, 1283 s, 1171 s, 1121 s, 885 m, 816 m, 695 m, 683 m. $^1$H NMR (CDCl$_3$)[$\delta$]: 7.56 (m, 1H, C$_6$H$_3$), 7.54 (m, 2H, C$_6$H$_3$), 4.52 (pt, $J_{HH}$ = 1.9 Hz, 2H, C$_5$H$_4$), 4.33 (pt, $J_{HH}$ = 1.9 Hz, 2H, C$_5$H$_4$), 4.26 (pt, $J_{HH}$ = 1.9 Hz, 2H, C$_5$H$_4$), 4.18 (pt, $J_{HH}$ = 1.9 Hz, 2H, C$_5$H$_4$), 4.07 (pt, $J_{HH}$ = 1.9 Hz, 2H, C$_5$H$_4$), 4.06 (pt, $J_{HH}$ = 1.9 Hz, 2H, C$_5$H$_4$), 3.99 (pt, $J_{HH}$ = 1.9 Hz, 2H, C$_5$H$_4$), 3.85 (pt, $J_{HH}$ = 1.9 Hz, 2H, C$_5$H$_4$). $^{13}$C{$^1$H} NMR (CDCl$_3$)[$\delta$]: 141.1 (C$_i$-C$_6$H$_3$), 131.5 (q, $J_{CF}$ = 33 Hz, C$_i$-C$_6$H$_3$), 125.4 (m, C$_6$H$_3$), 123.6 (q, $J_{CF}$ = 273 Hz, CF$_3$), 119.0 (m, C$_6$H$_3$), 84.8 (C$_i$-C$_5$H$_4$), 83.4 (C$_i$-C$_5$H$_4$), 82.5 (C$_i$-C$_5$H$_4$), 78.4 (C$_i$-C$_5$H$_4$), 71.6 (C$_5$H$_4$), 70.8 (C$_5$H$_4$), 70.5 (C$_5$H$_4$), 69.3 (C$_5$H$_4$), 68.4 (C$_5$H$_4$), 68.3 (C$_5$H$_4$), 67.8 (C$_5$H$_4$), 67.7 (C$_5$H$_4$). HR-ESI-MS (calc) {int} [m/z]: 659.9257 (659.9271) {100} [M]$^+$, 661.9240 (661.9249) {89} [M]$^+$. Crystal data for **E10**, C$_{28}$H$_{19}$BrF$_6$Fe, M$_r$ = 661.04 g·mol$^{-1}$, monoclinic, $P2_1/n$, $\lambda$ = 0.71073 Å, $a$ = 9.6500(2) Å, $b$ = 20.1919(4) Å, $c$ = 12.0152(3) Å, $\beta$ = 97.415(2) °, $V$ = 2321.61(9) Å$^3$, Z = 4, $\rho_{calcd}$ = 1.891 g·cm$^{-3}$, $\mu$ = 3.036 mm$^{-1}$, $T$ = 105.5(10) K, $\Theta$ range = 2.93 – 26.00 °, reflections collected: 21701, independent: 4547 ($R_{int}$ = 0.0330), $R_1$ = 0.0311, w$R_2$ = 0.0721 [$I$ > 2$\sigma$($I$)].

**Synthesis of 1-bromo-1'-dimethoxymethylferrocene (E11).** 1-Bromo-1'-formyl-ferrocene[277] (1.9 g, 6.49 mmol) was dissolved in 15 mL of trimethoxymethane and 0.1 mmol of 4-methylbenzenesulfonic acid monohydrate (20 mg) were added. The resulting solution was stirred at ambient temperature for 12 h. Afterward, the reaction mixture was hydrolyzed with 2 M NaOH (20 mL), the organic phase was separated and the aqueous layer was extracted exhaustively with diethyl ether. The combined organic phases were dried over $MgSO_4$ and filtered through a pad of alumina. After evaporation of all volatiles, compound **E11** was obtained as a bright orange oil. Yield: 2.19 g (6.46 mmol, 96 % based on 1-bromo-1'-formylferrocene). Anal. Calcd for $C_{13}H_{15}BrFeO_2$ (339.0): C, 46.06; H, 4.46. Found; C, 46.24; H, 4.55. IR data (NaCl)[cm$^{-1}$]: 3103 m, 2988 m, 2935 s, 2903 s, 2826 s, 1469 m, 1445 m, 1108 w, 1051 s, 823 s, 817 s. $^1$H NMR (acetone-$D_6$)[δ]: 5.46 (s, 1H, CH(OR)$_2$), 4.41 (pt, $J_{HH}$ = 1.9 Hz, 2H, $C_5H_4$), 4.32 (pt, $J_{HH}$ = 1.9 Hz, 2H, $C_5H_4$), 4.22 (pt, $J_{HH}$ = 1.9 Hz, 2H, $C_5H_4$), 4.17 (pt, $J_{HH}$ = 1.9 Hz, 2H, $C_5H_4$), 3.24 (s, 6H, OCH$_3$). $^{13}$C{$^1$H} NMR (acetone-$D_6$)[δ]: 102.0 (CH(OR)$_2$), 88.0 ($C_i$-$C_5H_4$), 79.0 ($C_i$-$C_5H_4$), 71.7 ($C_5H_4$), 71.3 ($C_5H_4$), 70.5 ($C_5H_4$), 69.0 ($C_5H_4$), 52.3 (OCH$_3$). HR-ESI MS (calc) {int} [m/z]: 337.9629 (337.9601) {100} [M]$^+$, 339.9607 (339.9579) {94} [M]$^+$.

APPENDIX AE3



| |
|---|
| N1(A) … O3(A) = 2.895(3) |
| N2–O3 … N1A = 162.67(15) |
| O1–N1 … O3A = 84.40(13) |
| A: 1-x,-y,2-z |

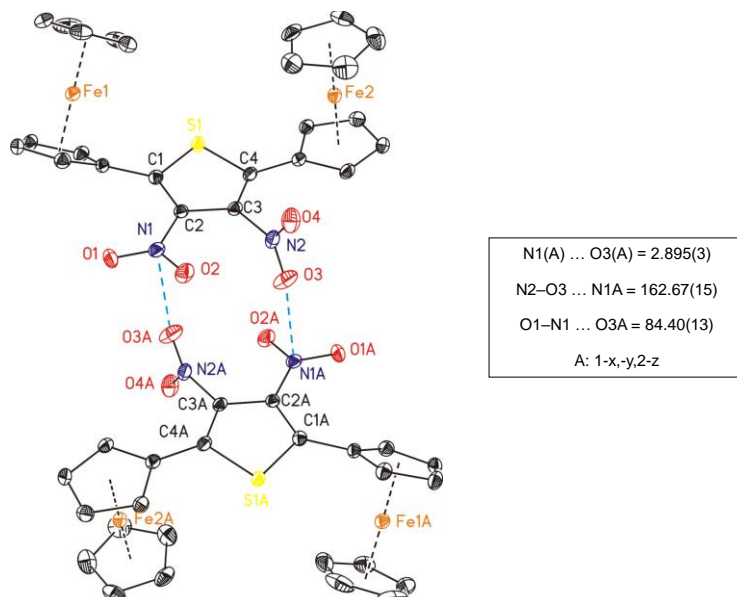**Figure AE3-1**. Dimeric structure of **E12** due to N-O interactions in the crystal packing.

**Table AE3-1. Plane intersections (°), bond distances (Å) and angles (°) involving the centroids of the cyclopentadienyls.**

| | Compd. | | | |
|---|---|---|---|---|
| | **E12** | **E13** | **E14** | **E15** |
| C$_4$S … C$_5$H$_4$ | 39.80(7)<br>11.95(8) | 35.95(10) | 22.8(2)<br>16.2(3) | 35.04(10) |
| torsions | 15.03(17)<br>8.91(16) | 14.0(3) | 1.68(4)<br>8.26(3) | 13.2(3) |
| D⋯Fe | 1.6494(3)<br>1.6540(3)<br>1.6445(3)<br>1.6514(3) | 1.655(14)<br>1.658(14) | 1.6473(6)<br>1.6402(6)<br>1.6419(6)<br>1.6515(6) | 1.650(11)<br>1.652(11) |
| D⋯Fe⋯D | 179.16(2)<br>178.72(2) | 179.3(9) | 178.64(4)<br>176.47(4) | 179.0(4) |

**Table AE3-2. UV-Vis absorption and multiple correlation analysis data of E12 and E14 according to Kamlet-Taft and Catalán.**

| solvent | $\tilde{\nu}_{max}$ [nm] | | $\tilde{\nu}_{max}$ [10$^3$ cm$^{-1}$] | | $\tilde{\nu}_{max}$ [10$^3$ cm$^{-1}$] (calculated according to Kamlet-Taft) | | $\tilde{\nu}_{max}$ [10$^3$ cm$^{-1}$] (calculated according to Catalán) | |
|---|---|---|---|---|---|---|---|---|
| | **E12** | **E14** | **E12** | **E14** | **E12**[a] | **E14** | **E12**[b] | **E14**[c] |
| 1,1,2,2,-tetrachloroethane | 531 | 610 | 18.832 | 16.393 | 18.729 | 16.439 | 18.794 | 16.380 |
| 1,1,1-trichloroethane | 517 | 611 | 19.342 | 16.367 | 19.322 | 16.418 | 19.252 | 16.450 |
| 1-butanol | 517 | 601 | 19.342 | 16.639 | 19.348 | 16.573 | 19.255 | 16.511 |
| 1-bropanol | 520 | 608 | 19.231 | 16.447 | 19.284 | 16.584 | 19.212 | 16.547 |
| 1-decylalkohol | 513 | 611 | 19.493 | 16.367 | 19.374 | 16.564 | 19.378 | 16.408 |
| 2,2,2,-trifluoroethanol | 526 | 605 | 19.011 | 16.529 | 19.013 | 16.486 | 19.305 | 16.504 |
| 2-propanol | 516 | 601 | 19.380 | 16.639 | 19.335 | 16.570 | 19.214 | 16.632 |
| acetone | 522 | 600 | 19.157 | 16.667 | 19.038 | 16.495 | 19.096 | 16.712 |
| acetonitrile | 524 | 596 | 19.084 | 16.779 | 18.987 | 16.496 | 19.054 | 16.707 |
| formic acid | -- | -- | -- | -- | 19.116 | 16.528 | -- | -- |
| anisole | 524 | 612 | 19.084 | 16.340 | 19.013 | 16.476 | 19.048 | 16.336 |
| benzene | 518 | 612 | 19.305 | 16.340 | 19.193 | 16.438 | 19.326 | 16.313 |
| benzonitrile | 530 | 610 | 18.868 | 16.393 | 18.793 | 16.492 | 18.733 | 16.393 |
| butyrolactone | 527 | 606 | 18.975 | 16.502 | 18.832 | 16.508 | 18.812 | 16.528 |
| CHCl$_3$ | 523 | 610 | 19.120 | 16.393 | 19.206 | 16.445 | 19.066 | 16.401 |
| cyclohexane | -- | 606 | -- | 16.502 | 19.954 | 16.396 | 19.770 | 16.382 |
| 1,1-dichlororethane | 524 | 607 | 19.084 | 16.474 | 18.909 | 16.448 | 18.986 | 16.464 |
| dichlorormethane | 524 | 608 | 19.084 | 16.447 | 18.897 | 16.453 | 18.984 | 16.486 |
| 1,4-dioxane | 519 | 604 | 19.268 | 16.556 | 19.245 | 16.476 | 19.406 | 16.426 |
| DMOE | 522 | 600 | 19.157 | 16.667 | 19.271 | 16.481 | 19.258 | 16.609 |
| DMSO | 546 | 606 | 18.315 | 16.502 | 18.664 | 16.554 | 18.655 | 16.483 |
| acetic acid | -- | -- | -- | -- | 19.129 | 16.534 | 19.285 | 16.386 |
| Et$_2$O | 512 | 602 | 19.531 | 16.611 | 19.606 | 16.478 | 19.591 | 16.618 |
| ethanol | 521 | 606 | 19.194 | 16.502 | 19.258 | 16.564 | 19.234 | 16.569 |
| EtOAc | 516 | 601 | 19.380 | 16.639 | 19.245 | 16.487 | 19.334 | 16.625 |
| ethylene glycol | -- | -- | -- | -- | 18.767 | 16.549 | 18.836 | 16.283 |
| form amide | -- | -- | -- | -- | 18.703 | 16.538 | 18.683 | 16.312 |
| n-hexane | 504 | 610 | 19.841 | 16.393 | 20.006 | 16.394 | 19.907 | 16.471 |
| hexafluoro-2-propanol | 550 | -- | 18.182 | -- | 19.116 | 16.499 | -- | -- |
| HMPA | 526 | 601 | 19.011 | 16.639 | 18.832 | 16.591 | 18.749 | 16.667 |
| methanol | 519 | 604 | 19.268 | 16.556 | 19.180 | 16.558 | 19.187 | 16.552 |
| N,N-dimethyl-acetamide | 536 | 604 | 18.657 | 16.556 | 18.819 | 16.548 | 18.802 | 16.586 |
| N,N-dimethyl-formamide | 533 | 604 | 18.762 | 16.556 | 18.819 | 16.538 | 18.819 | 16.585 |
| nitromethane | 527 | 601 | 18.975 | 16.639 | 18.858 | 16.452 | 18.937 | 16.597 |
| N-methylformamide | 540 | 601 | 18.519 | 16.639 | 18.793 | 16.578 | -- | -- |
| propionic acid | -- | -- | -- | -- | 19.206 | 16.531 | 19.455 | 16.330 |
| pyridine | 539 | 617 | 18.553 | 16.207 | 18.832 | 16.530 | 18.825 | 16.409 |
| triethylamine | -- | -- | -- | -- | 19.774 | 16.507 | 19.729 | 16.508 |
| carbon tetrachloride | 511 | 617 | 19.569 | 16.207 | 19.593 | 16.423 | 19.597 | 16.265 |
| tetramethylurea | 536 | 601 | 18.657 | 16.639 | 18.884 | 16.552 | 18.860 | 16.544 |
| tetrahydrofuran | 520 | 607 | 19.231 | 16.474 | 19.206 | 16.503 | 19.190 | 16.559 |
| toluene | 515 | 613 | 19.417 | 16.313 | 19.258 | 16.437 | 19.337 | 16.332 |
| water | -- | -- | -- | -- | 18.548 | 16.559 | 18.962 | 16.269 |
| xylene | 517 | 612 | 19.342 | 16.340 | 19.400 | 16.433 | 19.434 | 16.309 |

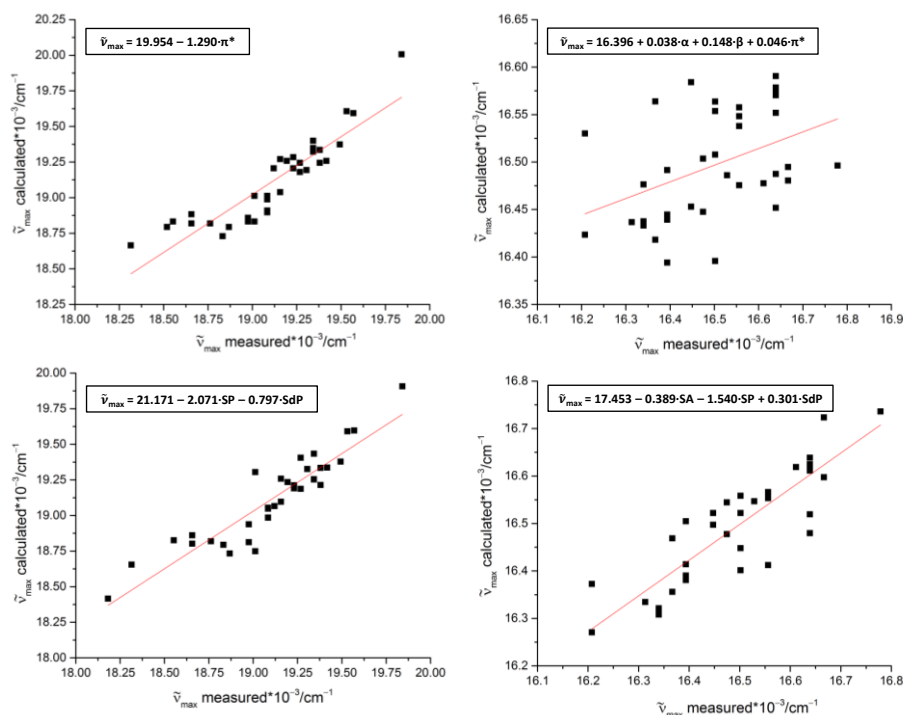[a] Without $\alpha$ and $\beta$. [b] Without *SA* and *SB*. [c] Without *SB*.

**Figure AE3-2**. Multiple correlation analysis of **E12** (left) and **E14** (right) according to Kamlet-Taft (top) and Catalán (bottom). The relevant data are depicted in Table AE3-2 (*vide supra*).

**Table AE3-3. Summarized results of the multiple correlation analysis of the Kamlet-Taft and the Catalán approach.**

| | *Kamlet-Taft – Equation (1)* | | | | | | |
|---|---|---|---|---|---|---|---|
| Compd. | $\tilde{\nu}_{max,0}$ [$10^3$ cm$^{-1}$][a] | a | b | s | n | $r^2$ | f |
| E12 | 19.980 | 0.034 | −0.150 | −1.240 | 35 | 0.82 | $< 4.36 \cdot 10^{-12}$ |
| | 19.954 | / | / | −1.290 | 35 | 0.81 | $< 1.56 \cdot 10^{-13}$ |
| E14 | 16.396 | 0.038 | 0.148 | 0.046 | 36 | 0.10 | $< 0.10$ |

| | *Catalán – Equation (2)* | | | | | | | |
|---|---|---|---|---|---|---|---|---|
| | $\tilde{\nu}_{max,0}$ [$10^3$ cm$^{-1}$][b] | a | b | d | e | n | $r^2$ | f |
| E12 | 21.350 | −0.161 | −0.006 | −2.317 | −0.768 | 34 | 0.79 | $< 2.13 \cdot 10^{-10}$ |
| | 21.171 | / | / | −2.071 | −0.797 | 34 | 0.80 | $< 5.09 \cdot 10^{-12}$ |
| E14 | 17.410 | −0.386 | 0.056 | −1.493 | 0.279 | 35 | 0.73 | $< 5.35 \cdot 10^{-9}$ |
| | 17.453 | −0.389 | / | −1.540 | 0.301 | 35 | 0.73 | $< 1.58 \cdot 10^{-9}$ |

[a] Corresponds to the absorption maximum in the reference system cyclohexane ($\alpha$, $\beta$ and $\pi^* = 0$ by definition). [b] Corresponds to the absorption maximum in gas phase (*SA*, *SB*, *SdP* and *SdP* = 0 by definition).
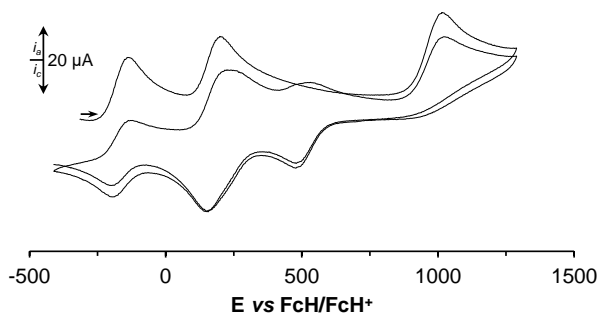


**Figure AE3-3**. Full range cyclic voltammogram of **E13**. Scan rate: 100 mVs$^{-1}$ in dichloromethane solutions (1.0 mM) at 25 °C, supporting electrolyte [N$^n$Bu$_4$][B(C$_6$F$_5$)$_4$] (0.1 M). The initial and the 2$^{nd}$ scan are shown.
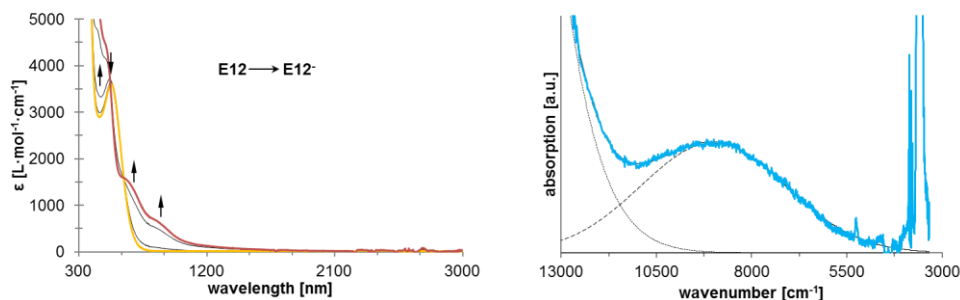
**Figure AE3-4**. Left: UV-Vis-NIR spectra of **E12** at decreasing potentials (–300 to –1100 mV). All potentials *vs.* Ag/AgCl at 25 °C in dichloromethane, supporting electrolyte [N$^n$Bu$_4$][B(C$_6$F$_5$)$_4$] (0.1 M). Right: Deconvolution of NIR absorptions (at 700 mV) for **E12**$^+$ (1.5 mM) using two distinct overlapping transitions with Gaussian shapes (dashed line indicates IVCT transitions). All potentials *vs.* Ag/AgCl at 25 °C in propylene carbonate, supporting electrolyte [N$^n$Bu$_4$][B(C$_6$F$_5$)$_4$] (0.1 M).
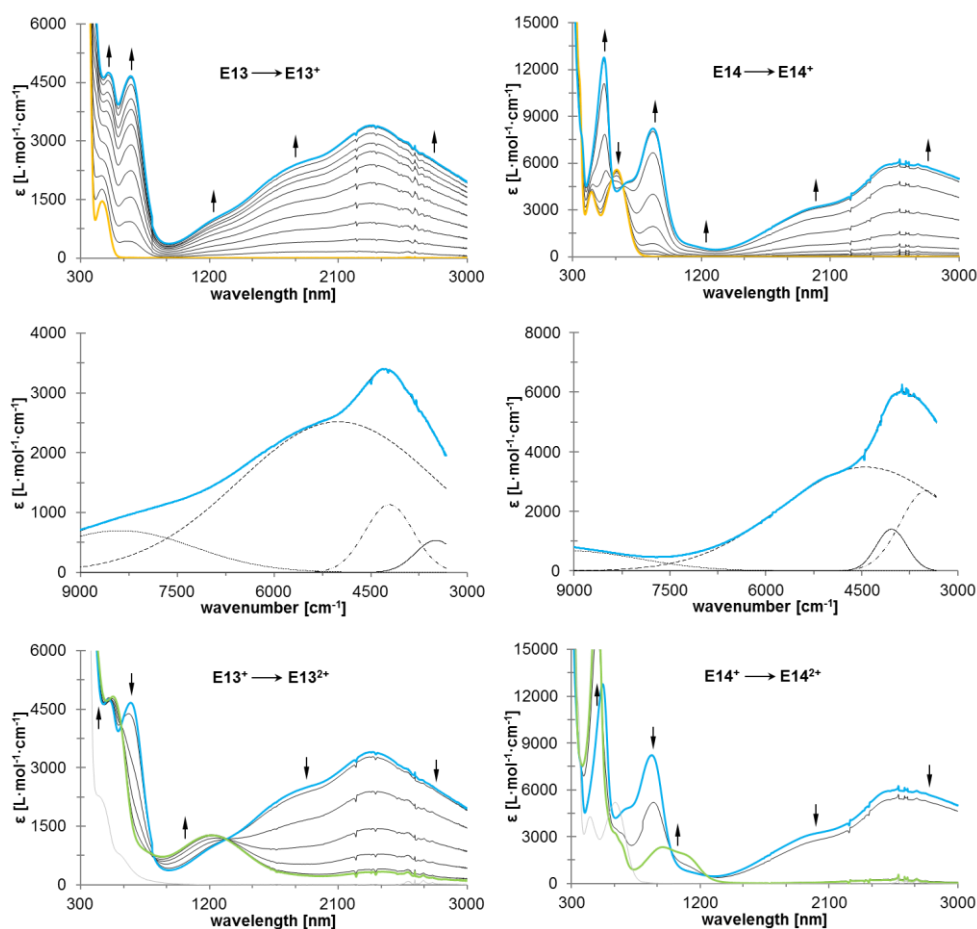


**Figure AE3-5**. Left: UV-Vis-NIR spectra of **E13** at rising potentials. Top: –100 to 600 mV. Middle: deconvolution of NIR absorptions at 600 mV using four distinct overlapping transitions with Gaussian shapes (dashed line indicates IVCT absorption, dotted line corresponds to absorptions caused by interactions between ligand and metal, solid line and dotted dashed line indicates IC transitions). Bottom: 600 to 800 mV (grey line represents re-reduction to the neutral species). Right: UV-Vis-NIR spectra of **E14** at rising potentials. Top: –300 to 450 mV. Middle: deconvolution of NIR absorptions at 450 mV using four distinct overlapping transitions with Gaussian shapes (dashed line indicates IVCT absorption, dotted line corresponds to absorptions caused by interactions between ligand and metal, solid line and dotted dashed line indicates IC transitions). Bottom: 450 to 550 mV (grey line represents re-reduction to the neutral species). All potentials *vs.* Ag/AgCl at 25 °C in dichloromethane, supporting electrolyte [N$^n$Bu$_4$][B(C$_6$F$_5$)$_4$] (0.1 M). Arrows indicate increasing or decreasing as well as shifting absorptions.
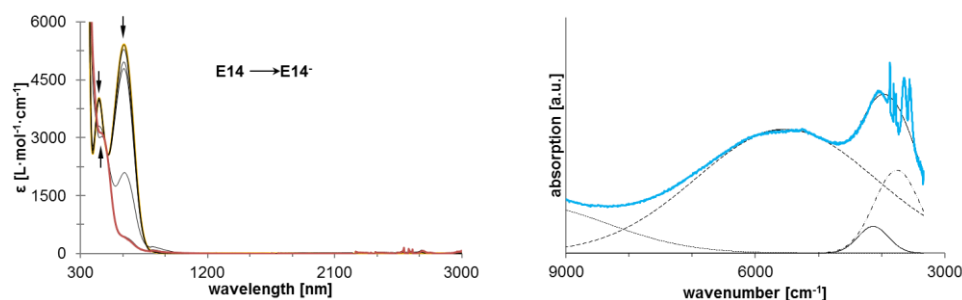
199

**Figure AE3-6**. Left: UV-Vis-NIR spectra of **E14** at decreasing potentials (–500 to –1400 mV). All potentials *vs.* Ag/AgCl at 25 °C in dichloromethane, supporting electrolyte $[N^nBu_4][B(C_6F_5)_4]$ (0.1 M). R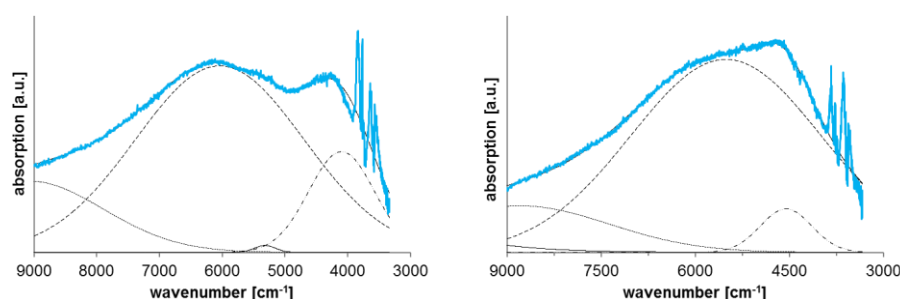ight: Deconvolution of NIR absorptions (at 560 mV) for **E14**$^+$ (1 mM) using four distinct overlapping transitions with Gaussian shapes (dashed line indicates IVCT transitions). All potentials *vs.* Ag/AgCl at 25 °C in propylene carbonate, supporting electrolyte $[N^nBu_4][B(C_6F_5)_4]$ (0.1 M).



**Figure AE3-7**. Left: Deconvolution of NIR absorptions (at 475 mV) for **E13**$^+$ (0.5 mM) using four distinct overlapping transitions with Gaussian shapes (dashed line indicates IVCT transitions). Right: Deconvolution of NIR absorptions (at 450 mV) for **E15**$^+$ (0.5 mM) using four distinct overlapping transitions with Gaussian shapes (dashed line indicates IVCT transitions). All potentials *vs.* Ag/AgCl at 25 °C in propylene carbonate, supporting electrolyte $[N^nBu_4][B(C_6F_5)_4]$ (0.1 M).
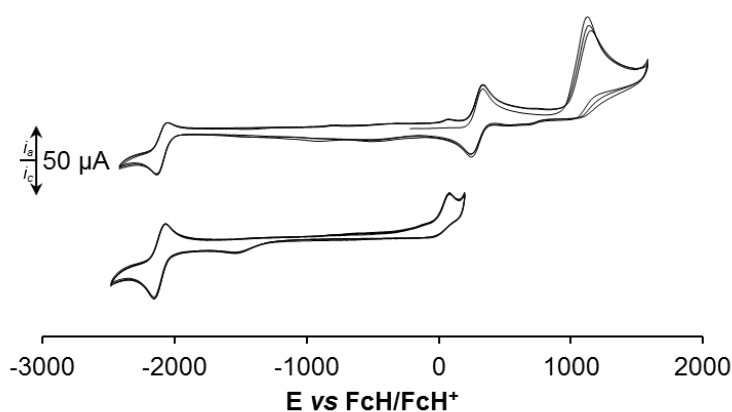
# APPENDIX AF

## APPENDIX AF1



**Figure AF1-1**. Cyclic voltammograms (multi scan) of **F1**. Scan rates: 100 mVs$^{-1}$ (top) and 500 mV$^{-1}$ (bottom) in dichloromethane solutions (1.0 mM) at 25 °C, supporting electrolyte $[N^nBu_4][B(C_6F_5)_4]$ (0.1 M).
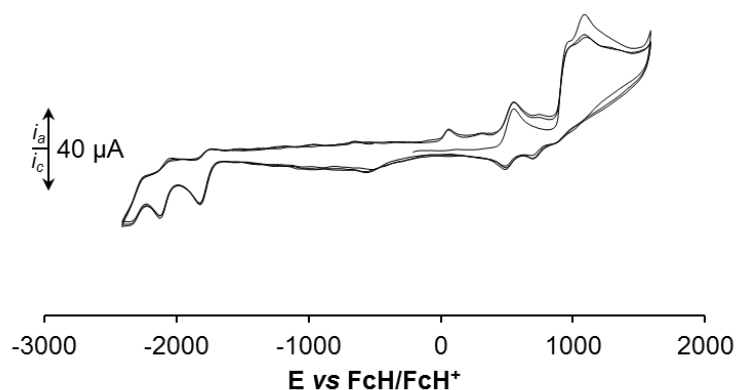
**Figure AF1-2**. Cyclic voltammogram (multi scan) of **F2**. Scan rate: 100 mVs$^{-1}$ in dichloromethane solutions (1.0 mM) at 25 °C, supporting electrolyte [N$^n$Bu$_4$][B(C$_6$F$_5$)$_4$] (0.1 M).
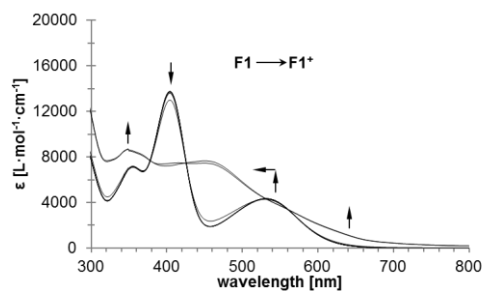


**Figure AF1-3**. UV-Vis spectra of **F1** at rising potentials (0 to 700 mV). All potentials *vs.* Ag/AgCl at 25 °C in dichloromethane, supporting electrolyte [N$^n$Bu$_4$][B(C$_6$F$_5$)$_4$] (0.1 M). Arrows indicate increasing or decreasing as well as shifting absorptions.
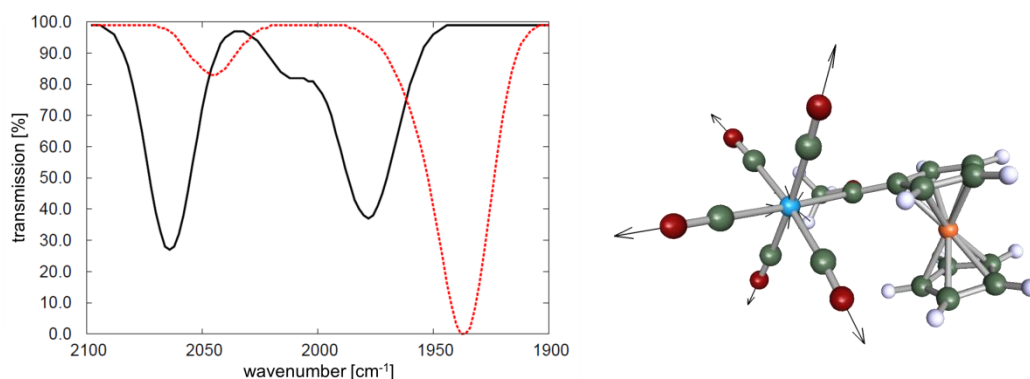


**Figure AF1-4**. Left: Calculated $\nu$(CO) stretching frequencies of **F1** (red line) and **F1**$^+$ (black line). Computational details are given in the Experimental Section. Right: Visualization of calculated $\nu$(CO) vibration mode for **F1** at 2045 cm$^{-1}$ (A$_1^{''}$, Figure AF1-4 left)
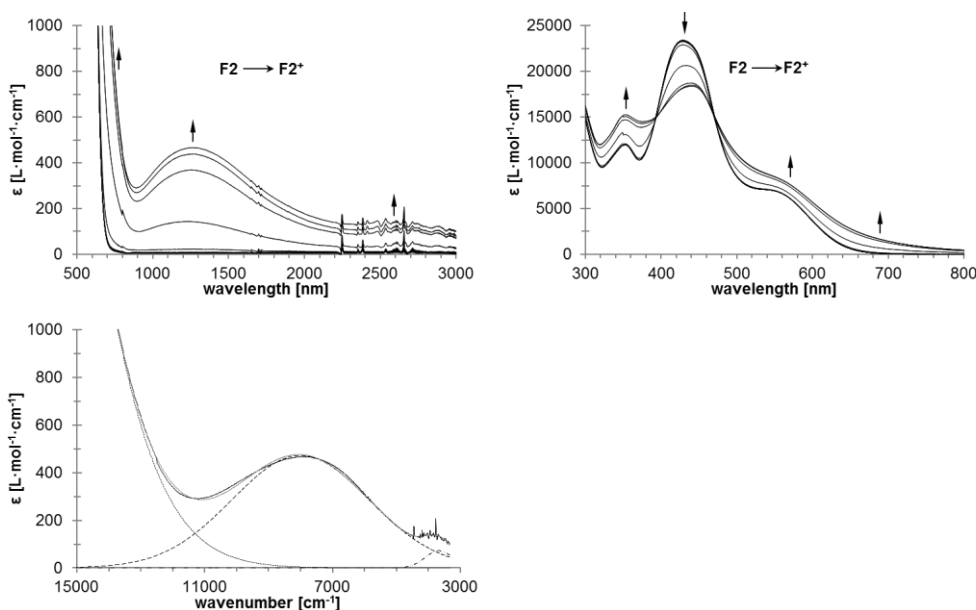
201

**Figure AF1-5**. UV-Vis-NIR spectra of **F2** at rising potentials (–100 to 1000 mV). Right: 300 – 800 nm. Left: 500 – 3000 nm. Bottom: deconvolution of NIR absorptions at 1000 mV, using three distinct overlapping transitions with Gaussian shapes (dashed line indicates MMCT absorptions, dotted line corresponds to absorptions caused by interactions between ligand and metal, dotted dashed line represents ligand field transitions). All potentials *vs.* Ag/AgCl at 25 °C in dichloromethane, supporting electrolyte [N$^n$Bu$_4$][B(C$_6$F$_5$)$_4$] (0.1 M). Arrows indicate increasing or decreasing as well as shifting absorptions.



**Figure AF1-6**. UV-Vis-NIR spectra of **F3** at rising potentials (left: –100 to 400 mV; right: 400 to 1000 mV). Top: 300 – 800 nm. Middle: 500 – 3000 nm. Bottom (left): deconvolution of NIR absorptions at 400 mV, using four distinct overlapping transitions with Gaussian shapes. Bottom (right): deconvolution of NIR absorptions at 1000 mV, using three distinct overlapping transitions with Gaussian shapes (dashed line

indicates IVCT (grey) or MMCT (black) absorptions, dotted line corresponds to absorptions caused by interactions between ligand and metal (black) as well as intrabiferrocenyl transitions (IBT, grey), dotted-dashed line represents ligand field transitions). All potentials *vs.* Ag/AgCl at 25 °C in dichloromethane, supporting electrolyte $[N^nBu_4][B(C_6F_5)_4]$ (0.1 M). Arrows indicate increasing or decreasing as well as shifting absorptions.
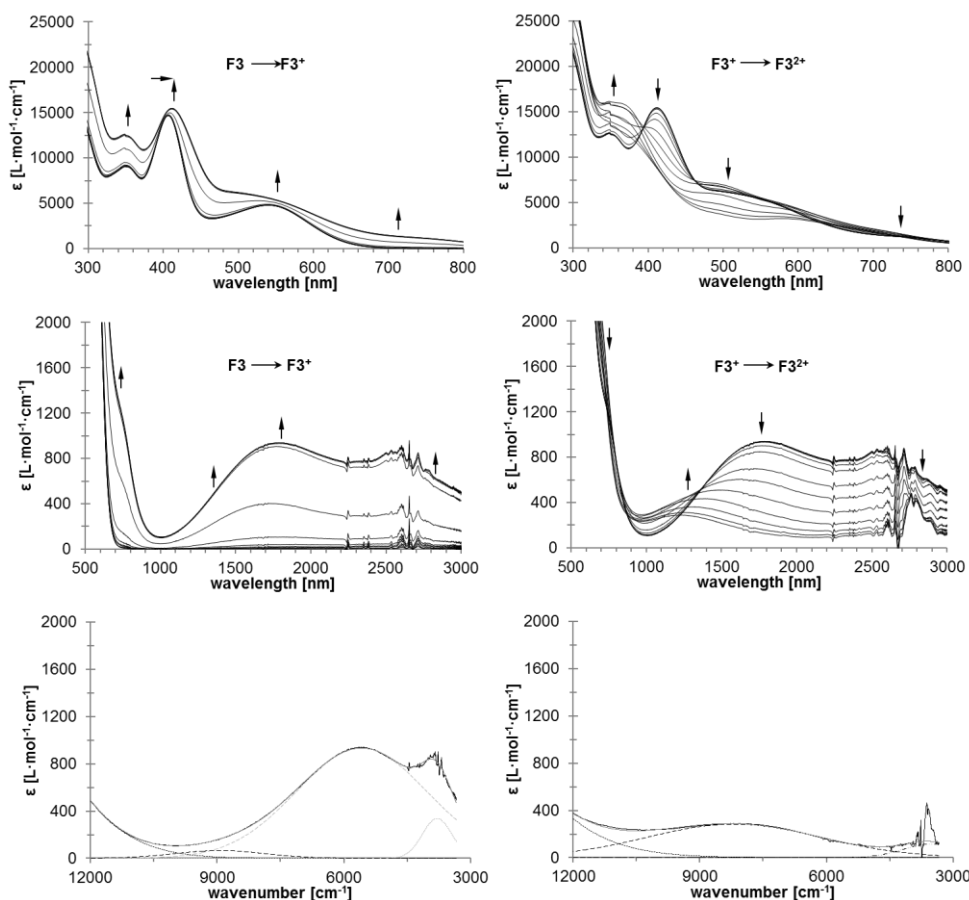


**Figure AF1-7**. UV-Vis spectra of **F4** at rising potentials (left: –100 to 600 mV; right: 600 to 1050 mV). All potentials *vs.* Ag/AgCl at 25 °C in dichloromethane, supporting electrolyte $[N^nBu_4][B(C_6F_5)_4]$ (0.1 M). Arrows indicate increasing or decreasing as well as shifting absorptions.
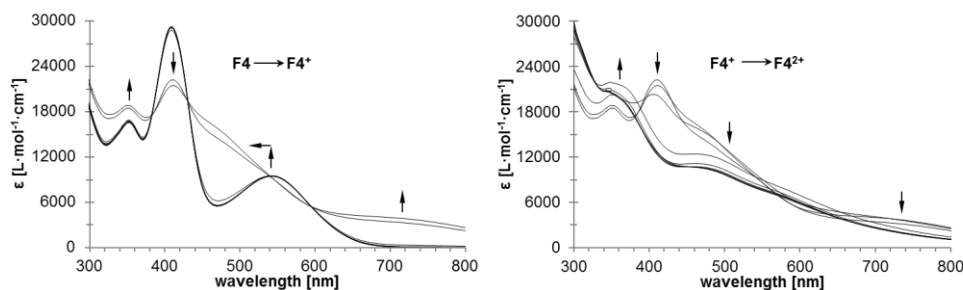
**Table AF1-1. Data Collection and Crystal Structure Details for F1 – F4.**

| | F1 | F2 | F3 | F4 |
|---|---|---|---|---|
| Chemical formula | $C_{17}H_{12}FeO_6W$ | $C_{24}H_{14}FeO_{12}W_2$ | $C_{27}H_{20}Fe_2O_6W$ | $C_{34}H_{22}Fe_2O_{12}W_2$ |
| Formula weight | 551.97 | 917.90 | 735.98 | 1101.92 |
| Crystal system, Space group | orthorhombic, $Pca2_1$ | orthorhombic, $Pbcn$ | triclinic, $P{-}1$ | monoclinic, $P2_1/n$ |
| $a$ [Å] | 20.2216(14) | 13.5817(8) | 7.2565(3) | 10.4968(3) |
| $b$ [Å] | 6.9527(5) | 14.2798(8) | 22.2626(7) | 13.1509(3) |
| $c$ [Å] | 11.7231(9) | 13.2044(6) | 31.8703(10) | 11.9019(3) |
| $\alpha, \beta, \gamma$ [°] | | | 105.358(3), 95.673(3), 98.626(3) | 97.546(2) |
| $V$ [Å$^3$] | 1648.2(2) | 2560.9(2) | 4856.5(3) | 1628.74(7) |
| $\rho_{calc.}$ [g cm$^{-3}$] | 2.224 | 2.381 | 2.013 | 2.247 |
| $F(000)$ | 1048 | 1712 | 2848 | 0.71073 A |
| Crystal dimensions [mm] | 0.4 x 0.2 x 0.05 | 0.4 x 0.4 x 0.01 | 0.40 x 0.28 x 0.02 | 0.40 x 0.40 x 0.40 |
| Z | 4 | 4 | 8 | 2 |
| Max., min. transmission | 1.000, 0.592 | 1.000, 0.386 | 0.890, 0.200 | 0.1426, 0.1426 |
| $\mu$ [mm$^{-1}$] | 7.884 | 9.585 | 5.946 | 7.979 |
| $\theta$ [°] | 3.10–25.25 | 3.09–25.23 | 2.90–25.25 | 3.10–25.24 |
| Index ranges | $-24 \le h \le 20$ | $-10 \le h \le 16$ | $-8 \le h \le 8$ | $-12 \le h \le 12$ |
| | $-5 \le k \le 8$ | $-17 \le k \le 17$ | $-26 \le k \le 26$ | $-15 \le k \le 15$ |
| | $-13 \le l \le 14$ | $-15 \le l \le 15$ | $-38 \le l \le 38$ | $-11 \le l \le 14$ |
| Total/unique reflections | 6596/2749 | 8750/2302 | 45035/17555 | 11708/2938 |
| Completeness to $F^2$ | 98.5 % | 99.2 % | 99.7 % | 99.2 % |
| Data/restraints/parameters | 2749/371/227 | 2302/308/182 | 17555/466/1297 | 2938/121/226 |
| $R_{int}$ | 0.0510 | 0.0726 | 0.0405 | 0.0332 |
| $R_1, wR_2, [I \ge 2\sigma(I)]$ | 0.0519, 0.1287 | 0.0564, 0.1372 | 0.0356, 0.0760 | 0.0184, 0.0414 |
| $R_1, wR_2$ (all data) | 0.0581, 0.1337 | 0.0673, 0.1457 | 0.0463, 0.0802 | 0.0204, 0.0422 |
| Goodness-of-fit (S) on $F^2$ | 1.061 | 1.049 | 1.033 | 1.075 |
| Largest diff. peak and hole [e Å$^{-3}$] | 4.828, –1.400 | 2.760, –1.980 | 2.662, –1.273 | 0.562, –0.487 |

Absolute structure parameter:[323] 0.30(2) for **F1**.
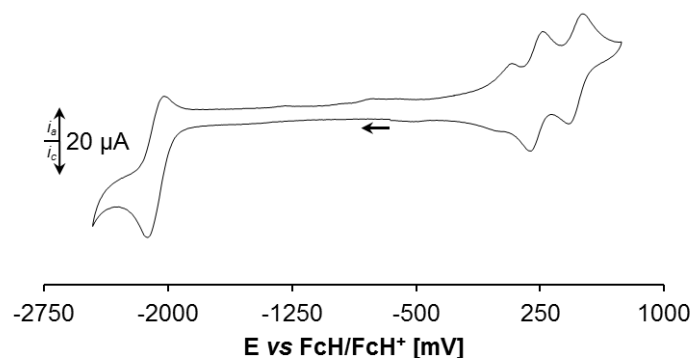
**Figure AF2-1**. Cyclic voltammogram of **F9**. Scan rate: 300 mVs$^{-1}$ in dichloromethane solutions (1.0 mM) at 25 °C, supporting electrolyte [N$^{n}$Bu$_4$][B(C$_6$F$_5$)$_4$] (0.1 mol$^{.}$L$^{-1}$)
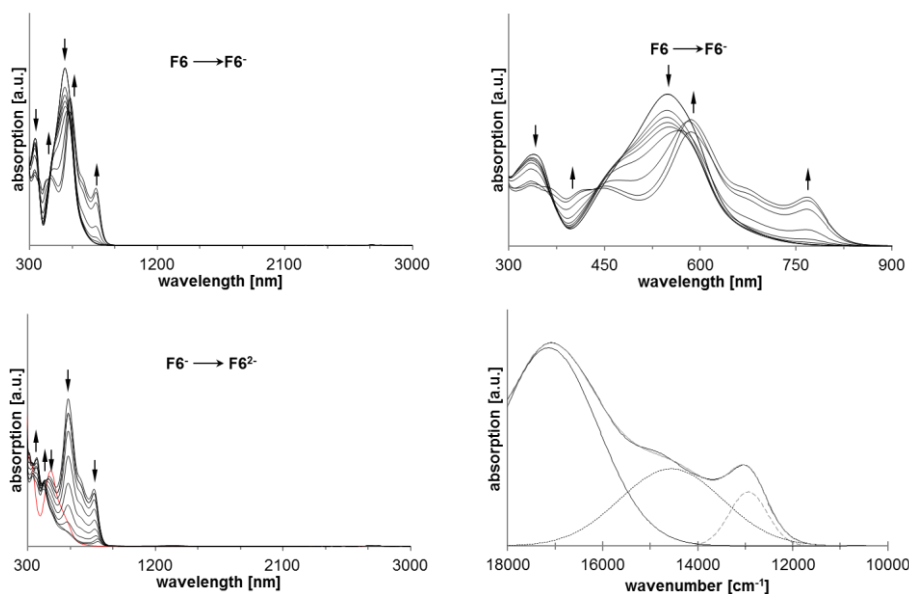


**Figure AF2-2**. Left: UV-Vis-NIR spectra of **F6** (2 mM) at rising potentials. Top: 200 to –610 mV. Bottom: –610 to –700 mV (red line represents reoxidation to the neutral species). Right: UV-Vis spectra of **F6** (2 mM) at rising potentials. Top: 200 to –610 mV. Bottom: deconvolution of UV-Vis absorptions at –610 mV, using three distinct overlapping transitions with Gaussian shapes. All potentials *vs.* Ag/AgCl at 25 °C in dichloromethane, supporting electrolyte [N$^{n}$Bu$_4$][B(C$_6$F$_5$)$_4$] (0.1 M). Arrows indicate increasing or decreasing as well as shifting absorptions.

**Table AF2-1. Crystal data and sturcture refinement for F7, F8 and F9.**

| | F7 | F8 | F9 |
|---|---|---|---|
| Chemical formula | $C_{11}H_6O_6SW$ | $C_{31}H_{22}Fe_2O_6SW$ | $C_{38}H_{24}Fe_2O_{12}SW_2$ |
| Formula weight | 450.07 | 818.10 | 1184.03 |
| $T$ [K] | 100(2) | 105.00(10) | 103.3(2) |
| $\lambda$ [Å] | 0.71073 | 1.54184 | 0.71073 |
| Crystal system, | monoclinic | monoclinic | triclinic |
| Space group | $P2_1/n$ | $P2_1/n$ | $P{-}1$ |
| a [Å] | a = 10.9273(5) | a = 14.3408(5) | a = 6.9273(4) |
| b [Å] | b = 11.1569(3) | b = 7.4003(2) | b = 10.4607(8) |
| c [Å] | c = 11.7633(4) | c = 26.4417(11) | c = 13.1390(13) |
| $\alpha, \beta, \gamma$ [°] | -, 116.617(5), - | -, 91.874(3), - | 96.050(7), 105.079(7), 99.971(6) |
| $V$ [Å$^3$] | 1282.13(8) | 2804.66(17) | 894.04(12) |
| Z, Calculated density | 4 | 4 | 1 |
| $\rho_{calcd}$ [g·cm$^{-3}$] | 2.332 | 1.937 | 2.199 |
| $\mu$ [mm$^{-1}$] | 9.190 | 16.672 | 7.332 |
| $F(000)$ | 840 | 1592 | 564 |
| Crystal size [mm] | 0.20 x 0.20 x 0.10 | 0.40 x 0.20 x 0.04 | 0.20 x 0.20 x 0.20 |
| $\Theta$ range [°] | 3.42 – 25.25 | 3.34 – 66.00 | 3.08 – 25.49 |
| Reflections collected / unique | 8217 / 2309 | 13589 / 4860 | 10980 / 3307 |
| $R_{int}$ | 0.0316 | 0.0387 | 0.0418 |
| Completeness to $\Theta$ | 99.1 % | 99.7 % | 99.4 % |
| Data / restraints / parameters | 2309 / 96 / 168 | 4860 / 0 / 370 | 3307 / 46 / 293 |
| Goodness-of-fit ($S$) on $F^2$ | 1.040 | 1.058 | 1.063 |
| $R_1$ , $wR_2$ [$I$>2sigma($I$)] | 0.0215, 0.0494 | 0.0423, 0.1138 | 0.0366, 0.1008 |
| $R_1$ , $wR_2$ (all data) | 0.0250, 0.0509 | 0.0435, 0.1152 | 0.0418, 0.1040 |
| Largest diff. peak and hole [eÅ$^{-3}$] | 1.261, –1.212 | 3.708, –1.539 | 2.486, –1.163 |

APPENDIX AG
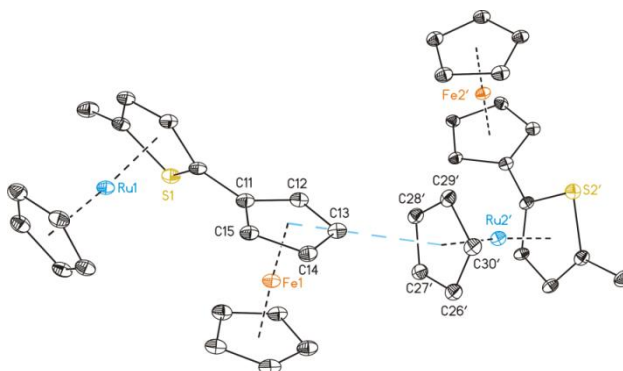


**Figure AG-1**. ORTEP diagram (30 % probability level) of the molecular structures of **G3** with selected atom-numbering scheme, showing the intermolecular *T*-shaped π interaction of 4.549(14) Å ($\alpha$ = 89.2(13) °). (Symmetry operation ('): 1–x, 2–y, 1–z)
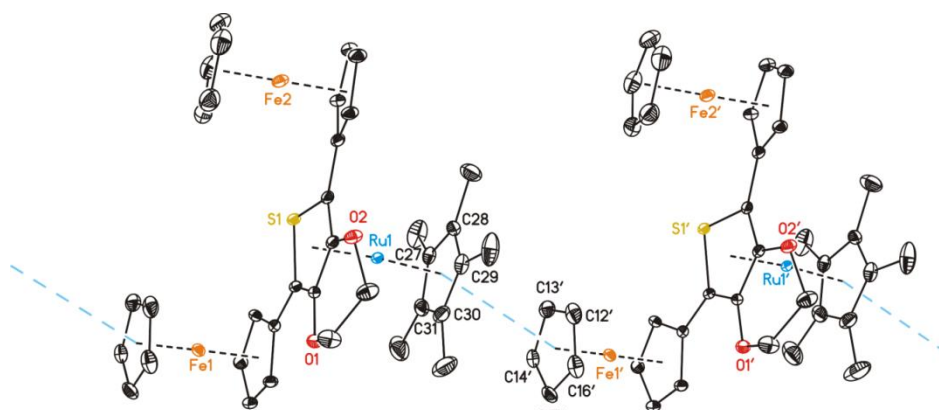
**Figure AG-2**. ORTEP diagram (30 % probability level) of the molecular structures of **G11** with selected atom-numbering scheme, showing the intermolecular parallel-displaced π-π interactions of 3.662(3) Å (α = 7.8(3) °) along [100]. (Symmetry operation ('): 1+x, y, z)

**Table AG-1. Selected bond distances (Å), angles (°) and torsion angles (°) of G3, G5, G7, G9 and G11.**

| Compound | G3 | G5 | G7 | G9 | G11 |
|---|---|---|---|---|---|
| Ct(C₅H₄) … Fe | 1.648(3) | 1.6409(9) | 1.6427(8) | 1.6438(5) | 1.6414(5) |
| | 1.650(3) | 1.6418(9) | 1.619(11) | | 1.6463(6) |
| | | 1.6559(9) | | | |
| Ct(C₅H₅) … Fe | 1.637(3) | 1.6415(9) | 1.6533(8) | 1.6535(5) | 1.6478(5) |
| | 1.666(3) | 1.6598(9) | 1.667(11) | | 1.6586(6) |
| | | 1.6671(9) | | | |
| Ct(C₄S) … Ru | 1.7956(16) | 1.8059(7) | 1.8089(5) | 1.7983(3) | 1.8195(3) |
| | 1.8069(16) | 1.8162(7) | 1.796(5) | | |
| | | 1.8206(6) | | | |
| Ct(C₅) … Ru | 1.8188(16) | 1.8156(7) | 1.7949(5) | 1.8109(3) | 1.8125(3) |
| | 1.8177(16) | 1.8253(7) | 1.830(5) | | |
| | | 1.8282(6) | | | |
| tors Fc | 8.9(16) | 0.4(5) | 23.1(4) | 12.1(3) | 6.8(3) |
| | 9.8(15) | 15.8(5) | 9.0(7) | | 14.0(3) |
| | | 6.9(4) | | | |
| tors ru (s) | 3.7(12) | 36.1(3) | 19.3(3) | 14.22(19) | 4.4(2) |
| | 15.5(11) | 36.6(4) | 16.4(3) | | |
| | | 0.0(0) | | | |
| Ct–Fe–Ct | 177.1(3) | 178.94(7) | 179.79(6) | 178.65(3) | 179.19(4) |
| | 178.4(2) | 178.74(7) | 175.2(10) | | 178.90(4) |
| | | 177.19(6) | | | |
| Ct–Ru–Ct | 174.49(10) | 174.94(4) | 173.51(3) | 174.84(2) | 173.34(2) |
| | 174.32(10) | 173.78(4) | 171.68(17) | | |
| | | 175.60(4) | | | |
| ang C₄S … C₅ | 59.4(9) | 32.52(19) | 7.9(4) | 44.06(15) | 1.52(16) |
| | 55.0(9) | 12.3(5) | 7.3(7) | | 14.93(12) |
| | | 5.5(5) | | | |
| rms (C₄S) | 0.0232 | 0.0233 | 0.0213 | 0.0252 | 0.0428 |
| | 0.0174 | 0.0221 | 0.0281 | | |
| | | 0.0133 | | | |
| rms (C₄) | 0.0014 | 0 | 0.0004 | 0.0021 | 0.0004 |
| | 0.0073 | 0 | 0.0149 | | |
| | | 0 | | | |
| distance S C4-plane | 0.10(3) | 0.096(14) | 0.087(8) | 0.102(6) | 0.175(6) |
| | 0.07(3) | 0.090(14) | 0.10(2) | | |
| | | 0.055(12) | | | |
| angle S…C4-plane | 4.8(3) | 4.48(11) | 4.14(7) | 4.82(5) | 8.26(5) |
| | 3.1(3) | 4.27(10) | 5.43(19) | | |
| | | 2.55(9) | | | |
| Cα-Cβ | 1.34(3) | 1.411(9) | 1.391(7) | 1.401(5) | 1.411(5) |
| | 1.44(3) | 1.401(9) | 1.435(7) | 1.411(5) | 1.415(5) |
| | 1.41(3) | 1.403(8) | 1.399(12) | | |
| | 1.39(3) | | 1.433(14) | | |
| Cβ-Cβ | 1.40(3) | 1.415(13) | 1.440(6) | 1.417(5) | 1.416(5) |
| | 1.41(3) | 1.418(14) | 1.443(13) | | |
| | | 1.428(12) | | | |
| Cα-S | 1.78(2), 1.75(2) | 1.774(7) | 1.742(5) | 1.753(3) | 1.765(4) |
| | 1.74(2), 1.75(2) | 1.767(6) | 1.760(5) | 1.756(4) | 1.776(4) |

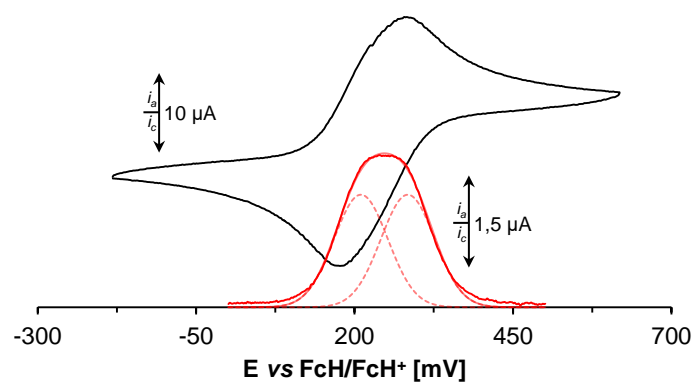|  |  |  |
|---|---|---|
|  | 1.763(6) | 1.768(9) |
|  |  | 1.723(13) |
| Zn13-Cl |  | 2.2112(11) |
|  |  | 2.2079(11) |
| Zn1-Cl… |  | 2.3544(10) |
|  |  | 2.3573(11) |
| Cl3-Zn1-Cl3 |  | 93.25(5) |
| Cl4-Zn1-Cl5 |  | 114.26(4) |
| Cl4/5-Zn1-Cl3 |  | 113.09(4) |
|  |  | 110.23(4) |



**Figure AG-3**. Cyclic and square wave (red) voltammogram of **G10** (0.5 mM) in dichloromethane at 25 °C. Scan rate: 100 mVs$^{-1}$ (SWV 1 Hz), supporting electrolyte [N$^n$Bu$_4$][PF$_6$] (0.1 M). Dotted lines elucidate deconvolution of the square wave voltammogram.

## CURRICULUM VITAE

*Personal Data*

Name:               J. Matthäus Speck

Data of Birth:      February 15, 1986

Place of Birth:     Meerane (Saxony)

Nationality:        German


*Education*

Sept. 1992 – June 1998      Staatliche Grund- und Regelschule, Langenleuba-Niederhain

Sept. 1998 – June 2004      Platanen- und Friedrichgymnasium, Altenburg

June 2004                   Abitur


*Civil Service*

July 2004 – Apr. 2005       Civil Service, Familienkommunität SILOAH e.V.


*University Education*

Oct. 2005 – Aug. 2010       Study of Chemistry, TU Chemnitz

Nov. 2009 – Aug. 2010       Diploma Thesis: "*Ferrocenylthiophene: Ferrocenyl-Substituierte Oligothiophene – Synthese und elektrochemisches Verhalten*"

Aug. 2010                   Diploma in Chemistry

Since Dec. 2010             Ph. D. Thesis, Anorganische Chemie, TU Chemnitz (Prof. Dr. Heinrich Lang)


*Fellowships/Awards*

2007                        Best Intermediate Diploma, awarded by the Gesellschaft Deutscher Chemiker (GDCh)

2011 – 2013                 Chemiefonds Fellowship of the Fonds der Chemischen Industrie (FCI)

# PUBLICATIONS

PUBLISHED MANUSCRIPTS

(1)   **Atropisomeric 3,3′,4,4′,5,5′-Hexaferrocenyl-2,2′-bithiophene: Synthesis, Solid-State Structure, and Electrochemistry.**

J.M. Speck, D. Schaarschmidt, H. Lang, *Organometallics* **2012**, *31*, 1975–1982.

(2)   **Synthesis, Electrochemistry, Spectroelectrochemistry, and Solid-State Structures of Palladium Biferrocenylphosphines and Their Use in *C,C* Cross-Coupling Reactions.**
M. Lohan, B. Milde, S. Heider, J.M. Speck, S. Krauße, D. Schaarschmidt, T. Rüffer, H. Lang, *Organometallics* **2012**, *31*, 2310–2326.

(3)   **Electron Transfer Studies on Ferrocenylthiophenes: Synthesis, Properties, and Electrochemistry.**
J.M. Speck, R. Claus, A. Hildebrandt, T. Rüffer, E. Erasmus, L. van As, J.C. Swarts, H. Lang, *Organometallics* **2012**, *31*, 6373–6380.

(4)   **Intramolecular electronic communication in ferrocene-based *β*-diketonato copper(II) complexes as observed by an electrochemical study.**
C.C. Joubert, L. van As, A. Jakob, J.M. Speck, H. Lang, J.C. Swarts, *Polyhedron* **2013**, *55*, 80–86.

(5)   **A Series of Se-Ferrocenyl Thiophene Carboselenoates – Synthesis, Solid-State Structure and Electrochemistry.**
D. Taher, F.F. Awwadi, U. Pfaff, J.M. Speck, T. Rüffer, H. Lang, *J. Organomet. Chem.* **2013**, *736*, 9–18.

(6)   **Metal-Metal Interaction in Fischer Carbene Complexes: A Study of Ferrocenyl and Biferrocenyl Tungsten Alkylidene Complexes.**
B. van der Westhuizen, J.M. Speck, M. Korb, J. Friedrich, D. I. Bezuidenhout, H. Lang, *Inorg. Chem.* **2013**, *52*, 14253–14263.

(7)   **Modification of a Hexadentate Amine based Ligand System by *N*-Methylation and Effects on Spin State and Redox Behavior of the Corresponding Transition Metal Complexes.**
S. Heider, H. Petzold, J.M. Speck, T. Rüffer, D. Schaarschmidt, *Z. Anorg. Allg. Chem.* **2014**, *640*, 1360–1367.

(8)   **Substituent Influence on Charge Transfer Interactions in α,α′-Diferrocenylthiophenes.**
J.M. Speck, M. Korb, T. Rüffer, A. Hildebrandt, H. Lang, *Organometallics* **2014**, *33*, 4813–4823.

(9)   **Synthesis, Crystal Structures, and Electrochemical Behavior of Fe−Ru Heterobimetallic Complexes with Bridged Metallocene Units.**
J. Schulz, F. Uhlík, J.M. Speck, I. Císařová, H. Lang, P. Štěpnička, *Organometallics* **2014**, *33*, 5020–5032.

(10)  **(Spectro)electrochemical investigations on (ferrocenyl)thiophenes modified by tungsten Fischer carbenes.**
B. van der Westhuizen, J.M. Speck, M. Korb, D. I. Bezuidenhout, H. Lang, *J. Organomet. Chem.* **2014**, *736*, 18–26.

(11)  **(Ferrocenylthienyl)phosphines for the Suzuki–Miyaura *C,C* coupling.**
C. Gäbler, M. Korb, D. Schaarschmidt, J.M. Speck, A. Hildebrandt, H. Lang, *Inorg. Chem. Commun.* **2015**, *54*, 96–99.

(12)  **Ferrocenes Bridged by Ethylenediamino Thiophene: Varying Charge Transfer Properties in a Series of 3,4-Di-*N*-substituted 2,5-Diferrocenyl Thiophenes.**
J.M. Speck, M. Korb, A. Schade, S. Spange, H. Lang, *Organometallics* **2015**, *34*, 3788–3798.

(13)  **(Ferrocenylthienyl)phosphines: Synthesis, Electrochemistry and Their Use in Suzuki-Miyaura *C,C* Coupling.**
C. Gäbler, J.M. Speck, M. Korb, D. Schaarschmidt, H. Lang, *J. Organomet. Chem.* **2016**, *813*, 26–35.

ORAL PRESENTATIONS

(1) **Ferrocenyl-substituierte Oligothiophene.**
J.M. Speck, R. Claus, H. Lang, 8. MANS, 23.09.2010, Halle.

(2) **Ferrocenyl Thienopyrazines – An interesting class of compounds for an application as active materials in non-aqueous redox-flow batteries.**
J.M. Speck, H. Lang, Nano-Energy Workshop - IFW Desden, 19.08.2015, Dresden.

(3) **Charge transfer in mixed-valent $\alpha,\alpha'$-diferrocenyl thiophenes – adjustable electronic coupling by substituent modification.**
J.M. Speck, H. Lang, 14th Ferrocene Colloquium, 22.02.2016, Konstanz.

POSTER CONTRIBUTIONS

(1) **Electron Transfer Studies on Ferrocenyl substituted Thiophenes.**
J.M. Speck, D. Schaarschmidt, H. Lang, 14th JCF-Frühjahrssymposium, 18. – 21.03.2012, Rostock.

(2) **Influencing the electronic interaction in diferrocenyl functionalized pyrrole and thiophene derivatives.**
S.W. Lehrich, J.M. Speck, H. Lang, 11th Ferrocene Colloquium 06. – 08.02.2013, Hannover.

(3) **Substituent Influence on Charge Transfer Interactions in $\alpha,\alpha'$-Diferrocenylthiophenes.**
J.M. Speck, M. Korb, T. Rüffer, H. Lang, 15th JCF-Frühjahrssymposium, 06. – 09.03.2013, Berlin.

(4) **Potential-dependent stochastic amperometry of multiferrocenylthiophenes in a nanofluidic device.**
K. Mathwig, H.R. Zafarani, J.M. Speck, S. Sarkar, H. Lang, S.G. Lemay, L. Rassaei, O.G. Schmidt, 13th Ferrocene Colloquium, 22. – 24.02.2015, Leipzig.

## SELBSTSTÄNDIGKEITSERKLÄRUNG

Hiermit erkläre ich an Eides statt, dass ich die vorliegende Arbeit mit dem Titel „*Ferrocenyl-substituted Thiophenes – Electrochemical Behavior and Charge Transfer*" selbstständig verfasst, nicht anderweitig zu Prüfungszwecken vorgelegt und keine anderen als die angegebenen Quellen und Hilfsmittel genutzt habe. Alle wissentlich verwendeten Textausschnitte, Zitate oder Inhalte anderer Verfasser wurden ausdrücklich als solche gekennzeichnet.

Chemnitz, den 16.03.2016

_____
Matthäus Speck